Contents

Chapter 1

What is Adsorption

1.1 INTRODUCTION

The region where one bulk phase ends and another begins is known as the interface or surface. A surface exists between a solid and a gas, a solid and a liquid, between two solids, between a liquid and a gas and between two liquids when they are immiscible. Concentration of the components in this region is different from their concentration in the bulk phases. The excess of an component in the interfacial region is known as the adsorbed amount.

In a gas, a large number of molecules are moving at random. In the course of their movement, the molecules collide with each other changing their velocity. If a molecule strikes the surface of a liquid or a sold, it may be reflected back elastically or may be retained on the surface for some time before returning to the gas phase. The molecule can be retained at the surface only if there is some kind of a force of attraction between the surface and the molecule. Unlike in their bulk, atoms on the surface of a solid or liquid have the neighbouring atoms only on one side. But the field of force due to the surface atoms extends on all sides including the space outside its boundary and this causes the attraction of the gas molecules. The captured molecule will be able to leave the surface only if the energy of thermal vibration of the molecule-surface bond is greater than the force of attraction. Adsorption will occur at any interface between a gas and a solid, a gas and a liquid, a liquid and a liquid, a liquid and a solid and between two solids. The component that is adsorbed is known as the adsorbate and the phase that offers the surface for adsorption is the adsorbent.

As it has been stated, molecules striking a surface may revert back

to the gas phase or may stay on the surface for a certain length of time. In the first case, molecules undergo elastic collision with the surface and do not exchange energy with it. If a molecular beam strikes a smooth surface at an angle θ, it may be reflected making the same angle. This is similar to the reflection of light. For this to happen, the unevenness of the surface should be less than the de Broglie wavelength of the molecular beam. If the surface is not as smooth, the molecules will be scattered randomly. The molecules that stick to the surface for a certain length of time cannot have any preferred direction while leaving the surface. Knudsen defined a term known as accommodation coefficient that gives an estimate of the extent of adsorption. Suppose the temperature of the gas before striking the surface is T_1, its temperature after exchanging some energy with the surface is T_2' and the temperature of the surface is maintained constant at T_2, Knudsen's accommodation coefficient is defined as

$$\alpha = \frac{T_2' - T_1}{T_2 - T_1} \tag{1.1}$$

When all collisions are elastic (there is no adsorption), $T_2' = T_1$ and $\alpha = 0$. When $T_2' = T_2$ (complete exchange of heat), $\alpha = 1$. Using a complicated experimental technique, accommodation coefficients were measured. For many adsorbent-adsorbate systems, α was found to be appreciable, and in some cases, even 1. The value of α is a direct measure of the quantity adsorbed.

Suppose η number of molecules strike one cm^2 of a surface per second and the molecules stay on the surface for an average time τ seconds, then the number of molecules (σ) that will be present on one cm^2 of the surface is

$$\sigma = \eta\tau \tag{1.2}$$

Striking rate τ cannot be measured directly. Hence, we shall try to relate it to some measurable quantity.

From kinetic theory of gases, we know $\eta = \frac{1}{4}N_1\overline{u}$ where $\overline{u}$ is the average speed of the gas molecules and N_1 is the number of molecules per cm^3. Kinetic theory of gases also gives the relation $p = \frac{1}{3}N_1 m\overline{u^2}$ where $\overline{u^2}$ is the root mean square speed and m is the mass of a molecule in gram. Form the relation between average speed and root mean square speed, we get

$$\overline{u} = \left(\frac{8RT}{\pi M}\right)^{\frac{1}{2}} \tag{1.3}$$

where $M = Nm$, the molar mass of the adsorbate and N is Avogadro's number. Note that $\overline{u}$ depends on temperature but is independent of pressure. If V is the molar volume of the gas, then $N_1 = \frac{N}{V} = \frac{Np}{RT}$. Substituting $\overline{u}$ and N_1 in equation (1.2), we get

$$\eta = \frac{Np}{\sqrt{2\pi MRT}} \tag{1.4}$$

Table 1.1: Magnitude of η for N_2 at different T and p.

Pressure, mm of Hg	Temperature, K	
	80	300
10^{-6}	7.4×10^{14}	3.8×10^{14}
1	7.4×10^{20}	3.8×10^{20}
760	5.6×10^{23}	2.9×10^{23}

Here, the units of mass, R, T and p are gram, erg/K, K and dyne/cm^2 respectively.

Equation (1.3) can be written as

$$\overline{u} = 460.13\sqrt{\frac{T}{M}} \tag{1.5}$$

and equation (1.4) can be simplified as

$$\eta = 2.62 \times 10^{19} \frac{p}{(MT)^{1/2}} \tag{1.6}$$

when p is in the unit dyne/cm^2. Expressing p in mm of mercury, the expression for η becomes

$$\eta = 3.52 \times 10^{22} \frac{p}{(MT)^{1/2}} \tag{1.7}$$

From equation (1.4), we see that the number of molecules striking the unit surface per second depends both on temperature and pressure. How large is this number and to what extent do they depend on pressure and temperature are given in Table 1.1.

Frenkel suggested the expression

$$\tau = \tau_o \exp(Q/RT) \tag{1.8}$$

where Q is the heat of adsorption. The quantity τ_o is the time of vibration of the surface atoms and is of the order 10^{-12} to 10^{-14} second. The variation of time of adsorption (τ) with the heat of adsorption (Q) is shown in Table 1.2. Here, we have taken $\tau_o = 10^{-14}$ second and T as the room temperature.

Table 1.2 shows that τ is very small for gases like hydrogen and helium. However, at higher temperature hydrogen can undergo chemisorption with high value of Q. The quantity η, on the other hand, has very large value even at a very low adsorbate pressure. The quantity adsorbed σ is the product of η and τ.

Table 1.2: Relation between τ and Q.

Q, kCal mol^{-1}	τ, s	Remarks
0.1	1.2×10^{-13}	
1.5	1.3×10^{-12}	Heat of adsorption of H_2 on many adsorbents
4.0	1.0×10^{-10}	Heat of adsorption of O_2, N_2, Ar etc. at room temp.
10.0	3.2×10^{-6}	Heat of adsorption of heavier hydrocarbons
20.0	1.0×10^{2}	Heat of chemisorption
40.0	1.0×10^{17}	Heat of chemisorption

Let us examine if hydrogen can undergo adsorption on a surface at room temperature and one atmosphere adsorbate pressure. Under these conditions, η for H_2 is 11.0×10^{23} per cm^2 per second. If we assume heat of adsorption as 1.5 kCal/mol, $\tau = 10^{-12}$ seconds, then $\sigma = 10^{12}$ molecules per cm^2. Let us compare this with the number of molecules of hydrogen present in one cm^2 in the gas phase. This will be $n^{2/3}$ where n is the number of molecules per cubic centimeter of the gas. At room temperature and one atmosphere pressure, $n^{2/3}$ is close to the value of σ calculated above. Since there no enrichment of hydrogen on the surface, it means that adsorption did not take place.

However, at a lower temperature, η can be much higher. For example, at a pressure one atmosphere and temperature 100 K, $\eta = 2 \times 10^{24}$ and $\tau = 10^{-10}$ seconds that gives $\sigma = 2 \times 10^{14}$ molecules per cm^2 which is much higher than the number of molecules in one cm^2 of the gas phase. This shows that enough adsorption should occur under these conditions. In case of chemisorption, Q is very much higher adsorption will take place even at very low pressure because of increased τ.

1.2 TYPES OF ADSORPTION

Adsorption occurs because of the unsaturation of the surface or the excess free energy of the surface. Based on the nature of interaction of the adsorbate molecules with the surface, we distinguish two types of adsorption: physical adsorption when the interaction is van der Waals type, and chemisorption when the interaction is chemical in nature. Generally, physical adsorption takes place at low temperature on a surface that is not highly valence unsaturated. But on the same surface, chemisorption may take place at a higher temperature.

It is not possible to draw a sharp line between the two types of adsorption. But a few experimental parameters are generally used to make a distinction between them. These are:

1. Change in electrical properties of the adsorbent

In chemisorption, there may be direct electron transfer from the solid to the adsorbate or vice versa. This would change the electrical properties like conductivity and work function of the solid. No such change is expected in physical adsorption.

2. Quantity adsorbed

Chemical forces are short range forces and such forces can form only a single layer of adsorption. Physical adsorption involves long range forces leading to multilayer adsorption, the upper limit of which is condensation of the adsorbate. Therefore the total quantity adsorbed in physical adsorption can be much higher.

3. Heat of adsorption

Heat of chemisorption is much higher, although in some cases heats of physical adsorption and chemisorption may be comparable.

4. Reversibility of adsorption

Physical adsorption is always reversible and the adsorbed molecules are in equilibrium with the gas phase. Because of the strong forces involved, chemisorption is almost irreversible. Chemisorbed species may be desorbed by raising the temperature, but in doing so there may be some chemical reaction. It was found that when chemisorbed CO is desorbed from some metal oxide surface by raising temperature, the desorbed gas is not CO but CO_2 instead.

5. Activated adsorption

As the adsorbate molecules approach a surface, they experience van der Waals forces even at a large distance from the surface. As they come

closer to the surface, they experience a force of repulsion which then changes to a strong force of attraction if they can come still closer. Only molecules with enough kinetic energy can overcome the force of repulsion to get chemisorbed. Chemisorption therefore should be an activated process and unlike physical adsorption, should involve an energy of activation. However, strong interaction between the adsorbed molecules themselves may make even physical adsorption activated.

6. Specificity

Physical adsorption is similar to condensation since both involve van der Waals forces. Physical adsorption therefore proceeds between any adsorbate-adsorbent system at suitable temperature and pressure. Chemisorption, on the other hand, is highly dependent on the chemical nature of the surface and the adsorbate.

1.3 SIMPLE ADSORPTION EQUATIONS

We are familiar with the adsorption equation

$$\sigma = \eta\tau = \frac{np\tau_o}{\sqrt{2\pi MRT}} \exp\left(Q/RT\right) \tag{1.9}$$

where σ is the quantity adsorbed per unit surface. Since M and τ_o are constants for a given adsorbate-adsorbent system, equation (1.9) can be written as

$$\sigma = \frac{k_o p}{\sqrt{T}} \exp\left(Q/RT\right) \tag{1.10}$$

when $k_o = \frac{N\tau_o}{\sqrt{2\pi RT}}$. Equation (1.10) has three variables σ, p and T. Adsorption experiments can be carried out by keeping an one of them constant and varying the other two.

If temperature T is maintained constant and if it is assumed that Q does not change during adsorption, equation (1.10) becomes

$$\sigma = k_1 p \tag{1.11}$$

when $k_1 = \frac{k_o}{\sqrt{T}} \exp\left(Q/RT\right)$. The effect of $\sqrt{T}$ on k_1 is small and has been neglected here and in subsequent cases. The above is the simplest form of adsorption isotherm equation that suggests linear increase of the quantity adsorbed with the adsorbate partial pressure. This is known as the Henry's isotherm. Such dependence is generally observed only at very low pressure.

If the quantity p in equation (1.10) is kept constant, we get

$$\sigma = k_2 \frac{\exp(Q/RT)}{\sqrt{T}} \tag{1.12}$$

This equation is known as adsorption isobar. Since the effect of $1/\sqrt{T}$ is negligible when compared to that of $\exp(1/T)$, one would expect exponential decrease of the quantity adsorbed with increase in temperature. If isobaric plots are made at two different pressures, the one obtained at the higher pressure will always lie above the one obtained at a lower pressure. Occasionally, an isobaric plots look like what is shown in figure 1.1.

Figure 1.1: *Quantity adsorbed against temperature plot showing change from physical adsorption to chemisorption.*

As seen in the figure, adsorption increases at some temperature after which it again decreases exponentially. Such a pattern indicates the change in the nature of adsorption from physical adsorption to chemisorption. There may be second break of similar nature indicating transition from chemisorption to absorption.

If the quantity adsorbed σ is kept constant in equation (1.9), we get

$$p = k_3 \sqrt{T} \exp(-Q/RT) \tag{1.13}$$

Neglecting the effect of $\sqrt{T}$, we can write

$$\ln p = -\frac{Q}{RT} + c \tag{1.14}$$

where c is a constant. This equation is known as adsorption isostere. At constant quantity adsorbed, a plot of $\ln p$ against $1/T$ will be a straight line from which the heat of adsorption Q can be found out.

Enormous experimental data has been generated on experimental adsorption isotherm measurement and many theories have been proposed to explain them. Some of these will be discussed in the next chapter.

SUGGESTED READING

1. De Boer, J.J., *The Dynamic Character of Adsorption*, Oxford, 1953.
2. Brunauer, S. *The Adsorption of Gases and Solids*, Princeton, 1945.

Chapter 2

Adsorption Isotherm

2.1 INTRODUCTION

Measurement of the quantity adsorbed on a solid surface at constant temperature at varying adsorbate pressure has been studied extensively. Measurement of σ as function of p at constant temperature is known as *adsorption isotherm*. A variety of adsorbents and adsorbates has been studied. From these measurements, five main types of plots emerged that have come to be known as the five BET types of isotherms (called after the proposers of this classification, Brunauer, Emmett and Teller)[1]. They are known as Types I, II, III, IV and V isotherms. These five types are shown in figure 2.1.

To understand the nature of the various types of experimental isotherm plots, different models have been proposed. The mathematical expressions for isotherms obtained from these models are then tested with experimental data. Although making such models is not an easy task because not much is known about the exact nature of the surface, some success has been achieved. Some of these equations have also found useful applications. Basically, isotherms are of two kinds one of which assumes a monolayer adsorption and the other assumes that adsorption is multilayer. Heat of adsorption has been been assumed to be constant in some cases and variable in other cases. Some of these cases will be examined here one by one.

2.2 MONOLAYER ADSORPTION

Some adsorption models assume that the adsorbed layer is only one molecule thick and that adsorption does not proceed beyond a monolayer.

[1] S. Brunauer, P. H. Emmett and E. Teller, *J. Am. Chem. Soc.*, 60, 309 (1938)

In deriving his isotherm equation, Langmuir further assumed that the heat of adsorption Q is constant for a given adsorbent-adsorbate system. Other workers examined the case when Q may vary with adsorption.

Figure 2.1: *Five basic types of BET isotherms.*

2.2.1 Monolayer Adsorption on Homogeneous Surfaces

To begin with, we shall consider the ideal situation when heat of adsorption is constant throughout the surface.

Langmuir isotherm

This model based on the assumption that adsorption does not go beyond a single layer of the adsorbate on the surface was proposed by Langmuir[2]. Monolayer adsorption means that every molecule striking the bare surface gets adsorbed and any molecule that strikes an adsorbed layer gets reflected back to the gas phase. This implies that adsorption does not proceed beyond the first layer. Langmuir also assumed that the energy of adsorption of each and every molecule of a given adsorbate is the same. Thus, the heat of adsorption Q is constant throughout the surface which means that the surface is energetically homogeneous. None of these two assumptions, namely monolayer nature of adsorption and homogeneous

[2]I. Langmuir, *J. Am. Chem. Soc.*, 40, 1361 (1918)

nature of the surface can be strictly correct. All the same, it leads to an equation that gives some insight into the nature of adsorption.

Let σ_0 be the number of molecules that will completely cover one cm^2 of a solid surface. This is generally known as the monolayer capacity of a solid. If σ is the number of molecules actually present on a unit surface at equilibrium, the fraction of the surface that is covered $\theta = \sigma/\sigma_0$. Fraction of the surface that is bare and available for further adsorption is $(1-\theta)$. Rate of adsorption and desorption are respectively $k_1(1-\theta)$ and $k_2\theta$ where k_1 and k_2 are the specific rates for adsorption and desorption respectively. At equilibrium,

$$k_1(1-\theta) = k_2\theta \tag{2.1}$$

By definition, $k_1 = \eta$, the number of molecules striking unit surface per second. The quantity $k_2\theta$ is the rate of desorption and is proportional to the number of molecules adsorbed per unit surface (surface concentration of the adsorbate). Hence, it is possible to write $k_2\theta = \nu\sigma_0\theta$ where ν is the frequency of vibration of the adsorbate-surface bond perpendicular to the surface with energy greater than Q. This shows ν is equal to $1/\tau_0$. Equation (2.1) becomes

$$\eta(1-\theta) = \frac{\sigma_0\theta}{\tau} \tag{2.2}$$

Rearranging, $\frac{1-\theta}{\theta} = \frac{\sigma_0}{\eta\tau}$ that can be written as

$$\frac{1}{\theta} = 1 + \frac{\sigma_0}{\eta\tau} = \frac{\sigma_0 + \eta\tau}{\eta\tau} \tag{2.3}$$

This gives

$$\theta = \frac{\eta\tau}{\sigma_0 + \eta\tau} = \frac{\eta\tau/\sigma_0}{1 + \eta\tau/\sigma_0} \tag{2.4}$$

Substituting for η and τ

$$\theta = \frac{\frac{Np}{\sqrt{2\pi MRT}\frac{\tau_0}{\sigma_0}e^{Q/RT}}}{1 + \frac{Np}{\sqrt{2\pi MRT}\frac{\tau_0}{\sigma_0}e^{Q/RT}}} \tag{2.5}$$

For a homogeneous surface (Q=constant) at constant temperature, the quantity $\frac{Np}{\sqrt{2\pi MRT}\frac{\tau_0}{\sigma_0}e^{Q/RT}}$ is a constant and let this be b. Then

$$\theta = \frac{bp}{1+bp} \tag{2.6}$$

This is known as the Langmuir's isotherm equation.

Langmuir's derivation of the equation is based on adsorption-desorption kinetics. Fowler derived the same equation from statistical thermodynamics where the quantity b turns out to be

$$b = \frac{h^3}{(2\pi m)^{1/3}(k/T)^{5/2}} \frac{f_a(T)}{f_g(T)} e^{q/T} \tag{2.7}$$

Here, $f_a(T)$ and $f_g(T)$ are the internal partition functions in the adsorbed and gaseous states respectively, q is the energy necessary to transfer an adsorbed molecule in its ground state to the gaseous ground state, k is Boltzmann constant, m is the molecular mass of the adsorbate and h is Planck's constant.

When $bp \ll 1$, Langmuir's equation reduces to $\theta = bp$ which means the quantity adsorbed increases linearly with adsorbate pressure. If, on the other hand, $bp \gg 1$, the equation becomes $\theta = 1$ that indicates completion of the monolayer. The plot of θ against p depends on the value of b. Such plots for different values of b are shown in figure 2.2

If a diatomic gas undergoes dissociation on adsorption, both atoms will occupy one site on the surface. In case of such dissociative adsorption, the rate of adsorption of each of the dissociated atoms will be proportional to $(1 - \theta)$, fraction of the surface that is empty. The rate of adsorption will be equal to $\eta(1 - \theta)^2$. Rate of desorption that is proportional to the surface concentration $\sigma_0\theta^2$. Equating rate of adsorption and desorption at equilibrium,

$$\eta(1 - \theta)^2 = \frac{\sigma_0}{\tau\theta^2} \tag{2.8}$$

This gives the equation

$$\theta = \frac{\sqrt{bp}}{1 + \sqrt{bp}} \tag{2.9}$$

Let us next consider the case of simultaneous adsorption of two gases A and B on the same surface. If we assume that the adsorbates A and B are competing for the same sites on the surface for adsorption, rate of adsorption of A will be $\eta_A(1 - \theta A - \theta_B)$ because the fraction of the bare surface is now $(1 - \theta_A - \theta_B)$. The rate of desorption of A is $\frac{(\sigma_0)_A\theta_A}{\tau}$. The quantity $(\sigma_0)_A\theta_A$ is the concentration of A on the surface. Equating the rates of adsorption and desorption,

$$\eta(1 - \theta_A - \theta_B) = \frac{\eta_A\tau}{(\sigma_0)_A} \tag{2.10}$$

Figure 2.2: *θ versus p for different values of b.*

This gives

$$\frac{\theta_A}{(1-\theta_A-\theta_B)} = \frac{\eta_A \tau}{\sigma_0)_A} = b_A p_A \tag{2.11}$$

b_A has the same meaning as b except that now it is related to the molecules of A only. Similarly,

$$\frac{\theta_B}{(1-\theta_A-\theta_B)} = \frac{\eta_B \tau}{\sigma_0)_B} = b_B p_B \tag{2.12}$$

Dividing (2.11) by (2.12),

$$\frac{\theta_A}{\theta_B} = \frac{b_A p_A}{b_B p_B} \tag{2.13}$$

This gives $\theta_B = \frac{\theta_A b_B p_B}{b_A p_A}$. Substituting for θ_B in equation (2.13),

$$\theta_A = b_A p_A (1 - \theta_A - \frac{\theta_A b_B p_B}{b_A p_A}) \tag{2.14}$$

Rearranging,

$$\theta_A = \frac{b_A p_A}{1 + b_A p_A + b_B p_B} \tag{2.15}$$

Similarly, it is possible to show

$$\theta_B = \frac{b_B p_B}{1 + b_A p_A + b_B p_B} \tag{2.16}$$

The general from of Langmuir equation for a multi-component adsorbate is

$$\theta = \frac{b_i p_i}{1 + \sum b_i p_i} \tag{2.17}$$

It is now necessary to test if the Langmuir equation is valid for a adsorbent-adsorbate system. The quantity $\theta = \frac{\sigma}{\sigma_0}$, can be replaced by $\frac{v}{v_m}$ where v and v_m are respectively the volume (at NTP) of the gas adsorbed at any pressure p and at saturation of the surface. A plot of $\frac{v}{v_m}$ against pressure should have the shape of the type I isotherm for Langmuir's assumptions to be justified. However, type I shape itself does not prove that the Langmuir's assumptions are correct for the system.

In order to test the Langmuir theory, we first convert the Langmuir equation into a linear form as the following

$$\frac{p}{v} = \frac{1}{bv_m} + \frac{p}{v_m} \tag{2.18}$$

The linearity of the p/v versus p plot will show that b and hence Q is a constant, which is a basic assumption of Langmuir's model.

Another linear from of the same equation is

$$\frac{v}{p} = v_m b - bv \tag{2.19}$$

According to this, a plot of v/p against v should give a straight line with a negative slope from which b can be obtained. Monolayer capacity v_m can be obtained from the intercept. Small values of the slope and the intercepts in these plots make the values of b and v_m inaccurate. All the same, linearity of the plots can be used as a test for the validity of the Langmuir's equation.

2.2.2 Adsorption on a Heterogeneous Surface

In deriving Langmuir's equation, it was assumed that the heat of adsorption for a given adsorbent-adsorbate system is constant. However, real surfaces are always heterogeneous. If heat of adsorption changes continuously say from Q_1 to Q_2, it may be assumed that all sites with a particular value Q_i will obey the Langmuir's equation. Including all values of Q within limits Q_1 to Q_2 will lead to

$$\theta = \int_{Q_1}^{Q_2} \frac{b_0 p e^{Q/RT}}{1 + b_0 p e^{Q/RT}} \tag{2.20}$$

Note that b has been replaced by $b_0 e^{Q/RT}$ because the quantity b is no longer a constant as Q is not a constant. The important point to consider is how does the number of adsorption sites vary with changing Q. One possibility is that all types of sites with their values of Q_i are

equal in number. The other possibility is that the number of sites vary as a function of Q. But such variations may be of different types.

Roginski[3] has done a mathematical analysis of non-homogeneous surfaces assuming different types of site distribution as a function of Q.

If $d\phi$ is the fraction of the surface with heat of adsorption lying between Q and $Q + dQ$, then $\frac{d\phi}{dQ}$ will give the distribution of sites with different Q on the surface. In principle, it is possible to consider many different distribution functions such as:

1. All types of sites are equal in number, i.e. $f(Q) = A$ where A is a constant.
2. Number of sites increases linearly with Q which can be written as $f(Q) = BQ + C$ where B and C are constants.
3. Number of sites decrease exponentially with increase of Q that can be written as $f(Q) = ne^{-Q}$, n and m being constants.

Temkin's isotherm

Temkin[4] assumed that all types of sites on the surface are equal in number ($f(Q) = A$) and wrote the equation

$$\theta = \int_{Q_1}^{Q_2} \theta(p, Q) f(Q) dQ \tag{2.21}$$

Substituting $f(Q) = A$,

$$\theta = \int_{Q_1}^{Q_2} \frac{Ab_0 e^{Q/RT} p}{1 + b_0 e^{Q/RT} p} dQ \tag{2.22}$$

Because A, b_0, R and T are constants and p does not depend on Q,

$$\theta = Ab_0 RTp \int_{Q_1}^{Q_2} \frac{e^{Q/RT}}{1 + b_0 p e^{Q/RT}} . d\Big(\frac{Q}{RT}\Big) \tag{2.23}$$

Solution of this integral gives

$$\theta = ART \ln \frac{1 + b_0 e^{Q_2/RT}}{1 + b_0 p e^{Q_1/RT}} = ART \ln \frac{1 + b_2 p}{1 + b_1 p} \tag{2.24}$$

[3]Roginskii, C.Z., *Adsorptsya i Kataliz na Neodnorodnykh Poverkhnostyakh* (in Russian), Izd. Akad. Nauk, Moscow, 1949.

[4]Temkin, M.I., *Zh. Fiz. Khim.*, 15,296 (1941).

Since $b_2p \gg 1$ and $b_1p \ll 1$, the equation (2.24) becomes

$$\theta = ART \ln b_2p \tag{2.25}$$

Temkin's equation suggests that if all types of sites are present on the surface in equal number, fraction of the surface covered and hence the quantity adsorbed should show a logarithmic dependence on adsorbate pressure. Frumkin and Shlygin[5] noticed such a dependence while studying adsorption of hydrogen on platinum electrode surface.

It appears highly unlikely that all types of adsorption sites are present on the surface in equal number. A more reasonable assumption may be that the number of sites with a given value of Q decreases linearly with Q. Adsorption begins at those sites where the heat of adsorption is maximum and as adsorption proceeds, sites with lower values of Q are covered with increasing p. If Q_2 is the upper limit of Q (when $\theta \to 0$), then $f(Q) = Q_2(1 - \alpha\theta)$, i.e. Q decreases linearly with increased surface coverage. The general isotherm equation (2.23) for a heterogeneous surface can now be written as

$$\theta = \int_{Q_1}^{Q_2} \frac{b_0pe^{Q_2(1-\alpha\theta)/RT}}{1 + b_0pe^{Q_2(1-\alpha\theta)/RT}} dQ = \int_{Q_1}^{Q_2} \frac{B_0pe^{-(Q_2\alpha\theta)/RT}}{1 + B_0pe^{-(Q_2\alpha\theta)/RT}} dQ \tag{2.26}$$

where $B_0 = b_oe^{Q_2/RT}$. The quantity $B_0e^{\frac{-Q_2\alpha\theta}{RT}}$ is similar to b in the Langmuir's equation. Therefore, it is possible to write

$$\frac{\theta}{1-\theta} = B_0pe^{\frac{-Q_2\alpha\theta}{RT}} \tag{2.27}$$

Taking logarithms and rearranging,

$$\ln B_0p = -\frac{Q_2\alpha\theta}{RT} + \ln \frac{\theta}{1-\theta} \tag{2.28}$$

The second term on the right hand side of the above equation will vanish at intermediate coverage, i.e. when $\theta = 0.5$ giving $\ln B_0p = (Q_2\alpha\theta)/RT$ finally giving

$$\theta = \frac{(\ln B_0p)}{Q_2\alpha} RT = (RT/Q_2\alpha) \ln B_0 + (RT/Q_2\alpha) \ln p \tag{2.29}$$

showing that quantity adsorbed should increase linearly with $\ln p$. Validity of this equation is restricted to the middle range of surface coverage only.

[5] Frumkin A.H. and Shlygin, A.I., *Acta Physicochim. URSS*, 3, 791 (1935)

Freundlich isotherm

Zeldovitch suggested a surface distribution given by $f(Q) = n_0 e^{-Q/Q_m}$ showing an exponential decrease in the number of surface sites with increasing Q. Here n_0 and Q_m are constants. This enables us to write the equation (2.21) as

$$\theta = \int_{Q_1}^{Q_2} \frac{b_0 e^{Q/RT} p}{1 + b_0 e^{Q/RT} p} n_0 e^{-Q/Q_m} dQ \tag{2.30}$$

An exact solution of this equation is difficult, but an approximate analytical solution under the condition $Q \gg RT$ gives

$$\theta = (b_0 p)^{RT/Q_m} \tag{2.31}$$

Since $v = v_m \theta$, we get $v = v_m (b_0 p)^{RT/Q_m}$. Taking logarithms,

$$\log v = \log v_m + (RT/Q_m) \log b_0 + (RT/Q_m) \log p$$

which predicts that $\log v$ vs $\log P$ plots at various temperatures will be straight lines. This result is similar to the empirical Freundlich isotherm equation generally written as

$$v = c p^{1/n} \tag{2.32}$$

which gives a straight line plot of $\log v$ against $\log p$.

2.3 MULTILAYER ADSORPTION

Unlike monolayer adsorption, multilayer adsorption assumes that the molecules striking the bare surface as well as the adsorbed layer stick to the surface.

BET isotherm

The most widely known adsorption equation for multilayer adsorption was derived by Brunauer, Emmett and Teller and this is known as the BET equation. Here again, it is assumed that the surface is energetically homogeneous which means that the heat of adsorption Q is constant. The first layer is a truly adsorbed layer and the subsequent layers are the condensed layers. This itself makes it doubtful may if the assumption that Q is constant can be correct. However, since the first layer is physically adsorbed that has Q close to the enthalpy of condensation, the constancy of Q may be accepted as an approximation.

The model assumes a dynamic equilibrium within each adsorbed or condensed layer. At equilibrium, the rate of formation of a layer is equal

to the rate of its destruction. It is not necessary for an early layer to be completed before the next layer starts forming. The conceptualized picture is shown in figure 2.3. This shows that the formation of a higher layer can begin even before an earlier layer is complete.

We assume that θ_1 is the fraction of the surface covered with a unimolecular layer, θ_2 is the fraction covered with a layer of two molecules and θ_i is the fraction covered by a layer that has i molecules one above another. This gives us the total number of molecules σ per unit surface

$$\sigma = \sigma_0\theta_1 + 2\sigma_0\theta_2 + 3\sigma_0\theta_3 \ldots + i\sigma_i\theta_i$$

where σ_0 is the monolayer capacity. Taking summation,

$$\sigma = \sigma_0 \sum_{i=1}^{i=\infty} i\theta_i \tag{2.33}$$

Figure 2.3: *The picture of multilayer adsorption as assumed in the BET model.*

The fraction of the surface that is bare under these conditions is

$$\theta_0 = 1 - \theta_1 - \theta_2 - \ldots - \theta_i$$

which gives

$$\theta_0 = 1 - \sum_{i=1}^{i=\infty} \theta_i \tag{2.34}$$

Let us now concentrate on the first layer. According to BET theory, the rate of adsorption of this layer is equal to its rate of desorption. We can write,

$$\eta\theta_0 = \nu\sigma_0\theta_1 \tag{2.35}$$

The first layer can be formed both by adsorption on the bare surface and by desorption of the second layer of a bimolecular layer. The net rate of formation of layer 1 is then $\eta\theta_0 + \nu_1\sigma_0\theta_2$ where ν_1 is the frequency of effective vibration of an adsorbed molecule in the second layer. Destruction of the first layer can take place by evaporation of the first layer as well as by condensation on the first layer and hence the net rate of destruction of the first layer is $\nu\sigma_0\theta_1 + \eta\theta_1$. Equating the rates of formation and destruction of the first layer,

$$\eta\theta_0 + \nu_1\sigma_0\theta_2 = \nu\sigma_0\theta_1 + \eta\theta_2 \tag{2.36}$$

Combining equations (2.35) and (2.36), we get

$$\nu_1\sigma_0\theta_2 = \eta\theta_1$$

Continuing the same logic, it can be shown that

$$\eta\theta_{i-1} = \nu_{i-1}\sigma_0\theta_i \tag{2.37}$$

Since all except the first layer are condensed layers, it is possible to write $\nu_1 = \nu_2 = \nu_{i-1}$ and they can be replaced by $\frac{1}{\tau_1}$.

From equation (2.35), we get

$\theta_1 = \frac{\eta\theta_0\tau}{\sigma_0}$.

$\theta_2 = \theta_1\frac{\eta\tau_1}{\sigma_0} = \beta\theta_1$, where $\beta = \frac{\eta\tau_1}{\sigma_0}$

$\theta_3 = \frac{\theta_2\eta\tau_1}{\sigma_0} = \beta^2\theta_1$

$\theta_i = \beta^{i-1}\theta_1$

Substituting the value of θ_1, we get

$$\theta_i = \beta^i\frac{\tau}{\tau_1}\theta_0$$

It is now possible to write equation (2.33) as

$$\sigma = \sigma_0\frac{\tau}{\tau_1}\theta_0\sum_{i=1}^{i=\infty} i\beta^i \tag{2.38}$$

And substituting for θ_i in equation (2.35),

$$\theta_0\left(1 + \frac{\tau}{\tau_1}\sum_{i=1}^{i=\infty}\beta^i\right) = 1 \tag{2.39}$$

Writing $\tau/\tau_1 = C$, equation (2.36) becomes

$$\sigma = \frac{\sigma_0 C\sum_{i=1}^{i=\infty} i\beta^i}{1 + C\sum_{i=1}^{i=\infty}\beta^i} \tag{2.40}$$

But $\sum_{i=1}^{i=\infty} i\beta^i = \frac{\beta}{(1-\beta)^2}$ and $\sum_{i=1}^{i=\infty} \beta^i = \frac{\beta}{1-\beta}$. So the equation (2.40) can be written as

$$\frac{\sigma}{\sigma_0} = \frac{C\beta}{(1-\beta)(1-\beta+C\beta)} \tag{2.41}$$

Except for the first layer, adsorption is same as condensation of the adsorbate. Infinite condensation is possible when p becomes equal to the saturation vapour pressure p_0. According to the equation (2.41), adsorption or $\frac{\sigma}{\sigma_0} \to \infty$ when $\beta \to \infty$. It thus possible to identify the term β with the measurable quantity $\frac{p}{p_0}$ and rewrite the equation as

$$\frac{\sigma}{\sigma_0} = \frac{Cp}{(p_0-p)[1+(C-1)p/p_0]} \tag{2.42}$$

The quantity σ/σ_0 can be conveniently replaced by v/v_m and the equation can be rearranged to a more convenient linear form as

$$\frac{p}{v(p_0-p)} = \frac{1}{Cv_m} + \frac{(C-1)p}{Cv_m p_0} \tag{2.43}$$

This is the familiar form of the BET equation. It predicts a straight line for a plot of $\frac{p}{v(p_0-p)}$ against $\frac{p}{p_0}$, with an intercept $1/v_m C$ and slope $(C-1)/v_m C$. The monolayer capacity v_m can be obtained from this plot.

The constant

$$C = \frac{\tau}{\tau_1} = \frac{e^{Q_a/RT}}{e^{Q_L/RT}}$$

where Q_a and Q_L are respectively the heat of adsorption and heat of condensation of the adsorbate. When heat of adsorption is very much greater than the heat of condensation ($Q_a \gg Q_L$), C is very much larger than β. Under this condition, the BET equation becomes similar to the Langmuir's equation.

$$\frac{v}{v_m} = \frac{C\beta}{1+C\beta}$$

because $C\beta = \frac{\tau\eta\tau_1}{\tau_1\sigma_0} = bp$ and hence

$$\frac{v}{v_m} = \frac{bp}{1+bp}$$

This is the equation for type I isotherm of the BET classification.

When $Q_a > Q_L$ such that C has values above 3, a type II isotherm is predicted. On the other hand, when adsorption is very weak ($Q_a \ll Q_L$), the BET equation predicts a type III isotherm.

Variation of the v/v_m versus p/p_0 plot for different values of the constant C is shown in figure 2.4.

A close scrutiny shows that the assumptions of the BET theory do not stand on firm ground. Its assumption that the surface is homogeneous can hardly be true for any real surface. Later studies confirm that most surfaces are highly heterogeneous and heat of adsorption falls with surface coverage that is directly proportional to partial pressure. Moreover, at higher coverage, there is likely to be lateral adsorbate-adsorbate interaction that will increase the heat of adsorption. It is likely that within some range of relative pressure (p/p_0), these two opposing effects cancel each other and a linear BET plot is obtained. Experiments show that the BET plot is linear in a certain pressure range with p/p_0 lying between 0.05 to 0.3.

Figure 2.4: *v/v_m versus p/p_0 plots for different values of C.*

In explaining the shape of type II isotherms, it can be thought that adsorption is rapid initially when the sites with high values of Q_a are being occupied. After the first layer is complete, heat of adsorption is replaced by heat of heat of condensation which is lower than Q_a. From this point onwards, adsorption increases slowly with p/p_0. The third part of the type II isotherm is due to rapid condensation when $p/p_0 \to 1$.

In case of type III isotherm, initial adsorption is very slow because of low value of Q_a. The convex nature of the plot in the next part is due to the fact that adsorption is now cooperative due strong adsorbate-

adsorbate interaction. The above hypothesis was tested by Kiselev[6]. Since strong adsorbate-adsorbate interaction is supposed to give a type III isotherm, adsorbates like water and ammonia that are capable of hydrogen bonding, should give type III isotherms on a nonpolar surface. However, if the adsorbent surface itself has hydroxyl groups (silica surface, for example), it will strongly interact with polar adsorbate molecules thus increasing adsorbate-adsorbent interaction that is likely to give a type II isotherm. Kiselev has demonstrated how the change in the nature of the surface changes the isotherm type in the following example. Benzene, gives a type II isotherm on hydrated silica. When polar –OH groups of the silica surface are progressively replaced by nonpolar $-OSi(CH_3)_3$, it changed to type III. Results obtained by Kiselev on the adsorption of benzene on treated silica surface are shown in figure 2.5.

Figure 2.5: *Benzene adsorption isotherms on hydrated silica surface treated with trimethylsilicon chloride; surface concentration of* $Si(CH_3)_3$*: 1 - 0; 2 - 60%; 3 - 70%; 4 - 80%; 5 - 90% and 6 - 100%.*

The kinetic derivation of the BET equation ignored the entropy factor. The same BET equation was derived by Goates and Hatch[7] from thermodynamic consideration. In their equation, the authors identified the constant C with $\exp \frac{\Delta G_L - \Delta G_{\mathrm{ad}}}{RT}$. Here ΔG_{ad} and ΔG_L are the Gibbs free energy of adsorption and condensation respectively. As adsorption proceeds, ΔH_{ad} becomes less and less negative and so does ΔS_{ad}. The opposing contribution of these two quantities to ΔG_{ad} helps in keeping it constant and hence the constancy of C is maintained within a range

[6]Kiselev, A.V., *Quart. Rev.*, 15, 116 (1961)
[7]Goates, J. and Hatch, C., *Soil Sci.*, 75, 275 (1953)

of p in spite of the fact that heat of adsorption changes.

With all its limitations, the BET equation has been useful in understanding the nature of the surface and its main application is in determining the surface area of solids that will be discussed later.

2.3.1 Polyani's Theory of Adsorption

Polyani developed a different approach to multilayer adsorption. The adsorbed layer is considered to be a thin film near the adsorbent-adsorbate interface. Since the force adsorption should decrease with the increase of distance from the surface, the adsorbed film lies in an intermolecular potential gradient. The force of attraction at any point in the film is given by an adsorption potential (ϵ) which is equal to the work done in bringing the molecule from the gas phase to that point. A surface on which all points have the same potential is called an equipotential surface. This is shown in figure 2.6.

Figure 2.6: *Adsorbed layers according to potential theory: each broken line represents an equipotential surface.*

Nearer the surface, the potential ϵ is high and it falls off as the distance from the surface increases. If v is the volume between the adsorbent surface and an equipotential plane, v will be maximum when the potential is zero, i.e. when the true gas phase begins. v will be lowest when the equipotential plane is nearest to the adsorbent surface, i.e. when ϵ is maximum. The building up of the adsorbed film may be described as $\epsilon = f(v)$. Since the potential is temperature independent, the same type of dependence ϵ on v should be valid for a given adsorbate-adsorbent system irrespective of temperature.

Since ϵ cannot be found by experimental measurement, Polyani tried to relate it to some experimentally measurable quantity. This approach

relates the potential of adsorption with the volume adsorbed and not with the distance from the surface. This has a big advantage. Although the distance is not known, volume v can be found out by multiplying the number of mole adsorbed (σ/N) by the molar volume v_ℓ of the liquid adsorbate such that $v = \frac{\sigma}{N} v_\ell$.

The potential ϵ too can be calculated. If p is the pressure of the adsorbate in the gas phase at equilibrium with the adsorbed phase and p_0 is its saturation pressure, the work done in taking molecule from an equipotential plane to the gas phase against the force of attraction of the surface (which is a measure of ϵ) is

$$\epsilon = RT \ln \frac{p}{p_0} \tag{2.44}$$

Figure 2.7: *(a) Adsorption isotherms of carbon dioxide on carbon surface at various temperatures; (b) The characteristic curve.*

An experimental adsorption isotherm can be expressed as σ vs $\frac{p_0}{p}$. Such a plot can be easily converted to a ϵ vs v plot. This is is known as a characteristic curve for a given adsorbate-adsorbent system and is independent of temperature. It has the advantage that if we construct a characteristic curve from the adsorption data obtained at one temperature, it can be converted to an adsorption isotherm at another temperature. Thus, from adsorption isotherm at one temperature, the same for another temperature can be reconstructed.This is possible because

$$v = \frac{\sigma_1}{N}(v_\ell)_1 = \frac{\sigma_2}{N}(v_\ell)_2$$

and

$$\epsilon = RT_1 \ln \frac{(p_0)_1}{p_1} = RT_2 \ln \frac{(p_0)_2}{p_2}$$

where the subscripts 1 and 2 everywhere refers to the quantities at temperatures T_1 and T_2 (for example, $(p_0)_1$ is the saturation pressure at T_1, $(v_\ell)_1$ is the molar volume of the liquid adsorbate 1, and so on). If adsorption is measured at different temperatures, they will all give the same characteristic curve. This has been illustrated in figure 2.7.

Polanyi's theory was further developed by Dubinin[8] that made it possible to convert the characteristic curve of one adsorbate-adsorbent system into the characteristic curve for another adsorbate on the same adsorbent.

Polyani's method is not applicable to monolayer adsorption and also for adsorption on solids with fine pores because in the latter case, the properties of the adsorbed layer is different from those of a ordinary adsorbate in the liquid state.

2.4 ADSORPTION ON POROUS SOLIDS

So far we have seen that the BET equation can explain the shapes of type I, type II and type III isotherms. Isotherms of type IV and V are shown by solids that has extensive pore structure. Moreover, adsorption and desorption follow different paths in many porous solids showing hysteresis. In such solids, a plot of the quantity adsorbed versus adsorbate pressure does not follow the same path for adsorption and desorption. In this section, an attempt will be made to understand the origin of the different types of adsorption-desorption hysteresis.

Physical adsorption inside the micropores of a solid will be treated here as capillary condensation of the adsorbate inside the pores. When the pores are very large, the surface inside and outside the pores are very similar and there is no difference between the surface inside the pores and the external surface. When the pores are very small (a few nanometers in radius), the surface force inside the pores is stronger because the adsorbate molecule is simultaneously close to a number of surface atoms. The pores may be treated as micro capillaries and the adsorbed layer as the condensed liquid layer. First formation of the liquid layer will occur at the narrowest part of the pore where the force of attraction is strongest. Further adsorption amounts to filling up of these pores by the liquid adsorbate.

[8]M. Dubinin, *Uspekhi Khimii*, 24 (1955)

Centre of curvature of the liquid film first formed lies in the adsorbate gas phase and the pressure difference between the gas and the liquid phase is given by the equation $\Delta P = \gamma(1/R_1 + 1/R_2)$, the total pressure being higher in the gas phase where the centre of curvature is located. R_1 and R_2 are the radii of curvature of the liquid film and γ is the surface tension of the liquid adsorbate. Chemical potential of the gas is $\mu' = \mu'_0 + RT \ln p$ where μ'_0 is the standard chemical potential and p is the vapour pressure of the gaseous adsorbate. Let μ'' be the chemical potential of the liquid adsorbate in the film. At equilibrium, $\mu' = \mu''$. The change in chemical potential $d\mu' = d\mu'' = RT d \ln p$.

Molar volume of the liquid

$$v_\ell = \left(\frac{d\mu''}{dP''}\right)_T \tag{2.45}$$

This gives

$$dP'' = \frac{d\mu''}{v_\ell} = \frac{RT}{v_\ell} d \ln p \tag{2.46}$$

Here P'' is the total pressure in the liquid phase of curvature $(1/R_1 + 1/R_2)$ and the corresponding vapour pressure is p. Let us assume that the total pressure in the liquid phase is P''_0 if the curvature of the film is zero. This will be the case when the film is formed on the surface outside the pore and the corresponding vapour pressure of the liquid film is its normal saturation vapour pressure p_0. One can now integrate dP'' between the limits P'' and P''_0

$$\int_{P''}^{P''_0} dP'' = \frac{RT}{v_\ell} \int_p^{p_0} d \ln p \tag{2.47}$$

Solving the integrals, we get

$$P''_0 - P'' = \frac{RT}{v_\ell} \ln \frac{p_0}{p} \tag{2.48}$$

For a plane surface, $P''_0 = P'_0$ where P'_0 is the total pressure in the vapour phase when the curvature is zero. Since the total pressure in the gas phase P' is constant, $P'_0 = P'$. Therefore,

$$(RT/v_\ell) \ln(p/p_0) = P''_0 - P'' = P' - P'' = \gamma(1/R_1 + 1/R_2)$$

It is now possible to write

$$p = p_0 \exp\left(-\frac{\gamma v_\ell (1/R_1 + 1/R_2)}{RT}\right) \tag{2.49}$$

Thus, inside the micropore where a concave liquid film is formed, the vapour will become saturated at a vapour pressure p that is lower than the usual saturation vapour pressure p_0 of the adsorbate. Condensation of the vapour inside a capillary then will begin at vapor pressure lower than p_0, the usual saturation vapour pressure. This is known as *capillary condensation*. It is important to note that the nature of the curvature of the meniscus of the initially formed film determines the pressure at which condensation will take place. Nature of the pore is important only as long as it determines the nature of this meniscus.

Depending upon the nature of the pore, two main types of meniscus can be formed. A spherical meniscus is formed at the narrowest part of a pore when the pore is closed at one end. If the pore is cylindrical and open at both ends, the first liquid film is formed all along the cylindrical wall and it has a cylindrical meniscus (see figure 2.8).

Figure 2.8: *Condensed liquid film showing (a) spherical meniscus and (b) cylindrical meniscus.*

For a spherical meniscus, $R_1 = R_2 = r_s$ where r_s is the radius of curvature of the spherical meniscus. For this, equation (2.49) becomes

$$\frac{p}{p_0} = \exp\left(-\frac{2\gamma v_\ell}{r_s RT}\right) \tag{2.50}$$

and for liquid film with cylindrical meniscus, one curvature is zero and hence equation (2.49) takes the form

$$\frac{p}{p_0} = \exp\left(-\frac{\gamma v_\ell}{r_c RT}\right) \tag{2.51}$$

when r_c is the radius of the meniscus of the cylindrical liquid film formed at the beginning. The equations (2.50) and (2.51) shows how adsorption on microporous solids should depend on the adsorbate pressure p.

Some typical case studies

Suppose the solid has cylindrical pores closed at one end. At the beginning, a spherical meniscus will form at the end of the pore (figure 2.8.(a)). Further adsorption will follow equation (2.50). As adsorption proceeds, the pore starts to fill up, but value of r_s remains unchanged. So, once the film is formed, the entire pore will be filled up with condensed adsorbate at the same pressure p. This is shown in figure 2.9.(a). The initial part of the curve shows that some increase in pressure is needed to initiate the formation of the film after which adsorption is complete at the same pressure. On completion of the pore filling, the meniscus remains spherical and desorption will follow the same equation. Thus, desorption will follow the path that is exactly the reverse of adsorption. No hysteresis will be observed.

Figure 2.9: *Adsorption-desorption isotherms in idealized (a) cylindrical pores closed at one end (b) cylindrical pores open at both ends.*

Next to be considered is a cylindrical pore with both ends open. The initial liquid film in this case will look like figure 2.8.(b). Adsorption which is nothing but filling up of the pore with the liquid adsorbate (capillary condensation) will follow the equation (2.51). As the film grows (see figure 2.8), the radius of the meniscus r_c will decrease and further adsorption will need even smaller value of p/p_0. But since the experimental value of p/p_0 is already higher than what is needed for further adsorption, entire adsorption process will be completed at a constant value of p/p_0. At the end of adsorption, the menisci at either end will become spherical as shown in the figure.

Desorption from this pore will begin with a spherical meniscus of the film according to equation (2.49). This means that desorption can begin only at a pressure lower than the pressure at which adsorption

took place. At some stage of desorption, the meniscus will change to cylindrical but by now the pressure is already lower than what would be needed for desorption from a film with cylindrical meniscus. Hence, the entire desorption will take place at the same pressure. The path followed by adsorption and desorption are separate in this case as shown in figure 2.9.(b).

Figure 2.10: *Gradual filling of a cylindrical pore open at both ends showing how the initially formed cylindrical meniscus changes to a spherical meniscus towards the end.*

Figure 2.11: *Different types of micropores: (a)Conical, (b) ink-bottle and (c) spheroidal pores.*

In the case of a solid with conical pores, the initial film will be spherical and adsorption will follow equation (2.50). r_s will increase with adsorption and hence further adsorption will need even lower adsorbate pressure. That is why adsorption will be complete at the pressure at which pore filling begins. In this case too, desorption path will be the reverse of the adsorption path and no hysteresis is expected.

Another type of pore is known as ink-bottle type shown in figure 2.11. Here, adsorption begins at the wider part of the pore with spherical meniscus that will need a higher pressure than what would be needed near the neck. So the pore will be filled up at the constant pressure. Desorption will begin near the neck where the radius is smaller and

hence will start at a pressure lower than the adsorption pressure. Hence hysteresis is expected. The same will be true for spheroidal pores.

Figure 2.12: *Types of adsorption-desorption hysteresis discussed by de Boer.*

Five different types of adsorption-desorption hysteresis diagrams that are shown in figure 2.12. has been considered by de Boer[9]

A straight forward interpretation of the experimental isotherm is not always possible. But obtaining the adsorption-desorption isotherms experimentally is very important in determining the pore volume and pore radius of solids. This will be discussed in Chapter 4.

SUGGESTED READING

1. De Boer, J.J., *The Dynamic Character of Adsorption*, Oxford, 1953.
2. Brunauer, S. *The Adsorption of Gases and Solids*, Princeton, 1945.
3. Gregg S.G., and Sing, K.S.W., *Adsorption, Surface Area and Porosity*, Acad. Press, 1967.
4. Brunauer, S., Copeland, L.E. and Kantro, D.L., *The Langmuir and BET theories* in *Solid Gas Interface, vol.1*, Flood, E.A. (Editor), Marcell Dekker, 1967.

[9]J.H. de Boer in *The Structure and Properties of Porous Materials*, D. H. Everett and F. S. Stone (Editors), Butterworth, Colston Papers, vol.10, London, 1958, p.68

Chapter 3

Adsorption Energetics

3.1 ADSORPTION THERMODYNAMICS

So far, we have considered a kinetic picture of the adsorption phenomenon. Since the physically adsorbed layer is in a dynamic equilibrium with the adsorbate bulk phase, it should be amenable to the methods of equilibrium thermodynamics. We shall consider here the general case of equilibrium between the two bulk phases and the adsorbed layer. This general treatment is due to Gibbs[1]. This approach does not require any specific knowledge of the nature of the surface or that of the adsorbate. The method is, however, not suitable for describing chemisorption.

Figure 3.1: *The adsorbed layer of small thickness t lying between the two bulk phases.*

Concentration of the components in the surface layer is different from those in the bulk phases. Let us consider the conditions of equilibrium of this heterogeneous system that consists of the bulk phases I and II and the adsorbed layer. The general condition of equilibrium of such a closed system is that its internal energy should be minimum at constant

[1]Gibbs,J.W., *THE COLLECTED WORKS, VOL.1. THERMODYNAMICS*, Longmans, New York, (1928)

total volume, constant total entropy and constant total concentration of each of the components. Let U, U' and U'' be the internal energies of the adsorbed layer, phase I and phase II respectively. Then at equilibrium,

$$d(U + U' + U'') = dU + dU' + dU'' = 0 \tag{3.1}$$

The expressions for the change in internal energy of the bulk phase I and II are known from thermodynamics.

$$dU' = T'dS' - P'dv' + \sum_i \mu_i' dn_i' \tag{3.2}$$

$$dU'' = T''dS'' - P''dv'' + \sum_i \mu_i'' dn_i'' \tag{3.3}$$

Here v, n, P, T and μ are the volume, entropy, number of moles, temperature and chemical potential of the respective bulk phase.

We shall have to find out the expression for dU, the change in internal energy of the adsorbed layer.The situation is pictorially shown in figure 3.1. The thickness t of the adsorbed layer is small as the surface forces falls off rapidly. Such a layer cannot be homogeneous throughout.

Let the area of the surface be α. The inhomogeneity of this layer will fall rapidly on either side of the interface if we position the interface at distance t_1 and t_2 respectively from the two bulk phases. We further assume that the position of the interface is fixed and does not change. This would mean that the volumes of the two bulk phases do not change too, i.e. $dv' = dv'' = 0$. So the internal energies of the bulk phases as well as that of the interface depend only on entropy and the respective n_i terms.

$$dU = TdS - \sum \mu_i dn_i \tag{3.4}$$

Now imposing the condition of equilibrium on the whole system,

$$\begin{aligned} T'dS' + \mu_1' dn_1' + \ldots + \mu_i' dn_i' + \ldots \\ +T''dS'' + \mu_1'' dn_1'' + \ldots \mu_i'' dn_i'' + \ldots \\ +TdS + \mu_1 dn_1 + \ldots + \mu_i dn_i + \ldots = 0 \end{aligned} \tag{3.5}$$

Since we have assumed the constancy of entropy of each phase,

$$dS' + dS'' + dS = 0 \tag{3.6}$$

Also, the total amount of each component in each of the phases is constant which gives

$$\begin{aligned} dn_1' + dn_1'' + dn_1 &= 0 \\ \cdots\cdots\cdots\cdots\cdots & \\ dn_i' + dn_i'' + dn_i &= 0 \\ \cdots\cdots\cdots\cdots\cdots & \end{aligned} \tag{3.7}$$

With these restrictions, the condition of equilibrium imposed by equation (3.6) can be satisfied if and only if $T = T' = T''$ and $\mu_i = \mu_i' = \mu_i''$. This means the system consisting of the two bulk phases and the adsorbed layer can be in equilibrium when the temperature in the entire system and chemical potential of each component in any part of the system are the same.

In reality, the energy, entropy and the number of moles of the components cannot be constant throughout the adsorbed layer as the surface force changes continuously throughout this layer. This is the reason why it is more convenient to talk about the excess of these quantities in this layer as compared to those in the same volume $t\alpha$ (where α is the area of the interface) in the phases I and II. It is then possible to write

$$U^\alpha = U - U' - U'' \tag{3.8}$$

$$S^\alpha = S - S' - S'' \tag{3.9}$$

$$n_i^\alpha = n_i - n_i' - n_i'' \tag{3.10}$$

We can term the excess U^α as the total surface energy, the quantity S^α the total surface entropy and n_i^α as the excess of the i-th component. In fact, the last quantity can be taken as equal to the total quantity adsorbed because the amount of the components in the surface layer far exceeds their amount in the bulk phases. The change in internal energy of the adsorbed layer can be now written as

$$dU^\alpha = TdS^\alpha + \sum_i \mu_i dn_i^\alpha \tag{3.11}$$

If the position of the surface changes such that the surface area α changes, the total surface energy will change by an additional amount given as $\left(\frac{\partial U^\alpha}{\partial \alpha}\right)_{S_i^\alpha, n_i^\alpha} d\alpha$ and the equation 3.11) becomes

$$dU^\alpha = TdS^\alpha + \left(\frac{\partial U^\alpha}{\partial \alpha}\right)_{S_i^\alpha, n_i^\alpha} d\alpha + \sum_i \mu_i dn_i^\alpha \tag{3.12}$$

The change in surface internal energy with surface area at constant surface entropy and constant quantity adsorbed $\left(\frac{\partial U^\alpha}{\partial \alpha}\right)_{S_i^\alpha, n_i^\alpha} = \gamma$, where γ is known as *surface tension*.

Surface tension γ is the two dimensional analog of pressure because $-P = \left(\frac{\partial U}{\partial \alpha}\right)_{S,n}$. The unit of γ is dyne/cm and it is related to the pressure difference ($\Delta P = P' - P''$). We shall next find out this relation.

The change in surface area by $d\alpha$ will change the volume of the bulk phases. If the volume phases I changes by dv', volume of phase II will change by $-dv''$ because the total volume is to remain constant, i.e. $dv' = -dv''$. At equilibrium, the change in internal energy is zero that gives $P'dv' - P''dv'' - \gamma\alpha = 0$). Thus we get

$$\Delta P dv' = \gamma d\alpha \tag{3.13}$$

where ΔP is the pressure difference between the two bulk phases I and II.

We shall consider here the general case of a curved surface with two principal radii of curvature R_1 and R_2. Let the point O_1 and O_2 be the origins of these two curvatures (figure 3.2) and θ_1 and θ_2 are the corresponding angles at the origin of these curvatures. Area of the surface is $\alpha = R_1\theta_1.R_2\theta_2$.

Figure 3.2: *A surface of area α changes to $\alpha + d\alpha$ by undergoing displacement towards phase II through a distance dx.*

If the surface moves through a distance dx, the volume change $dv' = -dv'' = \alpha dx$. In this process, the surface area would change from α to

$\alpha + d\alpha$, i.e. from $R_1\theta_1.R_2\theta_2$ to $(R_1 + dx)\theta_1.(R_2 + dx)\theta_2$ and the change in surface area can be written as

$$d\alpha = (R_1 + dx)\theta_1.(R_2 + dx)\theta_2 - R_1\theta_1.R_2\theta_2 \tag{3.14}$$

Neglecting $(dx)^2$ and rearranging,

$$\theta_1\theta_2 = \frac{\alpha}{R_1R_2} \tag{3.15}$$

and

$$d\alpha = \alpha\left(\frac{1}{R_1} + \frac{1}{R_2}\right)dx \tag{3.16}$$

Putting this expression for $d\alpha$ in equation (3. 13),

$$\Delta P = \gamma\left(\frac{1}{R_1} + \frac{1}{R_2}\right) \tag{3.17}$$

We have two special cases:

1. The surface is planar when $R_1 = R_2 = \infty$, $\Delta P = 0$ which means pressure in both the bulk phases are equal.
2. The surface is spherical when $R_1 = R_2 = R$ and $\Delta P = 2\gamma/R$.

Gibbs adsorption equation

The complete differential form of surface energy U^α (which is a first order homogeneous function of S^α, n_i^α and α) is

$$dU^\alpha = TdS^\alpha + S^\alpha dT + \gamma d\alpha + \alpha d\gamma + \sum_i \mu_i dn_i^\alpha + \sum_i n_i^\alpha d\mu_i \tag{3.18}$$

Comparing the above equation with equation (3.12), we see that

$$\alpha d\gamma + \sum_i n_i^\alpha du_i = 0 \tag{3.19}$$

The quantities U^α, S^α and n_i^α depend on the surface area α, i.e. they are extensive properties. It will be convenient if we express them per unit surface by writing $U_\alpha = U^\alpha/\alpha$, $U - \alpha = U^\alpha/\alpha$ and $\Gamma_i = n_i^\alpha/\alpha$. Dividing equation (3.19) by α, we write

$$-d\gamma = \sum_i \Gamma_i d\mu_i \tag{3.20}$$

This is Gibbs adsorption equation and the quantity Γ_i is known as the Gibbs surface excess. Gibbs equation tells us that the surface tension decreases with the amount adsorbed on the surface.

Change in surface tension

Surface tension decreases the spreading of a substance. In order to enhance the spreading property, the surface tension of the substance should be reduced. Gibbs equation shows that surface tension decreases with adsorption. Lets apply Gibbs adsorption equation to a two-component system, solid or a liquid adsorbent (1) and a gaseous adsorbate (2). For such a system, Gibbs equation is

$$-d\gamma = \Gamma_1 d\mu_1 + \Gamma_2 \mu_2 \tag{3.21}$$

We shall first assume that the adsorbent and the adsorbate are not soluble in each other. Then the chemical potential of the adsorbent at the surface and in its bulk will be the same, i.e. $d\mu_1 = 0$. The chemical potential of the adsorbate, however, will change on adsorption.The equation becomes

$$-d\gamma = \Gamma_2 d\mu_2 \tag{3.22}$$

Figure 3.3: *(a) Change of surface tension of water with vapour pressure of an alkane (b) corresponding isotherm plot.*

Assuming the adsorbate to be an ideal gas, $d\mu = RTd\ln p$ where p is the pressure of the adsorbate at temperature T. This gives

$$\Gamma_2 = -\frac{1}{RT}.\frac{d\gamma}{d\ln p} = -\frac{p}{RT}.\frac{d\gamma}{dp} \tag{3.23}$$

If the adsorbent is a liquid, it is possible to measure its surface tension as function of adsorbate pressure. Using equation (3.23), the data can be converted to an adsorption isotherm plot. Concave nature of the isotherm (type III) shown in figure 3.3(b) shows that the water surface-adsorbate interaction is very weak but the adsorbate-adsorbate interaction is comparatively strong.

The case when the adsorbate interacts with the adsorbent will be considered next. In this case, the chemical potential of the adsorbent too will change. However, if we consider the interface at a position where the adsorption is zero, we can still use the simplified form of Gibbs equation. A case in point is adsorption of ethanol on water surface. Since ethanol dissolves in water, chemical potential μ_1 of the adsorbent water will change. It is a matter of selecting the position of the interface such that self adsorption of water is zero, i.e. the number of water molecules per unit surface in this region is same as that inside water. One can then write

$$\Gamma_2 = -\frac{1}{RT}.\frac{d\gamma}{d\ln a_2} = \frac{-a_2}{RT}.\frac{d\gamma}{da_2} = -\frac{c_2}{RT}.\frac{d\gamma}{dc_2} \tag{3.24}$$

where a_2 and c_2 are the activity and concentration respectively of the adsorbate in a dilute solution.

Figure 3.4: *Orientation of surfactant molecules in a polar solvent.*

Let us consider systems where water is the solvent in which a long chain alcohol, fatty acid or an amine, all having a polar end and a non-polar end, is dissolved. In such cases, the water-water interaction in the bulk is stronger than the water-adsorbate interaction. Therefore the adsorbate molecules will be pushed to the surface. The concentration of such molecules will be much greater near the surface and hence surface tension of the solvent will be lowered. Such substances that lower the surface tension of the solvent are known as *surface active* materials or *surfactants*. The limiting value of this reduction in surface tension $-(\partial\gamma/\partial c_2)_{c_2\to 0}$ is known as *surface activity* of the substance.

When the concentration of the surfactant is very large, its molecules tend to cover the entire surface of the solvent. The flat orientation of the molecules present at low concentration changes to vertical orientation at high concentration with the polar end of the molecules lying inside the polar solvent and the nonpolar end oriented upwards (figure 3.4).

3.1.1 Surface Pressure

An adsorbate molecule will stay on the surface for the time τ before it is desorbed. During this period, the molecule is not stationary and moves on the surface executing a two-dimensional random motion. Thus, when a drop of oil is placed on the surface of water, it quickly spreads on the surface. The movement of the water molecules under it causes the spreading. A drop of water placed on a fabric quickly spreads and this causes wetting. Surface migration of the adsorbate on a solid surface may be caused by surface heterogeneity. Since the adsorbate molecules strike the solid surface randomly, it does not necessarily go the most energetic site. Once adsorbed, it may migrate from weaker to stronger adsorption sites. Even if the surface is perfectly homogeneous, surface migration will occur because the horizontal component of the velocity of the molecule striking the surface at any random direction.

The random movement of the adsorbate molecules along the surface is like a two-dimensional gas and this will give rise to a pressure along a line on the surface just like a the three-dimensional movement of a gas gives rise to a pressure on a surface. This two-dimensional analog of pressure is known as *surface pressure*. A thin metal strip placed on the surface of water taken on a trough will act as a barrier just like a piston in the case of gas pressure. If the trough has only pure water, the pressure on either side of the strip caused by the movement of the self-adsorbed water molecules are equal. If a drop of oil is added on one side, it spreads creating a contaminated surface on that side. This will cause a pressure difference on the two sides of the barrier and this will move the barrier through distance dx. If the length of the barrier is ℓ and π is the surface pressure, the work done in creating a contaminated surface of area ℓdx is $\pi \ell dx$. If surface tension of pure water is γ_0 and that of the contaminated surface is γ, it would mean that γ_0 amount of work should be done to create one square centimeter of pure surface. Work done by the system in removing ℓdx cm^2 of pure surface is $\gamma_0 \ell dx$ and this will create ℓdx cm^2 area of contaminated surface and the work necessary is $\gamma \ell dx$. The net work is $(\gamma_0 - \gamma)\ell dx$. Therefore,

$$\pi \ell dx = (\gamma_0 - \gamma)\ell dx \tag{3.25}$$

that gives

$$\pi = \gamma_0 - \gamma \tag{3.26}$$

Thus, surface energy is the pressure due to two-dimensional movement of the adsorbed molecules that is equal to the difference in surface tension of the clean and the contaminated surfaces.

For low adsorbate pressure, the amount adsorbed $\sigma = Kp$ when K is a constant. This means $\frac{\pi}{p} = \frac{d\pi}{dp}$. Therefore, no of mole adsorbed

$$\Gamma = \frac{\sigma}{N} = \frac{\pi}{RT} \tag{3.27}$$

But $N/\sigma = \alpha$. Remembering equation (3.23) that shows that $\Gamma_2 = \frac{p}{RT}\frac{d\pi}{dp}$, we get

$$\pi\alpha = RT \tag{3.28}$$

which is analogous to the ideal gas equation $PV = RT$ and is the equation of state of a two-dimensional adsorbed gas.

3.1.2 Free Energy of Adsorption

Helmholtz free energy A of a system consisting of adsorbent (1) and a liquid adsorbate (2) before adsorption has occurred can be expressed as

$$A = \gamma_1 + \Gamma_1\mu_1 + n_1\mu_2 \tag{3.29}$$

where γ_1 is the surface tension of the adsorbent, Γ_1 is the amount of its self-adsorption and μ_1 and μ_2 are the chemical potential if the adsorbent (1) and the liquid adsorbate (2) respectively. (We have chosen a liquid adsorbate and not a gas in order to make it more general. Free energy of the system after adsorption has reached equilibrium is

$$A' = \gamma + \Gamma_1'\mu_1' + n_2\mu_2 \tag{3.30}$$

Here, γ is the surface tension of the adsorbent after adsorption, Γ_1' and n_2 are the quantities of (1) and (2) adsorbed, μ_1' and μ_2' are the chemical potentials of adsorbent (1) and adsorbate (2) after adsorption. It is assumed here that the entire amount of the liquid adsorbate has been adsorbed. The change in free energy that we may call *free energy of adsorption* is

$$\Delta A_\alpha = A - A' = \Gamma_1'\mu_1' - \Gamma_1\mu_1 + N_2(\mu_2' - \mu_2) \tag{3.31}$$

Assuming that the bulk of the adsorbent does not interact with the adsorbate, chemical potential μ_1 of the adsorbent will remain unchanged

and $\mu_1' = \mu_1$ and $\Gamma_1' = \Gamma_1$. The system thus essentially becomes like an one-component system. Change in free energy now is

$$\Delta A_\alpha = \gamma - \gamma_1 + \Gamma_2(\mu_2' - \mu_2) = \Delta\gamma + \Gamma_2\mu_2 \tag{3.32}$$

But $\Delta\mu_2$ can be replaced by $RT \ln \frac{p}{p_0}$ where p_0 is the saturation vapour pressure of the liquid adsorbate and p is the vapour pressure of the same at equilibrium adsorption. Then,

$$\Delta A_\alpha = \Delta\gamma + \Gamma_2 RT \ln \frac{p}{p_0} \tag{3.33}$$

Since $-\Delta\gamma = \pi$, and at low coverage $\pi = \frac{RT}{\alpha} = RT\Gamma_2$, $\Delta\gamma$ in equation (3.33) can be replaced by $RT\Gamma_2$. This gives

$$\frac{\Delta A_\alpha}{\Gamma_2} = RT\left(\ln \frac{p}{p_0} - 1\right) \tag{3.34}$$

where ΔA_α is the molar free energy of adsorption. Differentiating this with respect to the quantity adsorbed Γ_2

$$\frac{\partial \Delta A_\alpha}{\partial \Gamma_2} = \frac{\partial \Delta\gamma}{\partial \Gamma_2} + RT \ln \frac{p}{p_0} \tag{3.35}$$

The first term of the right hand side in the above equation can be neglected in the case of a solid adsorbent. This gives

$$\frac{\partial \Delta A_\alpha}{\partial \Gamma_2} = RT \ln \frac{p}{p_0} = \Delta\mu_2 \tag{3.36}$$

Thus, the differential free energy of adsorption is the change in chemical potential of the liquid adsorbate in going from its initial state to the adsorbed state.

3.1.3 Enthalpy and Entropy of Adsorption

At equilibrium, $dA = -SdT - pdv$ and when volume v is constant, $(\partial A/\partial T)_v = -S$. Hence entropy of adsorption can be expressed as

$$\Delta S_\alpha = -\left(\frac{\partial \Delta A_\alpha}{\partial T}\right)_v \tag{3.37}$$

Differentiating,

$$\frac{\partial \Delta S_\alpha}{d\Gamma_2} = -\frac{\partial}{d\Gamma_2}\left(\frac{\partial \Delta A_\alpha}{\partial T}\right) = -\frac{\partial}{\partial T}\left(\frac{\partial \Delta A_\alpha}{\partial \Gamma_2}\right) \tag{3.38}$$

This shows that the differential entropy of adsorption is the decrease in differential free energy of adsorption with temperature. Substituting for $\frac{\partial \Delta A_\alpha}{\partial \Gamma_2}$ from equation (3.36), the differential entropy of adsorption of a liquid on a solid surface is

$$\frac{\partial \Delta S_\alpha}{d\Gamma_2} = -\left(\frac{\partial \Delta \mu_2}{\partial \Gamma_2}\right) \tag{3.39}$$

Or

$$\frac{\partial \Delta S_\alpha}{d\Gamma_2} = -R \ln \frac{p}{p_0} - RT\left(\frac{\partial \ln p}{\partial T}\right)_{\Gamma_2} + RT\left(\frac{\partial \ln p_0}{\partial T}\right) \tag{3.40}$$

Differential internal energy of adsorption can be written as

$$\frac{\partial \Delta U_\alpha}{d\Gamma_2} = \frac{\partial}{\partial \Gamma_2}(\Delta A_\alpha + T\Delta S_\alpha) \tag{3.41}$$

Or

$$\frac{\partial \Delta U_\alpha}{d\Gamma_2} = \frac{\partial \Delta A_\alpha}{d\Gamma_2} + T\frac{\partial \Delta S_\alpha}{d\Gamma_2} + \Delta S_\alpha \frac{\partial T}{\partial \Gamma_2} \tag{3.42}$$

At constant temperature,

$$\frac{\partial \Delta U_\alpha}{d\Gamma_2} = \frac{\partial \Delta A_\alpha}{d\Gamma_2} + T\frac{\partial \Delta S_\alpha}{d\Gamma_2} \tag{3.43}$$

Substituting for $\frac{\partial \Delta S_\alpha}{d\Gamma_2}$ and $\frac{\partial \Delta A_\alpha}{d\Gamma_2}$,

$$-\frac{\partial \Delta U_\alpha}{d\Gamma_2} = -RT \ln \frac{p}{p_0} + RT \ln \frac{p}{p_0} + RT^2\left(\frac{\partial \ln p_0}{\partial T}\right)_{\Gamma_2} - RT^2\left(\frac{\partial \ln p_0}{\partial T}\right) \tag{3.44}$$

Or simply

$$-\frac{\partial \Delta U_\alpha}{d\Gamma_2} = RT^2\left(\frac{\partial \ln p_0}{\partial T}\right)_{\Gamma_2} - RT^2\left(\frac{\partial \ln p_0}{\partial T}\right) \tag{3.45}$$

Decrease in internal energy with adsorption is the net heat or enthalpy of adsorption. The second term in the right hand side of the equation (3.45) is the latent heat of evaporation of the liquid adsorbate and the first term is the differential heat of adsorption. In the case when the

adsorbate is a gas in its standard state, the latent heat of evaporation is zero. Hence the differential heat of adsorption of a permanent gas

$$q = RT^2\left(\frac{\partial \ln p_0}{\partial T}\right)_{\Gamma_2} \tag{3.46}$$

The integral heat of adsorption can be obtained as

$$Q_{int} = \int_0^{\Gamma_2} q d\Gamma_2 \tag{3.47}$$

Adsorption is an exothermic process. However, the convention is to refer to heat of adsorption as a positive quantity. Since all real surfaces are heterogeneous, heat of adsorption decreases with increased adsorption.

Equation (3.46) can be written as

$$q = RT^2\left(\frac{\partial \ln p}{\partial(1/T)}.\frac{\partial(1/T)}{\partial T}\right)_{\Gamma_2} = RT^2\left(\frac{\partial \ln p}{\partial(1/T)}(-1/T^2)\right)_{\Gamma_2} \tag{3.48}$$

or

$$-\frac{q}{R} = \left(\frac{\partial \ln p}{\partial(1/T)}\right)_{\theta} \tag{3.49}$$

In the last equation, the subscript θ indicating constant surface coverage is used in place of Γ_2 that implies constant quantity adsorbed because they both have identical meaning. If adsorption isotherms are measured at various temperatures for a adsorbent-adsorbate system, the data may be used for obtaining the values p at different T at constant θ (constant quantity adsorbed). These data then can be used for getting isosteric ($\log p$ vs $1/T$) plots for different surface coverage. Differential heat of adsorption q can be found out from such plots using equation (4.6). The quantity q is also known as *isosteric heat of adsorption.*

Adsorption isosteric plots of ethane on a surface of graphitized carbon in the temperature range -125^o C to -60^o C have been obtained. At such low temperatures, the process is physical adsorption. The slope of these plots initially increased with surface coverage up to $\theta = 1$. This increase in heat of adsorption with coverage is due to increased adsorbate-adsorbate interaction. After $\theta = 1$, q decreases because further adsorption is essentially condensation of the adsorbate. Beebe and Stevens [2] measured the isosteric heat of physical adsorption argon, nitrogen and carbon monoxide using calorimetric method and found the

[2] R.A. Beebe and N.P. Stevens, J.Amer.Chem.Soc., 62, 2134 (1940)

values to be about 4 kCal/mol. Emmet and Brunauer [3] had studied the isosteric heats of adsorption of nitrogen at higher temperatures. Interestingly, it was found that the heats of chemisorption of oxygen, nitrogen and carbon monoxide on iron surface are approximately equal to the heats of formation of the oxide, nitride and carbonyl of iron. Rideal and Sweet [4] measured the isosteric heats of chemisorption of hydrogen on nickel film and noticed that that heat of adsorption falls with coverage. This points to the heterogeneous nature of the surface of the film.

Behaviour of heats of adsorption of various adsorbates on different surfaces can be summarized as:

- Heat of physical adsorption generally lies between 2-7 kCal/mol.
- For a given adsorbate, heat of physical adsorption is independent of the adsorbent.
- Heat of chemisorption is much higher and depends on both the adsorbate and the adsorbent.
- Heat of chemisorption falls off rapidly with increased coverage.
- Generally, calorimetric and isosteric heats of adsorption have same value.
- In the case of reactive gases, the heats of chemisorption is about the same as the heats of formation of the compound between the respective adsorbate and the adsorbent.

The works of the Russian scientists on the measurement of heat of adsorption has been reviewed by Kiselev [5]. Readers can also see an excellent review by Holmes [6].

3.2 THEORETICAL APPROACH

Surface is the region where one phase comes to an abrupt end. An atom present on the surface has neighbouring atoms only on one side. The force exerted by the field of such an atom or a molecule is saturated only on one side. But its field cannot come to an abrupt end and it extends into the space outside this phase. Any atom or molecule present

[3] P.H. Emmett and S. Brunauer, *J.Amer.Chem.Soc.*, 56, 35 (1934)
[4] E.K. Rideal and F. Sweet, *Proc.Roy.Soc.*, A257, 291 (1960)
[5] A.V.Kiselev, *Quart.Rev.(London)*, 15, 99 (1961)
[6] J.M. Holmes, in *SOLID GAS INTERFACE (Ed. E.A. Flood)*, Marcel and Dekker, NY, 1967, p.127

in this space will experience a force due to this field. This causes adsorption. There have been many attempts to understand the nature of this force and calculate the energy of interaction between the surface and the adsorbed atoms or molecules.

The force acting between a surface and a adsorbed molecule is mainly of two types. Force due to weak, long-range interaction like van der Waals force. In such an interaction, the equilibrium distribution of the electrons in the solid and the molecule remain essentially unchanged. The surface and the adsorbate molecule do not exchange electrons. The result is physical adsorption with low heat of adsorption. As the electron clouds start overlapping, a repulsive force sets in. Sharing or transfer of electrons between the solid surface and the molecule may take place if this force of repulsion is overcome. This leads to chemisorption. It is possible, in principle, to calculate the energy of interaction using the methods of quantum mechanics. Here, the method of calculating the physical force will be considered first.

3.2.1 Forces of Physical Adsorption

We are familiar with the situation that polar molecules attract each other. In order to understand the interaction between a nonpolar molecule and a nonpolar surface, we must first appreciate what leads to the attraction between two spherically symmetrical nonpolar molecules. London had developed a method for obtaining the intermolecular potential between two nonpolar molecules such as two hydrogen atoms. There is no dipole moment in such spherical molecules. London thought that the spherical symmetry of the hydrogen atom is only a time averaged picture. If the position of the electron is considered at any given instant, the atom may be considered as an instantaneous dipole that will induce a instantaneous dipole on the neighbouring atom too. The second dipole, in its turn, will induce a dipole moment in the first. Thus, the two oscillating dipoles will attract each other.

The wavefunction of two weakly interacting hydrogen atoms at large interatomic distance is

$$\psi^{(0)} = \chi_{1s_A}(1)\chi_{1s_B}(2) \tag{3.50}$$

where $\chi_{1s_a}(1)$ is the wavefunction of the electron 1 in atom A. Here, electron 1 is considered to be associated with atom A and electron 2 with atom B. The hamiltonian on interaction becomes

$$\hat{H} = \hat{H}^{(0)} + \hat{H}' \tag{3.51}$$

when $\hat{H}^{(0)}$ is the hamiltonian of the unperturbed system and the perturbation operator $\hat{H}'$ is

$$\hat{H}' = -\frac{e^2}{r_{A_2}} - \frac{e^2}{r_{B_1}} + \frac{e^2}{r_{12}} + \frac{e^2}{r} \tag{3.52}$$

Here r is the inter-nuclear distance, r_{A_2} is the distance between electron 2 and nucleus 1, r_{B_1} is the distance between electron 1 and nucleus B and r_{12} is the distance between electrons and 1 and 2.

It is possible to show that the first order perturbation energy that is given by the integral $< \phi^{(0)} \mid \hat{H}' \mid \phi^{(0)} >$ is zero. The second order perturbation gives the energy of interaction as

$$V_a(r) = -\frac{C_1}{r^6} - \frac{C_2}{r^8} - \frac{C_3}{r^{10}} \tag{3.53}$$

where C_1, C_2 and C_3 are constants. The first term in the right side of the above equation is the dipole-dipole interaction, the second term is the dipole-quadrupole interaction and the third term is the quadrupole-quadrupole interaction. The constant C_1 contributes 90 percent to the potential, C_2 about 10 percent and C_3 only about 1 percent. Here, the constant $C_1 = \frac{3}{2}\alpha_A \frac{I_A . I_B}{I_A + I_B}$ where α and I stand for polarizability and ionization energy respectively.

As the two interacting atoms A and B come close, a repulsive potential comes into play which is given by

$$V_r(r) = \frac{B}{r^n} \tag{3.54}$$

It has been observed that n can have values between 9 and 14, but the value 12 is suitable in most cases. Taking only the dipole-dipole interaction as the attractive potential, the net potential

$$V(r) = -\frac{C_1}{r^6} + \frac{B}{r^{12}} \tag{3.55}$$

The above expression for interaction potential is known as Lennard-Jones potential or simply as 6-12 potential. When this is plotted against r, it results in a curve as shown in figure 3.5. Lennard-Jones potential has been used widely for calculating interatomic potential.

In the case non-spherical polyatomic molecules, interaction potential depends, not only on the distance between the molecules, but also on their relative orientation. In such cases, Kihara's potential[7] is used.

[7] T. Kihara, *Adv.Chem.Phys.*,5, (1963)

Kihara's model assumes a hard electron core within the molecule and the intermolecular distance r in the Lennard-Jones equation is replaced by the shortest distance ρ between the two hard cores in the two interacting molecules. Kihara has also given a method for obtaining the shape and size of the hard core in a molecule.

Figure 3.5: *Potential energy for the interaction of two hydrogen atoms.*

The concept of weak interaction between two molecules may be extended to the interaction between a surface and a molecule. A surface may be polar or nonpolar in nature. Similarly, the adsorbate molecule too can be either polar or nonpolar. Depending on these, there may be four general cases such as (a) nonpolar molecule and nonpolar surface, (b)nonpolar molecule and polar surface, (c) polar molecule and nonpolar surface and (d) polar molecule and polar surface interacting with each other. These cases need to be handled separately.

a. Nonpolar molecule and nonpolar surface

Total interaction of a nonpolar molecule with a nonpolar surface can be obtained by summing up the interaction potential of a surface atom and the adsorbate molecule over all the surface atoms. This is the method of Lattice summation. If we consider the surface as a continuum, the potential becomes $\int_v V(r)\rho dv$ where v stands for volume and ρ is the number of lattice atoms per per unit volume. The integration is done over the entire solid. This leads to the expression for total potential

$$V(z) = -\frac{\rho A}{z^3} + \frac{\rho B}{z^9} \tag{3.56}$$

where z is the vertical distance of the adsorbed atom from the surface plane. The lattice summation method, however, ignores the detailed

structure of the solid surface. A better but more laborious method will be to calculate the bimolecular potential and sum it up over all the i atoms of the surface located at distances r_i from the adsorbate atom. For a surface like that of graphite, calculations justified the use of integration method as it has been found that the interaction potential depends mainly on the vertical distance and shows little dependence on the horizontal position of the surface atom. It should, however, be remembered that interaction forces are non-additive as the force between two atoms is affected by the presence of a third atom. In spite of this, lattice summation has been extensively used because of the difficulty in handling many-body problem.

b. Nonpolar molecule and nonpolar surface

Using the classical image method, Lennard-Jones obtained the interaction potential between a conducting metal surface and a nonpolar molecule as

$$V = -\frac{e^2 < r^2 >}{12z^3} \tag{3.57}$$

where e is the electronic charge, $< r^2 >$ is the mean square distance of all the electrons in the molecule from the centre of charge and z is the distance of the between the centre of charge and the surface. Such an approach ignores the repulsive force and also treats the surface as a structure-less continuum and ignores local variations on the surface.

Figure 3.6: *The (100) face of the KCl crystal.*

c. Nonpolar molecule and polar surface

The potential energy of a nonpolar molecule in an external field of magnitude ϕ is

$$V_1 = -\frac{1}{2}\phi^2 \tag{3.58}$$

Here α is the polarizability of the molecule. It is valid if the ϕ changes slowly over the space. This term should be added to the attractive potential due to dispersion in order to calculate the interaction energy of a nonpolar molecule with the surface of an ionic crystal. For an alkali halide crystal,

$$\phi = -\frac{8\pi e}{r_c^2}\exp\left(-\frac{r/r_c}{\sqrt{2}}\right) \tag{3.59}$$

where r_c is the shortest interionic distance and r is the vertical distance of the molecule from the surface. However, calculations show that ϕ is only about 2% of the dispersion potential.

Let us look at the surface of a simple ionic solid KCl by including both electrostatic potential ϕ and the dispersion potential. Calculations have shown that the potential of interaction not only depends on r, the vertical distance of the molecule from the surface, but varies from point to point on the surface. Figure 3.5 shows the (100) face of a KCl crystal. The potential energy of interaction V_{r_e} of an argon molecule at equilibrium vertical distance r_e at four different points marked a, b, c and d are given in Table 3.1.

Although the contribution of the electrostatic term is very less for a nonpolar molecule, this can be appreciable and may even exceed the dispersion potential if the adsorbate molecule is polar[8].

Table 3.1: Energy of interaction of the argon atom at the equilibrium distance (r_e) from the surface at different points.

Site	$V(r_e)$, kCal/mole
a	1.59
b	1.31
c	1.45
d	1.27

d. Polar molecule and polar surface

When a polar adsorbate molecule is present at a vertical distance r from the surface and the adsorbent surface is conducting (such as that of

[8]J.H.De Boer, *Adv.Catalysis*, 8, 33(1956)

graphite or a metal), the interaction of the molecule with the surface is the same as that of the molecule and its electric image located at the same distance r from the surface but inside the crystal. The expression for the the interaction potential is

$$V(\mu) = -\frac{\mu^2}{16r_e^2}(1 + \cos^2\beta) \tag{3.60}$$

$V(\mu)$ should be added to dispersion potential in order to calculate energy of adsorption of a polar molecule on a metal surface.

3.2.2 Chemisorption on Metals

Physical adsorption considers the adsorbate-adsorbent interaction as weak interaction without the formation of any chemical bond. In chemisorption, electron transfer or electron sharing takes place between the adsorbate molecule and the surface. The main problem in quantum chemical calculation is that the wavefunctions at the surface are not the same as in the bulk. Hence, some simple semi-quantitative methods have been developed. We shall consider here the valence bond method of calculating chemisorption energy on the surface of metals.

Valence bond method

Let us consider a surface atom S to which the adsorbed atom A is bonded. The normalized wavefunction for this bond is

$$\psi = c_i\psi_i + c_c\psi_c \tag{3.61}$$

where ψ_i and ψ_c are the normalized wave functions when the bond is purely ionic or purely covalent and c_i and c_c are mixing coefficients of the two wavefunctions. If E is the energy of adsorption, $\hat{H}\psi = E\psi$ and

$$E = <\psi|\hat{H}|\psi> \tag{3.62}$$

Minimizing E, one gets

$$\frac{1}{c_i^2} = 1 + \frac{E - H_{ii}}{E - E_{cc}} \tag{3.63}$$

where $H_{ii} = <\psi_i|\hat{H}|\psi_i>$ and $H_{cc} = <\psi_c|\hat{H}|\psi_c>$.

When $c_i^2 = 1$, $E = H_{ii}$ and the bond is ionic. When $c_i^2 = 0$, $E = H_{cc}$ and the bond is entirely covalent. If we can find out H_{ii}, H_{cc} and c_i^2, we shall be in a position to calculate the surface bond energy. It is not easy

to evaluate the above parameters and hence they are obtained from some experimental parameters indirectly. Thus, the quantity H_{ii} is obtained as

$$H_{ii} = A - I + U(r_e) \tag{3.64}$$

where A is the electron affinity of the acceptor atom, I is the ionization potential of the atom that gives the electron and $U(r_e)$ is the energy of attraction between S and A at their equilibrium distance. One can write $U(r_e) = -\frac{8}{9}\frac{e^2}{r_e}$ and $r_e = r_S + r_A$ where r_S and r_A are the covalent radii of the respective atoms.

The quantity H_{cc} is calculated as

$$H_{cc} = \frac{1}{2}(D_{AA} + D_{SS}) \tag{3.65}$$

where D stands for the bond dissociation energy. D_{AA}, the bond dissociation energy of the diatomic molecule A_2 that is undergoing dissociative adsorption by combining with the surface atom S. To obtain D_{SS}, one uses the latent heat of sublimation. If the solid is a fcc metal, each atom has 12 nearest neighbours and hence

$$D_{SS} = \frac{2}{12}\Delta H_{sub}$$

where ΔH_{sub} is the heat of sublimation of the metal. The quantity c_i^2 is obtained from the bond dipole moment μ as

$$\mu = c_i^2 e r_e$$

Thus, we are in a position to calculate E. The molar heat of adsorption of a diatomic gas A_2 is

$$q = N(2E - D_{AA}) \tag{3.66}$$

where N is Avogadro's number. For a monatomic gas,

$$q = NE.$$

Such calculation of heat of adsorption are highly approximate and often does not agree with the experimentally obtained values.

The main shortcomings of such an approach is that it assumes interaction of the adsorbate atom with a single atom of the surface. It is, however, possible that the adsorbate may interact with two or more surface atoms simultaneously.

Ligand field method

According to the ligand field theory, the five degenerate d orbitals of a transition metal atom is split into the t_{2g} triplet (d_{xy}, d_{yz}, d_{xz}) and e_g doublet $(d_{x^2-y^2}, d_{z^2})$ in a cubic field. The same splitting may be retained in a cubic metal. Which of the lobes of these orbitals emerges in space will depend on the outer plane where the atom is located.

Let us assume the outer plane to be (001) and it is the xy plane. We can visualize that two lobes each from d_{xz} and d_{yz} will emerge making angle 45^o with the surface. Another lobe of the d_{z^2} orbital will emerge perpendicular to the surface. Some of these lobes may participate in bond formation by overlapping with the orbitals of the adsorbate molecule. None of the lobes of the $d_{x^2-y^2}$ and d_{yz} will emerge because all their lobes lie on the xy plane.

Figure 3.7: *Adsorption of ethene on nickel (001) surface. The overlap of the ethene orbitals with the d orbitals of nickel is shown (only the lobes that emerge from the surface has been shown).*

The situation will be quite different if the surface atom lies on the (111) or (011) plane. The results are summarized in table 3.2.

According to ligand field approach, atomic hydrogen will be adsorbed on the (001) face of a fcc metal like nickel by overlapping with the d_{z^2} orbital. A molecule of ethene will find the (001) face most suitable for adsorption because the π orbital of ethene can easily overlap with the d_{z^2} of nickel and simultaneously, its σ orbital can overlap with the metal d_{yz} or d_{xz} orbital. This is shown schematically in figure 3.7. The (111) face of nickel will be least suited for adsorption of ethene because the lobes of d orbitals emerge making an angle that is not suitable for making good overlap.

3.2.3 Surface States

The abrupt end of the crystal lattice at the surface gives rise to energy states that are present only at the surface. These states known as surface states generally are located in the band gap between the top of the valence band and bottom of the conduction band. The motion of electron in a periodic lattice gives rise to electron energy bands as shown by the Kronig-Penney model.

Table 3.2: Lobes of the different d orbitals emerging from the different faces of a fcc metal.

Orbital	Crystal surfaces					
	(001)		(011)		(111)	
	Angle of emergence	No. of lobes	Angle of emergence	No. of lobes	Angle of emergence	No. of lobes
d_{xy}			30^o	2	30^0	1
d_{yz}	45^o	2	90^o	1	30^o	1
d_{xz}	45^o	2	30^o	2	30^o	1
d_{z^2}	90^o	1	45^o	1	$36^o16'$	1
$d_{x^2-y^2}$			45^o	1	$36^o16'$	2

Tamm has shown that the sudden break in the lattice at the surface gives rise to discrete energy states that split from the energy bands. Density of the surface states is $10^{16} - 10^{17}$ per cm^2. Surface states may also arise due to the presence of impurities or adsorbed atoms. Wave function of an electron in such a level has a sharp maximum near the adsorbed atom because of the immobilization of the lattice electron or hole near the adsorbed atom. This amounts to the formation of chemical bond between the lattice and the adsorbed atom. The effect of this on the energy bands of a semiconductor will be discussed in later chapter.

SUGGESTED READING

1. Clark, A., *Theory of Adsorption and Catalysis*, Academic Press, 1970.
2. Clark, A., *Chemisorptive Bond : Basic Concepts*, Academic Press, 1974.

Chapter 4

Catalyst Texture

Even a small change in the conditions of its preparation changes the quality of a catalyst. Hence, solid catalysts, commercial as well as laboratory preparations, need to be completely characterized for the purpose of standardization. Measuring the same properties before and after use of the catalyst helps in understanding the cause of catalyst deactivation. A large number of experimental techniques are used for this. Solid catalysts are generally porous in nature and the pores play a very important role in their application. In many catalysts, the large surface area is due to their porous nature. By texture of a catalyst we mean those properties that are associated with their porous nature. These are surface area (including the metal surface in case of supported metal catalysts) and pore structure of the catalysts.

4.1 SURFACE AREA

A solid may be nonporous or it may have pores. The pores may be large or they may be micropores as found in materials like zeolites. For measuring the surface area of a solid, it is necessary to know the number of molecules that cover the surface with a single layer of the adsorbate that is known as its monolayer capacity. If the area of cross section of the adsorbate molecule is known, the surface area can be calculated. For finding out the monolayer capacity of a solid, the BET equation is used. One form of the BET equation is

$$\frac{p}{v(p_0 - p)} = \frac{1}{Cv_m} + \frac{(C-1)p}{Cv_m p_0} \tag{4.1}$$

If the BET equation is valid, a plot of $\frac{p}{v(p_0-p)}$ against p/p_0 will be a straight line with slope $s = \frac{C-1}{v_m C}$ and intercept $i = \frac{1}{v_m C}$. Monolayer

capacity $v_m = \frac{1}{s+i}$. Since v_m is the volume in ml at standard temperature and pressure, the number of molecules is $\frac{v_m.N.}{22414}$, where N is Avogadro's number.

Total surface area of the solid is given by

$$\text{surface area} = \frac{v_m N}{22414} A_m \times 10^{-20} \text{m}^2 \tag{4.2}$$

where A_m is the area of cross section of an adsorbate molecule in the unit Å^2. Specific surface α (m^2/g) is obtained by dividing total surface area by the mass (gram) of the solid. Nitrogen adsorption at about 80 K gives a straight line BET plot in the p/p_0 range of 0.05 to 0.3, although occasionally it deviates from linearity even at a relative pressure = 0.1. The range 0 to 0.1 is generally used for surface area measurement. Molecular cross section area A_m is obtained from the relation

$$A_m = f\left(\frac{M}{\rho N}\right)^{2/3} \times 10^{16} \tag{4.3}$$

proposed by Emmett and Brunauer[1]. Here, M is the molar mass of the adsorbate, ρ is its density in the liquid state and f is a packing factor which becomes 1.091 assuming twelve nearest neighbours. (However, the mode of packing of the adsorbate depends on the nature of the solid surface). For nitrogen at its boiling temperature, the uncertainty in A_m is minimum and $A_m = 16.2$ Å^2.

Monolayer capacity can be measured either volumetrically or gravimetrically.

4.1.1 Volumetric Method

The volumetric apparatus commonly used for finding out surface area is based on a design by Emmett[2] as shown in figure 4.1. It has a sample holder, a manometer and a gas burette connected to a high vacuum line and a gas manifold. The gas burette has five or six bulbs of decreasing volume connected in series by short capillary tubes with etch marks and the volumes of the bulbs from one etch mark to the next is carefully calibrated. A series of bulbs with 250, 120, 50, 15 and 5 cm^3 capacity are often used.

A weighed quantity of the sample is taken in the sample bulb and it is degassed by heating and evacuating at the same time. The sample

[1]Emmett, P. J. and Brunauer, S., *J. Amer. Chem. Soc.*, 59, 1533 (1937).
[2]Emmett, P.J., *Advan. Colloid Sci.*, 1, 3 (1942).

and the vacuum line is then disconnected (by closing taps A and C). Next, the sample bulb is immersed in liquid nitrogen. Helium is then introduced with tap A closed. Mercury is now raised in the gas burette up to the first etch mark by opening the tap to the vacuum line and the pressure is noted in the manometer. Mercury is further raised to each of the etch marks and the volume of helium was found out from the pressure-volume relation at each pressure. Tap A is then opened allowing helium to expand and dead volume was calculated from the fall in pressure. After evacuating helium, nitrogen gas is introduced first with A closed to find out the volume of nitrogen taken by the same procedure as in case of helium. The tap A is then opened. This time pressure falls partly because of the expansion of gas into the dead volume and partly because of adsorption of nitrogen on the sample. Since the volume of the dead space is already known, the quantity adsorbed can be calculated.

Figure 4.1: *A simple volumetric adsorption apparatus after Emmett.*

All volumes are corrected to normal temperature and pressure conditions. In this way, the volume (v_m) of nitrogen adsorbed at five or six different values of p is obtained that is sufficient for a good BET plot.

Figure 4.2: *BET plot for nitrogen on silica.*

Figure 4.2 shows a BET plot of nitrogen on a silica sample. The plot is a straight line in the range of relative pressure 0 to 0.15. The intercept is very small. For a high surface area material like silica gel, it may be enough to make a single point measurement and join this point with the origin assuming zero intercept.

Monolayer capacity is some times obtained directly from the plot of volume adsorbed against relative pressure for a type II isotherm. The monolayer volume is as the volume adsorbed up to the point at which a sharp bend is noticed (point B in figure 4.3). Some workers suggest that the monolayer capacity should be found out by extrapolating the straight line part of the plot to the volume axis (point A). It has been found that the volume at point B (v_B) may be appreciably different from v_m obtained from the linear BET plot and that v_B/v_m is close to 1 only when the point B lies at a relative pressure which falls within the linear part of the BET plot.

A number of volumetric adsorption apparatus has been designed based on similar principles and the reader may refer to an excellent monograph by Gregg and Sing[3]. Automatic commercial instruments are

[3]Gregg, S.J. and Sing, K. S. W., *Adsorption, Surface Area and Porosity*, Acad.

also available most of which are based on flow method that will be discussed later.

Figure 4.3: *Type II isotherm showing points A and B.*

4.1.2 Gravimetric Method

In this method, the sample is suspended from a balance and the weight change of the sample due to adsorption at various adsorbate pressure is measured. A monolayer of nitrogen molecules on a 1 m^2 surface weighs 2.8×10^{-4} g. Therefore, the sensitivity of the balance to be used for gravimetric measurement depends on the surface area of the sample, but for accurate measurement, it should have a sensitivity of a few microgram. The other requirement is that the whole system including the balance should operate at a vacuum of at least 10^{-4} mm of mercury. Direct measurement of mass change has the advantage that no dead space correction is required, but a buoyancy correction is necessary. Both beam balance and spring balance are used.

The spring adsorption balance was introduced by Mcbain and Bakr[4] and similar design has been used by many.

The balance is a helical spring usually made of fused silica. A small light cup containing the sample hangs down from the spring. The sample

Press, New York, 1967.

[4]McBain, S. J. and Bakr, A. M., *J. Amer. Chem. Soc.*, 48, 690 (1926).

is placed inside a quartz tube which is connected to a flask containing nitrogen gas and to a vacuum line. Mcbain and Bakr followed the increase in mass from the elongation of the spring using a vertical traveling telescope. Sensitivity of the spring depends on the diameter of the coil and the diameter of the quartz fibre with which it is made. For high sensitivity, the coil diameter should be large but the fibre diameter should be small. It is not difficult to get spring with elongation of 1 mm per mg of mass. Since fused silica spring is fragile, phosphor-bronze springs may be used when larger weights are to be suspended.

Figure 4.4: *A modified McBain balance.*

Various recording type balances based on the same principle have been in use. One such unit using a LVDT is shown in figure 4.4.

Buoyancy correction is made using the relation

$$\Delta m = \frac{Mvp}{RT} \tag{4.4}$$

where v is the volume of the load (sample and sample holder), M is the molar mass of the sample and p is the adsorbate pressure. It is easy to check if the correction is significant, otherwise it can be ignored.

Vacuum microbalance of the beam type with better than one microgram sensitivity that can stand ultra-high vacuum are commercially available.

4.1.3 Flow Method

Flow method is rapid and does not require vacuum. Several modifications of the instrument that involve flow method are available. According to one[5], a mixture of helium and nitrogen is passed successively through a thermal conductivity detector (TCD), the sample tube maintained at room temperature and then through another matching TCD, all in a closed system. The two TCD detectors form two arms of a Wheatstone bridge circuit. The bridge gives steady output at constant flow of the gas mixture. The sample tube is then immersed in liquid nitrogen when some nitrogen from the gas mixture gets adsorbed on the sample. The change in the gas composition after adsorption is detected by the TCD. This changes the bridge output and is recorded by a potentiometric recorder in the form a peak. Area of the peak is proportional to the amount of nitrogen adsorbed and can be calibrated using various doses of nitrogen. When the liquid nitrogen trap is removed, a desorption peak is seen. By varying the partial pressure of nitrogen in the mixture and measuring the amount of nitrogen adsorbed at each partial pressure, it is possible to generate sufficient data to plot an isotherm.

Before adsorption, the sample must be degassed by heating in a stream of helium. It is possible to use, in principle, either the adsorption or the desorption peak. The latter may, however, lead to error if there is any hysteresis.

Irrespective of the method used for adsorption measurement, the main task is to find out v_m. All the three methods described here can be used to get a straight line BET plot at low p/p_0 from which surface area can be calculated.

BET method for surface area determination is used when an adsorbate-adsorbent system gives a type II isotherm. Since nitrogen at about 80 K gives a type II isotherm with most solids, it is extensively used as the adsorbate. Type I isotherm that shows saturation adsorption has also been tried by assuming that saturation indicates monolayer formation. Dubinin, however, argued that type I isotherm of physical adsorption actually indicates a gradual filling up of the micropores and it is not an indication of monolayer completion.

[5]Lobenstein, W. V. and Dietz, V. R., *J. Nat. Bur. Std.*, 46, 51 (1951).

Type III isotherm is shown when the value of the constant C in the BET equation is close to unity which means $Q_a \approx Q_L$. In this case and for all those cases when $Q_a < Q_L$, type II isotherm results. The quantity adsorbed at low partial pressure region for a type III isotherm is very small, and the measurements are likely to be inaccurate. Moreover, the BET equation gives the relation

$$v_m = \frac{C-1}{\alpha C} \tag{4.5}$$

showing that v_m is highly sensitive to the value of C when C lies close to 1. A small error in C will introduce a large error in the calculated monolayer capacity. This means that the conventional BET equation is not suitable for the determination of surface area by using an adsorbate that gives a type III isotherm.

4.2 PORE SIZE DISTRIBUTION

Many catalysts and catalyst supports are porous. Dubinin[6] classified pores according to their diameter as micropores (< 20) Å, macropore (> 200) Åand intermediate pores. Adsorption behaviour of solids are largely determined by the size and shape of the pores.

Pore size can be determined either from adsorption-desorption isotherm or by using mercury porosity meter.

4.2.1 Pore Size from Adsorption

We have seen the equation for capillary condensation for a spherical meniscus in Chapter II. From thermodynamic reasoning, Kelvin derived the relation for capillary condensation

$$\ln \frac{p}{p_0} = -\frac{2v\lambda}{rRT}\cos\theta \tag{4.6}$$

where θ is the contact angle that the liquid adsorbate makes with the wall of the pore and r is the radius of the capillary covered with the liquid film. Since the radius of the capillary (pore) is very small, θ will approach zero and the above equation becomes

$$\ln \frac{p}{p_0} = -\frac{2v\lambda}{rRT} \tag{4.7}$$

which is same as the equation that we derived for capillary condensation in Chapter II except that r_s (radius of the spherical meniscus) is replaced

[6]Dubinin, M. M., *Chem. Rev.*, 60, 235 (1960)

by r (radius of the capillary covered with a liquid film). Since $r = r_s \cos\theta$, one can surely replace r_s by r when $\theta = 0$. Since the liquid film is present even before capillary condensation begins, r in equation (4.7) gives the radius of the capillary (pore) coated with a liquid film and not the pore radius. The radius of the pore is

$$r_p = r + t \tag{4.8}$$

where t is the thickness of the liquid film.

Number of moles adsorbed at a given relative pressure p/p_0 can be found out from an adsorption isotherm. When multiplied by the molar volume of the liquid adsorbate, it gives the volume of the pore filled at that relative pressure. r at that relative pressure can be found out using equation (4.6). Film thickness t is the only quantity that remains to be found out in order to get r_p.

Thickness of the film t can be found out if adsorption is measured on a nonporous solid that is chemically similar to the porous material by assuming that the thickness of the adsorbate layer formed on both are same at identical relative pressure. If the film is made of n molecular layer, then $t = nt_m$, where t_m is the thickness of a monomolecular layer. If v_m is the monolayer capacity, $n = \sigma_p/\sigma_m$. t_m for nitrogen has been calculated to be 3.5 Åassuming hexagonal packing. Thus, it is possible to calculate r_p at different relative pressure of the adsorbate. The problem is that, it is not always possible to get a nonporous solid with the same adsorption properties as the porous substance.

Wheeler[7] proposed the equation

$$t = t_m \left[\frac{5}{\ln(p/p_0} \right] \tag{4.9}$$

for finding out film thickness. He suggested the value of $t_m = 4.3\mathring{A}$ assuming $\ldots$AAAAA$\ldots$ stacking.

Since both v_p and the corresponding r_p can be found out by this method, one can plot $\frac{\Delta v_p}{\Delta V_r}$ against r_p over the entire range of adsorption measurement. Such a plot, known as the structural curve, represents the relative abundance of pores of different radii in the solid. A typical adsorption-desorption isotherm and the corresponding structural curve using nitrogen as adsorbate (taken form Harris and Whitaker[8] is shown in figure 4.5.

[7]Wheeler, A., *Catalysis, vol.2*, Reynold, New York, 1955, p.118.

[8]Harris, M.H. and Whitaker, G., *J. Appl. Chem.*, 13, 348 (1963).

The main problem with this method is that it gives erroneous results in case of materials like zeolites when the pore size is very small ($3 - 8$ Å) the cause of which has been explained by Dollimore and Heal[9] as follows.

Figure 4.5: *Nitrogen adsorption on titania at* -195^o *C: (a) adsorption-desorption isotherm; (b) pore size distribution.*

Average pore radius is often calculated as

$$\overline{r}_p = \frac{2(V_p)_{\text{total}}}{\alpha} \tag{4.10}$$

where $(V_p)_{\text{total}}$ is the total pore volume (cm^3), and α is specific surface in cm^2/g. However, $(V_p)\text{total} = X_t/\rho$, where X_t (g/g) is adsorption at saturation and ρ (g/cm^3) is the density of the liquid adsorbate. Also,

$$\alpha = \frac{X_m N A_m}{M}$$

[9]Dollimore, D. and Heal, G. R., *Nature*, 1092 (1965).

where X_m (g/g) is the monolayer capacity.

Substituting this in the expression for $\overline{r}_p$ in equation (4.10) gives

$$\overline{r}_p = \frac{X_t}{X_m}\frac{2M}{\rho A_m N} \tag{4.11}$$

Here, $\overline{r}_p$ is in cm. When this equation is applied to solids with very small pores that gives type I adsorption isotherm, saturation adsorption is nearly the same as the monolayer capacity, i.e $X_t/X_m \approx 1$. Substitution in the above equation will give $\overline{r}_p = 7.08 \times 10^{-8}$ cm. Even if the pore is smaller than this, X_t/X_m will be near unity and the experimental average pore radius will be 7.08 Å. The method thus appears unsuitable for determining the pore size of the zeolites and other molecular sieves.

4.2.2 Mercury Porosity Meter

Mercury porosity meter makes use of the relation between the pressure needed to force mercury into a pore and the radius of the pore. A wetting liquid like water readily enters a capillary.

Figure 4.6: *Level and shape of the meniscus for (a) water and (b) mercury inside a capillary.*

In Chapter 2, we have seen that the hydrostatic pressure difference (ΔP) between two phases separated by a curved surface is

$$\Delta P = \gamma\left(\frac{1}{R_1} + \frac{1}{R_2}\right) \tag{4.12}$$

A solid with cylindrical pores closed at one end will initially form a spherical meniscus which means the two radii of curvature are equal, i.e $R_1 = R_2 = r_s$, where r_s is the radius of the spherical meniscus. The higher pressure in the vapour phase where the centre of curvature lies, forces the liquid into the pore causing capillary rise or automatic

pore filling. Pore radius r_p is related to the radius of the meniscus as $r_p = r_s \cos\theta$. For a non-wetting liquid like mercury, the centre of curvature lies inside the pore and hence the relation is $r_p = -r_s \cos\theta$. In the latter case, the liquid mercury will have to be forced into the pore since pressure inside the pore is higher. This is shown in figure 4.6.

The pressure difference in either case

$$\Delta P = \frac{2\gamma}{r_s} = \frac{2\gamma\cos\theta}{r_p} \tag{4.13}$$

Mercury can enter a pore of radius r_p only when the applied pressure exceeds ΔP. The average contact angle of mercury with a solid is taken to be 140^o and knowing the surface tension of mercury ($\gamma = 480$ dyne/cm at room temperature), r_p can be calculated from ΔP. This is the working principle of a mercury porosity meter.

Table 4.1: Relation between pore radius and pressure required to fill them.

Pore radius, Å	Pressure, atm.
500	140
100	700
50	1400
20	3500

In the mercury porosity meter instrument, the solid sample is immersed in a reservoir of mercury. Upper part of the reservoir ends in a capillary. The whole setup is placed inside a chamber that can be pressurized. When pressure is applied, mercury enters the pores of the solid and the level of mercury in the capillary falls. The fall is measured using a micrometer device. The difference in the volume of mercury is the volume of the pore v_p occupied by mercury at this pressure. Radius of the pore at this point is found out from equation (4.13). This procedure is repeated by raising the pressure to a higher level. Very high pressure is needed to fill up all the pores as shown in Table 4.1.

The main problem in this experiment is the difficulty in reaching very high pressure needed to fill up the micropores. From Table 4.1, we see how the pressure increases as the pore size becomes small. It is difficult to fill up pores that has radius smaller than 50 Å. For this limitation, adsorption-desorption method is more often used for pore size measurement. In those cases where the pore structure of solids has been measured (in the medium size range) by both the methods, the agreement was found to be good.

4.3 METAL SURFACE AREA

Supported metal catalysts is a very important class of industrial catalyst. The support is generally a high surface oxide on which small metal particles are deposited. Since many of them costly metals, it is necessary to make use of as many metal atoms as possible. This makes it necessary that they are distributed as small particles on a solid of large surface area to maximize the available metal surface. Catalytic activity is often reported as turn over number (TON) which means the number of molecules of the reactant converted per surface metal atom in one second. In order to know the number of metal atoms present on the surface per gram of the catalyst, the metal surface area should be known. Various experimental methods are used for this purpose some of which will be discussed here.

Chemisorption method

Methods for finding out chemisorption will be discussed in Chapter 5. For measuring the metal surface area, it is necessary to find out an adsorbate gas that is selectively adsorbed on the metal atoms only under the conditions of measurement. Supported platinum catalysts have been most extensively studied by this technique. Adsorption is allowed to reach the equilibrium and any physically adsorbed gas is removed by evacuation. For supported platinum catalysts, hydrogen is the most commonly used adsorbate and it is assumed that the gas is dissociatively adsorbed with the metal atom to hydrogen atom stoichiometry 1:1. This gives the number of platinum atoms in one gram of the catalyst exposed to the adsorbate. Metal surface is calculated using equation

$$S_M = 2 \times n_{H_2} \sigma_M = 2 \times n_{H_2}/n_s \tag{4.14}$$

where S_M is the metal surface area, n_{H_2} is the number of hydrogen molecules adsorbed, σ_M is the area occupied by one metal atom and n_s is the number of surface metal atoms. The quantity n_s depends on the Miller plane of the exposed metal surface. Assuming equal proportions of the low index planes (111, 110 and 100), this becomes 1.25 for platinum, 1.27 for palladium, 1.63 for ruthenium, 1.33 for rhodium, 1.59 for osmium and 1.51 for nickel. Applicability of hydrogen as an adsorbate is doubtful for many other atoms. For example, hydrogen is occluded in palladium forming $PdH_{0.6}$.

Metal dispersion D_M is defined as

$$D_M = n_s/n_T \tag{4.15}$$

Here n_s is the number of metal atoms on the surface and n_T is the total number of atoms, both per gram of the catalyst. n_T is found out by bulk chemical analysis or from the metal loading.

Adsorbates other than hydrogen have been tried. Among them CO presents the difficulty that it adsorbs on a number of metals in different surface stoichiometry. With nickel, it can not be used because of the formation of volatile nickel carbonyl. Hydrogen as an adsorbate has been most successful, in particular, for supported platinum catalysts.

In their attempt to measure hydrogen chemisorption more accurately, Benson and Boudart[10] introduced a surface titration method. Oxygen is first adsorbed according to the reaction

$$\mathrm{Pt_s} + \frac{1}{2}\mathrm{O_2} \rightarrow \mathrm{Pt_s} - \mathrm{O}$$

Then hydrogen gas is introduced in small doses that reacts as:

$$\mathrm{Pt_s} - \mathrm{O} + \frac{3}{2}\mathrm{H_2} \rightarrow \mathrm{Pt_s} - \mathrm{H} + \mathrm{H_2O}$$

Here $\mathrm{Pt_s}$ is a surface platinum. Since water formed during hydrogen titration is strongly adsorbed on the surface, this will not affect the partial pressure. The amount of hydrogen consumed can be measured volumetrically, gravimetrically or by pulse method. The titration method consumes three times more hydrogen than hydrogen chemisorption method and hence is more sensitive. An excellent review on this has been written by Lemaitre, Menon and Delanney[11].

4.3.1 X-ray Line Broadening

Average metal particle size can also be determined from X-ray line broadening. Sharp X-ray powder diffraction pattern is given by particles whose size lies between 10^{-5} to 10^{-3} cm. X-ray lines start to broaden when the particle size becomes smaller than 1000 Åand is most prominent when the crystal diameter is less than 200 Å. The average particle diameter D_M is given by the Scherrer equation

$$D_M = \frac{K\lambda}{\beta \cos\theta} \tag{4.16}$$

where λ is the wavelength of the X-ray, K is a constant that depends on the crystal system, β is the full width at half maximum height (FWHM)

[10] J. Benson and M. Boudart, *J. Catal.*, 4, 704, (1965).

[11] J. L. Lemaitre, P. G. menon and F. Delanney, in *Characterization of Catalysts*, Ed. F. Delanney, Marcell-Dekker, New York, 1984, p.299.

of the diffraction line and θ is the diffraction angle. Since β for different crystal systems lie between 0.9 and 1, it is customary to ignore the crystal system and accept the value 0.94 for K.

Line broadening, however, has several other causes. These include instrumental factors, stacking faults and strain in the crystal. For small crystals, it is possible to ignore the factors other than particle size and instrumental broadening. For getting the extent of instrumental broadening, X-ray powder diffraction of a good crystalline material recorded under identical condition is used. Normally, fine powdered sodium chloride or quartz is used as standards. Assuming the line shape to be Gaussian, the Warren's relation

$$\beta = \sqrt{B^2 - b^2} \tag{4.17}$$

is used. Here, B and b are observed FWHM for the sample and the standard respectively.

There are several limitations in finding out metal particle size by X-ray diffraction. The method can detect particle size not smaller than 50 Å. For small metal loading, low intensity of the diffraction lines of the metal is a serious problem. This is even more serious when the atomic number of the metal is not high. When several lines are available, the line that is most intense and symmetric is generally chosen. For supported platinum, palladium and nickel, the (111) line is generally chosen. But for platinum on γ-alumina, because the support itself has a diffraction line close to the (111) line of platinum and (311) reflection of platinum is the next choice. The rate of scanning is to be adjusted to get the best result and in most case 0.1 to 0.5 degrees per minute is used.

D_M obtained from Scherrer equation is actually the thickness of the metal particle perpendicular to the crystal plane. The actual size d_M of the metal particle is obtained as

$$d_M = D_{M(hkl)} \cdot g \tag{4.18}$$

where g is a geometric factor that depends on crystal plane and geometry as given in Table 4.2.

4.4 TRANSMISSION ELECTRON MICROSCOPY

Transmission electron microscopy (TEM) has been used extensively for measuring the size of small metal particles. The electron microscope uses an electron beam in place of visible light used by an optical microscope. The electron gun consists of a tungsten anode , an accelerating anode

Table 4.2: Crystal geometry and the geometric factor g.

Crystal geometry	g	Definition of size
Sphere	$\frac{4}{3}$	Diameter
Hemisphere	4	Diameter
Cube with (100) face with (hkl)		
100	1	Cube edge
110	1.061	Cube edge
111	1.155	Cube edge

and beam aperture control. An electron lens system (electric or magnetic field) can focuss the electron beam with very narrow cross section at the point where it strikes the specimen. The transmitted electrons passes through another set of electron optics to finally fall on a fluorescent screen where the image is produced and can be recorded on a photographic film.

The electron beam striking a specimen give rise to several other effects. The sample emits X-ray, Auger electrons, back scattered electrons, secondary electrons etc. Transmission electron microscopy uses transmitted electrons – un-scattered as well as elastically and inelastically scattered.

Figure 4.7: *A typical metal particle size distribution in a supported catalyst.*

Use of high energy electrons (100 keV or more) gives high resolution

and reduces chromatic aberration. The resolution of commercial instruments is 1 nm and the magnification is about 10^6 times. But higher resolution of even 0.2 nm has been achieved.

In the study of supported metal catalysts, the most important is the sample preparation. The catalyst is finely ground and then dispersed in a liquid (water, amyl alcohol etc.) and drop of this suspension is placed on a carbon film which rests on the electron microscope grid. The grid is a sieve woven from a thin metal wire, usually nickel or copper. A better method of sample preparation is the extraction and replication technique[12]. In this technique, a thin film of carbon is deposited on the catalyst by evaporation. The metal particles on the surface of the support remain encapsulated in the film and they are retained by the film when it is separated from the sample. Removing the support improves imaging as the contrast due to the support is eliminated.

TEM pictures gives the particle size and their distribution. The image is projected on a screen and the number of particles in different size range are counted. The size distribution in the measured range is then plotted as a histogram as shown in the figure 4.7.

SUGGESTED READING

1. Anderson, R. B. (Ed), *Experimental Mehtods in Catalytic Research*, Academic Press, New York, 1968.
2. Gregg, S. J. and Sing, K. S. W., *Adsorption, Surface Area and Porosity*, Academic Press, New York, 1967.
3. Linsen, B. G. and Van Den Heuvel, A., *Pore Structure* in *Solid-Gas Interface, Vol.2*, (E. A. Flood, Editor), Marcel Dekker, New York, 1967.
4. Delanney, F. in *Characterization of Heterogeneous Catalysts*, (F. Delanney, Editor), Marcell and Dekker, New York, 1984.

[12]G. Delami-Imelik, C. Leclercq and I. Martin, *J. Microscopy*, 20, 123, (1974).

Chapter 5

Chemisorption

Activation of small molecules on well defined metal surfaces has been the subject of numerous investigations. Earlier work on this has been adequately summarized by Trapnell and the summary is reproduced here from his book[1] (table 5.1).

Table 5.1: Activities of metal films in chemisorption: + chemisorption takes place; x no chemisorption.

Group	Metals	Adsorbate gases					
		N_2	H_2	CO	C_2H_4	C_2H_2	O_2
A	W, Ta, Mo, Ti, Zr, Fe, Ca, Ba	+	+	+	+	+	+
B	Ni, Pt, Rh, Pd	x	+	+	+	+	+
C	Cu, Al	x	x	+	+	+	+
D	K	x	x	x	x	+	+
E	Zn, Cd, In, Sn, Pb, Ag	x	x	x	x	x	+
F	Au	x	x	+	+	+	x

It can be seen that the main objective of this table is to delineate the metals that adsorb six typical molecules chosen and to clsssify the metals in terms of their adsorption abilities. The phenomenon has always been associated with the concept of active centres originally proposed by Taylor. Adsorption of such simple molecules can be visualized by some structural models based on their bonding characteristics in single molecular entities (see figure 5.1).

Experimental results on chemisorption of gases are mostly explained in terms of these models.

[1] B. M. W. Trapnell, *Chemisorption*, Butterworths Sc. Publ., 1955, p.173.

5.1 CHEMISORPTION OF HYDROGEN

The valence electrons of hydrogen atoms are involved in the H-H σ-bond in the molecule. The interaction with the surface uses the same σ-bond electrons as there are no other electrons available in the molecule. Consequently, chemisorption of hydrogen on metals is invariably a dissociative process in which the H-H bond is broken allowing each hydrogen atom to interact independently with the surface. The adsorbed species are therefore hydrogen atoms.

Figure 5.1: *Proposed structural models for the adsorption of some simple molecules: (a) hydrogen; (b) nitrogen; (c) carbon monoxide; (d) ethene; (e) ethyne; (f) oxygen.*

The exact nature of the adsorbed hydrogen complex is generally difficult to determine experimentally. The very small size of the hydrogen atom does mean that migration of hydrogen from the interface to the sub-surface layers can occur with relative ease on some metals (e.g., palladium and rare earth metals). The possibility of molecular hydrogen chemisorption at low temperature, however, can not be entirely excluded

as suggested by the formation of molecular hydrogen transition metal complex such as $W(\eta^2 - H_2(CO)_3(Pi - Pr_3)_3$, in which both atoms of the hydrogen molecule are coordinated to a single metal centre. Typical heats of adsorption of hydrogen on different metal surfaces are given table 5.2.

Table 5.2: Heat of chemisorption of hydrogen on metal surfaces.

Metal	Crystal structure	Q_{exp}	$Q^1_{Cal.}$	$Q^2_{Cal.}$	Q^{Eley}	Q^{Stvn}	Q^{Trst}
Ti	hcp	38.9	45	38 (40)			48.2
V	bcc		48	45			
Cr	bcc	45	41	38 (36)	16	24	38.4
Mn	bcc		43	36			
Fe	bcc	32.8*	30	32 (32)	17	31.6	34.4
Co	fcc	24±4	23	24 (28)		31	
Ni	fcc	27.5*	23	24 (27)		28.9	33.6
Zr	hcp		60	50			
Nb	bcc		60	58			
Mo	bcc	40	44	46 (45)		42.9	50.9
Tc	hcp		28	31			
Ru	hcp	26±2	24	28 (30)		38.1	
Rh	fcc	25.6*	22	25 (26)	24	32.3	
Pd	fcc	26	15	18 (22)		22.5	27.2
Hf	hcp		74	59			
Ta	bcc	45	71	67 (50)	32	49.6	56.8
W	bcc	48.7*	60	61 (45)	44	45.6	53.2
Re	hcp		32	36			
Os	hcp		30	34			
Ir	fcc	26±2	26	30 (24)		38.1	
Pt	fcc	24*	22	25 (25)		22.6	29.1

$Q^1_{Cal.}$ and $Q^2_{Cal.}$ are calculated using equations 5.1 and 5.2 respectively;
Q^* average of the available experimental values.

The values Q^{Eley} are taken from Eley[2], Q^{Stvn} from Stevenson[3] and Q^{Trst} taken from Trasatti[4].

Calculated values of heat of adsorption were obtained using equation

$$Q^1_{Cal} = \frac{(\beta E_{M-M} + E_{A-A_s})}{2} + 2.3[\gamma(\chi_M - \chi_A)]^2 \qquad (5.1)$$

[2]D. D. Eley, *Disscussions Faraday Soc.* 8, 34, (1950),
[3]R. P. Stevenson, *J. Chem. Phys.*, 23, 203 (1955).
[4]T. Trasatti, *Faraday Trans.*, 168, 229, (1955).

and

$$Q^2_{\text{Cal}} = \frac{(\delta E_{\text{M-M}} + E_{\text{A-A}_\text{s}})}{2} + 2.3[(\chi_{\text{M}} - \chi_{\text{A}})] \tag{5.2}$$

where E stands for bond energy, χ is electronegativity, and in this case, $\text{A} - \text{A}_\text{s}$ is a chemisorbed hydrogen molecule.

5.2 CHEMISORPTION OF O_2 AND N_2

Oxygen is a molecule which usually adsorbs dissociatively, but shows molecular adsorption on some metals like silver and platinum. In these cases where both types of adsorption are observed, it is the dissociative adsorption that has higher enthalpy of adsorption.

Interaction is relatively weak in the molecularly adsorbed state. The molecules are aligned such that the internuclear axis is parallel to the surface plane and it may bond to a single surface metal atom via any of the following bonding schemes:

1. σ-donor interaction in which the charge transfer is from the occupied molecular π-bonding molecular orbital (MO) of the oxygen molecule into the vacant orbitals of σ-symmetry of the metal ($\text{M} \leftarrow \text{O}_2$) (conveniently called donation), and
2. π-acceptor interaction, in which an occupied metal d-orbital of right symmetry overlaps with the empty π^* orbitals of the oxygen molecule and the charge transfer is from surface to oxygen ($\text{M} \rightarrow \text{O}_2$) popularly known as back donation.

Although the interaction of di-oxygen with the surface is generally weak, a substantial barrier to dissociation may be expected due to the high energy of the O=O bond. Nevertheless, dissociation of oxygen is found to be facile on most metal surfaces because the manner of interaction with the surface may mitigate the intrinsic bond energy thereby facilitating dissociation.

Oxygen atoms are strongly bound to the surface and tend to occupy the highest available coordination site. Strength of interaction of the adsorbate with the surface is such that the adjacent metal atoms are often seen to undergo significant displacement from their equilibrium positions on the clean metal surface. Such displacements may simply lead to a distortion of the surface in the immediate vicinity of the adsorbed atom (for example, the adjacent metal atoms may be drawn towards the oxygen reducing the metal-oxygen distance), or to a more extensive surface reconstruction.

Dissociative oxygen adsorption is often irreversible. Rather than leading to desorption, heating of an adsorbed oxygen overlayer often

results either in gradual removal of oxygen from the surface by diffusion into the bulk of the substrate (e.g., Si(111) or Cu(111)), or to the formation of surface oxides. Depending on the reactivity of the metal, further exposure at low temperature may result either in a progressive conversion of the bulk metal to oxide, or the oxidation process may effectively stop after the formation of a passivating surface oxide film of a particular thickness (e.g., in the case of aluminium).

Interaction of nitrogen with metal surfaces shows many characteristics similar to oxygen. However, nitrogen (N_2) is generally less susceptible to dissociation because of the weak M-N bond strength and the substantial kinetic barrier associated with N≡N triple bond.

5.3 CHEMISORPTION OF CARBON MONOXIDE

Depending on the metal surface, CO may adsorb either in the molecular from or in the dissociative fashion. In some cases, both types may coexist on a particular surface plane over a specific temperature range. The results may be summarized as:
1. On the reactive surface of the metals lying at the left-hand side of the periodic table (Na, Ca, Ti, rare earths), adsorption is almost always dissociative leading to the formation of adsorbed carbon and oxygen atoms (forming thereafter surface oxides or oxy-carbide compounds).
2. On surfaces of the metals lying on the right hand side of the *d*-block (Cu, Ag), the interaction is predominately molecular. The strength of interaction between CO molecule and the metal is weaker so that the M-CO bond may be readily broken and the CO may be desorbed by raising the temperature without the molecule getting dissociated.
3. For majority of the transition metals, however, the nature of adsorption (dissociative versus molecular) is very sensitive to surface temperature and surface structure (the Miller index plane and the presence of lower coordination sites like steps, kinks and defects).

Molecularly adsorbed CO binds to the single crystal metal surface in several ways - a behaviour analogous to the formation of molecular metal carbonyl complexes. These are shown in figure 5.2

While the above structural diagrams amply demonstrate the inadequacy of a simple valence bond description of the boding of the molecules to the surface, they do, to a limited extent, illustrate one of its features and strengths – namely that a given element (here carbon) tends to have a specific valence. Consequently, as the number of atoms to which carbon is coordinated increases, the C-O bond order accordingly decreases.

It should, however, be emphasized that a molecule such as CO does

not necessarily prefer to bind at the highest coordination site available. For example, there are 3-fold hollow sites available on a (111) surface of a fcc metal, but this does not mean that CO will necessarily adopt this site. The preferred site may still be a terminal or a 2-fold bridging site. Moreover, the site(s) which is occupied may change with surface coverage or temperature. The energy difference between the various adsorption sites available for chemisorption of molecular CO appears to be small.

Figure 5.2: *Various ways of adsorption of* CO *on metal surface: a. Terminal (all surfaces); b. Bridging (2-fold site, all surfaces); c. Bridging (3-fold hollow, fcc); d. Bridging (4-fold, hollow, fcc).*

The decrease in the C-O stretching frequency of the terminally bound carbon monoxide as compared to gaseous CO (2143 cm^{-1}) can be explained in terms of the Dewar-Chatt or the Blyholder model for bonding of CO to metals. The simple model considers the metal-CO bonding to be consisting of two main components:
1. A σ-bonding interaction due to the overlap of a filled σ-lone pair orbital on the carbon atom with metal orbitals of right symmetry that leads to an electron density transfer from the CO molecule to the metal atom.
2. A π-bonding interaction due to overlap of filled metal $d\pi$ (and $p\pi$) orbitals with the π^* antibonding molecular orbital of the CO molecule. Since this interaction leads to the introduction of electron density into the antibonding orbital of CO, there is a consequent reduction in the CO bond strength and its intrinsic vibrational frequency (relative to the isolated molecule).

5.4 UNSATURATED HYDROCARBONS

Unsaturated hydrocarbons (alkenes and alkynes) interact with the surface metal atoms fairly strongly. At low temperature (and on less reactive

metal surfaces), adsorption may be molecular, perhaps with some distortion of bond angles at the carbon atom. Ethene, for example, may bond to give a π-complex or a di-σ adsorption complex (see figure 5.3).

Figure 5.3: *Chemisorption of ethene: a. π-complex; b. di-σ complex.*

As the temperature is raised, or even at low temperature on more reactive surfaces (particularly those that bind hydrogen strongly), a stepwise dehydrogenation occurs. One particularly stable intermediate noticed in the course of dehydrogenation of ethene is the ethylidyne complex, whose formation also involves H atom transfer between the carbon atoms.

Based on the available data at the present time, metals can be classified into four groups on the basis of adsorption of these molecules either in molecular or in dissociated form (see table 5.3).

5.5 EXPERIMENTAL RESULTS

There exists a variety of spectroscopic techniques that have been employed to study chemisorption of gases on metal surfaces. For space constraints, only the adsorption of CO will be considered here.

5.5.1 Thermal Desorption Spectroscopy (TDS)

For example, typical TDS spectrum for CO adsorbed on typical metals has shown up to five desorption peaks[5] designated as α, β, γ, δ, and ϵ Usually the earlier peaks are attributed to desorption from multilayers and the last three are associated with desorption from the monolayer. This deduction is made on the basis of the amount of CO desorbed and also from the desorption energies usually deduced from TDS spectra obtained at various heating rates or from other variables. Usually the ϵ state desorbs over a wide temperature range and hence has to be associated with a single chemisorbed state. But the chemisorption energy, though may be assigned a single value, really means that desorption takes place with a spectrum of energies and hence the adsorbed state cannot

[5]R. W. Taylor, K. Hassan¡ A. A. Mehadi and J. W. Shuford *Comun. Soil Sc. Plant Anal.*, 26, 176, (1995).

be assigned to one single adsorbed molecular species. The spectrum of desorption energies can arise either due to the variations in the adsorption bond energy or due to repulsive interactions among the adsorbed species. Therefore, it has to be realized that the FWHM reflects on the desorption energies involved and hence there is no unique adsorbed species and there is a gradual variation of adsorption energies for the adsorbed species.

Table 5.3: Classification of transition metals based on their adsorption properties; P-Possible: N-Not possible.

Group	Metals	Dissociatve ads.					Non-dissociative ads.				
		H_2	O_2	N_2	NO	CO	H_2	O_2	N_2	NO	CO
A	Hf,Ta,Zr	P	P	P	P	P	N	N	N	N	N
A	Nb,W,Ti	P	P	P	P	P	N	N	N	N	N
A	V,Mn,Cr,Mo	P	P	P	P	P	N	N	N	N	N
B	Fe,Re	P	P	P	P	P	N	N	N	P	P
C	Ni,Co,Tc	P	P	N	P	P	N	N	N	P	P
D	Os,Ir,Ru	P	P	N	P	N	N	N	N	P	P
D	Pt, Rh, Pd	P	P	N	P	N	N	N	N	P	P

5.5.2 UPS Study

Ultraviolet photoelectron spectra are generally used for identifying the non-dissociative adsorption of gases, since the changes in the binding energy of the molecular orbitals of the adsorbate can be a measure of the strength of its bonding to the surface. Some typical data reported in literature are summarized in table 5.4.

In the case of non-dissociative adsorption of carbon monoxide on metals, one would examine the position of the photoemission peaks of 5σ, 1π and 4σ levels of carbon monoxide since they are the frontier orbitals. According to the Blyholder model which has been outlined earlier, the separation between 1π and 5σ levels are considerably reduced in the adsorbed state and even the relative positions are interchanged. The position of the 4σ level is altered considerably. Presence of these molecular energy levels in the photo-emission spectra is considered as fingerprint in identifying the non-dissociative (molecular) nature of adsorption. The extent of shift is considered as a reflection of the strength of the bond. Though these interpretations are well accepted and also appear to account for many of the observations, it should be pointed out that the eigenfunctions of the orbitals have certainly lost their molecular identity while interacting with the surface and hence the binding energy positions

of the oribitals could have been considerably altered on interaction with the wave functions of the surface. In such cases, one is not sure how much of the binding energy change is due to this orbital mixing and how much is due to the interaction energy. At best one can only assume that the trends of binding energy changes may be used to evaluate the relative order of interaction of the molecule with the surface. The absolute value of the change in binding energy may not be a suitable parameter to relate to the strength of the adsorption bond.

Table 5.4: UPS peak positions for CO adsorbed on metals.

Substrate	T, K	θ	Peak position, eV		
Cu(poly)[a]	20	≈ 0.5	$8.7(5\sigma)$	$11.6(1\pi)$	$14.5(4\sigma)$
	30	0.3	$8.5(5\sigma/1\pi)$	$11.8(4\sigma)$	$13.5(5\sigma)$
Cu(110)	> 77	(2x2)	$8.6(5\sigma/1\pi)$	$11.5(4\sigma)$	$13.5(5\sigma)$
Ag(110)[a]	50	<1	$9.1(5\sigma)$	$11.9(1\pi)$	$14.8(4\sigma)$
	50	$+1$	$9.5(5\sigma/1\pi)$	$12.1(4\sigma)$	$14.8(4\sigma)$
Au(poly)	40.8	9.8	12.3	13.3	
Au(110)	117	0.3	$10(1\pi)$	$12.5(4\sigma)$	$13.8(4\sigma)$
	> 77	< 0.5	$9.8(5\sigma/1\pi)$	$12.6(4\sigma)$	$13(5\sigma)$
	28	0.25	7.3, 9.4	12.5	13.8
		0.5	7.7, 9.4	10.3, 12.5	13.8, $13.3(4\sigma)$
		1.0	$7.8(5\sigma)$, 9.3	$10.4(1\pi)$, 12.5	13.8, $13.3(4\sigma)$
		> 2.0	$8.2(5\sigma)$,$11.2(1\pi)$	$14(5\sigma)$	
Gas phase I.P.			$14.01(5\sigma)$	$16.91(1\pi)$	$19.72(4\sigma)$
$-(\phi_0 + \Delta\phi)$			$9.59(5\sigma)$	$12.49(1\pi)$	$15.30(4\sigma)$

[a]- physical adsorption; all others- chemisorption.

5.5.3 Overlayer Structures by LEED

A number of LEED patterns have been reported for almost all gases adsorbed on metallic surfaces. For CO adsorption, a variety of LEED patterns are reported and changes of LEED patterns with coverage is well known. These patterns with various geometries especially the tilted geometries like $(\sqrt{3} \times \sqrt{3})R30$ are indications that localized bonding normally visualized in the form of adsorbed states shown in figure 5.1 might not represent the true bonding. Wavefunction of the adsorbate overlaps with the various frontier wavefunctions of the surface that gives rise to a series of adsorbed state LEED patterns. As the frontier orbital wavefunctions of the adsorbent can have different density contours it is possible that the adsorbed state geometries can vary with coverage. It may be possible that the whole set of LEED patterns observed for the adsorbed states is arising out of the orbital overlaps of the surface atoms with the valence orbitals of the adsorbate of suitable energy and

geometry. The model of localized bonding may be one of the extreme cases.

5.5.4 Work Function Measurement

Work function changes $\Delta\phi$ have been often interpreted in terms of electron exchange between the adsorbate and adsorbent and hence it is possible that $\Delta\phi$, can be positive or negative. In the case of adsorption of CO at initial stages (that is in the ϵ state), the work function of the adsorbate decreases indicating that the population of the lowest unoccupied states of the adsorbent from the valence electrons of the adsorbate. The magnitude of $\Delta\phi$ will depend on the energy, symmetry and degeneracy of such states of the adsorbent. The relative gradient of the variation of work function with coverage is a reflection of the extent of overlap of the orbitals of the adsorbent with those of the adsorbate. In this sense, this variation can be considered a measure of the strength of the adsorption bond.

5.5.5 NEXAFS Measurement

The near edge spectrum reflects the emission from the occupied states of the adsorbate and it is usually considered that the first resonance observed for CO adsorption on metal surfaces is due to π^* resonance and the next one is due to σ^* state of CO. These assignments reflect the overall symmetry of the wave functions from which the emission has been observed. Shape of the resonance emission gives indication of the change of the wave function due to overlap with the wave functions of the adsorbent. Variation of the shape of this resonance with coverage is an indication that the wave functions of the adsorbent with different energy and symmetry overlap with similar wave functions of the adsorbate.

5.6 KINETICS OF ADSORPTION

Kinetics of adsorption on metal surfaces has been treated by various models. One of the models that has been extensively used to treat the adsorption kinetic data is known as the Elovich equation. Elovich equation is written as

$$dq/dt = a\exp(-bq) \tag{5.3}$$

On integration with boundary conditions $q = q$ at $t = t$ and $q = 0$ at $t = 0$, the Elovich equation becomes

$$q = \frac{1}{b}\ln(1 + abt) \tag{5.4}$$

The linear form of Elovich equation is

$$q = \frac{1}{b}[\ln(ab) + \ln(t + t_0)] \tag{5.5}$$

where a and b are parameters of the equation and $t_0 = 1/ab$. This equation is commonly used in kinetics of chemisorption of gases on solids. The Elovich equation has rarely been applied to liquid state sorption. Recently, it has been successfully used to describe the sorption of zinc ions on soils and also for the sorption of metal ions on solvent impregnated resins. It has also been used for other adsorptions as well as for release of metal ions from soils. It has even been used to analyze thermal desorption and in the study of some other phenomena[6].

Values of the two constants a and b of this equation obtained from the slope and intercept of a plot of q versus $\ln t$ are related to the initial rate of the process and the nature of sites involved in the adsorption process. The general explanation of this form of kinetic law is based on the variation of the energy of chemisorption with the extent of coverage. Another plausible explanation could be that the active sites are heterogeneous in nature, and therefore exhibit different activation energies for chemisorption. These two considerations have been extensively utilized in interpreting the variations of the two constants of the Elovich equation with experimental parameters like temperature and pressure. While analyzing the kinetic data of adsorption of gases on metals, one has to take into account the fact that most of the adsorption takes place in the initial period and only the final 10 per cent of adsorption process follows the Elovich kinetic law. Even then this final adsorption kinetic data when analyzed by the Elovich equation as a plot of q versus $\ln t$ gives rise to gradient changes. Even though the surface heterogeneity or variation of the energy of adsorption with coverage are important parameters, their effect would be more meaningful for the initial fast adsorption than for the slow last 10 percent of adsorption when analyzed by the Elovich equation. The species arising from the initial fast chemisorption could have utilized most of the frontier orbitals of the adsorbent for overlap

[6]R. W. Taylor, K. Hassan¡ A. A. Mehadi and J. W. Shuford *Comun. Soil Sc. Plant Anal.*, 26, 176, (1995);
R. Juang and M. Chen, *Ind. Engg. Chem. Res.*, 36, 813, (1997);
C. W. Chung, J. F. Protter and G. Mcay, *Water Res.*, 35, 605, (2001);
O. Ferrandon, H. Bouabane and M. Mazet, *Rev. Sci. Eau*, 8, 183, (1995);
J. A. Helmer, K. J. Wahl, I. L. Singer and A. Erdemir, *Appl. Phys. Lett.*, 78, 2449, (2001);
H. Teng and C. Hsieh, *Engg. Chem, Res.*, 38, 292 (1999).

with the wave functions of the adsorbate and hence the charge density contours of the wave functions of the adsorbent involved in bonding with the last (slow) 10 percent adsorption could be associated with eigenvalues well below the frontier orbitals. Hence, this process of interaction would require distinct changes as with coverage that would give rise to gradient changes and not a uniform variation of the constants of the Elovich equation with experimental parameters. This is so because it is an inherent parameter of the system and not of the experimental variables.

Chemisorption on other surfaces like metal oxides can be treated in a similar manner. It should, however, be recognized that in such systems, we are dealing with more than one type of adsorption sites, namely metal ions and oxide ions. Hence, the surface structure of the adsorbed molecules will involve these surface ionic species. For example, carbon dioxide adsorption on oxide ions can give rise to carbonate type species and that of nitrogen dioxide can give rise to nitrate species. The energetics of these species too will be different. In essence, if one identifies the surface species and also the overlayer species, their bonding scheme may be worked out with known molecular entities.

5.7 CHEMISORPTION BOND

The chemisorption bond can be treated at various levels of sophistication. However, the fundamental theories of bonding can be applied to the treatment of the adsorption bond. In this section, the basis of some of these theories is briefly considered.

5.7.1 Covalent Bond

In physical adsorption, it is generally assumed that both adsorbate and adsorbent suffer only minor distortions as a result of van der Waals forces between them. In chemisorption, where electrons are shared or transferred and drastic redistribution of their equilibrium positions occur, the situation is more complex. The simplest methods of describing chemical forces of adsorption at metal surfaces, with analogies with simple chemical bonds will be considered here. The bond is pictured as existing between the adsorbed atoms and a single atom of the metal with the influence of the surrounding metal atoms. The bond existing between metal atoms at the surface is assumed to be intact, unaffected by the chemisorption bonds of other atoms with them. The empirical rules developed by Pauling between for bonding between single atoms have been extended to covalent type of adsorption bonds. Pauling's d character of metals has also been invoked to account for the varying strength of the chemisorption bonds formed with various metals.

Let us consider Eley's method of calculating adsorption bond energies. This method has been applied largely to the dissociative adsorption of hydrogen on metals.

$$2\mathrm{M} + \mathrm{H_2} \rightarrow 2\mathrm{M} - \mathrm{H} \tag{5.6}$$

The differential heat of adsorption at zero coverage is given by

$$q_D = 2D_{\mathrm{M-H}} - D_{\mathrm{H-H}} \tag{5.7}$$

where $D_{\mathrm{M-H}}$ and $D_{\mathrm{H-H}}$ are the dissociation energies of the metal-hydrogen bond and of the hydrogen molecule. Equation (5.4) assumes that no M-M bonds are broken on chemisorption which is not always true. To determine $D_{\mathrm{M-H}}$, Eley extended, Pauling's approximation of covalent bonds between free atoms to the adsorption bonds. Thus the bond energy in Kcal/mol is

$$D_{\mathrm{M-H}} = \frac{D_{\mathrm{M-M}} + D_{\mathrm{H-H}}}{2} + 23.06(\chi_M - \chi_H)^2 \tag{5.8}$$

where $\frac{D_{\mathrm{M-M}}+D_{\mathrm{H-H}}}{2}$ is the approximation for strictly covalent bond and $(\chi_M - \chi_H)^2$ corrects for the slight polarization effects resulting from the difference in electronegativities of M and H as defined by Pauling. The second term of equation (5.4) therefore, determines the small contribution of the ionic character of the bond. Substituting equation (5.5) for $D_{\mathrm{M-H}}$ into equation (5.4) the differential heat of adsorption becomes

$$q_d = D_{\mathrm{M-M}} + 46.12\mu^2 \tag{5.9}$$

where $\mu = (\chi_{\mathrm{M}} - \chi_{\mathrm{H}})$. The problem now is to determine $D_{\mathrm{M-M}}$ and the moment of the M-H bond that is at $\theta = 0$. The M-M bond energy ($D_{\mathrm{M-M}}$) is estimated from the latent heat of sublimation. In a face centered cubic metal, each atom has 12 nearest neighbours and since each bond involves two metal atoms

$$D_{\mathrm{M-M}} = \frac{\Delta H_{\mathrm{sub}}}{6} \tag{5.10}$$

Within the approximation of the calculation, equation (5.7) is also satisfactory for body centered cubic lattice, in which each atom has eight nearest neighbours and six next-nearest neighbours. Eley has calculated μ, the dipole moment of the chemisorbed bond in Debye at zero coverage. The equation is limited to very small values of μ. Dipole moment

at full coverage is given by $\mu_{\mathrm{f}} = V/300(4\pi n_s)$ where V is the surface potential in volts and n_s is the mean number of sites per cm^2. Surface potentials at full coverage are available from the work of Mignolet. If depolarization effects are assumed to be small, then μ_{f} may be equated to μ_0, the dipole moment at zero coverage. Values of $(\chi_{\mathrm{M}} - \chi_{\mathrm{H}})$ may also be obtained roughly from Pauling's table of electronegativities. Both the above methods are approximations even for diatomic molecules.

In an attempt to improve the method, Stevenson has made use of Mulliken's electronegativity values which are defined by $\chi_{\mathrm{M}} = \frac{1}{2}(Ie + A_0 e)$ where I, A_0 and e are the ionization potential, electron affinity and electron charge. For metals, both I and A_0 are set equal to ϕM, the work function of the metal, since the highest occupied and lowest unoccupied levels are at the Fermi surface. Stevenson writes $\chi^S_{\mathrm{M}} = 0.355\phi_{\mathrm{M}}$. where ϕ_{M} is in eV and 0.355 is a scaling factor. Stevenson's quantity χ^S_{M} is then directly used in equation (5.5) in place of χ_{M} along with Pauling's electronegativities for the adsorbate. The agreement between the calculated and experimental values of $D_{\mathrm{M-H}}$ is somewhat better using Stevenson's modification. But neither the original Eley method nor its modification gives completely satisfactory agreement with the experimental values for the initial heats of adsorption. For hydrogen on Fe, Co, Ni, Cu, Mo,Ta and W the agreement using Stevenson's procedure is moderately good, values for Pd and Pt are rather low and the value for Cr is very low, while the values for Ru, Rh and Ir are too high. In general the values for other gases are too low.

Various criticisms have been leveled at the details of Eley method. Erlich believes that the $D_{\mathrm{M-M}}$ estimated from heats of sublimation, using equation (5.7) should be lower. Erlich is particularly concerned about the fact that the heat of adsorption given by equation (5.6) is always positive, and thus predicts that adsorption will always be exothermic even for metals of low cohesive energy ($D_{\mathrm{M-M}}$). It is stated that the chemisorption of hydrogen on metals is detectable for $q_d \approx 3$ kcal/mol ($D_{\mathrm{M-H}} = 53$ kcal/mol) and, therefore, contrary to experiment, molecular hydrogen should be adsorbed on Al, Ag, Au, Zn, Cd, Sn and Pb. Pauling found that bond strengths for metal hydrides obtained from the geometric mean $(D_{\mathrm{M-M}}.D_{\mathrm{H-H}})^{1/2}$ give values that are in better agreement than those obtained from the arithmetic mean $\frac{1}{2}(D_{\mathrm{M-M}} + D_{\mathrm{H-H}})$.

Erlich investigated the use of the geometric mean in the chemisorption of hydrogen on metals. He found agreement for the transition metals, though chemisorption of hydrogen on Zn, Cd and Hg were correctly predicted as endothermic with values of $23.06(\chi_{\mathrm{M}} - \chi_{\mathrm{H}})^2$.

5.7.2 Ionic Bond

The energy change associated with the ionic mechanism of cationic adsorption of A on a metal

$$\mathrm{M} + \mathrm{A} \rightarrow \mathrm{M}^{-}\mathrm{A}^{+} \tag{5.11}$$

may be roughly estimated by breaking down the energy as follows:
(i) an electron is removed from the highest occupied level of an isolated atom A to infinity $(-Ie)$
(ii) the electron is then transferred to the Fermi surface of the metal $\mathrm{M}(\phi e)$
(iii) A^{+} is brought to its equilibrium distance z^* from the surface of the metal $(e^2/4z^*)$.
The heat of adsorption per gram atom at zero coverage may then be expressed as

$$q_d = (-Ie + \phi e + (9e^2/4z^*))N \tag{5.12}$$

where I and ϕ are respectively the ionization potential of A and work function of the metal and N is Avogadro number. $(e2/4z^*)$ is the classical image energy of attraction of the ion A^{+}. The metal is considered to be a semi-infinite plane and z^* is assumed to be the radius of the adsorbed ion. A similar expression can be given for the anionic adsorption of A.

$$\mathrm{M} + \mathrm{A} \rightarrow \mathrm{M}^{+}\mathrm{A}^{-} \tag{5.13}$$

giving

$$q_d = [A_0 e - \phi e + (e^2/4z^*)]N \tag{5.14}$$

where A_0 is the electron affinity of the adsorbate atom A. If the adsorption is dissociative, as in the case of hydrogen and some other diatomic molecules, then $-\frac{1}{2}(D_{\mathrm{A-A}})$, the heat of dissociation of A_2 per gram atom of A must be added to the right hand side of equations (5.9) and (5.10).
The main criticisms of these estimates are:
(i) the accuracy of the value assumed for z^* is questionable;
(ii) the classical image law is not quite applicable to distances comparable with lattice spacing; and
(iii) short range quantum mechanical forces of attraction and repulsions are ignored.
However, estimates of heats of adsorptions are in reasonably good agreement with experimental values for the cationic adsorption of alkali metal atom on tungsten.

5.7.3 Quantum Mechanical Approach

Higuchi, Ree and Eyring have introduced a simple quantum mechanical approach to calculate the percentage ionic character of covalent adsorption of bonds and heats of adsorption. This method has already been discussed in chapter 3 (see Valence bond method in page 56).

The results of Higuchi et al. show that bond such as Cs on W and of Na on V are purely ionic, but bonds of Ba with W and Sr with V are ionic with a small covalent character ($C_i^2 = 0.97$ for Ba). For gases on metals, the bonds are predominantly covalent with small ionic character (C_i^2 lying between 0.02 to 0.08). As would be expected in the case of strongly covalent systems, they find bond energies differing little from those obtained by Eley, since the present method offers only an alternative method of calculating $\chi_M - \chi_H$ which makes only a small contribution to the heat of adsorption (q_d).

Metals generally show a pronounced decrease in heat of adsorption with coverage. This has been attributed to various factors such as:
(i) adsorbate-adsorbate interactions,
(ii) change in work function of the metal due to chemisorption,
(iii) alteration of bonding with coverage, and
(iv) inherent non-uniformity of the metal surface.
Adsorbate-adsorbate interactions may be the result of mutual repulsions of parallel oriented dipoles of adsorbate, of short range repulsion forces, or of attraction between adsorbed atoms caused by van der Waals forces. However, these interactions can account for only a small part of the total decrease. For example, the bond moment of a hydrogen atom on tungsten is $\mu = 0.5D$ and the distance of separation of neighbouring dipoles r^* varies between 2.73 and 3.8 Å. Summing the interaction energy ($\mu^2/2r^3$) over the surface at full coverage gives 2-3 kcal/mol compared to an observed decrease of 25-30 kcal/mol. In a similar example, for nickel, the decrease due to dipole repulsion of hydrogen is at most 2 kcal/mol, while the experimental decrease is about 10 times as large. Only in the case of adsorption of alkali metal atoms is the dipole moment large enough for repulsive interaction to form an appreciable fraction of the observed decrease. For example, Cs and Na on W ($\mu = 3.6D$ and $5.4D$ respectively) give calculated decrease of 12 and 10 kcal/mol respectively. Short range forces are generally thought to be too small to give appreciable heat decrease because the chemisorbed particles are not sufficiently near for their electron clouds to overlap. Further, they are generally difficult to evaluate quantitatively. Van der Waals forces

between physically adsorbed molecules are usually observed at higher coverage and lead to the increase of the heat of adsorption roughly equal to the heats of condensation. No accurate estimate of such forces between chemisorbed particles has been made, but they are probably of the same magnitude as those found in physical adsorption.

Many experimental values of heats of adsorption show a drastic decrease at low coverage, whereas changes due to adsorbate-adsorbate interactions would be expected to show large effects only at high coverage ($\theta = 0.35$ or more). Several workers have suggested that the fall in the heat of adsorption can be attributed to ϕ_{f}, the decrease in the work function of the metal. Boudart suggested that $q_d = \frac{1}{2}Ne\Delta\phi$. Mignolet and also de Boer and coworkers gave $q_d = Ne\Delta\phi$.

Helmholtz equation as applicable to covalent adsorption can be written $V = 2pB\theta\mu$, where V is the contact potential which is the potential difference between the adsorbed layer and the metal surface and is therefore equal to $\Delta\phi$, the change in work function, B is the number of adsorption sites per unit area, θ is the fraction of sites covered. Now the contact potential V is the result of electron transfer accompanying covalent adsorption. In desorption, the electron is transferred back to the original position through the potential difference $V = \Delta\phi$. If the adsorbed species is positively charged, i.e., the electron is transferred to the metal, the potential would increase with coverage and favour more and more of the transfer of the electrons back to the ad-atom. If the adsorbed species is negatively charged, the potential as it increases with coverage, would favour more and more transfer of the electrons back to the metal. Thus, in both the cases, heat of desorption should decrease with coverage and will be given approximately by $q_d = Ne\Delta\phi$ which is in agreement with the suggestion of de Boer and Mignolet.

In the special case, where homo-nuclear diatomic molecules adsorb as atoms but desorb as molecule the above equation becomes $q_d = 2Ne\Delta\phi$. Higuchi et al. demonstrated good agreement between observed decreases in the heat of adsorption and calculated decreases in the heat of adsorption for hydrogen on iron and nickel. Dowden suggested that the chemisorption bonds are altered as coverage increases. He argued that some *dsp* hybrid bonds at the surface of a *d*-metal must exist essentially as free, as otherwise the Eley-Stevenson equation for chemisorption considered should contain an endothermal term for the initial breaking of metal-metal bonds. He further postulated that these *dsp* bonds, a reservoir of metal orbitals which are used only to a small extent, is pivotal in the resonance of metal-metal bonds. These orbitals are largely available

for chemisorption. As chemisorption proceeds, the metal orbitals of the free *dsp* type will still be used up. Thus with increasing coverage, the heats of chemisorption will fall because there will be increasing interference with pivotal resonance in the metal until a point is reached at which an endothermic term for breaking of metal-metal bonds must be included in any calculations of heat of adsorption. Although no quantitative verifications are possible, Dowden's theory cannot be categorically rejected.

Finally, there is considerable experimental evidence that an inherent non-uniformity of surfaces is a significant cause of decreasing heat of adsorption with coverage. Indeed, it appears to be the most reasonable cause when the heat decreases rapidly at low coverage.

5.7.4 Participation of d Electrons

The transition metals are distinguished by incompletely filled d-orbitals in their electronic structures. In the case of Ca and Ba, there is evidence to show that some electrons are present in the $3d$ and $5d$ bands in the metal crystals, although their isolated atoms contain no outer electrons in the $3d$ and $5d$ states respectively. Thus, in their crystalline state Ca and Ba resemble the transition metals in possessing a partly filled d-band structure. That the d electrons or orbitals of transition metals are in fact involved in chemisorption is supported by magnetic measurements which show that in a number of cases chemisorption markedly reduces the paramagnetic moment of the metal. Typical data on magnetic susceptibility changes, which were observed for Pd are given in table 5.5.

Table 5.5: Magnetic susceptibility of palladium powder samples.

Mole of $(CH_3)_2S$/g Pd	Percent	Percent	Percent calculated
0.27	10.1	8	13.5
0.23	7.9	6.0	111.5

In table 5.5, the second column shows the percentage change in susceptibility of the solid on chemisorption and third column shows the change in susceptibility of palladium alone after subtracting the diamagnetic susceptibility contribution of the adsorbed dimethyl sulphide from the total change. The last column gives the decrease in susceptibility of the palladium calculated on the assumption that the susceptibility of the surface atoms is reduced to zero. The calculated decrease is larger than the observed decrease, probably because the powder was not completely

free of initial contamination, and so not all the surface atoms were able to participate in chemisorption. However, the experimental change is of the same order of magnitude as would be expected for bonding with unpaired d electrons in the metal.

In going across the periodic table from left to right, there is a gradual increase in electrons available for bonding in the sequences K to Cr, Rb to Mo and Cs to W. There is also a corresponding gradual decrease in the atomic radii and therefore a decrease in M-M bond length. The latter is related to an increase in bond strength and to an increase in the number of bonding electron per atom. When Cr, Mo and W are reached, the atomic radii continue to be roughly constant in the transition series from Cr to Ni, Mo to Pd, and W to Pt. Pauling interpreted this to mean that the bond lengths are constant as are the bond strengths, and so the number of bonding electrons should also be constant. Since Cr has only six available electrons (five $3d$ and one $4s$), he assumed that the six is the common valence for the transition metals with more than six electrons in the d and s orbitals. For Mn, Fe, Co and Ni which have 7,8,9 and 10 $3d + 4s$ electrons respectively, it is postulated that only some (not all) $3d$ electrons may hybridize with $4s$ and $4p$ electrons (unused in bonding) free as atomic orbitals. The ferromagnetic saturation moment of iron, cobalt and nickel is attributed to unpaired non-bonding electrons in the atomic orbitals. On this basis, Pauling deduced the electronic structures of the transition metals.

To illustrate the arguments involved, the hybridized structures of Fe, Co and Ni are deduced as follows:
Iron has 8 electrons outside the argon core. Since its saturation magnetic moment is 2.22 Bohr magneton, it was presumed that it has 2.22 unpaired non-bonding electrons and hence the bonging electrons must be $8 - 2.22 = 5.78$. The non integral number of electrons represent a time average between two or more resonating valence states, in this case 78 percent in valence state 6 and 22 percent in valence state 5. In the pictorial representations given here, the following are used to distinguish between various types of electrons and orbitals: (a) unpaired and paired non-bonding electrons are indicated by arrows (these unpaired electrons account for the magnetic moment), (b) six bonding electrons (unpaired before bonding occurs) are represented by solid circles, and (c) metallic orbitals available for filling with bonding electrons are represented by open circles. The two possible valence states contribute in the ratio of 78:22 giving iron the necessary magnetic saturation moment of 2.22 B.M. This concept leads to a valency of 5.78. The two possible valence

states (shown below) contribute in the ratio of 78:22 giving iron the necessary magnetic saturation moment of 2.22 B.M. This concept leads to a valency of 5.78. The possible structures of iron are:

		$3d$	$4s$	$4p$	Sat. mag. moment
Fe(A) v=6	Ar core	↑↑ ● ● ●	●	● ● ○	2 BM
Fe(B) v=5	Ar core	↑↑↑ ● ●	●	● ● ○	3 BM

Cobalt has nine electrons outside the Argon core. Its saturation magnetic moment is 1.71 BM. The two structures possible each with six bonding electrons are:

		$3d$	$4s$	$4p$	Sat. mag. moment
Co(A) v=6	Ar core	↑↑↑ ● ●	●	● ● ●	3 BM
Co(B) v=6	Ar core	↑↓↑ ● ● ●	●	● ● ○	1 BM

Resonance between the two forms in the ratio 35A:65B will give a saturation moment of 1.71 BM.

Nickel has ten electrons outside the argon core. It has a saturation magnetic moment 0.6 BM.

		$3d$	$4s$	$4p$	Sat. mag. moment
Ni(A) v=6	Ar core	↑↓↑↑ ● ●	●	● ● ●	2 BM
Ni(B) v=5	Ar core	↑↓↑↓ ● ●	●	● ● ○	0 BM

Resonance in the ratio of 30A:70B will give a magnetic moment of 0.6 BM. Evidence from magnetic measurements indicated that Pd, Pt occupying the same group as nickel in the second and third long periods also contain on the average 0.55 to 0.6 unpaired electrons in the atomic orbitals. These elements as well as other metals of the second and third long periods are treated by Pauling in an identical fashion. Developing this concept for the elements following the transition metals, Pauling employed a system based on two observations:
(1) a linear relationship holds between the single bond radius and atomic number for bond of constant hybrid character and,
(2) for an element, the single bond radius is approximately linearly dependent on the d-character of the dsp hybrid bond orbitals.
The d character is defined as the number of bonding d-orbital electrons divided by the total number of bonding electrons and orbitals. Applying these principles, Pauling worked out the possible electronic structures for copper. Copper has eleven electrons outside the argon core.

		$3d$	$4s$	$4p$
Cu(A) v=7	Ar core	$\uparrow\downarrow\uparrow\downarrow$ ●●●	●	●●●
Cu(B) v=5	Ar core	$\uparrow\downarrow\uparrow\downarrow\uparrow\downarrow$ ●●	●	●●○

Resonance between structures A and B in the ratio of 25:75 gives copper a valency of 5.5.

Percent d-character

The percent d character for each metal is calculated from the distributions of the bonding electrons and orbitals and the resonance ratio as illustrated in table 5.6. The percent d-character of metals in first, second and third long periods can be calculated in a similar manner.

Table 5.6: Percent d-character of cobalt, nickel and copper.

Metal	Outer electrons			Resonance ratio	Percent d-character
	$3d$	$4s$	$4p$		
Co(A)	$\uparrow\uparrow\uparrow$ ●●	●	●●●	35	$\frac{35}{100} \times \frac{2}{6} + \frac{65}{100} \times \frac{3}{7} = 39.5$
Co(B)	$\uparrow\downarrow\uparrow$ ●●●	●	●●○	65	
Ni(A)	$\uparrow\downarrow\uparrow\uparrow$ ●●	●	●●●	30	$\frac{30}{100} \times \frac{2}{6} + \frac{70}{100} \times \frac{3}{7} = 40$
Ni(B)	$\uparrow\downarrow\uparrow\downarrow$ ●●●	●	●●○	70	
Cu(A)	$\uparrow\downarrow\uparrow\downarrow$ ●●●	●	●●●	25	$\frac{25}{100} \times \frac{3}{7} + \frac{75}{100} \times \frac{2}{6} = 35.7$
Cu(B)	$\uparrow\downarrow\uparrow\downarrow\uparrow\downarrow$ ●●	●	●●○	75	

There have been various attempts to relate percent d-character and catalytic activity. One of the famous correlations is between the percent d-character and the activity for hydrogenation of unsaturated compounds (see chapter 7). Though these correlations imply certain specific activation of the reactant molecules on the metal surfaces, it should be remarked that the variation in percent d-character among the catalytically active metals is limited and hence these correlations also do have only limited significance. However, that they lead to the understanding of the chemisorption bond is important to remember.

SUGGESTED READING

1. G. A. Somarjai, *Introduction to Surface Chemistry and Catalysis*, John Wiley and sons (1994).

2. B. Viswanathan, S. Sivasanker and A. V. Ramaswamy, Eds. *Catalysis: Principles And Applications*, Narosa Publishing House, New Delhi (2001).

3. B. M. W. Trapnell, *Chemisorption*, Butterworths Sceintific Publishers (1955).

4. R. P. H. Gasser, *An Introduction to Chemisorption and Catalysis by Metals*, Oxford Science Publishers, Clarendon Press, Oxford 1987.

5. A. J. Renouprez, H. Jobic, Eds., *Catalysis by Metals*, EDP Sciences, (1997).

6. G. C. Bond,*Catalysis by Metals*, Academic Press, New York, (1962).

7. V. Ponec, and G. C. Bond, *Catalysis by Metals and Alloys in Stud. Surf. Sci. Catal.*, Elsevier, Amsterdam, 1995.

Chapter 6

Catalysis - General Principles

6.1 INTRODUCTION

A chemical reaction takes place by lowering Gibbs free energy in going from reactants to the products. A reactant or reactants may undergo several reactions each giving a different set of products. The only requirement is that free energy should decrease during the reaction. The role of the catalyst lies in directing the reaction to one of the many thermodynamically permitted products by increasing the rate of only the desired reaction. Let us take decomposition of ethanol as an example. Ethanol may undergo dehydration to ethene, dehydrogenation to acetaldehyde or may give ethyl acetate as shown below:

Reactant	Catalyst	Product
C_2H_5OH	Al_2O_3	$C_2H_4 + H_2O$
"	Reduced copper	$CH_3CHO + H_2$
"	Doped copper	$CH_3COOC_2H_5 + 2H_2$

All the three reactions proceeds with lowering of free energy. In the absence of a catalyst, all the products will be present. But the specific catalyst directs the reaction to a particular set of products by increasing the rate of that reaction in preference to others. In fact, more than one of the reactions may take place in presence of one catalyst. The main thrust of research in catalysis is to find out a catalyst that will maximize the rate of the desired reaction without affecting the other reactions.

The importance of catalysis in chemical industry is unquestionable.

Many reactions that are thermodynamically possible may take place at an extremely slow rate and some times fortunately so. Nitrogen and oxygen combines in the atmosphere giving NO. Had this reaction been fast, the atmosphere would have no oxygen. Fortunately for us, the reaction is extremely slow. But in the manufacture of nitric acid, it is required that the reaction occurs very fast and here technology is dependent on a good catalyst. There is hardly a industrial chemical process without a catalyst and more than eighty per cent of the heavy chemicals are produced by catalytic process.

The actual catalytic process is extremely complex and it will be wrong to assume that catalysis has been well understood. As a result of colossal experimental research, many models have been proposed to explain the phenomenon of catalysis. Each model appears to work well for certain reactions, but fail to explain others. There is no general theory that can explain every catalytic reaction, but there are some common features in all of them.

Heterogeneous catalytic reaction involves the following steps:
1. Diffusion of the reactant from its bulk to the surface of the catalyst;
2. Chemisorption of the reactant on the catalyst surface;
3. Chemical reaction on the surface;
4. Desorption of the reaction products from the surface;
5. Diffusion of the product molecules from near the surface into the bulk.

Since a chemical reaction involves breaking and formation of chemical bonds, there must be a stage at which the bonds to be broken are sufficiently weak but still exists and the bonds to be formed are not yet complete. This stage is similar to the transition state of a homogeneous reaction with the exception that the transition state now includes the catalyst. We know enough about the reactants and the products, but very little of this transition state. Knowledge of the transition state is very important for understanding the energetics of a surface reaction.

6.1.1 Thermodynamic Considerations

For a chemical reaction to take place, free energy of the reaction should be negative. As the products accumulate, free energy of the reaction becomes less and less negative and finally it becomes zero at equilibrium when no further reaction apparently occurs. Actually the reaction does not stop, but the forward and the reverse reactions take place at the same rate at equilibrium and hence no further change in composition is noticed. This amounts to saying that the amount converted is maximum at equilibrium at a given temperature.

Free energy of a reaction

$$\Delta G_r = \Delta H_r - T\Delta S_r \tag{6.1}$$

where ΔH_r and ΔS_r are the enthalpy and entropy of the reaction. For a reversible reaction,

$$\Delta G_r = -RT \ln K \tag{6.2}$$

where K is the equilibrium constant. The presence of the catalyst does not change K and hence the maximum yield at equilibrium is the same irrespective of whether a catalyst is present or not. The catalyst accelerates the rates of both forward and backward reactions and brings the system to equilibrium quickly. This helps in reducing the time needed to get a certain amount of the product.

In a catalytic reaction, one is concerned with the energy state of the reactants, products and the transition state involving the reactant and the catalyst. Let us consider the reaction:

$$\mathrm{A} + \mathrm{B} \rightarrow \mathrm{C} + \mathrm{D}$$

In case of a catalytic reaction, it should be written as

$$\mathrm{A} + \mathrm{B} + \mathrm{M} \rightarrow [\mathrm{ABM}]^{\ddagger}$$

$$[\mathrm{ABM}]^{\ddagger} \rightarrow \mathrm{M} + \mathrm{C} + \mathrm{D}$$

where M is the catalyst and $[\mathrm{ABM}]^{\ddagger}$ is the transition state. If G_1 and G_2 are the free energy of the reactant and the product respectively, free energy of the reaction is $\Delta G_r = G_2 - G_1$. This, however, does not include the free energy of the transition state. We shall demonstrate here how the free energy of the transition state does not influence the thermodynamics of the reaction.

Since adsorption is always exothermic, we can write for an endothermic reaction

$$\mathrm{A} + \mathrm{B} + \mathrm{M} \rightarrow [\mathrm{ABM}]^{\ddagger} + \Delta H_{\mathrm{ad}}$$

$$[\mathrm{ABM}]^{\ddagger} \rightarrow \mathrm{C} + \mathrm{D} - \Delta H_r - \Delta H_{\mathrm{des}}$$

and for an exothermic reaction,

$$\mathrm{A} + \mathrm{B} + \mathrm{M} \rightarrow [\mathrm{ABM}]^{\ddagger} + \Delta H_{\mathrm{ad}}$$

$$[\mathrm{ABM}]^{\ddagger} \rightarrow \mathrm{C} + \mathrm{D} + \Delta H_r - \Delta H_{\mathrm{des}}$$

where ΔH_{ad} is the heat of adsorption of the reactant and ΔH_{des} is the heat of desorption of the product. Normally we assume that $\Delta H_{\text{ad}} = \Delta H_{\text{des}}$ and for the reaction only ΔH_r remains which is same for both catalysed and un-catalysed reactions. But the heat of adsorption is for the reactant and that of desorption is for the product and they are not equal. For a reversible reaction, we shall see that the heats of adsorption and desorption get canceled. If we take $\Delta H'_{\text{ad}}$ is the heat of adsorption and $\Delta H'_{\text{des}}$ is the heat of desorption for the reverse reaction, then,

$$\Delta H_{\text{ad}} = -\Delta H'_{\text{des}}$$

$$\Delta H'_{\text{ad}} = -\Delta H_{\text{des}}$$

Thermal effects of adsorption and desorption cancels out and the catalyst has no effect on the equilibrium. Since the only additional terms in the catalytic reaction as compared to the simple reaction are the energies of adsorption and desorption, nullifying their effect leaves the thermodynamics of the reaction unaffected in the presence of a catalyst. This is the general conclusion.

The above thermodynamic calculation that does not consider the non-equilibrium situation of the reactant, is not always sufficient. When hydrogen is adsorbed on the surface of platinum, hydrogen is present on the surface as atomic hydrogen that participates in reactions like catalytic hydrogenation. At the same temperature, there is hardly any atomic hydrogen in the gas phase. This non-equilibrium concentration of hydrogen atom on the surface arises from the use of the heat produced by adsorption.

Semenov and Shilov[1] noticed that the energy of activation E of many exothermic reactions between radicals and molecules is related to the heat of the reaction Q as

$$E = 11.5 - 0.25Q \tag{6.3}$$

The explanation is that a part of the heat of the reaction is utilized in activating the reactant molecule. Thus, utilization of the energy of the reaction by the system may significantly change the energy state of the reactant molecules.

When several products are possible, a catalytic reaction does not necessarily lead to the product that is most stable from usual thermodynamic consideration. This gives the possibility of selecting a catalyst for

[1]N. N. Semenov and A. E. Shilov, *Kinetika i Kataliz*, 6, 3 (1965).

getting the most desired one from a number of possible products. Let us consider the reaction between carbon monoxide and hydrogen between $300 - 400^o$ C.

Reactant	Catalyst	Product
	Cobalt	Paraffin
$CO + H_2$	Iron	Olefins
	ZnO+CoO	Methanol

Of these reactions, conversion to methanol takes place with the highest change of free energy, but it is possible to produce paraffin selectively using cobalt as catalyst.

Equally important is the orientation of the molecule in the adsorbed state in determining the course of a reaction. A simple molecule like CO may have several orientations in the adsorbed state. The nature of the product, to a large extent, depends on the orientation of the adsorbed molecule on the surface. Understanding the nature of the adsorbed species is of great importance in understanding catalysis.

Based on experimental evidence, some models have been proposed to explain catalysis. Some are based on the structure of the catalyst while others rely on their electronic property or acidity. Far from being universally applicable, these models have made the selection of a catalysis much easier. These will be discussed in the next two chapters.

6.1.2 Types of Solid Catalysts

A wide variety of materials are used as catalysts. Most common are metals, metal oxides and solid acids. Some metal sulphides too are used as catalysts as are some salts.

Metal and metal alloy catalysts have found application in hydrogenation and dehydrogenation. Semiconducting oxides are used as oxidation-reduction catalysts. Insulator oxides are generally used in dehydration and polymerization. Many salts and solid acids have found use in catalytic cracking, polymerization and isomerization.

Activity of a catalyst is defined as the amount of the product formed on unit mass of the catalyst in unit time. Often, the percent conversion of the reactant is used as a measure of catalytic activity. Catalytic activity is closely linked to the surface area available for adsorption. Metals have low surface area. In order to enhance surface area, metals are sometimes subjected to corrosive treatment so that they develop cracks and pores as in Raney nickel catalyst, or they are precipitated as extremely fine particles as in Urushibara catalysts.

In order to increase the surface area of a metal or that of a low surface metal oxide, they are often deposited on the surface of a solid with high surface area that is called the support. Alumina and silica are the most commonly used supports. Although catalytically inactive in most cases, a support may sometime act as a secondary catalyst.

Some compounds, when added in small quantities to the catalyst, enhances the catalytic activity many fold. Such compounds are known as promoters. Addition of 14 percent Al_2O_3 to nickel catalyst for conversion of CO to methane increases catalytic activity fifteen times. Potassium salts are added to V_2O_5 catalyst of SO_2 oxidation. The promoter may or may not have catalytic activity of its own. Promoter effect is related to the stabilization of the active surface or enhancement of the active centres on the surface. If the promoter itself has some catalytic activity, the catalyst is called a mixed catalyst. Many if of the important industrial catalysts are mixed catalysts. All these will be discussed elsewhere under Catalyst Preparation.

6.1.3 Catalyst Deactivation

No catalyst can retain its activity forever. Even the most stable among them gradually lose their activity with time. All catalysts have a finite life that may be hours, months or even years, but at some stage they will not be active any more. There are several reasons for this. The reason may be 1) chemical, 2) thermal or 3)mechanical.

Chemical Cause of Deactivation

There are two main chemical reasons that can bring about deactivation of a catalyst. When the catalyst surface reacts with a compound present as impurity in the reactant, it is known as poisoning of the catalyst. Presence of some chemicals in the reaction mixture retards the rate of certain chemical reactions and even stops the reaction completely. Such chemicals are termed catalyst poisons. Poisons have some specificity. Air, that activates a platinum catalyst used in oxidation, is a poison for some non-noble metal catalysts. As_2O_3 is a poison for platinum catalyst of hydrogenation, but does not affect the same catalyst when used for the oxidation of hydrogen peroxide. Only a small amount of the poison is sufficient to foul a catalyst. They get preferentially adsorbed on the active sites of the catalyst thus blocking them. Nickel, for example, has a strong affinity for sulphur and even traces of sulphur can poison a nickel catalyst.

It has been observed in many cases that during initial poisoning, the activity falls linearly with the concentration of the poison following a

relation

$$A = A_0 - \alpha\Gamma \tag{6.4}$$

where A_0 is the initial activity, A is the activity after poisoning, Γ is the concentration of the poison and α is a constant. In this connection, Maxted et al.[2] had made some interesting observation. This is shown in figure 6.1.

The reaction studied by them is hydrogenation of cyclohexene and the poison used was dimethyl sulphide. As the amount of the poison was increased, the consumption of hydrogen which is a measure of activity of the platinum catalyst, decreased linearly. The higher curves represent larger amount of the catalyst. α remains constant if the same poison is used for different amounts of the same catalyst under identical reaction conditions.

Figure 6.1: *Effect of* $(CH_3)_2S$ *on the activity of platinum catalyst in the hydrogenation of cyclohexene.*

During a chemical reaction, the catalyst may undergo structure change. It is known that the Fe_3O_4 ammonia synthesis catalyst loses its activity due to re-crystallization of the iron oxide. Addition of a small amount of alumina stabilizes it by forming of $FeAl_2O_4$. Again $ZnO.Cr_2O_3$ catalyst used in methanol synthesis from water gas gets reduced to zinc and thus becomes inactive.

[2]E. Maxted, K. Moon and E. Overlanger, *Discuss. Faraday Soc.*, 135 (1950)¿

Coking of the catalyst is another cause of deactivation. During reactions of unsaturated hydrocarbons or ring compounds, some high molecular weight carbon compounds are formed that block the surface. Two types of cokes, soluble (C/H<1) coke and insoluble coke (C/H$\geq$ 1), have been identified. Formation of coke depends on the operating conditions of the reactor. In processes like hydrodesulfurazition, when the reactor is operated at comparatively low temperature and high hydrogen pressure, the catalyst experiences low coking and has a long life. On the other hand, catalysts used in hydrocarbon cracking undergo deactivation due to coking in a few seconds because of the severe conditions (near atmospheric pressure and high temperature).

Another chemical cause of catalyst deactivation is the removal of the volatile compound formed by reaction between the catalyst and the reactant. Nickel catalyst loses its activity in reaction with CO under reducing conditions due to the loss of nickel as volatile nickel carbonyl.

Thermal cause of deactivation

During an exothermic catalytic reaction, there may be tremendous local heating effect. This may bring about a change in the chemical composition of a catalyst. In the case of a supported metal oxide, the support and the active phase may react forming a new compound on the surface that may not be an active catalyst. Sintering of the catalyst too may take place severely reducing the surface area of the catalyst. The active phase in many supported metal catalysts are nano-size metal particles. These may migrate along the surface forming bigger metal particles that may cause loss of activity. The support itself may undergo sintering in some cases.

Mechanical cause of deactivation

Industrial reactors operate under severe conditions. In a fixed bed reactor, the catalysts that are generally used as pellets of different shape and size, may crumble under the high pressure. Iron molybdate catalyst of oxidation of methanol to formaldehyde is used in the form of ring tablets. They break up because of the formation of iron and molybdenum oxide. In the fluidized bed reactor used in cracking, the catalyst particles undergo constant collision with each other and get powdered due to attrition and are blown out of the reactor such that additional catalyst is to be added periodically.

Prevention of deactivation

Deactivation of a catalysts may be reversible or irreversible. In the first case, it is possible to regenerate the catalyst. The method of regen-

eration may be as varied as the cause of deactivation. If the catalyst is a metal oxide that has lost activity due to its reduction, it may be regenerated simply by heating in air. If a metal catalyst loses activity due to its oxidation, its activity may be restored by heating in a stream of hydrogen. Alumina-silica catalysts used in cracking of hydrocarbons loses its activity due to coke formation and can be regenerated by burning off the coke. In many cases, it may not be possible to restore the catalytic activity. If such spent catalysts have costly metals, the metals are recovered and reused for making fresh catalysts.

6.2 REACTION KINETICS

Both catalyzed as well as un-catalyzed reactions follow the Arrhenius equation

$$k = A \exp\left(-\frac{E}{RT}\right) \tag{6.5}$$

where k is the specific reaction rate, A is the pre-exponential factor and E is Arrhenius energy of activation. The influence of the catalyst can be described by the reaction path shown in figure 6.2. Here, the reaction path is shown for an exothermic reaction. In order to undergo a chemical change, the reactant molecules should have energy higher than the energy of activation.

We have already listed the various steps of a reaction catalyzed by a solid. Ignoring the diffusion steps, three steps still remain. These are: 1) chemisorption of the reactant that may need some energy of activation (E_{ad}), 2) reaction on the surface that includes formation of an activated complex or transition state with the surface atoms, and 3) desorption of the product molecule that will always have some energy of activation (E_{des}).

In a simple reaction, formation of the active complex would require an energy of activation (E_{hom}) that is the difference of the enthalpy of the activated complex and that of the reactant. In the presence of a solid catalyst, the activated complex includes the surface atoms. Energy of activation is E_{het} that is determined experimentally. The true energy of activation of a heterogeneous catalytic reaction, however, is not E_{het}, but E_r which is equal to the sum of E_{het} and enthalpy of adsorption of the reactant ΔH_{ad}. Enthalpy of the reaction ΔH_r is not affected by the catalyst. As shown in the figure, E_{het} is significantly lower than E_{hom} by $\Delta H_a^{\ddagger}$.

Specific reaction rate of the catalyzed reaction can be expressed as

$$k_{\text{het}} = B \exp\left(-E_{\text{het}}/RT\right) \tag{6.6}$$

where B is the new pre-exponential factor.

Ratio of the two specific rates

$$\frac{k_{\text{het}}}{k} = \frac{B}{A}\exp\left(-\frac{E_{\text{hom}} - E_{\text{het}}}{RT}\right) = \frac{B}{A}\exp\left(-\frac{\Delta H_a^{\ddagger}}{RT}\right) \tag{6.7}$$

Both energy of activation and the pre-exponential factor for a catalytic reaction may be different from the non-catalyzed one. Changes in either of these may affect the rate of the reaction.

Figure 6.2: *Reaction path for a non-catalytic as well as that for a solid-catalyzed reaction.*

6.2.1 The Rate Determining Step

When we study a catalytic reaction in the laboratory, we try to find out how good is the catalyst for a given reaction in terms of both its activity and product selectivity. When we obtain the experimental results, can we be sure that the conversion data are truly representing these properties of the catalyst? Because of many complications, the true reaction rate may be masked by other effects. There are several steps involved in going from the reactant to the product for a heterogeneous catalytic reaction.

The overall rate of the reaction will be controlled by the rate of the slowest step because rate of all the steps are not equal. The reaction itself involves adsorption of the reactants, the chemical conversion and desorption of the products. If the rate of any of these three steps is the slowest, the reaction is said to be kinetically controlled. On the other hand, if diffusion of the reactant to the surface or that of the product away from the surface is the slowest step, the reaction is said to be in the diffusion control regime. There are several experiments that can verify whether the process kinetically controlled or it is diffusion controlled.

Diffusion needs a rather small energy of activation $(1 - 2$ kCal/mol), whereas the activation energy of the reaction is much higher. This means that the reaction rate increases much faster as compared to the diffusion rate with the rise of temperature . That is why high temperature chemical processes are generally controlled by the rate of diffusion. The term diffusion control does not mean that the actual reaction is taking place faster than diffusion. If diffusion is slow, the slow rate of supply of the reactant to the surface, or removal of the product from the surface will slow down the reaction rate too. Similarly, when the reaction is kinetically controlled, the slow rate of the surface reaction will slow down the rate of diffusion because the surface can not accommodate more molecules. This will lead to a steady state. The measured rate generally will be equal to the rate of the slowest step.

Figure 6.3: *Variation of* $\log k$ *with reciprocal temperature.*

Effect of temperature on $\log k$ of a catalytic reaction is shown in figure

6.3. In the low temperature region, the plot is very steep meaning its activation energy is high. Reaction rate is slow and this is the kinetically controlled region. Next, there is an intermediate region, in which the diffusion and reaction rates are comparable. This region is normally absent in a nonporous catalyst. The near flat part of the plot indicates low activation energy. In this high temperature region, reaction rate is too fast to be rate controlling and this is the diffusion control region.

Knowledge of the diffusion process (mass transfer) is very important in industrial catalysis. The subject of mass transfer and heat transfer will be discussed separately in a later chapter. The catalyst, however, is directly linked with the rate of the chemical reaction. In this section, we shall assume that the diffusion rates are high and the reaction is kinetically controlled and derive mathematical expressions for the reaction rate. Knowledge of the rate expression is helpful in improving the catalyst and also in understanding the mechanism of a reaction.

6.2.2 Rate Expressions

Rate of a chemical reaction on the surface of a solid is directly proportional to the concentration of the adsorbed molecule. The latter can be found by using the various adsorption isotherm equations. Generally, Langmuir isotherm equation is used and the derived expressions are said to follow Langmuir-Hinshelwood mechanism.

Let us consider a reaction

$$A \longrightarrow B$$

For a heterogeneous catalytic reaction, rate as expressed as the amount reacted in unit time per unit surface. Therefore, rate r is expressed as

$$r = -\frac{d[A]}{dt} = \frac{d[B]}{dt} = k'\theta_A \tag{6.8}$$

where θ_A is the fraction of the surface covered by $A$and k' is the true rate constant. Assuming the reactants and the products to be gases, concentrations are replaced by partial pressures p_A and p_B. Hence,

$$r = -\frac{dp_A}{dt} = \frac{dp_B}{dt} = k'\theta_A \tag{6.9}$$

If the product B gets adsorbed at the same sites as A, then

$$\theta_A = \frac{b_A p_A}{1 + b_A p_A + b_B p_B} \tag{6.10}$$

Substituting this in the rate equation,

$$r = \frac{k' b_A p_A}{1 + b_A p_A + b_B p_B} \tag{6.11}$$

This is the general rate expression for a reaction A going to B according to Langmuir-Hinshelwood model. Similar expressions can be written for reactions of other types involving more than one reactant or product.

Continuing with the above reaction, suppose both A and B are weakly adsorbed. In that case, $(b_A p_A + b_B p_B) \ll 1$ rate becomes

$$r = k' b_A p_A = k p_A \tag{6.12}$$

where the new constant k is known as the apparent rate constant. By studying the dependence of rate r on the p_A, one can find out the apparent rate constant. In order to find out the true rate constant k', one should know b_A or the heat of adsorption of A.

If adsorption of A is moderately strong but B is weakly adsorbed, the rate equation becomes

$$r = \frac{k p_A}{1 + b_A p_A} \tag{6.13}$$

in which case the reaction will have a fractional order. The apparent rate constant can be found out by appropriate curve fitting.

In the case when A is strongly adsorbed and B is adsorbed weakly, the quantity $(1 + b_B p_B) \ll b_A p_A$. The rate equation becomes

$$r = k' \tag{6.14}$$

In this case, the experimentally determined rate is the true rate constant.

In practice, different reaction mechanisms are assumed and the corresponding rate expressions are derived. These equations are then tested experimentally to ascertain the correct mechanism. It has been observed that the same reaction may follow different rate expressions depending on the catalyst, reaction temperature and partial pressure of the reactant. This is illustrated with the example of NO_2 decomposition as shown in the next table (data taken from Prichard and Hinshelwood[3].). Many more examples of this kind have been sited in the literature.

[3]C. R. Prichard and C. N. Hinshelwood, *Proc. Royal Soc.*, 108, 211 (1925), and C. N. Hinshelwood and C. R. Prichard, *J. Chem. Soc.*, 327 (1925).

Catalyst	Rate expression	E, kCal/mol
Au	$kp_{\mathrm{NO_2}}$	29.0
Pt	$\frac{kp_{\mathrm{NO_2}}}{1+bp_{\mathrm{O_2}}}$	32.5

Sometimes, a gaseous molecule may react with another adsorbed molecule in which case the rate does not depend on the partial pressure of the molecule that reacts from the gas phase. Such reactions are said to follow Rideal-Eley model. As an example, let us assume a reaction when an adsorbed molecule B reacts with a molecule A in the gas phase to give C. We can represent the reaction as

$$A_g + B_s \longrightarrow C_g$$

Here the subscripts s and g stand for adsorbed state and gaseous state respectively. The rate expression is

$$r = kp_A\theta_B = \frac{kp_Ab_Bp_B}{1 + b_Bp_B} \tag{6.15}$$

because only the reactant B is present on the surface. If either p_B or b_B or both are large,

$$r = kp_A \tag{6.16}$$

which shows that the reaction is first order with respect to A and is of zero order with respect to B.

We have seen that the specific reaction rate is related to Arrhenius activation energy as

$$\ln k = \ln A - \frac{E_{\mathrm{het}}}{RT} \tag{6.17}$$

Differentiating with respect to T,

$$\frac{d\ln k}{dT} = \frac{E_{\mathrm{het}}}{RT^2} \tag{6.18}$$

We have already seen that the experimentally determined specific rate k is related to the true rate constant k' such that $k = k'b_A$. True rate constant k' also follows the Arrhenius equation. Hence,

$$\frac{d\ln k'}{dT} = \frac{E_r}{RT^2} \tag{6.19}$$

when E_r is the true energy of activation of the reaction. But

$$k = k'b_A = A\exp\left(\frac{-E_r}{RT}\right)(b_A)_0\exp\left(\frac{Q_A}{RT}\right) \tag{6.20}$$

where Q_A is the heat of adsorption of A. This gives

$$\ln k = -\frac{E_a}{RT} + \frac{Q_A}{RT} + \text{constant} \tag{6.21}$$

Differentiating the above equation with respect to T, we get

$$\frac{d \ln k}{dT} = \frac{E_r - Q_A}{RT^2} \tag{6.22}$$

Comparing equations (6.17) and (6.21), we see that

$$E_{\text{het}} = E_r - Q_A \tag{6.23}$$

When the product is strongly adsorbed, it can be shown that

$$E_{\text{het}} = E_r - Q_A + Q_B \tag{6.24}$$

It is not easy to know the true activation energy of heterogeneous catalytic reaction since it needs the knowledge of the heats of adsorption. Even when the heats of adsorption have been measured, it should be remembered that they change with surface coverage since most catalytic surfaces are heterogeneous in nature.

6.3 LABORATORY REACTORS

The main use of a laboratory reactor lies in obtaining accurate data on the rate of a catalytic reaction occurring in the kinetically controlled region. It tries to eliminate the effect of heat and mass transfer. These reactors are generally operated under constant temperature conditions. It becomes imperative to use a small catalyst bed (1-2 cm in length, or even smaller) for accurate temperature control. Assuming continuous flow of the reactant and steady rate, we can write

$$r dw = F dx \tag{6.25}$$

where r is the rate of conversion of the reactant (mol or mass of the reactant converted per unit mass of the catalyst per unit time), x is conversion, w is the mass of the catalyst and F is the number of mol of the reactant fed in unit time. Writing in the integral form,

$$\frac{w}{F} = \int_{x_0}^{x_t} -\frac{1}{r} dx \tag{6.26}$$

Here, x_0 and x_t are the conversion at 0 and w mass of the catalyst respectively. r can be found out by differentiating a plot of x against

w/F. When this expression is used in obtaining rate, the reactor is called an integral reactor. It should be noted that the partial pressure of the reactant changes while it passes through the catalyst bed due to its conversion. It is highest when it enters the catalyst bed and lowest when it leaves it. If the conversion is maintained at a very low level, the partial pressure of the reactant may be assumed to be nearly constant throughout the catalyst bed. One can then use equation (6.25) to get rate. This is the rate obtained in the integral reactor when $w/F \rightarrow 0$. This is known as the initial rate and can be used as a measure of the intrinsic activity of the catalyst.

Laboratory reactors may be 1) Flow reactors or 2) Static reactors. Each type have many variations.

Figure 6.4: *A simple tubular flow reactor.*

6.3.1 Flow Reactor

A simple flow rector is a cylindrical tube of stainless steel, glass or quartz. The tube length and diameter is decided by the amount and particle size of the catalyst. For good isothermal condition, the catalyst amount should be small since smaller diameter and length of the catalyst bed makes it easy to maintain constant temperature. For maintaining plug flow condition, the ratio $d_b/d_p > 6$ and $\ell_t/dp > 100$ where d_b is the diameter of the catalyst bed, d_p is the average diameter of the catalyst particle and ℓ_t is the length of the catalyst bed. The tube is generally held vertically. A jacket or a thermo-well is provided for placing a thermocouple near the catalyst bed without actually coming in contact with

the catalyst. A flow reactor is schematically shown in figure 6.5.

The reactor is placed inside a tubular furnace such that the catalyst bed lies at the middle of the furnace. The temperature is controlled by an accurate temperature controller. Gaseous reactants from cylinders are fed through a mass flow controller. Liquid reactants are pumped using a syringe pump or a peristatic pump, vaporized in a preheater and carried into the reactor by a inert carrier gas. A simple flow reactor is shown in figure 6.4.

Such a reactor can be used both in the integral and the differential modes (at very low conversion). The differential reactor provides the rate directly without resorting to any graphical or analytical solution. But the chemical analysis should be precise since very low conversion is used, a problem that has been solved by using precision gas chromatographs.

Figure 6.5: *A recirculation reactor.*

A steady state recirculation reactor can overcome some of the difficulties of a simple flow reactor. A simple flow reactor is a single pass reactor meaning the reactant passes through the catalyst bed only once. In a recirculation reactor, the reactant after passing through the catalyst bed is recirculated after removing a small amount of it and adding a small amount of the reactant to make up for the amount converted. Thus, isothermal conditions are maintained more efficiently and the rate will be free from the possibility of being controlled by mass transfer. The circulation rate is maintained 10-15 times faster than the feed rate which, however, can be varied so that mass transfer is fast enough. At low conversion, rate of the reaction is given as

$$r = \frac{y_0 - y_f}{w/F} \tag{6.27}$$

where y_0 and y_f are the mole fraction of the reactants and the entry and

the exit respectively. It is important that the circulation pump does not contaminate the reactant.Chambers et al.[4] has described the design of a contamination-free recirculation pump.

Static reactor

In this case, the reactor is a closed system consisting of the catalyst and the reactant. Concentration of the reactant is measured form time to time either *in situ* or by removing a small amount from the system. If the reactants and the products are all gaseous and the reaction proceeds with a change in volume, the rate can be followed simply by following the change in pressure. Rate is expressed as

$$r = \frac{M}{w}\frac{dx}{dt} \tag{6.28}$$

where M is number of mol of the reactant, W is the mass of the catalyst, x is the fraction converted and t is time.

The main difficulty in this case is that the concentration of the reactants may be considerably higher on the surface than in the gas phase where the measurement is made. This can happen because of the slow rate of diffusion. This can be overcome by stirring the reactor vigorously if the reactants are liquids, or by using a recirculation pump in case of gaseous reactants. Chambers and Boudart[5] described the design of a recirculation pump. Carberry[6] designed a reactor in which large catalyst particles are placed in baskets that form the wings of a central rotating stirrer. In this case, the dead space is large and it is not easy to seal the system. Such basket type reactors can be used both in the flow as well as in the static mode.

Pulse reactor

A pulse reactor is a microreactor which takes a small amount (0.2-0.5 g) of the catalyst. Flow of an inert carrier gas, sometimes mixed with one of the reactants (hydrogen in case of a hydrogenation reaction), is maintained through the catalyst. The reactor is fitted with a valve or an injection port through which a known quantity of the reaction mixture or the second reactant can be introduced. The outlet is connected to a gas chromatograph for chemical analysis. A pulse reactor is shown in figure 6.6.

[4]R. P. Chambers, N. A. Diugharty and M. Boudart, *J. Catal.*, 4, 625 (1965).
[5]R. P. Chambers and M. Boudart, *J. Catal.*, 5, 517 (1966).
[6]J. J. Carberry, *Ind. Eng. Chem.*, 56, 39 (1964).

A pulse reactor is convenient as it can quickly provide conversion data and can be used for initial screening of a large number of catalysts. It is useful in carrying out specially designed experiments in which reactants are pulsed in different sequences. It is, however,not suitable for kinetic studies.

Figure 6.6: *Micro pulse reactor.*

Eliminating heat and mass transfer effects

In order to get the true rate data that would indicate the activity of the catalyst, it is necessary to operate the laboratory reactor in the kinetically controlled regime so that the rate is not influenced by mass and heat transfer effects.

Heat and mass transfer effects that may influence the measured reaction rate arises from temperature and concentration gradients 1) within a catalyst particle (intra-particle), 2) between the catalyst surface and the bulk of the reactant (interphase), and 3) from one region to another within the catalyst bed (inter-particle). Care should be taken to see that none of these influence the measured rate.

Intra-particle diffusion effect can be tested by varying the particle size of the catalyst. The absence of any dependence of rate on the particle size ensures that intra-particle diffusion does not effect the rate. The effect of heat and mass transfer in the interphase region is tested by checking the dependence of flow rate (F) on conversion at constant space velocity (w/F) by carrying out such tests over a wide range of flow rates.

Inter-particle heat transfer effect is minimized by diluting the catalyst with inert materials such as α-alumina or glass beads. Axial con-

centration gradient is minimized by maintaining plug flow condition. To achieve this, length of the reactor tube (L) should be such that by $\frac{L}{d}$ ratio is greater than 30, where d the diameter of the reactor tube. Heat and transfer effects in catalysis will be discussed in a separate chapter.

SUGGESTED READING

1. Ashmore, P.G., *Catalysis and Inhibition of Chemical Reactions*, Butterworths, London.
2. Thomas, J. M. and Thomas, W. J., *Introduction to the Principles of Heterogeneous Catalysis*, Acad. Press, London and New York, (1967).
3. Bond, G. C., *Catalsis by Metals*, Acad. Press, London and New York, (1962).
4. R. Hughes, *Deactivation of catalysts*, Acad. Press, London, 1984.
5. L. L. Hegedus and R. W. McCabe, *Catalyst Poisoining*, Marcel Dekker, New York, 1984.
6. Doraiswamy, L. K. and Tabjl, D. G., *Laboratory Catalytic Reactors*, in *Catal. Rev. Sci. Engg.*, (Ed. E. Heinemann), Marcell and Dekker, New York, 1969.

Chapter 7

Theory of Catalysis by Metals

A wide variety of solids have been used as catalysts. These are metals, oxides of transition metals, oxide of nonmetals and also some special types of solid materials. There is no single theory that can explain the catalytic behaviour of all these solids. The commonly accepted idea is that the entire surface is not catalytically active. There are some sites on the surface at which the reactant molecules are chemisorbed in order to undergo chemical conversion. These sites are known as active centres. The active centre may be a single surface atom or a group of atoms. That the entire surface is not active in catalysis is evident from the behaviour of a catalyst poison. It has been found that a poison in concentration far less than needed for complete coverage of the surface, is sufficient to completely deactivate the catalyst. This clearly indicates that the poison is preferentially adsorbed at the active centres making them unavailable for the reactant molecules. If it has no preference for the active centres, it will not be a poison for the catalyst.

A good catalyst should have a large concentration of the active centres per unit surface. The concept of active centre has led to define catalytic activity as turn over number or turn over frequency which is the number of molecules reacting per active centre per second.

Theories of heterogeneous catalysis tries to identify the nature of the active centres based on the structure of the surface or the electronic property of the surface. Because of their basic differences as solids, catalysts are classified as metals, semiconductors and insulators. Attempts have been made to develop separate theories of catalysis on the basis of this

classification. In this chapter, we shall consider the theories of catalysis by metals.

7.1 GEOMETRIC FACTOR IN CATALYSIS

Catalytic properties of metals are linked variously either to the structure of the metal or to their electronic property. Because structure is determined by the size of the metallic radius which also determines its bond strength to some extent, there is little doubt that the two are not unrelated. We shall first discuss the importance of structure or the so called geometric factor in catalysis.

7.1.1 Balandin's Multiplet Theory

The catalyst, as it is known, facilitates the breaking of a set of chemical bonds and the formation of another set of bonds during a reaction. Balandin based his argument on the fact that the atoms should come close to each other in order to form a chemical bond between them. The function of the surface atoms of a catalyst is to bring these atoms (between which bonds are going to be formed) close to each other. The the surface atoms achieve this by drawing them simultaneously close to the surface atoms themselves. This would require that the reactant molecule is adsorbed on the surface through more than one of its atoms. In other words, Balandin's model[1] assumes a multi-point adsorption involving more than one atom of the reactant molecule and an equal number of surface atoms. Atoms of the molecule between which rearrangement (breaking or formation) of bonds takes place are called the index group. In order to achieve multi-point adsorption of the right kind, arrangement of the index group should have a geometric relationship with the arrangement of the atoms of the surface to which they will be linked.

The simplest reaction, according to this model, is a doublet reaction that involves a two-point adsorption of the reactant involving a pair of surface atoms. This is shown in figure 7.1.

In the above scheme. A, B, C and D are index group atoms that may be linked to substituent groups that are of minor importance in this scheme. The active centres on the surface are shown by small circles. Intervention of the surface atoms weakens the $A-B$ and $C-D$ bonds leading to the formation of the active complex that includes the surface atoms. The active complex may go to form $A-C$ and $B-D$ or may revert back to the reactants. The $A-B$ and $C-D$ bond distances and

[1] A. A. Balandin, *Adv. Catal.*, 10, 96 (1958).

those between the active centres should have a close relationship for easy formation of the active complex.

Figure 7.1: *Chemical reaction through a doublet formation.*

Depending on how it is chemisorbed, the same molecule may undergo different reactions. The two modes of adsorption of the ethanol molecule, one leading to dehydrogenation and the other to dehydration have been illustrated in figure 7.2.

Figure 7.2: *Two different ways of adsorption of the ethanol molecule leading to (a) dehydrogenation and (b) dehydration.*

The bond distance between the index groups in these two types of adsorption are different and so should be the distance between the surface atoms in order that the formation of the active complex is facilitated.

The geometric concept was most successfully applied by Balandin to explain the dehydorgenation of cyclohexane to benzene. A molecule of cyclohexane can be adsorbed on the surface along its edge involving two atoms (doublet mechanism) or the cyclohexane molecule may sit on the surface flat using all six carbon atoms (sextet formation) that is possible if six surface atoms are present forming an equilateral triangle as shown figure 7.3. Such orientation of the surface atoms is available on the close packed planes like the (111) plane of a fcc metal or the base plane of a hexagonal metal. The planar configuration of cyclohexane is not the most stable one and the molecule in this position will not be stable.

The metal atoms should facilitate the formation of carbon-carbon π bond and removal of six hydrogen atoms, one from each carbon to form three molecules of adsorbed hydrogen. This would require a optimum

distance between the metal atoms of the (111) plane of a fcc metal or the base plane of a hexagonal metal. Balandin computed the distance between the hydrogen atoms of cyclohexane and the nearest metal atom to which hydrogen may get transferred. From this, he concluded that a distance between 2.48 Åand 2.77 Åis most suitable. The former is the interatomic distance in metallic nickel and the latter in metallic platinum (both fcc metals), on their (111) plane. Both these metals are excellent catalysts for dehydrogenation of cyclohexane and hydrogenation of benzene. Further, if the interatomic distance in the metal is off these limits, the reaction becomes difficult because in such a case, either the hydrogen atoms are far away from the metal atoms, or all the six carbon atoms of the molecule cannot be arranged on the surface.

Figure 7.3: *(a) Cyclohexane sitting on a close packed plane of a metal surface; (b) formation of adsorbed benzene and hydrogen.*

Although there is a fair amount of experimental support for the Balandin's theory, examples are also there that do not agree with it. Thus, the oxide Cr_2O_3 is a good catalyst for the above reaction which is not in accordance with Balandin's model. However, it may may be argued that a molecule of cyclohexane may undergo chemisorption along its edge using only two carbon atoms (doublet mechanism). This too will give benzene in three successive steps forming cyclohexene in the first step and cyclohexadiene in the second step and finally giving benzene. Sokolskii and Druz[2] have indeed reported the presence of cyclohexadiene in the product by using chromia catalyst. It should also be remembered that the interatomic distances used by Balandin are taken from X-ray

[2]D. V. Sokolskii and V. A. Druz, *Theory of Heterogeneous Catalysis*, Nauka, Alma-Ata, 1968, p.116.

diffraction that are true for the atoms in the bulk. Low energy electron diffraction results have clearly shown that these distances are somewhat higher when the atoms are on the surface. This may question the validity of Balandin's conclusions.

7.1.2 Valence Angle Conservation

Rideal and Twig[3] took a different geometrical approach in order to explain the catalytic hydrogenation of an unsaturated hydrocarbon. We know that the reactant molecule forms an active complex with the catalyst. If the formation of the active complex gives rise to further strain in the valence angle of the hydrocarbon structure, it will be be formed with difficulty. In such case, the energy of activation will be high and the reaction will be difficult. In other words, a good catalyst should facilitate the formation of the active complex without straining the valence angle.

The adsorption mechanism in this case is similar to Balandin's doublet. This is shown in figure 7.4. If c is the carbon–carbon distance, a is the lattice parameter of the metal used as catalyst and θ is the angle formed at the carbon atom by the other carbon and a surface metal atom, then

$$a - c = 2\mathrm{KA} = 2b\cos\phi = 2b\cos(2\pi - \theta) \tag{7.1}$$

In the above diagram, K is a metal atom, C is a carbon atom and CA is the perpendicular distance of the carbon atom from the surface. The rest is clear from the diagram.

Figure 7.4: *Adsorption of ethane on a metal through two points showing the relation between lattice parameter and valence angle.*

The above equation can be rearranged to get

$$\frac{a - c}{2} = b\cos(180 - \theta) \tag{7.2}$$

[3]G. H. Rideal and B. K. Twig, *Proc. Roy. Soc.*, A 146, 630 (1934).

Knowing b, c and θ, the distance a can be calculated. If the metal is nickel, the distance K–C can be taken as 1.82 Å(from the Ni–C distance in the compound $Ni(CO)_4$). Taking the C–C distance is 1.54 Åfor a single bond and Ni–Ni distance in metallic nickel is 2.48 Å, the angle Ni–C–C becomes $105^o28'$. This is close to the tetrahedral angle formed by carbon. So nickel can easily adsorb ethane without straining the valence angle and should be a good catalyst for ethane dehydrogenation and also for ethene hydrogenation. If the lattice parameter has a value that gives valence angle far different from the tetrahedral angle, the active complex will need a high energy of activation and the reaction rate will be slow. The angle K–C–C will be closest to tetrahedral angle if the lattice parameter is 2.74 Åwhich is close to the lattice parameter of palladium (2.74 Å) and platinum (2.77 Å). Both these metals are excellent catalysts for ethene hydrogenation.

7.1.3 Kobozev's Ensemble Model

In order to explain catalysis by supported metals, Kobozev[4] proposed the ensemble theory. Use of a support not only increases the specific activity (activity per gram of the metal) sharply, but also minimizes the decrease in activity due to sintering. The metal atoms present on the surface of the support can undergo surface migration, eventually leading to sintering of the metal. According to Kobozev, the defect structure of the support restricts the surface migration of the metal atoms within a zone that largely prevents sintering. Molecules of the catalyst poisons too are adsorbed on the entire support and not only on the catalytically active metal atoms. This reduces the poisoning effect considerably. According to this model, the defect structure of the support plays an important role in preventing surface migration of the active phase. This retains the high dispersion of the metal in the form of atoms or small cluster of atoms that Kobozev called an ensemble.

During the preparation of a supported metal catalyst of low metal loading, isolated atoms are formed on the support surface. Surface coverage is expressed as

$$\theta_M = \frac{A_M N_0}{\alpha_I} \tag{7.3}$$

where A_M is the area of a metal atom, α_I is the specific surface of the inert support and N_0 is the number of metal atoms per gram of the support. Crystallization starts when $\theta_M > 0.1$. Ensemble model

[4]N. I. Kobozev, *Acta Physicochem. USSR* 9, 1, (1938).

is concerned mainly about how the fraction of different ensembles of composition M_n ($n = 1, 2$ etc.) changes with the change of θ_M.

If N_0 is the number of metal atoms to be distributed among L zones of free migration and if all such zones are equivalent, the probability that n number of atoms enter one zone is

$$W_n = \frac{\nu^n}{n!} \exp(-\nu) \tag{7.4}$$

where $\nu = N_0/L$, the average number of metal atoms per zone. How the probability of formation of ensembles of different number of atoms change with ν is shown in figure 7.5.

What kind of ensemble will predominate depends on ν, and at constant L, on N_0. If it is possible to know the ensemble type that is active for a reaction, it may be tried to prepare a catalyst with maximum number of ensembles of that type. To achieve this, the catalytic activity will have to be determined experimentally.

Figure 7.5: *Variation of the probability of formation of an n-atomic zone having different average number of atoms n with the average number of zones.*

Two types of catalytic activity will be defined: 1) total activity A which is the number of molecules reacting per second on all the metal

atoms present on one gram of the supported catalyst, and 2) specific activity expressed as $a = A/N_0$, number of molecules reacting per metal atom per second. (The latter activity is also known as turn over number, TON). If all types of ensembles are equally active for a reaction, total activity A should increase with N_0 until crystallization begins, whereas the specific activity should remain constant. On the other hand, if only a particular n-atomic ensemble is active for a reaction, total activity should be proportional to W_n which means A should increase with ν or with $(N_0/L)^n$ up to a point and then fall exponentially.

What type of ensemble will be active for a particular reaction has been found as follows. The number ensembles having n atoms is

$$L_n = L\frac{(N_0/L)^n}{n!}\exp(-N_0/L) \tag{7.5}$$

Let r_n be the activity of one n-atomic ensemble. Then,

$$A_n = r_n L_n = r_n.L\frac{1}{n!}(N_0/L)^n \exp(-N_0/L) \tag{7.6}$$

and

$$a_n = \frac{A_n}{N_0} = \frac{r_n}{n!}(N_0/L)^{n-1}\exp(-N_0/L) \tag{7.7}$$

where A_n and a_n are respectively the total and specific activity of an n-atomic ensemble. Differentiating the last two equations with respect to N_0, we get

$$n = N_0(A_{\max})/L \tag{7.8}$$

and

$$n - 1 = N_0(a_{\max})/L \tag{7.9}$$

where $N_0(A_{\max})$ and $N_0(a_{\max})$ are respectively the values of N_0 at which total activity and specific activity are maximum. Solving the above two equations simultaneously, we get

$$n = \frac{N_0(A_{\max})}{N_0(a_{\max}) - N_0(a_{\max})} \tag{7.10}$$

If we find out experimentally the value of N_0 at which catalytic activity is maximum, we can find out n that shows the number of atoms in the ensemble responsible for this reaction. If a_n vs N_0 plot does not have a maximum, then the monoatomic site is the active site.

From accumulated experimental data, size of the ensemble responsible for catalysis has been identified for a large number of reactions. Some results are summarized in table 7.1.

Kobozev's model assumes that the zone of free migration of the metal atoms is determined by the defect structure of the support. This makes the crystal structure of the metal irrelevant and thus is opposed to Balandin's concept. A modified form of Kobozev's model has been put forward by Boudart and coworkers[5] when they classified reactions as structure sensitive or *demanding* and structure insensitive or *facile*. However, Kobozev's approach is concerned only with those reactions that are facile, whereas Balandin was concerned with the demanding reactions only.

Table 7.1: Active ensemble size for reactions on supported metals.

Reaction	Catalyst	Support	Active ensemble
$2SO_2 + O_2 \rightarrow 2SO_3$	Pt or Pd	Alumina gel Silica gel	$[Pt]_2$; $[Pd]_1$
$4NH_3 + 5O_2 \rightarrow 4NO + 6H_2O$	Pt	Alumina gel Silica gel	$[Pt]_1$
$C_2H_2 + H_2 \rightarrow c_2H_6$	Pt	Silica gel	$[Pt]_2$
$3H_2 + N_2 \rightarrow 2NH_3$	Fe	Carbon	$[Fe]_3$
$C_6H_8 + 2H_2 \rightarrow C_6H_{12}$	Pt	Silica gel	$[Pt]_2$; $[Pt]_6$

7.1.4 Demanding and Facile Reactions

If a reaction takes place on a metal surface, one would expect catalytic activity to increase linearly with metal surface area. However, Boreskov and coworkers[6] while studying oxidation of sulphur dioxide and hydrogen on platinum found no dependence of catalytic activity and specific metal surface. Boudart and associates[7] found the rate of hydrogenlysis of neopentane to isobutane and methane to be very much dependent on the metal specific surface. This led to the classification of supported metal catalysts to structure sensitive or *demanding* and structure insensitivity or *facile*. This difference becomes clear if reaction rate is expressed as turn over number (TON). For a facile reaction, TON should be independent of metal particle size (metal dispersion), but should increase linearly with metal dispersion if the reaction is demanding. Examples of facile and demanding reactions are given in table 7.2.

The reason why some reactions are demanding and others are facile was explained by Anderson and Avery[8] as follows. If the reaction requires

[5]M. Boudart, A. W. Aldag, J. E. Benson, N. A. Dougharty and C. G. Harkins, *J. Catal.*, 6, 92 (1966).

[6]G. K. Boreskov and V.S. Chesalova, *Zh. Fiz. Khim.*, 30, 2560 (1956) and G. K. Boreskov, M. G. Slinko and V. S. Chesalova, *Zh. Fiz. Khim.*, 30, 2787 (1956).

[7]M. Boudart, A. W. Aldag, L. D. Ptak and J. E. Benson, *J. Catal.*, 11, 35 (1968).

[8]J. R. Anderson and N. R. Avery, *J. Catal.*, 5, 466 (1966).

the chemisorption of the reactant molecule to take place through three or more surface atoms, the surface atoms should have certain type of arrangement and the reaction will be demanding. If, on the other hand, the reaction takes place by chemisorption of the molecule through a single point or a doublet, the arrangement of the surface atoms is of little importance and the reaction is facile. Classification of reactions as demanding and facile is valid only for catalysts of high dispersion. This will have no validity when the metal loading is high.

Table 7.2: Examples of facile and demanding reactions.

Catalyst	Reaction	Facile/ Demanding
Pt/Al_2O_3	Hydrogenation of benzene	Facile
	Isomerization of neopentane	Facile
	Hydrogenlysis of cyclopentane	Facile
	Dehydrogenation of isopropanol	Facile
	Hydrogen-deuterium excange	Demanding
	Hydrogenation of CO	Demanding
	Hydrogenolysis of neopentane	Demanding

7.2 ELECTRONIC EFFECT IN CATALYSIS BY METALS

There are two major approaches in describing the electron property of metals. The band theory and the valence bond method.

7.2.1 Band Theory

The band theory that is based on the assumption that the outermost electrons of the atoms in a metal are free to move in the entire crystal in a periodic potential field of the positive metal ions. This gives rise to the electron energy bands in the crystal in place of the discrete energy levels of the outer orbitals. The inner orbitals remain unaffected. The bands may be s p or d bands formed by the overlap of the respective types of orbitals, or they may be hybrid bands formed when two different kind of bands overlap. The details of band theory is available in any standard textbook of solid state chemistry or physics.

Since there are several energy bands in a metal, some of them may be completely filled, others may be empty or partly filled by electrons. If the highest energy band is only partially filled, electrons can easily move in the band without supply of any energy since the bands are made of continuous energy levels. Such solids are metals. Electrical conductivity of metals should be independent of temperature, but this not so because

electrons are randomly scattered by heat (phonons). Electrical resistance of a metal actually increases with temperature.

If the highest energy band is empty is the band lower to this is completely full, the two bands are separated by a forbidden region and the solid is an insulator. If the energy separation between these two bands are small (< 1 eV), it is possible for some electrons from the full band (called the valence band) to jump across the band gap to the empty upper band (known as the conduction band) even at room temperature. Now the electrons in the conduction band can move freely because there are enough number of empty states in that band. Removal of the electrons from the valence band creates an equal number of positive holes in this band. The positive holes can move in the valence band. Under the influence of small electric field, the electrons and the holes move to the opposite electrodes, both contributing towards electrical conductivity. Solids with small energy gap between the valence band and the conduction band are called *semiconductors*. The band diagrams of the three types of crystalline solids are shown in figure 7.6.

In transition metals, the s-band is broad and the nearby d-band is considerably less so because the d-orbitals overlap to a much lesser extent. In a crystal, s- and d-bands may overlap forming a hybrid band. The experimental criteria that gives the idea about the electron distribution in the bands is the magnetic moment of the metal.

Assuming separation of the s- and d-parts of the hybridized band, and also assuming the electrons to be present in two different but overlapping bands formed by the $3d$ and $4s$ orbitals of the transition metal atoms, the saturation magnetic moment (in Bohr magneton, BM) per atom at 0 K should be equal to the number of holes in the d-band which is the same as the number of unpaired electrons in the d-band. Since the total number of $4s$ and $3d$ electrons in the band are known, number of electrons (per atom) in the s-band can be calculated (see Table 7.3).

Figure 7.6: *Energy band diagram of different solids: a. metal, b. semiconductor and c. insulator. Shaded part of the bands are occupied by electrons.*

In an isolated atom of iron, for example, there are six $3d$ and two $4s$ electrons. In the metal, there is continuous exchange of electrons between the s and d bands and the configurations d^6, d^7 and d^8 are all present. The weighted average is $d^{7.8}$. Then 0.2 electrons per atom in the s band are responsible for binding. This band model, however, does not explain satisfactorily how iron with only $0.2s$ binding electrons has such high melting point.

Table 7.3: Electron distribution in metals of the iron group.

Metal	$s+d$ electrons	Saturation moment (BM)	d-band holes	d-band electrons	s-band electrons
Iron	8	2.2	2.2	7.8	0.2
Cobalt	9	1.7	1.7	8.3	0.7
Nickel	10	0.6	0.6	9.4	0.6

7.2.2 Pauling's Valence Bond Method

In order to describe bonding in transition metals, Pauling used the valence bond method. It considers the nine outermost, five (n−1)d, one ns and three np, orbitals where n is the principal quantum number of the outermost level. These available orbitals are divided into (i) dsp hybrid bonding orbitals, (ii) d nonbonding orbitals and (iii) metallic s orbitals. Bonding orbitals are responsible for cohesion of the metal, the electrons in the nonbonding d orbitals are localized at the respective atoms and are responsible for magnetic moment, and the electrons in the metallic orbital are responsible for electrical conduction.

The cohesion in the metal, that determines the size of the ionic radius and melting point of a metal, will be maximum when the dsp hybrid bonding orbitals are maximum. It is found that in the transition series, atomic radius decreases and melting point increases regularly up to the chromium group (Cr, Mo and W) and after that, they do not change much. This led Pauling to assume that dsp hybrid bonding orbitals attain a maximum at the chromium group and then remain the same up to the copper group. Since chromium metal has saturation magnetic moment 0.22 BM, there must be 0.22 localized d electrons per chromium atom. Knowing that chromium has a total six electrons ($3d^4 4s^2$) in its d and s orbitals, number of electrons in the dsp bonding orbitals is $6 - 0.22 = 5.78$. Since the cohesive properties do not change after chromium in the series, the same number of bonding dsp electrons are assumed to be present in all elements from chromium to copper. Now it is easy to write down the electron distribution in the bonding, nonbonding

and metallic orbitals of the rest of the transition metals.

Table 7.4: Electronic structure of the metals of the first transition series according to valence bond theory.

Metal	Total $s+d$ electrons	Bonding *dsp* orbitals	Nonbonding *d*-electrons, spin		Saturation moment, BM	
			$+1/2$	$-1/2$	Calc.	Obs.
Ti	4	4.00	0	0	0	0
V	5	5.00	0	0	0	0
Cr	6	5.78	0.22	0	0.22	0.22
Mn	7	5.78	1.22	0	1.22	1.22
Fe	8	5.78	2.22	0	2.22	2.22
Co	9	5.78	2.44	0.78	1.66	1.61
Ni	10	5.78	2.44	1.78	0.66	0.61
Cu	11	5.78	2.44	2.44	0	0

dsp hybrid orbitals are used in forming metal-metal bonds. Valence of these metals are fixed at 5.78. Hybridization requires some electrons from the s and d orbitals to be promoted to the p orbitals. This energy is provided by resonance between more than one electronic configuration of a metal. Nickel, for example, exists in two configurations and the same is true for cobalt (see figure 6.6). Here, arrows represent electrons in localized atomic orbitals, solid circles represent bonding electrons in hybrid orbitals and the hollow circles are the electrons in metallic orbitals.

Actual electronic configuration is a resonance hybrid of the two forms. Ni-A has two unpaired electrons and Ni-B has none. Pauling suggested that the metal has 30 percent Ni-A and 70 percent Ni-B. Saturation moment will be $0.3 \times 2 + 0.7 \times 0 = 0.6$ BM. Similarly, 35 percent Co-A and 65 percent Co-B will give a magnetic moment 1.7 BM.

Figure 7.7: *Two different electronic configuration of cobalt and nickel.*

The *dsp* hybrid orbitals are used in forming metallic bond. It is possible to calculate the extent of *d*-orbital participation in metallic bonding.

Pauling called this as percent d-character of the metallic bond. Ni-A has two bonding d-electrons and six available orbitals and Ni-B has three such electrons and seven available orbitals. Hence d-character of the metallic bond in nickel is $33\% \times \frac{2}{6} + 70 \times \frac{3}{7} = 40\%$. Similarly, 35% of Co-A and 65% of Co-B leads to 39.7% d-character.

Percent d character of metallic bond of the transition metals are shown in Table 7.5.

Acceptance of the fixed valence of 5.78 for a number of transition metals raised serious objection from many. However, it was useful in rationalizing the physical properties like melting point, hardness, atomic radius etc. of the metals.

Table 7.5: Percent d-character of metallic bond in transition elements.

Element	d-character	Element	d-character	Element	d-character
Sc	20	Ti	27	V	35
Fe	35.5	Co	39.7	Ni	40
Cu	36	Y	19	Zr	31
Nb	39	Mo	43	Tc	46
Ru	40	Pd	46	Ag	36
La	19	Hf	29	Ta	39
W	43	Re	46	Os	49
Ir	49	Pt	44		

7.2.3 Electronic Structure and Catalysis

Beeck[9] tried to relate the heats of chemisorption of hydrogen and ethene at very low surface coverage with percent d-character of the metallic bond. It was assumed that the chemisorptive bond is formed between the adsorbate and the atomic d-orbital of the metal. Hence, heat of chemisorption should decrease with increase in d-character of the metallic bond. The experimental correlation is shown in figure 7.7.

Although there is some decrease of heat of adsorption with increase in d-character for the Group VIII metals, there is a sharp fall in the heat of adsorption from tantalum to iron although d-character shows little change, and tungsten stays away from the curve.

Beeck has also studied catalytic activity of the transition metals for hydrogenation of ethyne. Dependence $\log k$ against d-character of the metal (figure 7.8) shows a linear increase for the Group VIII metals, but little variation for the metals from tantalum to iron. Tungsten still remains away from the curve.

[9] O. Beeck, *Discuss. Faraday Soc.*, 8, 118 (1950)

Saturation magnetic moment of the metals changes with adsorption of hydrogen. Saturation moment of palladium (0.6 BM) becomes zero when hydrogen adsorption is complete. Stoichiometry of this is $PdH_{0.6}$. Thus, the number of hydrogen atoms per atom of palladium is exactly equal to the number of *d*-band holes of palladium. It was suggested that the chemisorptive bond is formed by donation of electrons from the adsorbate to fill up the *d*-band holes of the metal.

Figure 7.8: *Initial heat of adsorption as a function of percent d-character; adsorption of (a) hydrogen, (b) ethene.*

We have been discussing chemisorption of hydrogen because hydrogenation and dehydrogenation are two major reactions catalyzed by metals. Assuming that the metal–hydrogen bond is covalent, strength of this bond can be calculated using the equation

$$Q_{\mathrm{M_H}} = \frac{1}{2}[D_{\mathrm{H-H}} + D_{\mathrm{M-M}}] + 23.06(\chi_{\mathrm{M}} - \chi_{\mathrm{H}})^2 \qquad (7.11)$$

where $Q_{\mathrm{M-H}}$ is the heat of adsorption, $D_{\mathrm{H-H}}$ is the bond dissociation energy of hydrogen. $D_{\mathrm{M-M}}$ is the bond dissociation energy of the metal which is equal to $L_s/6$ where L_s is its heat of sublimation.

Bond found a good correlation between calculated and experimental heats of adsorption of hydrogen on metals except that for chromium, ruthenium, rhodium and irridium. Since these calculations assume covalent bond formation between the metal and the adsorbate, it obviously will not be successful for those adsorbates that form more ionic bond. But even for such gases that form covalent bonds such as N_2, CO, C_2H_2 and C_2H_4, significant departure from expected values have been observed. Form these results, Bond[10] concluded that for the group VIII metals, where the atomic radii are minimum (meaning strongest

[10]G. C. Bond, *Catalysis by Metals*, Acad. Press, London & New York, 1962

metallic bond), considering the *d*-character of the metallic bond may be useful. Properties like heat of sublimation reaches a maximum value in group VI, and here the heat of sublimation of the metals may be a better criteria for predicting chemisorption and catalysis.

Figure 7.9: *Variation of catalytic activity of metals with d-character for hydrogenation of ethyne.*

Participation of the *d*-band electrons can be demonstrated by taking the alloys of Group VIII metals with copper group atoms as examples.. Nickel, palladium and platinum has 0.6 *d*-band holes per metal atom. When alloyed with copper, these *d*-band holes gets gradually filled up because of the transfer of *s* electrons of copper into these bands. The *d*-band will be full at 60 percent copper. One may expect a gradual change of catalytic activity on alloying of these metals with copper up to 60 percent addition of copper, after which it may change drastically. Some trend of this kind has been noticed, but not as frequently as expected.

Catalytic hydrogenation reactions depend, to a large extent, on the activation of hydrogen. What form of hydrogen actually facilitates the catalytic reaction? Studies on ortho-para conversion of hydrogen and that of hydrogen-deuterium exchange shows that hydrogen undergoes dissociation on the surface. Ratio of the rates hydrogenation to the rates of deuteration has been found to be equal to the rate of hydrogen-deuterium exchange. This supports the assumption that the active form of hydrogen is the atomically adsorbed form. But there are also reports of alternative form of hydrogen active in some hydrogenation reaction. For

example, Frakas et al.[11] found that a nickel surface covered with ethene does not support ortho-para conversion although it catalyzes ethene hydrogenation suggesting that hydrogenation of ethene on nickel may not need hydrogen to be present on the surface in the dissociated form. There are also examples of hydrogenation by dissolved hydrogen in metals[12]. Hydrogenation may also follow radical mechanism as it has been found that hydrogen is present in some platinum metals as protons[13].

Figure 7.10: *Surface structure of the various low Miller index planes in a metal.*

The generally accepted mechanism of hydrogenation of a unsaturated hydrocarbon is that hydrogen is adsorbed in a dissociated form, the unsaturated alkene is simultaneously adsorbed by opening up the carbon–carbon double bond followed by a two-step transfer of hydrogen to these carbon atoms. This is supported by the infrared spectroscopic evidence that showed that the chemisorbed alkenes do not show the

[11] A. Frakas, L. Frakas and E. K. Rideal *Proc. Roy. Soc.*, A146, 630 (1934).
[12] O.Schimdt, *J. Phys. Chem*, 118, 193 (1925)
[13] M. Stackleberg and P. Weber, *Z. Electrochem.*, 56, 806 (1952).

carbon-carbon double bond.

7.3 STUDIES ON SINGLE CRYSTAL SURFACES

It has been already said that the coordination number of the metal atoms on the surface are lower than that in the bulk. Low index surfaces of a fcc metal are shown in figure 7.10.

Coordination number of an atom on the (100) face is 8 (4 on the same plane and 4 in the plane below). The same for the (110) face is 7 and for the (111) face is 9. The coordination number of an bulk atom in a fcc metal is 12. We see that a atom on the (110) surface has more valence unsaturation than an atom on the (111) surface. Higher index surfaces have more steps and kinks. Studies on single crystal surfaces have shown higher chemisorption and catalytic activity at steps and kinks.

Figure 7.11: *Adsorption of nitrogen on the various surfaces of iron single crystal.*

For a better understanding of the phenomenon, studies on adsorption and catalysis were conducted on clean single crystal surfaces. Such ultra-high vacuum techniques of surface studies will be discussed later. Some interesting results will be presented in this section. Although the surface of a practical catalyst is quite different and much more complex than a model single crystal surface, studying the latter is the only way of getting some insight into the fundamental process taking place on the surface. Using single crystal surface as catalysts, it is possible to identify the geometry of the active site. There are examples when results on single crystal catalyst and supported metal were found to be in good agreement. This is possibly due to the fact that at high metal loading, the metal particles may be present on the surface of the support with

its (111) or (100) planes exposed. Methanation of CO by hydrogen on nickel (100) single crystal surface shows the same energy of activation as on Ni/Al_2O_3 catalyst.

Nitrogen on the (111) surface of iron is found in two molecular forms, one bound through a single nitrogen atom (end-on position) called the γ-nitrogen and the other bound to the surface through both nitrogen atoms (side-on position) known as α-nitrogen. The latter has a much weakened $N - N$ bond as suggested form infrared vibration[14]. α-form is the precursor to the adsorbed atomic nitrogen. Chemisorption of nitrogen[15] has the highest rate on the (111) surface and lowest on the (110) (see figure 7.11). The (111) plane also showed the highest rate for ammonia synthesis[16]. The ratio of the rate was found to be 418:25:1 for (111):(100):(110).

Figure 7.12: *Adsorption scheme for nitrogen on clean and modified iron surfaces.*

Nitrogen adsorption on single crystal iron surface has been studied because of its importance in ammonia synthesis. Since potassium is a

[14]M. Grunze et al., *Phys. Rev. Lett.*, 53, 850 (1984)
[15]F. Bozzo, E. Ertl and M. Weiss, *J. Catal.*, 50, 519 (1977)¿
[16]N. D. Spencer, R. C. Schoomaker and G. A. Somorjai, *J. Catal.*, 74, 129 (1982).

promoter for iron catalysts of ammonia synthesis, the effect of partly covering the (111) iron surface with potassium was studied. Presence of potassium markedly increased the rate of ammonia synthesis[17] on the (111) surface of iron. The overall effect of pre-adsorbed potassium is to increase the energy of adsorption of N_2 and lower the energy barrier for N_2 dissociation.

Figure 7.13: *N(1s) spectra of adsorbed nitrogen on clean and modified iron surface.*

Since chlorine is a poison for the ammonia synthesis catalyst, Rao *et al.*[18] studied a iron surface modified with chlorine by XPS. It was found that the end-on molecular form (γ) of nitrogen is stabilized. The beneficial effect of electropostive atoms such as potassium, and the negative effect of electronegative atoms like chlorine suggest that the effect is electronic in nature. The various possible ways of nitrogen adsorption on iron and modified iron surface are shown in figure 7.12.

Nitrogen adsorption on polycrystalline iron surface has been studied by XPS. Whereas clean iron surface shows both end on and side on adsorption, surface modified with barium shows only the side on adsorbed species as revealed by N($1s$) spectra (figure 7.13).

Adsorption of CO on metal surface shows several modes of adsorption

[17]S. R. Bare, D. R. Strongin and G. A. Somorjai, *J. Phys. Chem.*, 90, 4726 (1986).
[18]C. N. R. Rao and G. Ranga Rao, *Chem. Phys. Lett.*, 146, 557 (1988).

of the molecule. The molecule can be bonded to the surface through one, two or three surface atoms as been shown by infrared and high resolution electron energy loss spectroscopy.

Although identifying the adsorbed species on the surface is very important, it should be remembered at the same time that the most prevalent species on the surface may not be always responsible for a catalytic reaction. At present, there seems no alternative to the experimental determination of catalytic activity and selectivity because catalytic activity cannot be predicted *a priori*. However, the various models that has been discussed here can act as guideline for proper selection of a catalyst.

SUGGESTED READING

1. Bond, G. C., *Catalysis by Metals*, Acad. Press, London and New York, (1962).
2. Thomas, J. M. and Thomas, W. J., *Introduction to the Principles of Heterogeneous Catalysis*, Acad. Press, London and New York, (1967).
3. G. C. Bond, *Heterogeneous Catalysis, 2nd Ed.*, Oxford University Press, 1987.
4. Roberts, M. W. and McKee, C. S., *Chemistry of the Metal-Gas Interface*, Clarendon, Oxford, 1982.
5. Rao, C. N. R. and Ranga Rao, G., *Surface Science Reports*, 13, 221, (1991).

Chapter 8

Catalysis by Semiconductors

8.1 INTRODUCTION

A large number of transition metal oxides used as catalysts have semiconducting properties. The possible involvement of semiconductors in catalysis may be even more frequent than it appears. Metal catalysts of oxidation have a thin layer of oxides on the surface and since catalytic reactions take place on the surface, semiconducting property of the oxide layer may control catalysis. Oxides that are insulators too may behave as extrinsic semiconductors because of the presence of defects and impurities. These widens the scope of semiconductors as heterogeneous catalysts.

8.2 INTRINSIC AND EXTRINSIC SEMICONDUCTORS

For a solid at 0 K, the valence band is completely full and the conduction band is empty. Since the energy gap between these two bands in a semiconductor is small, a number of electrons are raised across the band gap to the conduction band leaving a equal number of holes in the valence band at $T > 0$ K. Under a small applied electric field, the electrons and the holes can move in the solid leading to electrical conduction. Such materials are *intrinsic semiconductors*. In an intrinsic semiconductor, electrons and holes equally contribute to conduction.

Electrons in a solid experience a potential that fluctuates periodically across the lattice. If this fluctuation is very large, the bands become narrow and conduction cannot be explained as due to the electron movement in this band. In such cases, the electrons become localized at the cations (forming valence defects) or at lattice vacancies. Such electrons

(or holes) can jump from one site to another equivalent site leading to *hopping conduction*.

Figure 8.1: *Energy diagram of n- and p-type semiconductors.*

A real crystal has point defects like (a) vacant lattice sites, (b) interstitial atoms and (c) impurity atoms. There may be more than one kind of defects in a crystal and they may be in various states of ionization. Such defects form localized energy levels in the forbidden region. The defect (normally an impurity) may form a filled energy level, called a donor level, that lies just below the conduction band. Electrons from the donor level can be easily raised to the conduction band. Such semiconductors will have electrons as the majority charge carriers and they are known as *n*-type semiconductors. If the impurity forms a normally empty energy level lying in the band gap just above the valence band, this is called an acceptor level. It can easily accept an electron from the valence band. Electrons raised to the acceptor levels are localized, but the holes formed in the valence band can move across the solid. In such materials, holes are the majority charge carriers and these materials are known as *p*-type semiconductors. Figure 8.1 shows the energy diagram of *n*- and *p*-type semiconductors. Both *n*- and *p*-type semiconductors are called *extrinsic semiconductors*.

8.2.1 Fermi Energy

According to Fermi-Dirac statistics, the probability f that an electron has an energy E_i is

$$f = \frac{1}{\exp[(E_i - E_f)/kT] + 1} \tag{8.1}$$

At 0 K, $f = 0$ when $E_i > E_F$, and when $E_i < E_F$, $f = 1$. This shows that Fermi energy E_F is the energy below which all energy levels are full and above which all levels are empty at 0 K. At any other temperature, $f = \frac{1}{2}$ when $E_i = E_F$. This gives a workable definition of Fermi energy

at any real temperature: it is the energy state at which the probability of finding an electron is equal to $\frac{1}{2}$. It is possible to show that Fermi energy is the partial molal free energy of the electrons or it is the electrochemical potential.

The number of electrons n_i in the state E_i is

$$n_i = \frac{g_i}{\exp[(E_i - E_F)/kT] + 1} \tag{8.2}$$

where g_i is the degeneracy. When $E_i - E_F \gg kT$, it is possible to write

$$n_i \approx g_i \exp[(E_F - E_i)/kT] \tag{8.3}$$

Thus, if the band gap is sufficiently large as in many oxides, the concentration of electrons in the conduction band is

$$n = N_c \exp \frac{E_F - E_C}{kT} \tag{8.4}$$

where N_C is the density of (energy) states in the conduction band and E_C is the energy of the bottom of the conduction band.

The density of states

$$N_C = \left(\frac{8\pi m_e^* kT}{h^2}\right)^{\frac{3}{2}} \tag{8.5}$$

where m_e^* is the effective mass of an electron.

Concentration of holes p in the valence band

$$p = N_p \exp \frac{E_V - E_F}{kT} \tag{8.6}$$

where N_V is the density of states in the valence band and E_V is the energy at the top of the valence band.

$$N_V = \left(\frac{8\pi m_h^* kT}{h^2}\right)^{\frac{3}{2}} \tag{8.7}$$

where m_h^* is the effective mass of a hole.

For an intrinsic semiconductor, $n = p$. Equating equations (8.4) and (8.6) and rearranging, we get

$$E_F = \frac{E_V + E_C}{2} + \frac{3kT}{4} \ln \frac{m_e^*}{m_h^*} \tag{8.8}$$

If the effective masses of electrons and holes are equal, Fermi energy of a semiconductor would lie half way between the valence band and the conduction band. In the case of an n-type semiconductor, Fermi energy lies much higher, very near the bottom of the conduction band. For a p-type semiconductor, the same lies just above the top of the valence band. Doping (deliberate addition of impurity) is a handle to control the position of the Fermi level in a semiconductor.

8.2.2 Electrical Conductivity

Electrical conductivity of a semiconductor can be expressed as

$$\sigma = ne\mu_e + pe\mu_p \tag{8.9}$$

where μ_n is the mobility of the electrons in the conduction band and μ_p is the mobility of the holes in the valence band. For an intrinsic semiconductor, $n = p$ and conductivity

$$\sigma = ne(\mu_e + \mu_p) \tag{8.10}$$

Figure 8.2: $\ln \sigma$ *vs* $1/T$ *plot for a defect semiconductor.*

Substituting values of n and p,

$$\sigma = 2e\left(\frac{2\pi kT}{h^2}\right)^{3/2}(\mu_e + \mu_p)\exp\left(-\frac{E_C - E_V}{kT}\right) \tag{8.11}$$

For constant mobility in a given solid

$$\sigma = \sigma_0 \exp\left(-\frac{E_g}{2kT}\right) \tag{8.12}$$

where $E_g = E_C - E_V$ is the energy band gap. Plot of $\ln \sigma$ against $1/T$ gives a straight line where the slope is $E_g/2k$.

In a defect (extrinsic) semiconductor, $\ln \sigma$ vs $1/T$ plot have three distinct regions. The low temperature region represents extrinsic conductivity due to the defects and this may be either n- or p-type. The constant conductivity region represents the exhaustion region when all the electrons (or holes) from the defect levels are exhausted. The high temperature region is due to intrinsic conductivity and the slope obtained in this region is $-E_g/2k$.

Change in electrical conductivity of a solid during chemisorption helps in understanding the type of chemisorbed species formed.

8.3 BOUNDARY LAYER THEORY OF CHEMISORPTION

According to boundary layer theory, the adsorbate and the surface exchange electrons during adsorption. As a result, the adsorbed species are charged particles. If an adsorbate molecule C accepts an electron from the surface, it becomes C^- on the surface. The surface is covered with negatively charged species. As a result, a positive charge develops just below the surface. This makes it difficult for more electrons flowing to the surface and forming more of C^-. This makes further adsorption difficult. If the solid is a n-type semiconductor with low impurity concentration, concentration of electrons in the conduction band will not be very high and will soon be exhausted. Since supply of electrons will have to come now from much lower energy levels, chemisorption may stop even before the monolayer is complete. This type of chemisorption that stops before long is known as *depletive chemisorption.* Oxygen molecule can undergo chemisorption either as O_2^- or dissociatively as O^-. Oxygen adsorption is therefore quite restricted on n-type ZnO.

When an electronegative element such as oxygen is adsorbed on a p-type material in which the electrons will have to be supplied from the valence band, initial adsorption is difficult. But as the negatively charged species are formed on the surface, a positive space charge develops below the surface. This will make it easy for more electrons to move to the surface facilitating further chemisorption. At elevated temperature, O^{2-} too is formed. Experiments show appreciable chemisorption of oxygen on p-type NiO and Cu_2O. This increased in adsorption of oxygen on NiO is *cumulative adsorption.* Negatively charged adsorbed particle on a n-type oxide leads to depletive chemisorption whereas positively charged adsorbed species on the same gives cumulative chemisorption. The reverse is true for a p-type oxide. The results are summarized in

Table 8.1.

Carbon monoxide may be adsorbed reversibly as well as irreversibly. Reversible adsorption of CO follows the reaction.

$$CO + 2O^{2-} \rightarrow CO_3^{2-} + 2e$$

The surface is thus enriched with electrons by CO adsorption and this facilitates further adsorption of oxygen. Pre-adsorption of CO on a oxide always gives higher oxygen adsorption.

$$\frac{1}{2}O_2 + 2e \rightarrow O^{2-}$$

CO is reversibly adsorbed on ZnO and the mechanism is not well understood.

Table 8.1: Chemisorption on Semiconductors.

Adsorbed species	Semiconductor type	Chemisorption
C^-	n-type	Depletive
C^-	p-type	Cumulative
C^+	n-type	Cumulative
C^+	p-type	Depletive

According to boundary layer theory, adsorption takes place by charge transfer only. This can be easily followed by measuring the electrical conductivity of the catalyst pellet during adsorption. Boundary layer theory, however, cannot account for those chemisorption processes that do not involve charge transfer.

8.4 WOLKENSTEIN'S THEORY

Wolkenstein developed an elegant theory of catalysis by semiconductors. In this method chemisorbed species are treated as structural defects on the surface. The interaction between the adsorbate and the surface may be localized or non-localized. Non-localized adsorption occurs due to interaction of the electrons of the adsorbate with the surface atoms and transfer of electrons from or to the surface is excluded. This results in weak perturbation and formation of a weak chemical bond between the adsorbate and the surface. The bond is not localized and the adsorbate can migrate along the surface. Mixing of the wavefunction of the adsorbate and the surface electron leads to localized chemisorption by formation of a strong chemisorption bond. Thus, there are:
(1) *Weak chemisorption* in which the free electron or hole of the surface

do not take part and the adsorbate molecule is charge neutral. We shall designate such species as CL where L stands for the crystal lattice.
(2) *Strong chemisorption* in which the adsorbate molecule holds on to an electron or a hole of the surface. This results in strong chemisorption bond. If the adsorbate takes up an electron from the conduction band of the solid, it forms a strong *acceptor bond* (n-bond) and is designated CeL. This occupies an energy level A in the band gap close to the bottom of the conduction band. A chemisorbed particle that has localized a hole of the lattice forms a strong *donor bond* (p-bond) and is designated CpL. This occupies a state D in the band gap that lies higher than the top of the valence band. These are shown in figure 8.3. Note that the terms strong acceptor bond (n-bond) and strong donor bond (p-bond) are based on whether the adsorbate is an acceptor or donor of electron. Here, eL stands for a free lattice electron and pL for a free lattice hole. The same adsorbate can, however, be an acceptor or a donor of electron. Such behaviour of structural defects are well known in solids, e.g. F centres and F' centres. Chemisorbed molecules may change from one type to another.

8.4.1 Electron Transition in Chemisorption

As has been said, the chemisorbed species may change from one type to another. This simply means different states of ionization of the species. Such different states of ionization of point defects in solids are well known. These transformations also bring in change in the localized energy level of the species. Thus if a weakly chemisorbed species CL changes to a strong acceptor species CeL by interacting with a free electron of the lattice, it will give up an amount of energy V^-. On the other hand, if CL is to become CpL, it will give an electron to the valence band (localize a hole from the lattice) and this will give out energy equal to W^-. Inter-conversion of the species and the corresponding energy are shown by the following equations:

$$\mathrm{eL} + \mathrm{pL} \rightleftharpoons \mathrm{L} + E_g \tag{8.13}$$

$$\mathrm{CL} + \mathrm{eL} \rightleftharpoons \mathrm{CeL} + V^- \tag{8.14}$$

$$\mathrm{CL} + \mathrm{pL} \rightleftharpoons \mathrm{CpL} + W^+ \tag{8.15}$$

$$\mathrm{CeL} + \mathrm{pL} \rightleftharpoons \mathrm{CL} + V^+ \tag{8.16}$$

$$\mathrm{CpL} + \mathrm{eL} \rightleftharpoons \mathrm{CL} + W^- \tag{8.17}$$

These energy changes are also shown in figure 8.3

If an electron is removed from a species attached to the surface by a strong acceptor bond, it changes to a weak chemisorption bond. The same would lead to desorption according to the boundary layer theory. According to Wolkenstein's model, chemisorbed species can change from one type to another and every change involves some energy change too.

Figure 8.3: *Energy change in changing one type of chemisorbed species to another.*

8.4.2 Equilibrium of Various Chemisorbed Species

An adsorbate molecule may be present on a surface in all three forms of adsorption. Let N^0, N^- and N^+ represent the number of particles linked to the surface by weak chemisorption bonds, strong acceptor bonds and strong donor bonds respectively. If N is the total number of adsorbed molecules, then

$$N = N^0 + N^- + N^+ \tag{8.18}$$

Let $\eta^0 = N^0/N$, $\eta^- = N^-/N$ and $\eta^+ = N^+/N$ be the mole fraction of the three types of adsorbed molecules. Then

$$\eta^0 + \eta^- + \eta^+ = 1 \tag{8.19}$$

Wolkenstein has shown that the relative concentration of the different forms of the chemisorption is dependent on Fermi energy of the solid. This is shown in figure 8.4.

As shown in the figure, E_F is the energy difference between the Fermi level and the top of the conduction band. The dependence of the mole fractions on E_F is shown on the right hand side. If E_f is high, η^- is high too. If the solid has a low E_F as in a p-type semiconductor, η^+ is high. If the Fermi level is manipulated, it is possible to control the type of chemisorbed species on the surface. One way of controlling the Fermi level of a semiconductor is by doping with donor or acceptor impurities.

The product of the reaction depends on the type of chemisorbed species. One kind of chemisorbed species may give one product, whereas

another kind may give a different product during catalysis. Wolkenstein's ideas than can be tested by doping a semiconductor and using it as a catalyst.

Figure 8.4: *Change in the mole fraction of the adsorbed forms with Fermi level.*

8.4.3 Catalysis by Semiconductors

One form of chemisorbed molecule may lead to a given product whereas another form may be either inactive or may lead to a different product during a reaction. Hence, a reaction rate equation should contain the terms term η^0, η^- or η^+ and hence the energy E_f.

Reactions that are accelerated by raising Fermi level are called the *acceptor reactions* and the reactions that accelerated by lowering of the Fermi energy are known as the *donor reactions*.

Relating the reaction rate with Fermi level is however not so simple. A heterogeneous catalytic reaction in the kinetically controlled situation has several steps such as adsorption of the reactant, surface reaction and desorption of the product. One of the steps is slowest and is rate determining. In order to increase the reaction rate, the rate of the slowest step will have to be increased. For a given reaction in a given set of experimental conditions, chemisorption of the reactant may be favoured by high Fermi energy, but desorption of the product may be helped if Fermi energy is low. Whether raising of Fermi level will help the reaction depends on what is the rate determining step. If chemisorption is the rate determining step in this reaction, rate will increase by raising Fermi level. If, on the other hand, desorption of the product is rate determining, increase of Fermi energy will slow down the reaction.

Further complications are caused by the fact that for the same reaction on the same catalyst, the rate determining step at high temperature may be different from that at low temperature. We shall take here CO oxidation as an example. The reaction

$$CO + O_2 \rightarrow CO_2 \tag{8.20}$$

takes place both on ZnO (n-type) and NiO (p-type) semiconductors. Parravano[1] has shown that doping of NiO with Li^+ increases p-type conductivity (lowering of Fermi level) and this lowers the rate of CO oxidation. Doping with Cr^{3+}, on the other hand, decreases its conductivity (raises the Fermi energy) and this increases the reaction rate. Schwab and Block[2], on the other hand, observed the opposite effect. Parravano had studied the reaction at low temperature, but Schwab and Block had employed comparatively high temperature. This difference has been explained by Wolkenstein[3] as due to different rate determining steps at different temperatures.

Correct understanding of the rate determining step is very important while interpreting the result.

8.4.4 Fermi Level and the Surface

It is seen that concentration of one of the three forms of chemisorbed molecules depend on the position of the Fermi level. Depending on the type of the species formed, the solid may develop positive or negative charge just below the surface. This will cause the energy bands to bend near the surface.

If the surface accumulates negative charge, the valence band and the conduction band will bend upwards near the surface. This will lead to an increase in the work function ϕ of the solid. If the surface accumulates positive charge, the energy bands will bend downwards near the surface thus reducing the work function. No such changes will be there if the surface is uncharged. These are shown in figure 8.5. Here, $E_{f.s}$ is the energy difference between the Fermi level and the top of the valence band at the surface. Position of the energy bands remain unchanged in the bulk of the solid. Band bending takes place only near the surface and disappears in the crystal at some distance from the surface.

Measurement of work function of a solid before and after adsorption is an important indicator of the nature of the species. A chemical reaction should actually be effected by $E_{f.s}$ rather than by E_F since the reaction takes place on the surface of the catalyst. In most cases, however, an increase in E_F leads to an increase in $E_{f.s}$ and *vice versa*. This makes

[1] G. Parravano, *J. Amer. Chem. Soc.*, 75, 1452 (1952)

[2] G. M. Schwab and J. Block, *Z. Phys. Chem.* 1, 42 (1954)

[3] F. F. Wolkenstein, *Electronic Theory of catalysis on Semiconductors, Moscow*, p.88 (1960)

it possible to relate E_F to catalytic activity. This will not be so when surface states plays the dominant role in chemisorption and catalysis. In that case, the band theory of solids cannot be applied to explain catalysis.

Figure 8.5: *Band bending at the surface causing change of work function: (a)negative surface charge, (b) positive surface charge, (d) no surface charge.*

Wolkenstein has developed the most general theory of catalysis by semiconductors. The difficulty in applying it correctly also lies in its generality. There are too many parameters involved and it is not easy to know which of them is more important in a given set of experimental conditions.

8.5 ELECTRONIC EFFECT IN SUPPORTED CATALYSTS

Schwab[4] applied the concepts of band theory of solids to explain the catalytic properties of supported metals. Like Wolkenstein, he too classified reactions as donor and acceptor reactions. If the rate-determining step of a reaction involves an electron transfer from the reactant molecule to the catalyst, it is a donor reaction. The reverse of this is an acceptor reaction. He classified hydrogenation, dehydrogenation, deuterium exchange etc as donor reactions and decomposition of hydrogen peroxide as an acceptor reaction. According to this concept, n-type semiconductors will support acceptor reactions and p-type semiconductors will support donor reactions that has been experimentally found to be true in many cases. He then extended this concept further to supported metal catalysts.

[4]G. M. Schwab, *Adv. Catal.*, 27, 1 (1978)

A support may merely help in spreading the metal and increase the catalytic activity per gram of the metal. Alternatively, the support may synergetically promote the catalytic activity by increasing the rate and decreasing the energy of activation of the reaction. In a series of published work, Schwab and co-workers tried to verify whether such synergy is due to electronic effect. When a small amount of an active metal is supported on a semiconducting oxide, Fermi level of the metal will adjust with that of the support in contact. Change in the Fermi level of the support can also be achieved by doping. A clear example of electronic effect is formic acid decomposition (a donor reaction) on Fe/Al_2O_3 catalyst. Doping of the support with K_2O changed n-type Al_2O_3 to p-type and as expected, this lowered the energy of activation of the reaction. Doping with GeO_2, on the other hand enhanced its n-type conductivity and this raised the energy of activation of the reaction[5]. K_2O doped Fe is used as ammonia synthesis catalyst. However, doping of Fe with K_2O showed an increase in the energy of activation in ammonia synthesis. In this case, K_2O serves the purpose of stabilizing the active phase and is not used for increasing catalytic activity.

SUGGESTED READING

1. Wolkenstein, F. F., *Electronic Theory of Catalysis on Semiconductors*, Moscow, 1960.
2. Wolkenstein F.F., in *Advances in Catalysis*, Vol.12, 189, 1960.
3. Clark, A., *Theory of Adsorption and Catalysis*, Academic Press, London, 1970.
4. Schwab, M., *Advances in Catalysis*, Acad. Press, Vol.27, 1, 1978.

[5]M. Schwab and R. Putzer, *Chem. Ber.*, 92, 2132 (1959).

Chapter 9

Catalysis by Acidic Solids

9.1 INTRODUCTION

Many organic reactions are catalyzed by mineral acids. Ioffe and Roginskii[1]have shown that the same reactions are also catalyzed by solids that have acid properties. Most important in this class of solids are the aluminosilicates. Silica and alumina have surface hydroxyl groups that are weakly acidic and they themselves are not very useful. Binary oxides of silicon and aluminium in which the two elements have different oxidation states show good acid properties and are useful as catalysts. In the aluminosilicates, Si^{4+} and Al^{3+} are present in the tetrahedral environment of shared oxygen. The presence of Al^{3+} creates a charge imbalance that can be compensated by a positive ion. When this positive ion is a proton, the solid becomes a Brönsted acid. When such a solid is heated, one $Al-O$ may be broken due to dehydration and the aluminium is now linked to only three oxygen. This aluminium with a missing electron pair acts as a Lewis acid. The Lewis acid site can interact with an neighbouring silanol group forming a strong Brönsted acid centre. This is illustrated in figure 9.1.

Aluminosilicates may be amorphous or crystalline. Crystalline aluminosilicates are known as zeolites.

Amorphous aluminosilicates with varying SiO_2 to Al_2O_3 ratio have been prepared. Other additives used are MgO, ThO_2, ZrO_2 and some other metal oxides. The method used for their preparation varies. They may be prepared by mixing separately precipitated silica and alumina gels, by co-precipitation of the gels, or by impregnating silica gel with the

[1]I. I. Ioffe and S. Z. Roginskii, *Zh. Fiz. Khim.*, 31, 612 (1957).

solution of an aluminium salt. These materials are X-ray amorphous. Industrial catalysts are generally prepared by the co-precipitation method with a total aluminium of about 12 percent. Amorphous aluminosilicates are gradually being replaced by zeolites.

Figure 9.1: *Brönsted and Lewis acid sites in the aluminosilicate.*

9.2 ZEOLITES

Zeolites are crystalline aluminosilicates with the general composition

$$M^{n+}_{x/n}[(AlO_2)_x(SiO_2)_y]zH_2O$$

where M^{n+} is a cation with charge n+, an x, y and z are numbers. The ratio $y/x \geq 1$, but it can be very large in some structures and it has been possible to synthesize zeolites containing no aluminium at all. Zeolites have become important technological materials because of certain structural features and the flexibility in its structure and composition.

9.2.1 Structure

The primary building unit in the zeolites is the SiO_4 tetrahedron as in any silicate or silica. The tetrahedra has great flexibility for the $O - Si - O$ angle and the $Si - O$ distances. All the four oxygen atoms are shared by neighboring tetrahedra. Under the geothermal conditions of their formation in nature, some of the silicon atoms are replaced by aluminum. Thus a zeolite has both SiO_4 as well as AlO_4 tetrahedra. The atoms at the centre of the tetrahedra are generally referred to as T atoms.

Joining of the tetrahedra by shared oxygen atoms in a variety of ways gives rise to different structures. As an example, 24 such tetrahedra can join giving rise to a cubooctahedron that is known as the *sodalite* unit (figure 9.2 a). Each corner has a silicon or an aluminium atom and the oxygen atoms (not shown) are present at the midpoint of the lines

joining the corners. In the sodalite unit, each T atom is linked to three O atoms and the T atoms can link to a fourth O by joining with another sodalite unit. The sodalite units can be joined to give different structures. When each of the four-silicon rings are shared by two sodalite units with common T atoms, the structure formed is found in the mineral *sodalite* (figure 9.2 b). When the sodalite units are joined through common oxygen atoms, the structure generated is that of zeolite A (figure 9.2 c). If the sodalite units are connected by sharing the oxygen atoms of the six-silicon rings, the structure formed is the same as that found in the natural zeolite *faujasite* (figure 9.2 d).

Figure 9.2: *Formation of zeolite structures:* a. *sodalite unit; b. sodalite; c. zeolite A; faujasite.*

We have seen that the sodalite unit has four and six T atom rings. But faujasite formed by joining these rings has twelve-T rings in the structure. It should be remembered that each ring has as many oxygen atoms as there are T atoms and the rings are generally referred to by the number of oxygen atoms in a ring such as six-oxygen ring, 12-oxygen ring and so on.

The sodalite unit is one of the many types of secondary building blocks in a zeolite. There are many other types of building blocks. As another example, we shall see how the structure of the well known synthetic zeolite ZSM-5 is made. This is shown in figure 9.3. This shows a five-member ring (9.3 a and b) and how they link up forming a chain (9.3 c).

Figure 9.4 a shows how two chains link up forming the ZSM-5 struc-

ture. Joining of the chains generate 10-oxygen rings that form channels in the structure of approximately 5.6 Ådiameter. Figure 9.4 b gives a picture that ignores the smaller channels. This shows that the channels with 10-oxygen rings are straight in one direction and run zigzag in the perpendicular direction intersecting the straight channels. Classification of zeolites based on pore opening is given in table 9.1.

Table 9.1: Classification of zeolites based on pore/channel system.

Zeolite type	Channel system[1 a]	Cavity, Å
Small pore		
Linde A	4.1, (8, 3-dimension)	6.6 and 11.4
Erionite	3.6x5.2 (8, 3-dimension)	6.3x13
Medium pore		
ZSM-5	5.4x4.8 (10, 1-dimension)	Interconnected
	5.1x5.6 (10, 1-dimensiom)	channels
Ferrierite	3.4x4.8 (8, 1-dimension)	Interconnected
	4.3x5.5 (10, 1-dimension	channels)
Large pore		
Faujasite	7.4 (12, 3-dimension)	6.6 and 13
Mordenite	2.9x5.7 (8, 1-dimension)	Interconnected
	6.7x7 (12, 1-dimension)	channels

[1]shows size of channel in Å; no. of O atoms in the ring and channel directions are shown in parentheses.

Pore structure plays an extremely important role in determining the properties of zeolites. The other important aspect is the Si/Al ratio.

9.2.2 Zeolite Pores

One important aspect of zeolite chemistry is the presence of micropores of molecular dimension. Although macropores too exist in the intercrystalline space, they are of much less consequence. Nearly the entire surface area of the zeolites are the surface inside the micropores. The pores that are accessible to molecules are the pores of made 8, 10 and 12 oxygen ring. These rings may be circular or elliptical because of the flexibility of the bond angles. Different types of oxygen rings are shown in figure 9.6. A few structures with extra-large pores (14 or more member rings) have been reported.

Pore size can be directly found out by X-ray crystallography. But it is often difficult to grow single crystals. The indirect method of determining the pore size in a zeolite is adsorption of probe molecules. A compound can undergo appreciable adsorption in a zeolite only if its molecules are able to enter into the micropores. This implies that the

diameter of the pore is larger than the kinetic diameter of the probe molecule. Kinetic diameter of some probe molecules as obtained using Lennard-Jones potential are listed in table 9.2.

Figure 9.3: *Formation of the chain from five-member oxygen ring; the chains join to form the ZSM-5 pore structure.*

Zeolites that are made of 5-oxygen double rings are termed pentasils. Both ZSM-5 (MFI-type) and ZSM-11 (MEL-type) are of pentasil variety. Unlike ZSM-5, ZSM-11 has straight channels. Both have very high Si/Al ratio.

Figure 9.4: ZSM-5 *structure: a. formation of 10-O ring, and b. straight and zigzag channels in ZSM-5.*

Zeolites of the ferrierite (FER) family has a special configuration of

5-O rings. Ferrierite is one of the high silica natural zeolites with Si/Al ratio between 16 and 28. The structure has columns of 8-O rings along the b-axis and chains of 5-O rings that are interconnected successively through 6-O and 10-O channels parallel to the c-axis. The 8- and 10-ring channels intersect perpendicularly. A number of synthetic zeolites having names such as ZSM-35, ZSM-38 and Fu-9 belong to the FER family.

MTT is another important family of zeolites. Here, the 10-ring pores are separated by sinusoidal chains 5-O rings that are connected by 6-O rings. The 10-ring pores are egg-shaped and run only in one direction. Synthetic zeolites ZSM-23, ISI-4, KZ-1, EU-1, EU-4 belong to this family. They have unidirectional channels running parallel to the a axis.

9.2.3 Synthesis

Synthesis of zeolites have been extensively studied by Barrer[2] and his group. Synthesis is carried out hydrothermally by heating a mixture of the solutions of sodium silicate and an aluminium salt in alkaline condition at about 100^o C and at a pressure higher than one atmosphere. The initially formed gel slowly crystallizes forming the zeolite structure.

Figure 9.5: *Two dimensional framework of (a) ferrierite; (b)* ZSM-23.

Factors that are important in the synthesis of a zeolite are: (a) the silicate source, (b) the ratio of Si to Al (c) pH of the gel, (d) quantity

[2]Barrer, R.M., *Hydrothermal Synthesis of Zeolites*, Academic Press, London, 1982.

of water added, (e) temperature and duration of heating. The pressure used is self-generated and is often not accurately monitored. The use of some organic compounds, that are believed to serve as the template around which crystallization begins, is often necessary.

The presence of free OH^- is necessary as it complexes easily with silicon and aluminium ions. The $T - OH$ units can join with the elimination of water forming $T - O - T$ linkage. The presence inorganic and organic cations (present in the hydrated form) can act as templates around which structure formation can begin. Higher temperature hastens the crystallization process, but this may also give rise to the formation dense phases with quartz or crystobalite structure instead of zeolites. It should be remembered that zeolites are meta-stable phases that tend to pass to the stable structures, a transition from less dense to more dense phases. Hence, the temperature and duration of heating should be carefully chosen. Often, this is done by trial method.

Table 9.2: Kinetic diameter of probe molecules

Molecule	Kinetic diameter, Å
carbon dioxide	3.3
ammonia	2.6
sulphur hexafluoride	5.5
ethene	3.3
i-butane	5.0
cyclohexane	6.0
neopentane	6.2
n-butane	4.3
benzene	5.85

Presence of inorganic cations (present in hydrated form) greatly influences crystallization. Thus, it has been found that the presence of sodium or potassium ion gives much bigger crystals as compared to the presence of ammonium ion.

Although it is believed that the organic molecules, generally weak organic bases, acts as templates, their actual role is far more complex. It has been found that different templates can be used to synthesize the same zeolite and also the same template may lead to different structures depending upon other conditions. This is because the organic template may assume different structures depending upon the extent of its hydration. Some common organic templates are tetramethyl ammonium, tetraethyl ammonium and tetrapropyl ammonium ions, 1,2-

diaminoethane, 1,3-diaminopropane etc.

9.2.4 Acidity of Zeolites

It has been already told that the zeolites are solid acids and have both Brönsted and Lewis acid sites.

Two aspects of acidity are important in zeolites: concentration of acid sites and strength of the acid sites. The first increases with the relative amount of aluminium in the structure as increased amount of aluminium generates more negative charge in the zeolite framework. Strength of acid sites, on the other hand, is greater when the amount of aluminium is lower. This is related to higher electronegativity of silicon as compared to that of aluminium. Higher amount of the more electronegative silicon makes it a stronger acid. However, low silica zeolites can not be synthesized with higher value of Si/Al ratio. In order to increase the Si/Al ratio in them, they are subjected to treatment for partial removal od aluminium from the structure. This is known as dealumination and is carried out by high temperature steaming, acid treatment or treatment with EDTA of the zeolite.

Figure 9.6: *8-member, 10-member and 12-member oxygen rings found in erionite,* ZSM-5 *and faujasite.*

A zeolite may have $Si-O-Si$ and $Si-O-Al$ linkages. However, the $Al-O-Al$ linkage is never found in a zeolite. This is known as Lowenstein's rule. The reason for this is that the presence of two large Al atoms side by side in place of Si makes the structure unstable. Following Lowenstein's rule, there can be five different types of silicon environment in a zeolite if one considers the near-neighbour T atoms only. These are

silicon linked (via oxygen) 0, 1, 2, 3, and 4 aluminium atoms respectively. The zero-aluminium environment does not have any $Si - O - Al$ linkage and hence does not generate an acid site. The proton is associated with the oxygen of the $Si - O - Al$ bond and there are four such hydroxyls possible as shown in figure 9.7. In these structures, the silicon atom having the hydroxyl is linked to one, two, four and three aluminium atoms respectively. These would give rise to four distinct types Brönsted acid sites.

Figure 9.7: *Four possible types of bridged hydroxyls in a zeolite.*

There are several methods for determining acidity of a zeolite. The most commonly used are (a) titration with a base in a nonaqueous medium, (b) infrared spectra of adsorbed bases and (c) temperature programmed desorption of an adsorbed base.

Acid-base titration

The strength of acids and bases is expressed by the equilibrium constant of the reaction

$$B + H^+ \rightleftharpoons BH^+ \tag{9.1}$$

However, equilibrium constant cannot be directly calculated in cases of strong acid solutions and strong acidic surfaces. Acidity in such cases is expressed as Hammett's acidity function (H^0)[3]

$$-\log [H^+] = pK - \log \frac{[BH^+]}{[B]} \tag{9.2}$$

The base B should have a colour different from that of BH^+. By selecting a number of indicators of different pK values, Hammett's acidity function can be found out. This method, originally applied to solutions, has

[3]Hammett, L.P., *Physical Organic Chemistry*,McGraw-Hill, New York, 1940.

been extended to measure surface acidity. This is possible because the indicator adsorbed on the surface of the solid also changes colour on changing to the protonated form. If the acid function of the surface is lower than that of the indicator, colour will change.This method has been extensively used by Benessi[4], Dzisko and Borisova [5] and many others. In order to find out the total number of acid sites, the zeolite is suspended in a nonpolar solvent (normally heptane) and a suitable indicator is adsorbed on the surface. It is then titrated with a solution of butylamine in heptane.

Infrared spectroscopic method

This method has been used widely. Spectra of a thin wafer of the solid is recorded in a high vacuum infrared cell with provision for heating that enables to record spectra as a function of heat treatment of the sample.

Figure 9.8: *Infrared spectra of* ZSM-5 *wafer with adsorbed pyridine at various temperature; both hydroxyl and pyridine regions are shown. (a): after pyridine adsorption at 150º C, (b), (c) and (d): after evacuating at 250, 350 and 450 degree C respectively.*

Two infrared bands are commonly seen in the hydroxyl stretching region at about 3740 and 3600 cm^{-1}. The higher wave number band is associated with surface silanol and that around 3600 $cm^{-}1$ is due to bridging hydroxyl present inside the zeolite pores. Quantum-chemical

[4]Benesi, H.A., *J.Am.Chem.Soc.*,21, 5490 (1956).
[5]Dzisko, V.A. and Borisova M.S., *Kinet. Kataliz*, 1, 144 (1960).

calculations by Kazanskii[6] has shown that the bridged hydroxyls are the stronger acid sites. There can be four different types of bridging hydroxyls in zeolites (figure 9.8).

Infrared spectra of adsorbed molecules can distinguish Brönsted and Lewis acid sites. Pyridine is generally used as the probe. It forms pyridinium ion with H^+ and also gets coordinated to valence-unsaturated aluminium (Lewis acid site). The pyridine ring vibration appearing at 1540 cm^{-1} belongs to pyridinium and that at 1445 cm^{-1} is due to coordinated pyridine. Satyanaryana and Chakrabarty[7] has studied both the hydroxyl region and the pyridine ring vibration region at different temperature for the same ZSM-5 samples. Pyridine was adsorbed at (a) 150^0 C and evacuated at (b) 250, (c) 350 and (d) 450^o C respectively.

The intensity of the hydroxyl increased as more and more pyridine was desorbed by heating and the intensity of the bands due to adsorbed pyridine decreased. At the highest temperature, most pyridine at the Lewis acid sites was desorbed, but some pyridine attached to the strongest Brönsted sites prevailed (figure 9.8).

Temperature programmed desorption

Because of the simplicity of the experimental technique, temperature programmed desorption (TPD) of a pre-adsorbed base like ammonia or pyridine is the most commonly used method for evaluation of acidity of a zeolite. Being a small molecule, ammonia (kinetic diameter 2.62 Å) can reach almost all the acid sites in a zeolite. Use of pyridine, on the other hand, may give information of the acid sites located in the pores and channels that are catalytically more significant. The method uses a programmed heating of the zeolite sample on which ammonia has been adsorbed. The desorbed gas is continuously monitored using a gas chromatographic detector and a plot of temperature against the detector signal is obtained. The TPD profile may show one or more separated or overlapping peaks that may be resolved using a suitable computer program. Each peak is identified with acid sites of a particular strength. Peak area is a measure of the number of acid sites that may be calibrated by introducing appropriate doses of ammonia into the detector. A typical TPD of a sample of acidic ZSM-5 is shown figure 9.9.

In summary, some zeolite structures such as zeolite A can tolerate Si/Al ratio that is marginally higher than one. Some structures may have

[6]Kazanskii, V.V.,*Structure and Reactivity of Modified Zeoites*, Elsevier, Amsterdam 1984, p.61.

[7]Satyanaryana C and Chakrabarty D.K., *Ind. J. Chem.*, 30A, 422 (1991).

very high Si/Al ratio approaching infinity (ZSM-5). Number of acid sites decrease with the decrease in Si/Al ratio. For example, it is possible to retain the ZSM-5 structure with only silicon and no aluminium (silicalite 1) and this has no acidity at all. Strength of the acid sites, on the other hand, increases as Si/Al ratio increases. This is because of the increase in the average electronegativity of the framework. Thermal stability of the zeolite structure too increases by decreasing the quantity of aluminium in the structure. Catalytic activity of the zeolites can be manipulated by controlling several factors like framework structure, pore size as well as acidity.

Figure 9.9: *Temperature programmed desorption profile of ammonia from a* ZSM-5 *sample.*

9.2.5 Shape Selective Catalysis

Catalysis by zeolites can be applied to those reactions that are generally catalyzed by acids. Besides their acidity, pore structure of the zeolites is important in determining the catalytic activity and selectivity and this leads to shape selective catalysis.

The concept of shape selectivity was first introduced by Frilette, Weisz and Golden[8]. They noticed that calcium exchanged A (a small pore zeolite) dehydrated 1-butanol, but there was no dehydration of 2-butanol on this catalyst. This was unexpected as 2-butanol should undergo easy dehydration on an acidic zeolite. Weisz and his coworkers quickly realized that this happens because of the larger kinetic diameter of 2-butanol. Since the reaction is to take place inside the zeolite pores where most acid sites are located, 2-butanol could not reach the sites

[8]Frilette, V.J., Weisz, W.B. and Golden, R.L.,*J. Catal.*, 1, 301 (1962).

because the small pores of zeolite A were partially blocked by the calcium ions. 1-butanol with smaller kinetic diameter could enter the pores to reach the acid sites and could undergo conversion, whereas the bigger 2-butanol molecule failed to do so. Thus, it was established that catalysis on microporous materials not only depend on the chemical behaviour of the molecules, but also on the shape of the molecules. The authors called this shape selective catalysis. What we have described here is an example of *reactant shape selectivity.*

Figure 9.10: *Shape selective reactions on* ZSM-5*: a. reactant shape selectivity; b. product shape selectivity and c. transition state shape selectivity.*

The product pattern depends not only on the shape and size of the reactants, but also those of the products. Of the several products that may be formed inside the zeolite cavity, only those that can diffuse out through the pores will be present in the product. Other molecules will undergo further reaction. Methylation of toluene to xylene gives selectively p-xylene on modified ZSM-5, although thermodynamics predicts m-xylene as the major product. All the three xylenes are actually formed at the channel intersection of this zeolite to form an equilibrium mixture that has the m-, p- and o-isomers in the ratio 2:1:1 approximately. However, the para isomer can diffuse out more easily because of its smaller kinetic diameter. As the concentration of p-xylene inside the zeolite pore

decreases, more of the other two isomers get converted to it to maintain the equilibrium concentration. This is an example where shape of the product molecules decides the product selectivity. This is known as product shape selectivity.

Sometimes, the zeolite cavity does not have enough space to accommodate a particular transition state necessary to from a product. Thus, disproportionation of o-xylene in ZSM-5 gives toluene and 1,2,3-trimethylbenzene, but no 1,3,5-trimethylbenzene is formed. This is because the bulky transition state that could have led to the last product cannot be formed in the limited space. This transition state, however, can easily form in zeolite Y that has a much bigger cavity. This is an example of *transition state shape selectivity*. These examples are illustrated in figure 9.10.

Frilette and coworkers[9] introduced a term *constraint index* (CI) which is the ratio of the reaction rate constants for cracking of n-hexane and 3-methylpentane. Since CI for the medium pore zeolites were independent of crystal size, it can not be attributed to the diffusion constraint of the reactants. They suggested that CI is a measure of the steric constraint of the reaction intermediate (transition state) inside the zeolite cavity. Weitkamp and coworkers[10] introduced a quantity called *spaciousness index* (SI) defined as the yield ratio of iso-butane and n-butane in the hydrocracking of C_{10} naphthene. It was found that SI increased with pore width of the 12-O ring zeolites, but not very appropriate for 10-O ring zeolites.

9.2.6 Zeolite Based Processes

Despite its tremendous potential, relatively small number of chemical processes based on zeolite catalysts have so far been commercialized. The number of patents and published papers, however, demonstrate the great interest in this area. Any reactions that are catalyzed by sulphuric acid can be carried out on a suitable zeolite. The advantage of using a solid acid over the conventional acids are manifold. Because the catalyst is a solid, the problem of separating it from the product is not there. It is non-corrosive and non-polluting. These are in addition to the advantage of shape selectivity. It is impossible to present here all the reactions that have been carried out on zeolites. Only a few selected examples will be considered.

---

[9] V. J. Frilette, W. O. Haag and R. M. Lago, *J. Catal.*, 67, 218, (1981).

[10] J. Weitkamp, S. Ernst and R. Kumar, *Appl. Catal*, 27, 207, (1986).

One way of classifying the reactions based on zeolite catalysts is to divide them into: 1) chemicals related, 2) gas related and 3) oil conversion related, although there may be considerable overlap between them because at the present time, the principal raw material for all organic chemicals is petroleum and natural gas. However, such a classification will simplify a complex task.

Chemicals related processes

Some of the important chemical processes that uses zeolites as catalysts are given in table 9.2.

Production of ethylbenzene from benzene and ethene (Mobil-Badger process) over ZSM-5 has several advantages. Besides the usual advantages of a solid acid, a high throughput and much lower catalyst deactivation are the additional benefits. The long life of the catalyst is due low coke formation that is related to the medium pore size and the absence of cavity in this zeolite. This prevents the formation of large organic molecules that are the precursors to coke. Formation of polyethylated products are prevented due to product shape selectivity.

Table 9.3: Important chemicals that uses zeolite catalysts

Process	Catalyst
Benzene to ethylbenzene	ZSM-5
Xylene production	Modified ZSM-5
Tolune to p-ethyltoluene	ZSM-5
Benzene and propene to cumene	H-Y
Methanol to lower olefins	Erionite
Olefin to amine	Modernite
Detergent alkylates	RE-Y or Modernite
Phenol to alkylphenol	K-L
Nitration of chlorobenzene with NO_x	Several
Cyclohexanone oxime to caprolactum	ZSM-5
Fischer-Tropsch to low olefins	Ru-Y
Side chain alkylation of toluene	Ca/B-X

The C_8 cut in the refinery consists of all three xylenes and ethyl benzene. Isomerization on modified ZSM-5 gives p-xylene which is the raw material for the production of terephthalic acid. It is formed not only by isomerization of the other two isomers o- and m-, but also by conversion of ethylbenzene. Use of ZSM-5 prevents disproportionation of xylene to toluene and trimethylbenzene because the transition state

leading to their formation is bulky and cannot be accommodated inside the pores of modified ZSM-5. Small amount of platinum on ZSM-5 is used for isomerization of C_8 fraction since it allows the isomerization of xylenes as well that of ethylbenzene to p-xylene. Conversion of ethylbenzene needs hydrogenation-dehydrogenation function (platinum) and xylene isomerization needs the acid sites. This catalyst is superior to the traditionally used platinum on silica/alumina that is less selective due to hydrocracking[11]. Disproportionation of toluene gives benzene and p-xylene and Mobil has developed an improved process based on ZSM-5[12]. In a similar manner, toluene can be ethylated with ethylene directly to p-ethyltoluene over ZSM-5 selectively and, cumene can be obtained from benzene and propene over H-Y. Alkylation of benzene with isobutanol gave mostly secondary butylbenezene with acidic Y, ZSM-5, ZSM-12 etc., zeolite unusually large amount of isobutylbenzene was formed using zeolite beta[13].

Many acid catalyzed reactions of functionalized hydrocarbons have been studied using zeolites. These include alkylation of phenol[14], halogenation[15], amine formation[16] and many other reactions.

Gas-conversion related processes

With growing information on proven natural gas reserves, the importance of processes based on methane or other C_1 compounds that can be obtained from methane, is increasing. The idea is to convert C_1 compounds to higher carbon compounds. Conversion of methane is achieved via synthesis gas route to methanol which is then further converted to other useful products. Important processes are methanol to gasoline (MTG), methanol to olefins (MTO), light paraffin to aromatics, to mention a few.

Methanol to gasoline

The Mobil MTG is based on medium pore zeolite like ZSM-5 that yield primarily aromatics, lower olefins and some C_{5+} non-aromatics[17]. Use

[11] F. G. Dwyer, *Chemical Industries, No.5*, Dekker, New York, 1981.

[12] W. O. Haag, D. H. Olson and P. B. Weisz, *Chemistry for the Future, Proc. IUPAC Congress*, Cologne, Pergamon-Oxford, 1984.

[13] A. Mitra, S. Subramanian, D. Das, S. V. V. Chilukuri and D. K. Chakrabarty, *Appl. Catal. A*, 153, 233 (1997).

[14] U. S Patent, 4 371 714 assigned to Mobil Oil

[15] *Eur. Chem. News*, June 24, 19 (1985)

[16] C. D. Chang and P. D. Perkins, *Zeolites*, 3, 298 (1983)

[17] C. D. Chang and A. J. Silvestri, *Chemtech*, 624 (1987).

of ZSM-11 increases C_{5+} aliphatics at the expense of C_3 whereas ZSM-4 gives a lot more C_{11+}. Light olefins are first formed in this process which than get converted through oligomerization and hydrogen transfer.

Methanol to olefin
By suitable choice of conditions such as temperature, space velocity, methanol partial pressure and total pressure, it possible to carry out either MOG or MTG[18]. Wide pore zeolites give heavy aromatics, but lead to high coke formation.

Figure 9.11: *Olefin oligomerization by Shell process.*

LPG to aromatics
Another interesting route is direct conversion of light petroleum gas (LPG) into aromatics that may be used for mixing with gasoline for octane raising as well as source of petrochemicals. Galium-impregnated zeolite has been found useful for this[19]. The route to these products is via dehydrogenation of paraffins followed by oligomerization and cyclization where gallium acts as the dehydrogenation component.
Olefin oligomerization
Olefin oligomerization is another important process. Although this has been known for some time, the advantage of the new zeolite based catalysts is that the product pattern can be changed by adjusting the process conditions[20]. Product distribution in the Shell process is shown in figure 9.11. The process gives large amount of kerosene fraction, but also good quantity of both gasoline and diesel. By modifying the process

[18] C. D. Chang, *Catal. Rev. Sc. and Engg.*, 26, 323 (1984).
[19] US Patent 4 528 412.
[20] S. A. Tabak and J. H. Beech, *Paper presented at AIChE Spring National Meet*, Houston, 1989.

conditions, it is possible to switch between gasoline that is the preferred product in the Western countries, and middle distillate that is more in demand in the developing world.

Oil conversion related processes

Some of the important processes in this category are

Hydroisomerization

Prohibition of lead tetraethyl as additives to motor fuel has led to the search for alternative methods to boost the octane number. Thus, it has become important to hydroisomerize the C_5 and C_6 paraffins to branched products. Since isomerization is favoured at lower temperature[21], zeolites catalysts are preferred because they work at moderate temperature. The feed is C_5 and C_6 paraffins and mordenite is used as the catalyst. Since isomerization is incomplete, zeolite A is used for separating the branched paraffins from the normal and the latter is recycled into the isomerizer. Higher paraffins are not used because they undergo cracking rather than isomerization.

Figure 9.12: *Total isomerization process*

Hydrodewaxing

Wax essentially consists of normal paraffin molecules and they are undesirable for quality lubricating base oil. Hence, the base oil needs to be processed to remove the n-paraffins. This can be doe by solvent extraction, but the new method used is catalytic dewaxing. This is done in the presence of hydrogen using a platinum-containing medium pore shape selective zeolite such as ZSM-5. Long normal paraffin molecules are are selectively hydrocracked to get lighter molecules.

Hydrocracking

Hydrocracking based on zeolite catalysts were developed in the United

[21] J. Weitkemp, *ACS Symposium Series 20, Am. Chem. Soc.*, (1075)

States mainly for naphtha processing and these catalysts were not required to be highly selective. But high demand for middle distillates like diesel and kerosene in the developing countries in particular, required that the catalysts be more selective for these products.

Fluidized catalytic cracking showed a dramatic improvement after zeolite Y was introduced as catalyst mostly as its rare earth exchanged form (REY). But this catalyst gave increased amount of paraffins leading to decreased octane number. Ultra-stable Y (USY) zeolite that has a higher Si/Al ratio and hence lower concentration of acid sites has improved the situation. A mixed catalyst consisting of REY and USY has given much better performance. There is still much scope for the improvement of FCC catalyst.

9.3 ALUMINOPHOSPHATE MOLECULAR SIEVES

Success of the zeolites as catalysts led to the search of newer type of molecular sieves other than aluminosilicates. Since both phosphorus and aluminium in their usual oxidation states (5+ and 3+ respectively) form oxygen-sharing tetrahedra, attempts have been made to prepare aluminum phosphate molecular sieves. The first success was reported by Wilson *et al.*[22] when they synthesized micro-porous sieves by hydrothermal treatment of a reactive alumninophosphate gel in the presence of an organic template. Structures of this type are made of alternating AlO_4 and PO_4 tetrahedra with shared oxygen between them. They form a variety of structures some of which are analogous to known zeolite structures. These are called "alpo" and one structure $AlPO_4$-5 has the structure of the zeolite faujasite and the framework structure of $AlPO_4$-34 is similar to that of the zeolite chabazite. All the known structures contain $Al-O-P$ linkage and none have either $Al-O-Al$ or $P-O-P$ linkages. These compounds are charge neutral and do not have any exchangeable ions and hence are neither acidic nor basic. These, therefore, have no use as solid acid catalysts.

Some of the $AlPO_4$ structures do not form in the absence of silicon at the T sites. For example, a silicon-containing chabazite-like structure SAPO-34 can be readily synthesized although $AlPO_4$-34 is not known. Silicon substituted aluminophosphate sieves were reported by the same group[23] who found that Si^{4+} replaces P^{5+} in the structure. This im-

[22] S. T. Wilson, b.M. Lok, C. A. Messina, R. T. Gajek, R. L. Patton and E. M. Flanigen, *J. Am. Chem. Soc.*, 104, 1146 (1982).

[23] B. M. Lok, C. A. Messina, R. L. Patton, R. T. Gajek, T. R. Cannan and E. M. Flanigen, *J. Am. Chem. Soc.*,106, 6092 (1984).

parts a negative charge to the framework that is compensated by protons. These class of compounds known as SAPOs are therefore Brönsted acids. It is also possible to substitute metal ions which, according to available evidence, replaces the Al^{3+} ions. If the metal ions are divalent like Mg^{2+}, that too will give a negatively charged frame and hence will be acidic. Such compounds are called MeAPOs. A very large number of $AlPO_4$, SAPO, MeAPO and MeSAPO structures have been reported so far. Metal substitution in the $AlPO_4$ frame is easier as compared to the zeolite frame. This is because the zeolites are synthesized from slightly basic medium and under these conditions, metal hydroxides precipitate out. Aluminophosphate sieves, on the other hand, are synthesized from slightly acidic solution that makes metal substitution easier. Aluminophosphate and substituted aluminophosphate sieves with small pore (8-O ring), medium pore (10-O ring) and large pore (12-O ring) structures have been reported.

Catalysis by SAPO

SAPOs are weaker acids as compared to the zeolites and this property can be beneficially utilized in catalysis. In the methanol conversion reaction that proceeds via ether to alkenes and finally gives alkanes and aromatics, the first two steps requires mild acidity, whereas the formation of aromatics needs strong acid sites. Use of a variety of SAPO-34, medium pore material gives more than 95 percent alkenes as compared to 20 percent by ZSM-5, which mainly gives aromatics and alkanes[24]. Vapour phase oligomerization takes place efficiently on medium pore SAPO-34 and SAPO-31 as compared to the medium pore zeolite ZSM-5 which gives a high yield of aromatics. This is because formation of aromatics needs hydrogen transfer that can take place only on strong acids[25]. In most cases, the low acid strength of SAPO as compared to the their zeolite counterparts has been exploited to advantage.

Among the various SAPO materials, SAPO-41, a structure with highly elliptical 10-oxygen pore openings has been found to have a large number of strong acid sites. Its activity for toluene methylation with methanol was found to be higher than even that of ZSM-5. The product also contained a large amount of 1,2,4-trimethylbenzene formed mostly due to further alkylation of p-xylene. This appears an interesting material as it has a strong acidity among SAPOs[26].

[24] C. D. Chang, *Catal. Rev. Sci. and Engg.*, 25, 1, (1983).

[25] J. A. Rabo, R. J. Pellet, P. K. Coughlin and E. S. Shamshoum, *Stud. Surf. Sci. Catal.*, 46, 1, (1989).

[26] A. M. Prakash, S. V. V. Chilukuri, R. P. Bagwe, S. Ashtekar and D. K.

9.4 CLAYS

Clays belong to a class of sheet silicates also called phyllosilicates. If we consider a silcate sheet, its composition will be $(Si_2O_5)_n^{-2n}$ with all the unshared oxygen lying on one side of the sheet. If a layer of γ-gibbsite $Al(OH)_3$ is placed over this sheet such that the Al atoms share the terminal oxygens of the silicate sheet, the OH can be eliminated. The aluminium atoms are six-coordinated. A 1:1 or TO (tetrahedral-octahedral) structure formed in this way gives the clay called kaolinite that has the formula $Al_2(OH)_4(Si_2O_5)$. If a second silica sheet combines with the other side of the aluminium layer, it gives 2:1 (TOT) structure of composition $Al_2(OH)_2(Si_2O_5)_2$ known as pyrophyllite (see figure 9.13).

Figure 9.13: *(a) TO (kaolinite) and (b) TOT (pyrophillite) clay structure.*

If a $Mg(OH)_2$ layer is placed over the silicate sheet to form a two-layer structure, it gives chrysotile $Mg_3(OH)_4(Si_2O_5)$.

If silicon (oxidation number +4)in the tetrahedral sites are substituted by aluminium (oxidation number 3+), the sheet becomes negatively charged. The negative charge is compensated by positive metal ions placed between the layers. Exchange of the metal ions by protons makes the clays Brönsted acids that makes them solid acid catalysts.

One clay mineral that has been extensively studied for its catalytic activity is montmorillonite that has the composition;

$$M_{x/n}^{n+}.xH_2O(Al_{4-x}Mg_x)_{oct}(Si_8)_{tet}O_{20}(OH)_4.$$

Chakrabarty, *Microporous Mat.*, 6, 89, (1996).

It is no longer necessary to be restricted by the naturally occurring clay minerals as it is possible to synthesize them with much wider variation of composition in which the octahedrally coordinated aluminium can be replaced by transition metal ions[27]. Synthesis is also possible with varying Si:Al ratio and substitution of hetero-atoms at both tetrahedral and octahedral sites and all these can be used to control acidity of the clay.

9.4.1 Intercalation of Clays

Clays swell in water and other polar solvents because of the hydration of the inter-lamellar cation. This is actually an example of intercalation in which the host structure of the clay accommodates the guest solvent molecules. Organic molecules undergo catalytic conversion through intercalation followed by activation at the acid sites. Host structure has to expand to accommodate the guests. The inter-lamellar water may be one-, two- or three-layered and they can be readily replaced by organic molecules. In recent years, many transition metal complexes have been intercalated.

Figure 9.14: *Formation of pillared clays shown schematically.*

It has been shown that when hydrated Cu^{2+} is intercalated in montmorillonite the metal ion is present as square-planar $[Cu(OH_2)_4]^{2+}$ parallel to the silicate sheet. This shows strong tendency to coordinate organic molecules[28]. Pinnavaia and Welty[29] prepared intercalated $[Rh(PPh_3)_n]^+$ in the clay hectorite by treating intercalated $[Rh_2(OAc)_{4-x}]^{x+}$ with triph-

[27] J. M. Thomas and C. R. Theocharis in *Modern Synthetic Methods*, Vol.5 Springer Verlag, 249, (1989).

[28] M. M. Mortland and T. J. Pinnavaia, *Nature*,229, 75, (1971).

[29] T. J. Pinnavaia and P. K. Welty,*J. Am. Chem. Soc.*, 97, 3819 (1975).

enyl phosphine. Many other metal complexes have been intercalated[30],[31] in clays and some of them may be used as anchored homogeneous catalysts.

9.4.2 Pillared Clays

Although proton exchanged clays have good acidity, they cannot be used at high temperature because of the collapse of the inter-lamellar space due to removal of water. The collapse can be prevented by pillaring the clays by introducing inorganic material into the inter-lamellar space. By placing the pillars evenly, a new type of shape selective acid catalysts can be created. For this, polynuclear cationic species of silicon, aluminium, titanium, zirconium etc. are ion-exchanged by soaking the clay in solutions containing such species. The resulting pillared clays have high thermal stability[32].

9.4.3 Catalysis with Clays

As in the case of zeolites, acid sites in clays may be Brönsted as well as Lewis type that are interconvertible through dehydroxylation-rehydration. Reactions that are acid catalyzed can be carried out on clays. These are dimerization, hydrogen transfer, ether formation, ester formation, to name a few. As has been stated, clay has the disadvantage of structural collapse at high temperature that can be prevented by pillaring. Some reactions on pillared clays will be considered here.

Catalysis on Pillared Clays

One interesting reaction is the conversion of trimethylbenzene (TMB) that undergoes both isomerization and disproportionation. This has been studied on clays pillared with polymeric aluminium oxide. Among the trimethylbenzene isomers, 1,2,4-TMB that has the smallest molecular kinetic diameter has been found to be most active and this has been attributed to transition state shape selectivity[33]. Zirconia pillared clays has been found to be active for methanol to olefin conversion[34]. Iron oxide pillared clay is active for Fischer-Tropsch conversion of synthesis gas with high selectivity for C_1-C_5 hydrocarbons.

[30] A. Yamagishi, *J. Coord. Chem.*, 16, 131, (1087).
[31] R. A. Dellagardia and J. K. Thomas, *J. Phys. Chem.*, 87, 990 (1983).
[32] D. E. W. Vaughan, *Chem. Engg. Progr.*, 25 (1988).
[33] T. J. Pinnavia and P. K. Welty, *J. Am. Chem. Soc.*, 97, 3819, (1975).
[34] R. Burch and C. I. Warburton, *J. Catal.*, 97, 511 (1986).

Catalysis on ion-exchanged clays

Proton-exchanged montmorillonite can catalyze the conversion of toluene to nitrotoluene using *in situ* prepared $PhCOONO_2$ as the nitrating agent[35]. The reaction stops at mononitration stage. Another reaction that is very effectively catalyzed by ion-exchanged montmorillonite is addition of propene to toluene to give isopropyl derivatives.

Other important reactions include intermolecular elimination of ammonia from amines, reaction between acetone and formaldehyde to give methyl vinyl ketone, cyclization of α,ω-dicarboxylic acids, chlorination of aromatics.

Many reactions catalyzed by clays are stereoselective. Also, clays absorb preferentially one optical isomer and thus can be used in asymmetric synthesis. Because of the possibility of tailoring the inter-lamellar spacings and acidity, clays are going to be important catalytic material for many more reactions.

9.5 MESOPOROUS MATERIALS

These are inorganic solid material that have uniform pores ranging from 20-500 Å. The most important of them is the structure known as MCM-41. Last ten years have produced a large number of publications on these materials. They are synthesized in the presence of a surfactant such as cetyltrimethylammonium halide. The method of synthesis is similar to that of zeolites. It has been suggested that the surfactant molecules arrange themselves into cylindrical micelles with the polar groups pointing outwards towards the surface of the cylindrical arrangement. Si-OH groups of the silicate species get attracted towards these polar groups. Two or three layers of the silicate precursors get deposited on the micellar formation forming the structure. After crystallization, the organic molecule is expelled by heating making the substance mesoporous (see figure 9.15). If this mechanism of their formation is valid, then the chain length of the alkyl ammonium halide will be crucial in determining the pore size.

Metal substitution for silicon could achieved only to a very limited extent. Often, it has found that substitution makes the structure highly unstable. Synthesis of such materials has been reviewed by Ying. Menhert and Wong[36]. Main problem in using them in catalysis lies in their poor acidity and low thermal stability. Once these problems are solved,

[35] A. Cornelis, A. Gerstmans and P. Laszlo, *Chemistry Letts.*, 1839 (1988).

[36] J. Y. Ying, C. P. Menhert and M. S. Wong, *Angew Chem. Int. Ed.*, 38, 57, (1999).

Figure 9.15: *Cylindrical micelle leading to the formation of* MCM-41 *and related structures.*

they will be advantageous in that the pore size restriction imposed by the zeolites and other molecular sieves can be overcome.

SUGGESTED READING

1. Breck, D. W., *Molecular Sieves*, John Wiley, New York, 1974.
2. Szostak, R., *Molecular Sieves: Principles of Synthesis and Identification*, Van Nostrand, New York, 1989.
3. Barrer, R., *Hydrothermal Chemistry of Zeolites*, Acad. Press., London, 1982.

Chapter 10

Mechanism of Some Reactions

10.1 INTRODUCTION

Normal catalytic reactions proceed in five simple reaction steps. These are: 1. diffusion of the reactants to the surface, 2. their adsorption, 3. reaction of the adsorbed species, 4. desorption of the products and 5. diffusion of the products away from the surface (see Chapter 6). Among these five steps, step 3 (surface reaction) can have two distinct mechanisms. If the surface reaction involves the interaction between two adjacent chemisorbed species, then the reaction is termed as Langmuir-Hinshelwood (L-H) mechanism. If on the other hand the reaction involves interaction between one chemisorbed species and the other species is either physically adsorbed or reacts from the gas phase then the reaction is termed as Rideal-Eley (R-E)mechanism. These two reaction mechanisms is represented as

H D
| | $\rightarrow$ 2M + HD Langmuir-Hinshelwood mechanism
M – M

H D
| | + D_2 $\rightarrow$ | | + HD Rideal-Eley mechanism.
M – M M – M

Even though the examples shown have only one step involving either the Langmuir-Hinshelwood mechanism or Rideal-Eley mechanism, there can be in a reaction sequence many such steps. An example is

the hydrocarbon production on metals from CO and hydrogen by the Fischer-Tropsch process involving the formation of surface methylene and methyl radicals by the interaction between chemisorbed CO and physically adsorbed hydrogen. It must be clear that the strength of the chemisorption bond decides the mechanism to be followed. If the chemisorption bond is weak, it is possible to expect the predominance of Rideal-Eley mechanism. In this chapter we shall discuss mechanism of some typical catalytic reactions of importance and demonstrate how they have been elucidated.

10.2 O-P CONVERSION AND H_2-D_2 EXCHANGE

The reactions under consideration are

$$\begin{aligned} \mathrm{p-H_2} &\Longleftrightarrow \mathrm{o-H_2} \\ \mathrm{o-D_2} &\Longleftrightarrow \mathrm{p-D_2} \\ \mathrm{H_2 + D_2} &\Longleftrightarrow \mathrm{2HD} \end{aligned}$$

In each of these cases, the course of the reaction can be followed by measuring thermal conductivity of the gas phase. Ortho-para conversions can be catalyzed by the magnetic fields. This conversion takes place by the reversal of the nuclear spins without the dissociation of the molecule. Since non-dissociative pathway cannot account for the hydrogen-deuterium exchange, the mechanism of spin reversal brought out by the magnetic fields will not be considered here any further. Therefore, the first postulate one makes in the elucidation of the mechanism of these conversions and exchange is the dissociative adsorption of the diatomic hydrogen molecule H_2 or D_2. The available experimental observations can be summarized as follows:

(i) The relative velocity ratios on Pt surface were found to be para-H_2 conversion:ortho-D_2 conversion: H_2/D_2 exchange = 1:0.54:0.67 while on iron films this ratio was found to be 5:2:1.

(ii) There are two postulates for the mechanism of these reactions:

$$\mathrm{2M + p-H_2} \Longleftrightarrow \mathrm{2MH} \Longleftrightarrow \mathrm{2M + o-H_2} \quad (\mathrm{L-H\ mechanism})$$

$$\mathrm{MH + D_2} \Longleftrightarrow \mathrm{MD + HD} \quad (\mathrm{R-E\ mechanism})$$

One of the options to resolve between these two mechanisms is to find out the velocity of the transformations because the velocity of the transformation is related to the velocity of adsorption and desorption. One can either measure these velocities or calculate them assuming any of the two mechanisms and compare them. It was initially thought that hydrogen adsorption occurred on metal filaments at low temperature

but desorption could occur only at high temperature (> 673 K). However, the hydrogen deuterium exchange on metal films could be observed even at low temperature. Hence, it was deduced that the surfaces were saturated with atomic hydrogen at low temperatures (between 90 and 273K).
(iii) Isothermal heats of the reversible adsorption decrease continuously with increasing adsorption from 15.2 kcal/mol to 3 kcal/mol. Since these values are higher than what one can expect for physical adsorption, it is probably chemisorption.
(iv) Although it is probable that hydrogen adsorption on metal surfaces is reversible at low temperature, the variation of the surface coverage θ with temperature is rather small and hence requires precise measurements to ascertain the changes in the coverage.
(v) Assuming that hydrogen adsorption is non-activated and that the adsorbed hydrogen are mobile (the evidence for this comes from spill over of hydrogen atoms from the metal surface to oxide supports. In the case of gold nano-particles, this spill over and consequent H/D exchange has been demonstrated), the velocity of hydrogen adsorption can be written as[1]

$$u = \frac{\sigma p}{\sqrt{2\pi mkT}}(1-\theta)^2 \tag{10.1}$$

where θ is the surface coverage and σ is the condensation coefficient. u has the unit mol/cm^2.s. The other terms have the usual meaning. In this case, the rate of para hydrogen conversion must be given by the difference between the rates of adsorption and desorption. Thus,

$$r = \frac{\sigma p}{\sqrt{2\pi mkT}}(1-\theta)^2 - u' \tag{10.2}$$

where p is the pressure of para hydrogen and u' is the desorption rate. When equilibrium is established between para and ortho hydrogen, the equilibrium pressure of para hydrogen is p' and this can be deduced from the following equation

$$u' = \frac{\sigma p'}{\sqrt{2\pi mkT}}(1-\theta)^2 \tag{10.3}$$

since $r = 0$ under equilibrium conditions. Putting this value of u' in equation (10.2) gives

$$r = \frac{\sigma(p-p')}{\sqrt{2\pi mkT}}(1-\theta)^2 \tag{10.4}$$

[1]M. Lazar, C. Ducu, V. Almasan, N. Aldea, B. Barz, P. Marginean, C. Sutan and V. Malinov, *Roman. J. Phys.*, 51, 273, (2006).

This expression makes it possible to calculate r that can be compared with the experimentally obtained values.

Table 10.1: Kinetic data on conversion of para hydrogen on tungsten.

No.	Parameter	Experimental	Calculated
1	Activation energy	1950 kcal/mol	1650 kcal/mol
2	Order at 173 K	0.1 to 0.5	0.6
3	r at 173 K	1.8×10^{18}	2.2×10^{17}
	and 1 Torr	molecules/cm^2.s	molecules/cm^2.s

One can make use of equation (10.4) and calculate the order of the reaction and also evaluate the value of the activation energy. It is also possible to get the relative rates at constant pressure at two chosen temperatures T_1 and T_2 from the expression

$$\frac{r_1}{r_2} = \sqrt{\frac{T_2}{T_1}}.\frac{(1-\theta_1)^2}{(1-\theta_2)^2} \tag{10.5}$$

This can also be used to calculate the value of the activation energy. The kinetic parameters calculated using equation (10.4) and the experimental values are given in table 10.1 for comparision[2].

The differences between the experimental and calculated values could have arisen due to errors involved in estimating accurately the value of θ, the surface coverage.

Langmuir-Hinshelwood mechanism as applicable for the para ortho hydrogen conversion is called Bonhoeffer-Farkas mechanism. Evidence in support of the mechanism is the low order that is observed. If the reaction were to follow the Rideal-Eley mechanism then the rate will be proportional to $\theta.\theta'$ where θ' is the fraction of the coverage by the physically adsorbed state. The adsorption isotherms generated in this temperature range showed that the physical adsorption layers are hardly present and the surface gets saturated with a monolayer. This conclusion is based on the observation that the physically adsorbed layer or the coverage (θ') that should be proportional to pressure, hardly changes with p. If the reaction were to follow the Rideal-Eley mechanism then the order of the reaction has to be greater than unity. The fact that the order of the reaction is small shows that the reaction does not follow Rideal-Eley mechanism.

[2]D. D. Eley and E. K. Rideal, *Proc. Roy. Soc.*, A178, 429, (1941).

10.3 HYDROGENATION OF ETHYLENE ON METAL

In the case of para to ortho hydrogen conversion and the hydrogen-deuterium exchange reaction, the final decision on the reaction mechanism is taken by comparing the observed experimental rate with the rate calculated on the basis of the assumed mechanism. This is one of the ways of deciding the reaction mechanism. However, in elucidating the mechanism of other surface transformations, many more evidences are used. In this section, a more complex reaction namely, hydrogenation of ethylene on metal surfaces will be considered. The available experimental evidences are:

1. The initial heat of adsorption of ethylene on metallic surfaces is higher than that of hydrogen. This implies that the surface of the metals is essentially covered by adsorbed ethylene. This assumption is supported by the following observations as well: (i) the reaction is first order with respect to ethylene and zero order with respect to hydrogen on most of the metal surfaces, and (ii) even though metals like nickel are capable of catalyzing the H_2-D_2 exchange reaction, no exchange takes place when ethylene hydrogenation is carried out using a $H_2 + D_2$ mixture.

2. On metal surfaces, ethylene adsorption takes place by the dissociation of the molecule.

$4M + C_2H_4 \rightarrow M_2C_2H_4 + 2MH$

The adsorbed hydrogen reacts with the gas phase ethylene to form ethane according to the reaction

$$\begin{array}{ll} H & H \\ | & | \\ M & - M \end{array} + C_2H_4 \rightarrow 2M + C_2H_6$$

The surface acetylene generated may react with gas phase hydrogen to give ethylene

$M_2C_2H_2 + H_2 \rightarrow 2M + C_2H_4$

However, as has been already stated, the surface may be covered with the acetylene species formed by dissociative adsorption of ethylene.

3. If hydrogenation is carried out by using deuterium, then all the four deuterated ethylene are obtained such that

$$C_2H_3D > C_2H_2D_2 > C_2HD_3 > C_2D_4.$$

4. Redistribution of deuterium among the molecules may be taking place simultaneously with the hydrogenation reaction with deuterium. If these reactions were to occur independent of the hydrogenation reaction, all the six deuteroethnanes ($D_1 - D_6$) may be expected and not the only hydrogenation product $C_2H_4D_2$.

Redistribution reaction can occur at temperature lower than that of hydrogenation and hence it should be an independent reaction. This redistribution of deuterium in the saturated molecule is not entirely random. In the case of hydrogenation of *cis*-2-butene with deuterium on nickel surface, the relative amount of the deuterated butenes was not found to follow a binomial distribution suggesting that a fraction of the product has been formed by direct reaction without going through the redistribution route. The relative extent of redistribution to direct hydrogenation of olefins depends on the nature of the olefin, the metal surface and temperature.

Based on these observations, a reaction mechanism for the hydrogenation of ethylene has been proposed. The mechanism should reflect the exchange and the redistribution processes separately if deuterium was to be used as the hydrogen source.

For direct hydrogenation, formation of an adsorbed ethyl radical may be the first step. This may form in two ways
(a) Reaction between an adsorbed hydrogen and an impinging ehtylene molecule (R-E mechanism)

(b) Reaction between two adsorbed species (L-H mechanism)

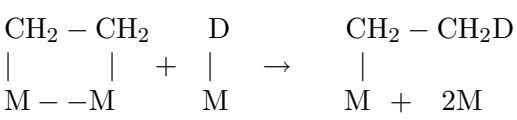

(c) Reaction between adsorbed ethylene molecule with a gaseous hydrogen molecule (R-E mechanism)

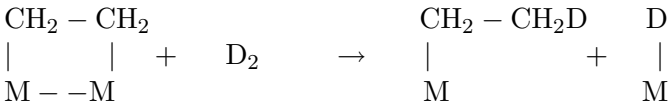

Even if a dissociative adsorption of hydrogen involving four sites has been visualized, two-site non-dissociative adsorption as shown in the schemes (b) and (c) is also possible. The redistribution reaction can take place according to the following steps

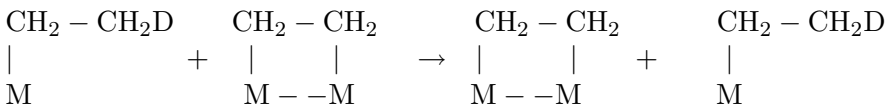

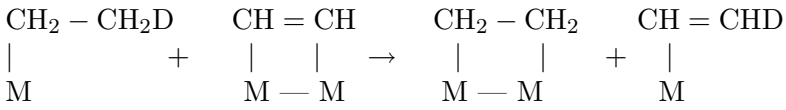

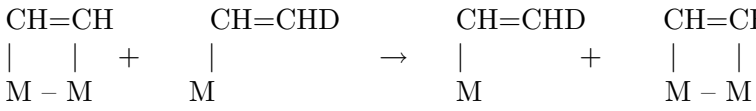

Hydrogenation will take place according to the scheme 2 (page 184). The velocity of the reaction will then be proportional to $\theta_H^2 . p_{C_2H_4}$. Since surface coverage θ_H^2 is proportional to $p_{H_2}/p_{C_2H_4}$, velocity of the reaction is proportional to the hydrogen pressure. However, scheme 2 cannot be the essential step since the ethyl radicals formed on the surface can also undergo the redistribution steps.

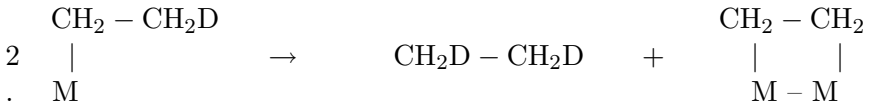

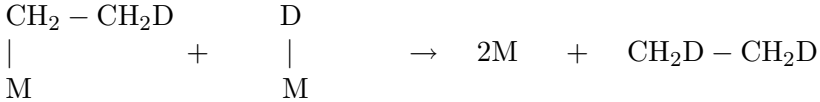

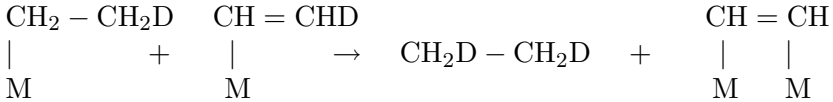

These surface ethyl radicals can thus redistribute before undergoing hydrogenation. The occurrence of redistribution itself is an evidence of the presence of the half-hydrogenated species on the surface.

Other experimental evidences in support of the Rideal-Eley mechanism are:

1. Heat of adsorption (about 30 kcal/mol);
2. Activation energy of hydrogenation too is of the same order of mag-

nitude;
3. The above two observations imply that ethylene is not adsorbed on the surface under these experimental conditions;
4. The reaction is independent of ethylene partial pressure and is proportional to either p_{H_2} or $p_{H_2}^{\frac{1}{2}}$.

It is therefore clear that this reaction is a typical example of the operation of the Rideal-Eley mechanism on metal surfaces.

10.4 CO OXIDATION ON OXIDE SURFACES

This reaction follows two different mechanisms depending on the temperature of the reaction. At low temperature, the velocity of the reaction is proportional to the pressure of oxygen and is independent of the pressure of CO, while at high temperatures, the reaction velocity is proportional to the pressure of CO and is independent of pressure of oxygen.

Low temperature reaction

The experimental results on oxidation of CO on cuprous oxide around 293 K shows that
1. Under the reaction conditions, the surface seems to be predominantly covered with CO. The adsorption of oxygen on cuprous oxide under these temperature conditions increased the conductivity while adsorption of CO decreased the same. If a mixture of the gases is exposed to a surface pre-saturated with oxygen, conductivity slowly falls as catalysis proceeds until it reaches the value for a CO covered surface. On the other hand, if the mixture is exposed to a surface pre-saturated with CO, the catalytic reaction proceeds without change in conductivity. This means that under these conditions, the surface covered with CO is the steady state.
2. If the completely free surface is exposed to a mixture of the gases, immediate adsorption of CO takes place followed by a slow fall in pressure due to the reaction which is proportional to one volume of oxygen and two volume of CO. This result indicates that a slow catalytic reaction takes place on CO covered surface.
3. Oxygen adsorption on CO covered surface is higher and the heat of oxygen adsorption is also higher than on the bare surface. This indicates that oxygen adsorption on the bare surface is different from the oxygen adsorption on CO covered surface.
4. The probable reaction taking place on the CO covered surface can be described as

$$CO + \frac{1}{2}O_2 + O^{2-} \longrightarrow CO_3^{2-} \tag{10.6}$$

leading to the formation of a surface carbonate like species. Formation of surface carbonate is also confirmed from calculation and measurement of the heat of adsorption (≈100 kcal/mol). All these results indicate that the mechanism of oxidation of CO is the formation of surface carbonate followed by its decomposition according to the equation

$$CO_3^{2-} \longrightarrow CO_2 + O^{2-} \tag{10.7}$$

However, it is known that surface carbonates do not decompose at such low temperature to give CO_2 as evidenced from the independent experiments on surface carbonate decomposition. But if CO is added to a carbonate covered surface formed by CO_2, adsorption is rapid and in the reaction, two volumes of CO_2 is evolved for every volume of CO that is adsorbed. Hence, the reaction can be represented as

$$CO_3^{2-} + CO_s \xrightarrow{k_3} 2CO_2 + 2e^- \tag{10.8}$$

This is the most probable mechanism of oxidation of CO on oxides at low temperatures. It is possible to confirm this by considering the kinetics of the reaction. It is likely that adsorption of CO takes place on the surface metal ions. As in the case of hydrogen-deuterium exchange, the mechanism of the reaction in this case too can be established by considering the kinetics of the oxidation process. In this reaction, the gas phase oxygen strikes the surface sites to form surface carbonate species as

$$CO_s + 2O_s \xrightarrow{k_2} CO_{3,s} \tag{10.9}$$

Adsorbed oxygen is produced by the impingement of gaseous oxygen molecules on the available sites and adsorbed oxygen is removed by the formation of carbonate species (equation 10.9). Applying steady state approximation for the coverage of surface adsorbed oxygen and also for the surface carbonate species one gets

$$\frac{d\theta_O}{dt} = k_1 p_{O_2}(1 - \theta_O)^2 - k_2 \theta_{CO} \theta_O^2 = 0 \tag{10.10}$$

where θ_O, θ_{CO} and θ_{CO_3} are respectively the surface coverage of O, CO and CO_3 and k_1 is the rate constant for dissociative adsorption of oxygen. Since θ_O is small, $(1 - \theta_O)$ can be approximated to unity then the

expression for θ_{CO} is written as

$$\theta_{CO} = \frac{k_1}{k_2}\frac{p_{O_2}}{\theta_O^2} \tag{10.11}$$

Similarly the surface carbonate is formed by equation (10.9) and is destroyed by equation (10.8). Under steady state conditions,

$$\frac{d\theta_{CO_3}}{dt} = k_2\theta_{CO}\theta_O^2 - k_3\theta_{CO_3}\theta_{CO} = 0 \tag{10.12}$$

where $\theta_{CO_3} = \frac{k_2}{k_3}\theta_O^2$.
The rate of the reaction is then given by

$$k_3\theta_{CO_3}\theta_{CO} = k_1 p_{O_2} \tag{10.13}$$

Thus, the reaction should be first order in oxygen and zero order with respect to CO. The calculated rate is simply equal to the rate of adsorption of oxygen. The experimental observations agree with this prediction showing the validity of the mechanism proposed.

At high temperature, CO oxidation on oxides (e.g., on cupric oxide at 573 K or above) follows a kinetic law which is first order in CO and independent of the pressure of oxygen. Adsorption of CO on metal ions of the oxides will be weak in this temperature range. Hence, the reaction may not involve the reaction between the adsorbed CO and surface carbonate species as shown in equation (10.8). In this temperature range the adsorption of CO will take place solely as surface carbonate

$$CO + 2O^{2-} \rightarrow CO_3^{2-} + 2e^- \tag{10.14}$$

The oxide ions participating in the reaction are from the lattice. The anionic vacancies that will be generated by this reaction will be filled up by the adsorption of oxygen from the gas phase as

$$\frac{1}{2}O_2 + 2e^- \rightarrow O^{2-} \tag{10.15}$$

Of these two steps (equations 10.14 and 10.15), the adsorption of CO as carbonate will involve considerable activation barrier and equation (10.15) i.e., replenishment of the oxide ions of the lattice by adsorption of gas phase oxygen will be the fast process. Therefore, the reaction at high temperature would take place by the decomposition of the surface carbonate species and the slow step will be the formation of surface carbonate by adsorption of CO. If this postulate were to be true, the

reaction will be first order with respect to CO and zero order with respect to oxygen. This reaction mechanism implies that the reaction takes place through reduction and re-oxidation of the surface involving the oxide ions for the surface carbonate formation. The removal and reformation of oxide ions is a rapid process and this redox mechanism is known as Mars-van Krevelen mechanism.

10.5 HYDROCARBON CONVERSION REACTIONS

There have been many attempts to examine the mechanism of hydrocarbon conversion reactions using a variety of experimental techniques. The reaction which has received extensive attention is the cracking of hydrocarbons for the production of fuel grade molecules. In the initial stages, cracking of high molecular weight hydrocarbons was carried out thermally. However, this is no longer practised because thermal cracking of n-hexadecane mostly gives C_1 to C_3 hydrocarbons and the reaction follows a radical pathway making control of the cracking process difficult. Catalytic cracking is mostly employed these days and the catalysts used are amorphous silica-alumina and synthetic or natural aluminosilicates. The catalytic function of these systems is the acidic nature of these materials. Individually, silica or alumina is not active for catalytic cracking but in combination, they catalyze the cracking reaction. It has been already recognized that the physical and chemical properties of the aluminosilicates are different from those of their constituents. The catalyst in the form of fine powder or particles are fluidized by the vapours of the crude oil to be cracked and the catalytic cracking reaction leaves carbon deposit on the catalyst particles requiring frequent regeneration of the catalyst. The design of the reactors is such that both regeneration and cracking reactions can be alternatively performed. Subsequent reformation of the hydrocarbon molecules involving hydrogen transfer, isomerization and aromatization can also be promoted in the same reactor. Like polymerization-depolymerization, catalytic cracking can also follow a four stage reaction scheme. They are (i) initiation or formation of carbocation, (ii) cracking or decomposition of carbocation, (iii) propagation or formation of new carbocations from the already formed ions, and (iv) termination or removal of the carbocations. Generally, the carbocations are formed by the loss of a hydride ion from the molecule combining with a proton of the catalysts. This reaction for hydrocarbon substrates can be shown as:

$$R_1.CH_2.CH_2.CH_2.CH_2.R_2 + HA$$
$$. \quad \rightarrow R_1.C^+H.CH_2CH_2CH_2.R_2 + A^- + H_2$$

In the case of an olefin, a proton from the catalysts may be transferred to one of the carbon atoms involved in the double bond.

$$R_1R_2C = CR_3R_4 + HA \rightarrow R_1R_2C^+ - CHR_3R_4 + A^-$$

In the case of alkyl aromatics, the proton is transferred to the ring, but the positive charge created is resonating within the ring structure

It is known that olefins crack faster than the corresponding paraffins and it is likely that in an industrial process, the cracking is initiated by the small amount of olefins present in the feed. Then the carbocations generated in the olefin molecule undergoes exchange reaction with the paraffin molecules.
(ii) Cracking: This reaction has some specific rules. It is generally observed that the bond between the two carbon atoms adjacent to the charged carbon atom breaks and hence cracking can be carried out selectively.

$$R_1CH.CH_2CH_2CH_2CH_2.R_2 \rightarrow R_1CH = CH_2 + C^+H_2.CH_2.R_2$$

This rule is termed as the rule of least rearrangement and hence involves only shifting of the electron.

In the case of alkylaromatics the same rule of cleavage applies.

Further, cracking of the new carbocations can proceed. However, the new ion formed is a primary carbocation and if this were to crack then ethylene will mostly be formed. However, the amount of C_2 olefins formed in cracking is small and hence it is obvious that the primary carbocations undergo isomerization before further cracking. In the example considered, the primary carbocations isomerizes to

$$C^+H_2.CH_2.R_2 \rightarrow CH_3C^+H.R_2$$

Therefore, the cracking of the isomerized carbo cations can yield other products.
(iii) Propagation: Carbocations of low molecular weight is inert to cracking since only a small amount of C_1 and C_2 hydrocarbons are formed. When a low molecular weight ion is formed after cracking, they exchange with a new paraffin molecule as shown

$$R_1R_2C^+ - CHR_3R_4 + R_1CH_2CH_2CH_2CH_2R_2$$
$$. \qquad \rightarrow R_1R_2CH - CHR_3R_4 + R_1C^+HCH_2CH_2CH_2R_2$$

With alkyl aromatic molecules like isopropyl benzene, propagation takes place according to the following reaction.

(iv) Termination: Termination of the chain of the cracking reaction can take place by the proton abstraction reaction namely,

$$R_1R_2C - CHR_3R_4 + A^- \rightarrow R_1R_2C = CR_3R_4 + HA$$

(v)Isomerization: As stated earlier, isomerization often precedes cracking and typical isomerization reaction is shown as

$$CH_3.CH_2.C^+(CH_3).CH_2CH_2R \rightarrow C^+H_2.C(CH_3)H.CH_2CH_2.R$$
$$. \qquad \rightarrow CH3.C^+(CH_3).CH_2.CH_2.R \rightarrow CH_3C(CH_3) = CH_2 + C^+H_2.R$$

10.6 CATALYTIC DECOMPOSITION OF N_2O

Catalytic decomposition of nitrous oxide is a simple test reaction. The decomposition products are simple and stable molecules and the product accumulation does not affect the reaction rate. The reaction is

$$N_2O \rightarrow N_2 + \tfrac{1}{2}O_2$$

The kinetics of the reaction can be easily monitored by following the change in pressure as a function of time in a closed system. The detailed mechanism of this reaction is fairly well known.

$$N_2O \rightarrow N_2O_s$$

$$N_2O_s + e^- \rightarrow N_2O_s^-$$

$$N_2O_s^- \rightarrow N_2 + Os$$

$$O_s \rightarrow \tfrac{1}{2}O_2 + e^-$$

$$O_s + N_2O \rightarrow N_2 + O_2 + e^-$$

At the molecular level, N_2O is one of the simple molecules with well defined frontier orbitals. The nitrogen and oxygen atoms undergo *sp* hybridization for σ bonding. One localized π electron pair between the two nitrogen atoms and one pair of π-electrons get delocalized over all the three atoms in the N_2O molecule. One lone pair is present on *sp* hybrid orbital of nitrogen and two lone pairs of electrons on *sp* and *p* orbitals of oxygen and the rest two electrons are present in the antibonding π^* orbital.

In the kinetics of N_2O decomposition, the only adsorption of importance is that of oxygen. Hence, the following three kinetic equations have been proposed

$$-\frac{dp}{dt} = k_1 p_{N_2O} \tag{10.16}$$

$$-\frac{dp}{dt} = k_2 \frac{p_{N_2O}}{p_{O_2}^{1/2}} \tag{10.17}$$

$$-\frac{dp}{dt} = k_3 \frac{p_{N_2O}}{(1 + p_{O_2}^{1/2})} \tag{10.18}$$

corresponding to no inhibition, (equation 10.16), strong inhibition (equation 10.17) and weak inhibition (equation 10.18) by oxygen adsorption.

There have been a number of studies on the decomposition of N_2O on metals which include Ag, Au, Pb, Fe, Ni, Pd, Ir, Pt, W and alloys like Ag-Au and Ag-Ca. In all these cases, the rate determining step is adsorption of N_2O leading to the formation of oxide on the surface. This aspect of N_2O decomposition has also been used for evaluating the metal surface area of various supported catalysts.

N_2O decomposition has also been studied on oxide surfaces. It has been shown that *p*-type oxides were more active than *n*-type oxides and

insulators. This was interpreted considering (i) cumulative nature of anionic adsorption of N_2O on p-type oxides and depletive nature of adsorption on n-type oxides and (ii) more facile desorption of oxygen on p-type oxides than on n-type oxides as shown.

p-type oxides
Step 1
$N_2O \rightarrow N_2O_s + [+]$
Or, $N_2O \rightarrow N_2 + O_s^- + [+]$
Step 2
$[+] + O_s{}^- \rightarrow \frac{1}{2}O_2$
Or, $[+] + O_s{}^- + N_2O \rightarrow O_2 + N_2$
n-type oxides
step 1
$N_2O + [-] \rightarrow N_2O_s^-$
Or, $N_2O + [-] \rightarrow N_2 + O_s{}^-$
Step 2
$O_s{}^- \rightarrow \frac{1}{2}O_2 + [-]$
Or, $O_s{}^- + N_2O \rightarrow N_2 + O_2 + [-]$

The results obtained on ZnO doped with Li_2O or Ga_2O_3 revealed that there is a correlation between conductivity and activation energy or specific rate of the reaction. Further detailed studies on rare earth oxides have shown that various correlations exist between activity and different physico-chemical properties of the catalysts. Kinetics of N_2O decomposition is influenced by added adsorbed gases as well as various pre-treatments given to these catalysts. Voorhoeve[3] has discussed the role of magnetic ordering of the solid on the decomposition of N_2O on several oxide systems. Winter has studied the decomposition of nitrous oxide on rare earth sesquioxides and other oxides and has established the following linear correlations: (i) lattice parameter of the oxides used and activation energy for N_2O decomposition, (ii) lattice parameter of the oxides used and the rate for nitrous oxide decomposition at a given temperature, (iii) lattice constants and pre-exponential factors for the nitrous oxide decomposition, (iv) the activation energy for nitrous oxide decomposition and that for oxygen isotopic exchange reaction, (v) pre-exponential factor for nitrous oxide decomposition and that for oxy-

[3]R. J. H. Voorhoeve, *Paper presented at 19th Annual Conference of the American Institute of Physics at Boston*(1974).

gen isotopic exchange reaction, (vi) rate of exchange reaction at a particular temperature with the rate of nitrous oxide decomposition, and (vii) activation energy for nitrous oxide decomposition and the nearest oxygen-oxygen distance in the various oxides. These and other similar correlations showed the similarity between the exchange reaction and the nitrous oxide decomposition reaction and emphasized the importance of the desorption step in the decomposition reaction.

The kinetics of nitrous oxide decomposition was found to follow different rate equations at different pressure ranges. At 50 torr pressure, the decomposition rate was not inhibited by oxygen and the kinetics is first order with respect to nitrous oxide (equation 10.16). At 200 torr, the rate is inhibited by oxygen and the equations (10.17) or (10.18) are applicable. A volcano shaped correlation between catalytic acidity and standard heat of formation was also reported by Vijh[4] and others[5]. Decomposition of nitrous oxide has been shown to be a model reaction for suprafacial catalysis. The adsorbed form of nitrous oxide can resemble a cationic, an anionic or radical species, and the corresponding Wieberg-bond indices are given in table 10.2.

Table 10.2: Wieberg bond indices in N_2O species.

System	$N-N$ bond	$N-O$ bond
N_2O	2.34	1.49
N_2O^+	2.17	1.62
N_2O^-	1.87	1.20
N_2O^+ (nonlinear)	1.53	1.54

10.7 DECOMPOSITION OF ISOPROPANOL

Isopropanol can undergo dehydrogenation and dehydration simultaneously according to the following reactions

$$CH_3CH(O)HCH_3 \rightarrow CH_3COCH_3 + H_2$$
$$CH_3CH(OH)CH_3 \rightarrow CH_3CH = CH_2 + H_2O$$

This is a simple catalytic reaction where the selectivity preference can be studied. Thermodynamically, both the reactions are equally possible as seen from the data presented in table 10.3. Decomposition of

[4] A. K. Vijh, *J.Catal.*, 31, 51,(1973).

[5] G. Nagasubramanian, M. V. C. Sastri and B. Viswanathan, *Ind. J. Chem.*, 16A, 242, (1979).

isopropanol and formic acid is often used for evaluating the relative activity or selectivity of catalysts for dehydrogenation and dehydration. It is implied that the selectivity determined in each case will reflect only the relative rates of the two modes of decomposition. In order to ensure this, it is necessary to carry out the decompositions under conditions of equal thermodynamic selectivity for dehydrogenation and dehydration so that any deviation from a selectivity of 0.5 may be attributed to the catalytic activity. From the data presented in table 10.3 it is seen that a thermodynamic selectivity of 0.5 is maintained above 700 K for the decomposition of isopropyl alcohol. This justifies the use of the reactant for the evaluation of the selectivity of the catalysts.

Table 10.3: Thermodynamic data for isopropanol decomposition

Temp.,	ΔG_f^o, kcal/mol			ΔG_r^o,	$\log K_p$	Select.for
K	IPA	water	propene	kcal/mol		dehydrogenation
400	-33.17	-53.52	18.62	-1.73	0.904	
500	-24.66	-52.36	22.45	-5.25	1.000	0.4541
600	-15.94	-51.16	26.46	$-8,76$	1.000	0.4818
700	-7.07	-49.92	30.60	-12.25	1.000	0.5000
800	1.87	-48.65	34.84	-15.70	1.000	0.5000

Decomposition of isopropanol has been extensively employed as a test reaction for the investigation of oxide catalysts. The specific advantage of this reaction for the investigation of oxide catalysts is that apart from the activity data, selectivity of the catalyst with respect to two important types of reactions – dehydration and dehydrogenation can be studied. The term 'selectivity' is used to express the ratio of the rate of the particular mode of decomposition (either dehydrogenation or dehydration) to the total decomposition rate.

Sabatier and Milhe[6] were the earliest to carry out systematic study of isopropanol decomposition on a number of oxides. The variation of the selectivity for the decomposition on different metal oxides has drawn the attention of several investigators. If the dehydrogenation and dehydration reactions are of the same order, then the selectivity actually measures the kinetic selectivity and hence its value will depend on the temperature at which these constants are measured. However, if the reactions are of different orders, the selectivity factor depends on the pore structure of the catalyst with the rate increasing in favour of the products obtained in the reaction of lower kinetic order. From the influence of sintering temperature on the activity and selectivity of catalysts,

[6]P. Sabatier and A. Milhe, *Ann. Chim. Phys.*, 20, 289, (1910).

Schwab and Schwab-Agallidis[7] have concluded that the dehydration reaction occurs in the narrow pores and that the dehydrogenation reaction occurs on the flat surface. Therefore, according to Schwab's proposal one expects that sintering should enhance selectivity for dehydrogenation as sintering will destroy the active sites of dehydration. However, it is generally felt that the effect of the pretreatment of the oxide at high temperatures on the selectivity is more complicated. A modification in the texture of the catalyst as well as changes in the surface properties of the oxide can result from pretreatment at high temperature. Reduction of the catalyst either to metallic state or to lower oxidation states can occur, and this will change the electrical properties of the catalyst and also its selectivity.

Based on their study of decomposition of isopropanol on several oxides, Eucken and Wicke[8] found that the surface hydroxyls are essential for the dehydration process and the surface cations of the metal oxides are responsible for dehydrogenation reaction. For dehydration process, they proposed the following mechanism

According to Eucken and Wicke, the hydrogen atom of the OH bearing carbon atom is polarized negatively and is transferred to the positive metal ion of the surface, while the positively polarized hydrogen atom of the hydroxyl group binds to an oxygen atom of the surface. The two separately bound hydrogen atoms combine to form a hydrogen molecule.

Eucken[9] attempted to correlate the nature of the oxide with the selectivity for dehydrogenation of alcohols. He assumed that the dehydrogenation reaction will be favoured by a strong polarization of the atoms

[7] G. M. Schwab and E. J. Schwab-Agallidis, *J. Am. Chem. Soc.*, 71, 1806, (1949).
[8] A. Eucken and E. Wicke, *Z. Naturforschung*, 2A, 163, (1947).
[9] A. Eucken, *Naturwissenshaften*, 32, 161, (1944).

of the catalysts surface and that the screening of the cations of the surface by the oxygen ions is minimum. This screening will be stronger when the size of the cation is small and the the charge is high. Based on these, Eucken proposed a selectivity function η such that

$$\eta = r_c^3/(V_M.Z) \tag{10.19}$$

where η is a measure of the selectivity, r_c is the radius of the cation, V_M the molecular volume of the oxide expressed per cation and Z is the valence. With the aid of this selectivity function, Eucken obtained a reasonable correlation with the experimental selectivity data. The drawback of Eucken's correlation is that it does not take into consideration the influence of the crystal structure and the nature of the exposed crystal planes. Mars obtained a similar correlation for the dehydration reaction based on the assumption of a close relationship between dehydration rate and the number of surface OH groups considered as the source of protons. Balandin considers the dehydrogenation and the dehydration of alcohols and other reactions such as the dehydrogenation of hydrocarbons and amines as doublet reactions involving two active sites of the catalyst in the formation of the intermediate reaction complex. The reacting atoms of the molecule constitute a group, called the index group which is characteristic of a given reaction. In the dehydration (I) and dehydrogenation (II) of alcohol, the following atoms of the alcohol skeleton are involved, respectively.

According to Balandin[10], the course of the reaction is determined by the value of the adsorption potential, which is the sum of the bond energies between the atoms of the index group and the catalyst. When the adsorption potential is low that is the affinity between the catalyst and reactant is weak, the formation of multiplet complex will control the reaction rate. On the other hand, if the value of the adsorption potential

[10] A. Balandin, *Adv. Catal.*, 10, 96, (1958).

is high, the multiplet complex will readily be formed and hence the rate of the overall reaction is controlled by the decomposition of the stable intermediate complex into the reaction products. In the multiplet theory, the selectivity of a catalyst will depend on the values of the adsorption potentials for the two competitive reactions. For many metal oxides, the bond energies of the atoms of carbon, hydrogen and oxygen with the catalyst (necessary for the determination of the adsorption potentials) were obtained from kinetic investigations by Balandin and coworkers. From this data, Balandin and coworkers attempted to classify the selectivity of the oxides on energy considerations. However, the following objections were raised against Balandin's integral approach to the phenomenon of catalysis.
(i) In the determination of the energy parameters between the catalyst and atoms, it is assumed that the bond energies are the same for different types of reactions. Consequently, reactions such as dehydration and dehydrogenation are supposed to occur on the same type of active sites.
(ii) Once the index group is established, the emphasis is on energy factors only, and the effect of pre-exponential factor on the reaction rate is ignored.

Many investigators have searched for a correlation between the catalytic activity and the electronic properties of the catalyst. The decomposition of alcohols on oxide catalysts was also investigated from this point of view. Wolkenstein[11] and Hauffe[12] have dealt with this subject on the basis of theoretical considerations. Like Eucken and Wicke and Balandin, Wolkenstein also assumed that the course of the reaction depends on the mode of adsorption of alcohol. However, he introduced the new aspect of the involvement of charge carriers (electrons or holes) of the catalyst in the chemisorption of the alcohol molecule. For the dehydrogenation reaction he considered that the O-H bond of the alcohol molecule is split and that the alcohol molecule is adsorbed with the transfer of electron from the catalyst surface to the substrate molecule (acceptor). Hence the adsorbed species becomes negatively charged. For the dehydration process, however, rupture of the C-OH bond occurs and the substrate molecules become positively charged (donor). Wolkenstein considers that the adsorption step determines the course of the reaction while dehydration is a donor reaction. The relative activity of a catalyst with respect to both reactions, according to Wolkenstein, is controlled

[11] A. Wolkenstein, *Adv. Catal.*, 12, 189, (1960)
[12] K. Hauffe, *Adv. Catal.*, 7, 251, (1955); *Angew. Chem.*, 67, 189, (1955).

by the position of the Fermi level at the surface of the catalyst and the selectivity of a catalyst would vary within wide limits by a shift of the Fermi level.

Contrary to the assumptions of Wolkenstein, Hauffe considered the desorption of acetone as the rate controlling step for the dehydrogenation reaction. According to the scheme given by Hauffe, (see figure 10.1), it follows that free electrons are released to the catalyst during the desorption of acetone. Therefore he concludes that the dehydrogenation reaction is a donor process and that a p-type semiconductor should be a good dehydrogenation and poor dehydration catalyst. However, postulates of both Wolkenstein and Hauffe were not based on any kind of electrical measurements.

Figure 10.1: *Schemes for isopropanol dehydration and dehydrogenation according to Hauffe.*

Bielanski[13] Zhabrova[14] and Krylov followed the dehydrogenation of alcohols on p-type and n-type oxide catalysts by the measurement of the changes of electrical conductivity and work function during the reaction.

[13]A. Bielanskii, J. Deren, J. Haber and J. Sloczinski, *Proc. 2nd. Internat. Cong. Catal.*, 2, 1653, (1961).

[14]G. M. Zhavrova, *Chem. Tech.(Berlin)*, 15, 193, (1963).

They observed that chemisorption of isopropanol, ethanol, acetone and acetaldehyde all increased the conductivity of n-type oxides suggesting that the same process, namely transfer of electrons from the adsorbed molecule to the conduction band of the solid occurs. Based on these results, Zhabrova proposed the following mechanism for the dehydrogenation of isopropanol.

$$(CH_3)_2CHOH \rightarrow [(CH_3)_2CHOH]^+ + e^-$$
$$[(CH_3)_2CHOH]^+ \rightarrow [(CH_3)_2CO]^+ + H_2$$
$$[(CH_3)_2CO]^+ + e^- \rightarrow (CH_3)_2CO$$

The alcohol molecule chemisorbed in the first step of the reaction gets positively charged by release of an electron. In the second step, the substrate molecule is converted to a positively charged acetone molecule after the release of hydrogen. The final step of the desorption of chemisorbed acetone molecule is rate-determining and is an acceptor step involving the transfer of electron from the conduction band to the chemisorbed molecule. This mechanism implies that the dehydrogenation reaction can be regarded as an acceptor reaction. Though the final conclusion is similar to the one arrived at by Wolkenstein, there are significant differences in the details of the mechanism. Involvement of the electrons from the catalyst surface in the dehydration reaction has not been proved. This suggests that the conclusion of Wolkenstein, namely, change in the position of the Fermi level changes both dehydrogenation and dehydration reaction rates and hence the selectivity seems unlikely. However, the changes observed in the selectivity for decomposition with the change in the position of the Fermi level may be accounted for by the dependence of the dehydrogenation rate on the position of the Fermi level alone.

Garcia de la Banda[15] and coworkers investigated the mechanism of dehydrogenation of isopropyl alcohol on chromia based catalysts. The main feature of their studies is the measurement of the conductivity of the catalyst under reaction conditions with the feed consisting of isopropyl alcohol diluted with various amounts of products. They analyzed the data by means of various kinetic equations and concluded that:
(i) two equal active sites on the catalyst surface are involved in the reaction,
(ii) isopropanol, acetone, and hydrogen all are adsorbed on these sites, and

[15] J. F. Garcia de la Banda, *J. Catal.*, 1, 136, (1962).

(iii) surface reaction involving the transformation of adsorbed isopropanol to adsorbed acetone is the rate controlling step in the dehydrogenation process.

Mechanism of dehydration

It is seen from the above discussion that the dehydration differs in character considerably from the dehydrogenation reaction. Hence, a separate examination of the mechanism of dehydration of alcohols is called for. Most of the investigations have been carried out on alumina and silica based catalysts. De Boer[16], Dzisko[17], Whitmore[18] and Bremner[19] consider that the dehydration proceeds through the intermediate formation of a carbonium ion. They suggested the following mechanism:

$$C_2H_5OH + H_s^+ \rightleftharpoons [C_2H_5OH_2]_s^+$$
$$[C_2H_5OH_2]_s^+ \rightleftharpoons [C_2H_5]_s^+ + H_2O$$
$$[C_2H_5]_s^+ \rightleftharpoons C_2H_4 + H_s$$

In the case of some catalysts, however, the dehydration rate was not affected when the acidic sites were poisoned with sodium ions. From this, Topchieva et al.[20] concluded that the dehydration reaction proceeds via the formation of a surface compound of the alcoholate type, which is easily, decomposed into the reaction products. They consider that the hydroxyl groups present on the surface constitute the active sites for the dehydration process. The reaction sequence proposed for the dehydration of ethyl alcohol on alumina by Topchieva is the following:

As mentioned earlier, Eucken and Wicke also consider that the surfacial hydroxyl groups are the active centres for the dehydration process. Pines and Manassen proposed that in addition to weakly acidic sites weakly basic sites are necessary for the dehydration of alcohols.

From the discussion, it is seen that the mechanisms of both the modes of decomposition of isopropanol have been thoroughly investigated. Be-

[16]J. H. de Boer, *Ind. Chem. Belge*, 21, 1159, (1956).
[17]V. A. Dzisko, *Proc. 3rd Internat. Congr. Catal.*, 1, 422 (1965).
[18]F. C. Whitmore, *J. Am. Chem. Soc.*, 54, 3274, (1932).
[19]J. G. M. Bremner,*Research (London)*, 1, 282, (1948).
[20]K. V. Topchieva, K. Y. Pin and J. V. Smirnova, *Adv. Catal.*, 9, 799, (1957).

side the decomposition of isopropyl alcohol when employed as a test reaction gives the data on the activity and selectivity of the oxide catalysts for two important types of reaction, namely, dehydrogenation and dehydration. Thus it is seen that even though conceptually one can visualize only two sets of mechanisms for the heterogeneously catalyzed reactions, the intricate mechanism may involve many exchanges which include charge transfer as well as atom or molecule rearrangements on the surface of the catalysts. It is necessary to probe these transformations carefully to elucidate the detailed mechanism of surface transformations.

SUGGESTED READING

1. O. V. Krylov, *Catalysis by Non-metals*, Academic Press New York, 1970.
2. E. K. Rideal, *Concepts in Catalysis*, Academic Press, London 1968.
3. P. Mars, *The Mechanism of Heterogeneous Catalysis*, (Ed. J.H. de Boer), Elsevier, Amsterdam, 1959.
4. A. Balandin, *Advances in Catalysis*, 10, 96 (1958).
5. Th. Wolkenstein, *Advances in Catalysis*, 12,189 (1960).
6. Th. Wolkenstein, *The Electronic Theory of Catalysis on Semiconductors*, Pergamon, London, 1963.
7. A. Bielanski, *Catalysis and chemical Kinetics*, Academic Press, New York, 1964.
8. K. V. Topchieva, K. Yun Pin and J. V. Smirnova, *Advances in Catalysis*, 16, 49(1966).
9. K. Haufffe, *Angew. Chem.*, 67, 189 (1955).
10. J. F. Garcia de la Banda, *J.Catal.*, 1, 136 (1962).

Chapter 11

Surface Structure

11.1 INTRODUCTION

There are three important aspects of study of the surface. These are: 1) geometric structure of the surface, 2) chemical composition of the surface and 3) study of the molecules adsorbed on the surface. We have already seen the importance of the exposed planes of a metal in connection with Balandin's multiplet theory and in case of adsorption on clean metal single crystal surfaces. The three-dimensional crystal structure of the solid is generally studied by X-ray diffraction. X-ray has high penetration power and the structural information obtained from X-ray diffraction gives the bulk structure. Low energy electrons with energy of 50–100 eV have de Broglie wavelength of the order of an Angstrom that is same as those of X-ray used in diffraction study. Hence, electron diffraction can be a tool for study of crystal structure. However, the penetration of the low energy electrons are restricted to the top planes of the crystal and this has been used for studying the geometry of the crystal surface. This method is known as low energy electron diffraction (LEED). Another method that gives information of the surface structure but has limited use is field emission microscopy (FEM). Both LEED and FEM methods will be discussed in this chapter.

Chemical composition of a surface can be found out both qualitatively and quantitatively by X-ray photoelectron spectroscopy (XPS) and Auger electron spectroscopy (AES). There are a variety of methods of finding out the state and chemical composition of a solid, but all of them are not surface specific. These methods include spectroscopic techniques such as XPS, AES, UVPS, NMR, EPR, Mössbauer, IR and Raman spectroscopy, various thermal methods, HEELS etc. Many of these

techniques can be suitably modified for studying the adsorbed molecules. The underlying principles of these methods and their selective applications will be discussed in the various chapters that will follow. In this chapter, we shall restrict to the study of the structure of single crystal surfaces by low energy electron diffraction and FEM.

11.2 LOW ENERGY ELECTRON DIFFRACTION

In the year 1928, Thomson demonstrated that a beam of high energy electrons is diffracted by a metal foil, confirming de Broglie's prediction about wave nature of particles. High energy electrons penetrate about 100 atomic layers and the pattern is similar to X-ray diffraction. Davisson and Germer have shown that low energy electrons are reflected from the surface with very little penetration. If diffraction is produced by the top layer of atoms, the two-dimensional grating will give characteristic diffraction pattern. The diffraction pattern is produced by constructive interference of the electrons scattered by all the possible rows of atoms of the surface. This is analogous to Bragg's three-dimensional diffraction. The electron beam is allowed to fall normal to the surface. Constructive interference will occur when the condition

$$n\lambda = d\sin\phi \tag{11.1}$$

is satisfied. Here ϕ is the angle of reflection.

Wavelength λ is given as

$$\lambda = \frac{h}{p} = \frac{12.27}{V^{\frac{1}{2}}(1 + 0.978 \times 10^{-6}V^{\frac{1}{2}})}\mathring{A} \tag{11.2}$$

At low voltage

$$\lambda = \left(\frac{150}{V}\right)^{\frac{1}{2}} \tag{11.3}$$

Electrons with 100 eV energy gives wavelength $\lambda = 1.226$ Åwhich is of the order of lattice separation. Electron beam having energy in this range will undergo diffraction.

The scattering cross section for X-ray is small (10^{-6} Å^2) and the intensity of the scattered beam is very weak as compared to the incident beam. Scattering cross section for LEED is large (1 Å^2). Thus, the amplitude of the scattered beam is of the same order as that of the diffracted beam and the latter may act as a source and again undergo scattering. Low energy electrons may thus undergo multiple scattering. The elastic scattering cross section decreases with electron energy. At

100 eV energy, only 5% of the back scattered electrons are elastic and carry the structural information. Intensity of the diffraction spots depends on:
1. the degree of surface order over 500 Å; imperfection leads to broadening;
2. energy of the electrons; higher energy leads to greater penetration and lower intensity;
3. multiple scattering.

Figure 11.1: *Schematic view of a LEED instrument.*

If the electrons penetrate, the lower planes too will participate in diffraction. Constructive interference will occur when λ equals the distance between successive planes. Since λ changes with voltage, the successive planes will undergo interference constructively at some voltages and not at other voltages. As a result, intensity of the spots will show successive maxima and minima. Generally, measurements are made at several voltages to get a complete picture about the surface structure.

Diffraction pattern gives rise to a pattern that corresponds to the reciprocal lattice of the real structure. Since the reciprocal lattice has the same geometry as the real lattice, the diffraction pattern will look similar to the real lattice.

11.2.1 LEED Instrument

A LEED instrument consists of an electron gun (heated tungsten cathode), the electron optics system to get a narrow electron beam of right energy, the sample holder and a fluorescent screen (see figure 11.1). The

sample is placed at the centre of curvature of the screen. Orientation of the crystal can be changed by a crystal manipulator. The electron beam normal to the crystal surface produces a diffraction pattern on the screen. A set of spherical-shaped 100 mesh grid of nickel-plated tungsten is placed in front of the screen. The grid is biassed to suppress the diffiusedly scattered electrons that has energy lower than those of the incident beam. The electron beam can be adjusted to any energy from 10 to 500 eV. Facilities are provided for heating and sputter cleaning the crystal surface. An ultra-high vacuum system maintains the chamber at 10^{-10} torr.

Figure 11.2: *LEED patterns from the various exposed surfaces of metallic nickel.*

Figure 11.3: *LEED pattern of the (111) surface of platinum single crystal at (a) 51 V, (b) 63.5 V, (c) 160 V and (d) 181 V.*

11.2.2 Study of Clean Metal Surface

A clean metal surface can be produced by cleaving the crystal or by sputtering the surface inside the UHV chamber. At such high vacuum, a fresh surface will take more than an hour to be covered by the residual gas and making the study of a clean surface possible. Most studies have been concerned with the primary planes (100), (110) and (111).

Arrangement of the atoms on these planes of a fcc metal is shown in chapter 7. The corresponding LEED patterns are presented in figure 11.2. It can be seen that the LEED patterns have the same symmetry as the arrangement of the surface atoms in the respective planes.

Relative distance between the spots depends on the voltage as shown by the LEED pattern of the (111) surface of a platinum single crystal recorded at different voltage (figure 11.3)

The LEED patterns that have been considered so far are of surfaces with minimum defects. A surface may, however, have steps and kinks. The atoms present at such sites are least coordinatively unsaturated and are of greater catalytic importance. The presence of such defects change the LEED pattern as shown in the figure 11.4 taken from G. A. Somorjai. If the steps occur at regular intervals, additional spots are seen as shown in the figure. If the steps are irregular, blurring of the spots will be seen instead of the second set of spots.

Figure 11.4: *LEED pattern of platinum (111) surface: (a) regular surface; (b) surface with regular steps.*

11.2.3 Study of Adsorbed Layer

It should be realized that the atoms on the surface are not rigidly fixed but have a certain degree of mobility even for the most refractory metals. Under the influence of a adsorbed gas, the surface atoms can move some distance along the surface. As a result, the surface may undergo restructuring before the monolayer is complete and may give a new LEED pattern.

Designating the overlayer structures

If the diffraction pattern of the surface overlayer is identical with the original clean surface, it is designated (1x1) structure. If the unit cell of the overlayer is twice the unit cell of the clean surface, it is (2x2). There may be two different types of of this designated c(2x2) and p(2x2). When the adsorbate atoms have unit cell with the same lattice distance as that of the clean surface along one axis and twice the distance along the other axis, it is designated (2x1). These differences are shown in figure 11.5.

Figure 11.5: *Different overlayer structures.*

Adsorption of oxygen on nickel

Adsorbed oxygen can form different types of overlayers on the surface of nickel. Two of such adlayers are sown in figure 11.6 with the corresponding LEED patterns. For convenience, nickel and oxygen are shown as

having same dimension where the open circles represent nickel and the shaded circles represent oxygen.

The surface layer may be mixed, i.e. the top layer may contain both substrate atoms and adsorbate atoms due to surface reconstruction, or they may be unmixed which means that the adsorbate atoms sit on the top of the substrate atoms. Figure 11.6 (a) shows a mixed surface in which three fourth of the original number of nickel atoms are present and one fourth is oxygen. This conclusion is deduced from the LEED pattern shown in figure 11.6 (c). Further adsorption leads to a mixed surface where half of the surface atoms of the mixed surface are oxygen. This gives the pattern shown in figure 11.6 (d). It should be born in mind, however, that the same geometric pattern will appear in LEED if the surface atoms are reversed, i.e. pattern 11.6 (c) will be shown if the three fourth of the mixed surface is oxygen and one fourth is nickel.

Some times, a mixed structure and a overlayer structure may give similar geometry of the LEED patterns. In such cases, it is very important to carry out an intensity analysis.

Figure 11.6: *(a) and (b): (2x2) structures of nickel (100) surface; (c) and (d) the corresponding LEED patterns.*

11.3 FIELD EMISSION MICROSCOPY

This method is based on the fact that the work function (ϕ) of a metal is different for different surfaces. It is higher for those surfaces that are more densely packed with atoms. For an fcc metal, for example, ϕ is higher for the (111) surface than for the (100). This difference is used in FEM.

When a gas is adsorbed on the surface of a metal, work function of the metal changes. The adsorbate may be considered a dipole. If the positive end of the dipole is directed to the surface, a negative charge will be induced just below the surface and this will try to prevent an electron from arriving at the surface. The work function of the metal will increase as a result. If the negative end of the dipole is directed towards the surface, work function will decrease. The field emission microscope can be used to study the change of work function of the various crystallographic planes surface as a function of adsorption.

Emission of electrons is achieved by applying a high voltage in which a sharp metal tip is the cathode. The current emitted i is independent of temperature (at least up to 300 K) and is given by the Fowler-Nordheim equation

$$\frac{i}{V^2} = S \exp\left(-\frac{B(e\phi)^{\frac{3}{2}}}{KV}\right) \tag{11.4}$$

where V is the applied voltage, e is electronic charge, and B, S and K are constants. The current emitted is dependent on ϕ at constant voltage.

Figure 11.7: *Schematic representation of a field emission microscope.*

The design of a field emission microscope is schematically shown in

figure 11.7. It consists of a sharp, rounded metal tip (radius of curvature (1000-3000 Å) which is the cathode. The anode is a fluorescent screen. The system is connected to high vacuum.

Since the metal tip (the sample) as well as the screen are spherical, emitted electrons from the different planes of the tip will travel radially to the screen where bright spots will be formed. Distance between the spots is a measure of magnification that is proportional to R/r where R is the distance of the screen from the metal tip and r is the radius of curvature of the tip. Each exposed plane of the metal tip will give a bright spot on the screen. After getting the image of the clean metal tip, the adsorbate is introduced and the pattern is observed as function of adsorption. It is possible to identify the surface that is most affected by adsorption by observing the change in the spots.

Because of the small mass of the electrons, all the electrons emitted by a plane will not hit the same spot on the screen because of uncertainty principle. This uncertainty can be minimized and the spots can be made to appear very sharp if the mass of the emitted particles could be increased. It is with this idea that field ion microscopy (FIM) was developed.

Figure 11.8: *(a) Field emission and (b) field ion micrographs of a tungsten tip.*

The principle is same as that of FEM. A very small quantity of helium gas is leaked into the system. The helium atoms undergo ionization at the tip and the ions move out from the different planes radially towards the screen very much like the electrons. Helium atoms being much heavier, sharp spots are obtained on the screen. Figure 11.8 shows a FEM and

FIM micrographs. Each small spot in the field ionization micrograph represents a surface atom in the terraces of the tip. The limitation of this method is that the sample will have to be prepared in the form of tip and the material should be quite strong.

SUGGESTED READING

1. J. W. May, *Electron Diffraction and Surface Chemistry*, Ind. Engg. Chem., 57, 18 (1965).
2. A. U. MacRae, *Low Energy Electron Diffraction*, Science, 139, 379 (1963).
3. R. S. Hansen and N. C. Gardner, *Field Electron and Field Ion Microscopy*, in Experimental Methods in Catalytic Research, (Ed. R. B. Anderson), Acad. Press, New York.

Chapter 12

Infrared, Raman and EELS

The vibrational energy levels of a molecule can be studied by infrared and Raman spectroscopic methods. The vibrational frequencies of complex molecules depend on the strength of the bonds as well as on the symmetry. Polyatomic molecules can be treated as an assembly of harmonic oscillators and it is possible to calculate the vibration frequencies theoretically. But the components of vibration may be very complex for large molecules as well as for adsorbed species making such calculations impossible. However, various chemical groups may be assigned group frequencies and these may be used for identification of chemical groups. In the study of vibrational spectra of adsorbed molecules, use is made of the group vibration frequencies that are already available in the vast published literature.

12.1 INFRARED SPECTROSCOPY

In the early period of development of this technique, low signal to noise ratio of the instrument was the major hindrance in the way of getting a good spectrum. After the introduction of computers, it became possible to scan the same spectrum many times and store the data. The signal to noise ratio (S/N) can be improved because where S is proportional to the number of scan (n), N is proportional to $n^{\frac{1}{2}}$. After n scans, the ratio S/N improves $n^{\frac{1}{2}}$ times.

The intensity problem has been greatly solved after the Fourier transform infrared (FTIR) spectroometer was introduced. In this method, the sample is exposed to all the frequencies at the same time. The incident beam is split by a beam splitter. The split beam falls on a fixed mirror and the other half on a moving mirror. The reflected beams from the two

mirrors meet at the beam splitter where they interfere constructively or destructively depending on the optical path difference (position of the moving mirror). For any single wavenumber, the intensity should vary sinusoidally as function of the mirror position, and hence as a function of time. The time dependent intensity $I(t)$ is related to the intensity $B(\overline{\nu})$ of the detected wavenumber $\overline{\nu}$ as

$$I(t) = B(\overline{\nu})\cos(4\pi\overline{\nu}Vt) \tag{12.1}$$

where V is the velocity with which one of the mirrors move. Thus, $I(t)$ is a cosine Fourier transform of $B(\overline{\nu})$. The time dependent spectrum is converted to a frequency dependent spectrum by fast Fourier transform. The source, however, is not monochromatic and for each wavenumber, the same thing will happen. Since all the wavenumbers are simultaneously used, it is much faster. Since no grating is used, much higher throughput can be used. Since a laser is used to monitor the position of the moving mirror, the wavenumber accuracy is much greater. Figure 12.1 shows schematically a FTIR instrument.

Figure 12.1: *Schematic diagram of a FTIR instrument.*

12.1.1 The IR Cell

For studying the spectra of adsorbed molecules on the surface of a catalyst, a special infrared cell is needed. This easy to fabricate cell should have the provisions for 1) evacuation, 2) in-situ heating of the sample and 3) entry of adsorbate gases. The path length of the beam within the sample chamber should be small to minimize the effect of the gas spectrum.

Many designs are available in the published literature[1]. A simple design is shown here (figure 12.2). The cell is a stainless steel tube with flanges on which the windows could be mounted by viton o-rings. A glass tube is attached vertically to the metal tube that has a pulley system. the sample holder is a thin metal disc with a central home where the sample in the form of a thin wafer can be placed. The sample holder can be raised (by the pulley attached to a ceramic magnet that can be manipulated from outside) in the tube to the position of a heater and also can be positioned at the path of the IR beam. The glass tube is connected to vacuum and a gas handling system. Much more sophisticated designs are available, but this simple cell could give very good spectra.

Figure 12.2: *A simple high vacuum IR cell*

12.1.2 Application in Catalysis

Early works on the application of IR spectroscopy in catalysis can be traced in the works of the Russian scientists[2] and those of Eishens and

[1] J. B. Peri, in *Catalysis Science and Technology*, Eds. J. R. Anderson and M. Boudart, Springer Verlag, Berlin, 1984.

[2] A. V. Kiselev and V. I. Lygin, *Infrared Spectra of Surface Compounds*, John Wiley, New York, 1975.

co-workers[3]. Assuming that a FTIR instrument is available for recording the spectrum, a few other point deserves attention. First, how the spectrum is recorded. Most workers prefer the transmission mode where the radiation transmitted through the sample is recorded by the detector. The spectrum can also be recorded in the diffuse reflectance mode. The theory of diffuse reflectance can be found elsewhere[4]. A diffuse reflectance spectrum can be converted to absorption spectrum using standard routines. This technique is very useful for a highly scattering sample like a solid catalyst.

Closely spaced spectral lines often overlap giving a broad band. Such bands are resolved by the Fourier self deconvulation technique[5].

Small spectral changes can be noticed by the use of the technique of difference spectroscopy in which the background spectrum can be subtracted computationally to get a dramatically improved spectrum of the adsorbed molecule.

Since most FTIR spectra of the adsorbed molecules are recorded in the transmission mode, sample preparation needs some care. The finely powdered sample is prepared in the form of a thin self-supporting wafer. It should be thin enough to transmit enough radiation and at the same time should contain enough catalyst to hold a sufficient number of adsorbed molecules. About 10-20 mg cm^{-2} serves well this requirements.

Infrared spectroscopy has a variety of applications in catalysis. These are:
1. Determination of bulk structure of the catalyst. This is particularly important for newly synthesized zeolites of unknown structure;
2. Information on some of the peculiarities of the surface such as the presence of surface hydroxyl groups can be obtained. For porous materials like the zeolites, the majority of the hydroxyl groups are on the surface (inside the pores) and there is hardly any difference between bulk and surface in this regard;
3. Study of molecules adsorbed from solution or from the gas phase and their transformation;
4. Study of Brönsted and Lewis acidity of solids; and
5. Identification of the transition state.
Of these, the last one is most difficult and involves much speculation.

[3]R. P. Eishens and W. A. Pliskin, *Adv. Catal., Vol.10*, Acad. Press, New York, 1958.

[4]P. Kortum, W. Braun and C. Herzog, *Angew. Chem. Int.*, 2, 333, (1963).

[5]J. K. Kauppinen, D. J. Moffat, H. H. Mantsch and D. G. Cameron, *Apl. Spectrosc.*, 35, 271, (1981).

Study of zeolite structure

Group vibrations of the zeolites can be classified into two categories: 1) internal vibrations of the TO_4 tetrahedron that are insensitive to the rest of the structure, and 2) external vibrations meaning vibrations related to the linkages between the tetrahedra. The internal stretching modes are sensitive to Si/Al ratio and generally shift to lower frequency with the increasing amount of aluminium. The second class of vibrations depend on the overall structure. These vibrations and their origin are given in table 12.1.

In the zeolite beta (a large pore, high-silica zeolite), for example, the peaks at 526 cm^{-1} and 560-570 cm^{-1} are due to double ring vibrations. The intense peak at 526 cm^{-1} is possibly due to double four ring vibrations because the structure has a large proportion of such units. The peak at 785 cm^{-1} is due to external linkages of AlO_4 tetrahedra whereas the peak at 1080 cm^{-1} is due to internal TO_4 tetrahedra. Infrared spectrum of zeolite beta (Si/Al = 20) is shown in figure 12.3.

The presence of absorption bands at 550 and 1200 cm^{-1} indicate the presence of chains and blocks respectively of five-membered rings of the pentasil zeolites[6]. Since amorphous silica gives an IR band at 450 cm^{-1}, the optical density ratio of the 550 and 450 cm^{-1} bands is used as a measure of crystallinity of the ZSM-5 zeolite[7].

Table 12.1: IR frequencies observed in zeolites.

Internal vibration	cm^{-1}	External vibrations	cm^{-1}
asymmetric stretch	$950 - 1250$	double ring	$500 - 650$
symmetric stretch	$650 - 720$	pore opening	$300 - 420$
$T - O - T$ bending	$420 - 500$	symmetric stretch asymmetric stretch	$750 - 820$ 1050-1150

Surface hydroxyl

Terminal hydroxyl groups attached to a atom like silicon or aluminium in their oxides are weakly acidic and infrared vibration at 3700-3800 cm^{-1} whereas for bridging hydroxyl group that is a stronger acid site, it

[6]P. A. Jacobs, H. K. Beyer and J. Valyon, *Zeolites*, 1, 161, (1981).
[7]J. C. Jansen, F. J. Vander Gaag and H. Van Bekkum, *Zeolites*, 4, 369, (1984).

appears at 3650-3700 cm^{-1}. A very broad band at about 3500 cm^{-1} is ascribed to the presence of strong hydrogen bonds[8].

Figure 12.3: *IR spectrum of zeolite beta with Si/Al ratio 20.*

Adsorption of CO on metal surface

Adsorption of small molecules like CO on metal has been extensively studied by IR spectroscopy. These include adsorption on well defined single crystal surface, polycrystalline metal and also on supported metal catalysts. The stretching frequency of the gaseous carbon monoxide molecule is at 2143 cm^{-1} and this is generally lowered on chemisorption. The assignments are based on the observed CO vibration frequencies in molecular metal carbonyl compounds. Based on this, the assignments for the various types of chemisorbed CO are:

Type of adsorbed CO	dicarbonyl	linear terminal	double bridge	triple bridge
frequency, cm^{-1}	2050-2150	1950-2050	1800-1950	< 1800

The different forms of adsorbed CO are shown below:

Lowering of the CO stretching frequency may mean that the C–O bond has weakened as a result of bonding to the surface. Adsorption of

[8] A. Zecchina, and C. O. Arean, *Chem. Soc. Revs.*, 1996, 187.

CO on nickel and palladium single crystal surface shows a variation of the frequency with coverage. Energy of adsorption on these surfaces too show similar variation with coverage. Both show a steep change at one-third coverage that has been attributed to adsorption from hollow site to double bridge site[9]. These assignments to specific types of adsorption, however, may not be meaningful at higher coverage.

Figure 12.4: *FTIR spectra of* CO *on* Ru/SiO_2 *(after background subtraction): a. 100 torr* CO *at 100°C after 1 hour; b. the same as a after 2 hours; c. b after 100 torr* H_2 *at 100 °C; d. oxidized with 100 torr oxygen at 100 °C followed by 100 torr* CO *at 150°C.*

Physically adsorbed CO on transition metal oxides shows a shift of the frequency to higher than that for gaseous CO is rationalized by considering the existence of a strong electric field due to the metal ions[10].

CO adsorption on supported metal

Of much greater interest is the adsorption of CO on supported metals. Ru/SiO_2 catalysts showed a three band spectrum on CO adsorption at 2140, 2075 and 2005 cm^{-1}. By comparing with the spectra of various ruthenium carbonyl compounds, these bands were assigned to a mixture surface di- and tri-carbonyls. On treatment with hydrogen, the peaks due to tricarbonyl only disappeared showing that the tricarbonyls to be more reactive[11] (figure 12.4). The same three-band spectra is seen when

[9] F. M. Hoffmann, Surf. Sci. Rep., 3, 107 (1983).
[10] P. G. Harrison and E. W. Thornton, *J. Chem Soc, Faraday I*, 72, 2703, (1976).
[11] A. A. Desai and D. K. Chakrabarty, *Inorg. Chim. Acta*, 133, 301, (1987).

CO is adsorbed on Ru/SiO_2 catalyst is prepared by thermo-evacuation of $Ru_3(CO)_{12}/SiO_2$, only each band were now located at 5 cm^{-1} higher.

Gupta and coworkers[12] have extensively studied the adsorption of CO + H_2 at room temperature on Ru/TiO_2 catalysts. They identified multicarbonyl as well as linearly bonded CO on Ru. They suggest that the role of hydrogen lies in extracting oxygen from weakly held carbonyls to give active carbon that is responsible for hydrocarbon formation.

Table 12.2: Observed IR bands of adsorbed CO on metal oxides.

Metal oxide	Frequency, cm^{-1}	Type of species
Cr^{3+}/SiO_2	2200	terminal CO
Cr^{2+}/SiO_2	2190,2184	terminal CO
Fe^{3+}/SiO_2	1590,1305,1030	bidentate CO_3^{2-}
Co^{2+}/SiO_2	2177	terminal CO
Cu^{2+}/SiO_2	2170	terminal CO
	1675	bicarbonate
	1585	carboxylate
	1350	carbonate
Mn^{2+}/SiO_2	2200	weakly adsorbed CO
	1590,1320,1030	bidentate CO_3^{2-}

Tanaka and White[13] studied the IR spectra of adsorbed CO on Pt/TiO_2 which is an important photo catalyst. Their results show that linearly adsorbed CO on terrace has a higher frequency (2094 cm^{-1}) as compared to the adsorption at steps (2077 cm^{-1}). Adsorption on the steps shows greater reversibility. When the catalyst is in the SMSI (strong metal-support interaction) state, no bridged mode of adsorption is seen and adsorption on terraces is appreciably less.

[12]N. M. Gupta, V. S. Kamble, R. M. Iyer, K. R. Thampi and M. Gratzel, *J. Catal.*, 137, 473, (1992).

[13]K. Tanaka and J. M. White, *J. Catal.*, 79, 81, (1983).

CO adsorption on metal oxides

It has been reported that adsorption of CO on metal ions may shift the CO stretching to higher frequency. CNDO calculations[14] suggest that higher shift is possible if CO attaches to a cation through the carbon end, or to an oxide ion through the oxygen end. So far, there does not appear to be any experimental evidence of the second type of adsorption.

IR spectra of adsorbed CO on metal oxide surfaces depends on the pretreatment given to the oxide. Presence of surface oxygen lead to the formation of surface carbonates. Similarly, presence of surface hydroxyls give rise to formate. Some results are given in table 12.2.

Adsorption of NO

Infrared spectra of adsorbed NO have been extensively studied by Terenin and co-workers[15] and have been reviewed by Shelef and Kummer[16]. Types of bonding of NO with surface atoms has been classified by these authors. The infrared vibration regions and the corresponding assignments are shown in table 12.3.

Table 12.3: Metal-nitric oxide bond type and ν(NO) region.

Type of bonding	νNO, cm^{-1}
purely ionic, NO^+	2100-2400
coordinative ionic, ...N=O	1900-2100
double bond ionic, $=N^+=O$	1800-1900
coordinative, :N=O	1700-1870
covalent, –N=O	1600-1800
purely ionic, NO^-	1500-1700

Harrison and Thornton[17] found that for NO adsorbed on Fe^{3+} exchanged SnO_2, the peak at 1832 cm^{-1} shifted progressively to lower frequency down to 1770 cm^{-1} by exposure to CO at higher temperature. The band was assigned to Fe-N=O where the Fe^{2+} is the adsorption site. It is even suggested that NO probe molecule can distinguish between Fe^{2+} at octahedral and tetrahedral sites giving NO bands at 1810 and 1735 cm^{-1} respectively[18].

[14]N. S. Hush and M. L. Williams, *J. Mol. Spectros.*, 50, 349, (1984).

[15]L. M. Roev and A. N. Terenin, *Opt. Spektr.*, 7, 759, (1959).

[16]M. Shelev and J. T. Kummer, *Chem. Engg. Progr. Symp.*, 67, 74, (1971).

[17]P. G. Harrison and E. W. Thornton, *J. Chem. Soc., Faraday I*, 2703, (1975).

[18]K. Tanabe, H. Ikeda, T. Iizuka and H. Hattori,*React. Kinet. Catal. Lett.*, 11, 149, (1979).

12.1.3 Determination of Acidity of Solids

Infrared spectra of adsorbed pyridine and the effect of pyridine on the infrared hydroxyl bands are helpful in determining the acidity of solids.

Pyridine forms pyridinium ions with protons (Brönsted acid site) and is coordinated to electron-pair deficient sites (Lewis acid centres). It is known that the pyridinium ion shows three IR bands. A typical IR spectrum of pyridine adsorbed on the zeolite ZSM-5 is shown in figure 12.5. The N–H stretching band is not seen because of its broadness. The ring vibration of coordinated pyridine shows infrared bends at 1450 and 1490 cm^{-1}. The observed spectrum showed three bands at 1450-1455, 1490 and 1545 cm^{-1}. Thus the band near 1450 cm^{-1} is exclusively due pyridine at Lewis acid sites and the one at 1545 cm^{-1} belongs to pyridine at Brönsted acid sites. As the sample is heated, the band due to Lewis acidity loses intensity rapidly showing that this is the weak acid site.

Figure 12.5: *FTIR spectra of pyridine adsorbed on* HZSM-5 *after evacuation at: a. 423 K; b. 523 K; c. 523 K and d. 723 K.*

12.1.4 Reaction Intermediates

IR spectroscopy can be used for identifying the intermediates formed on the surface during a catalytic reaction. Study by Moser, Chiang and Thompson[19] by reflectance infrared technique of the decomposition of ethanol on HZSM-5 zeolite is interesting. In this technique, powder catalysts could be used without requiring pelletization (see figure 12.6).

Figure 12.6: *IR spectra (a) hydroxyl region and (b) alkoxy region of ethanol on* HZSM-5 *at various temperature.*

In the presence of ethanol at 100 °C, the low silica ZSM-5 sample (Si/Al=35) the peak at 3740 cm^{-1} due terminal silanol remained unaffected but the peak at 3605 cm^{-1} due to aluminol disappeared completely. The latter reappeared at 250 °C and did not change much up to 350 °C. Ethylene appeared in the gas phase (peak at 946 cm^{-1}) only at 200 oC. An ethoxy peak (1214 cm^{-1}) too appeared at this temperature and the aluminol peak is also restored. On further heating, the ethoxy peak disappeared and the aluminol peak was fully restored. The results suggest that adsorption of ethanol proceeds at the Al-OH-Si site via ethoxide formation which then goes to ethylene. IR studies on the high silica ZSM-5 (Si/Al=1062), on the other hand showed that ethanol is adsorbed at hydrogen bonded silanol and dehydration needs a higher temperature.

Chang, Conner and Kokes[20], 77, 1957, (1973) followed the isomerization of 1-butene on zinc oxide both by rate measurement and infrared

[19]W. R. Moser, C. Chiang and W. Thompson, *J. Catal.*, 115, 532, (1989).
[20]C. C. Chang, W. C. Conner and R. J. Kokes, *J. Phys. Chem.*

spectroscopy. By exposing ZnO to butenes, several infrared bands were observed. The assignments of these bands are shown in table 12.4.

Figure 12.7: *IR spectra of 1-butene on* ZnO.

Table 12.4: C=C stretching frequencies in cm^{-1}.

Molecule	Gaseous	π-complex	π-allyl
trans-butene	1676[a]	1640	1582
cis-butene	1660	1625	1572
1-butene	1645	1610	1572

[a] Raman active only

It is seen that butenes on ZnO form both π-complexes and π-allyls. Figure 12.7 shows the IR spectra after 1-butene is introduced to ZnO. Initially, a sharp band is seen at 1610 cm^{-1} due to the π-complex and one at 1572 cm^{-1} due to the *anti* π-allyl. With time, the band at 1610 cm^{-1} weakens and two bands appears at 1640 cm^{-1} (due to π-complex of *trans*-butene) and at 1625 cm^{-1} (π-complex of *cis*-butene). This indicates that isomerization is already occurring. As equilibrium approaches, only the π-complex of *cis*-butene and the *anti* π-allyl (the only π-allyl that *cis*-butene can form) remains prominent.

The change in the intensty of the bands due to the *anti* π-allyl and the three π-complexes with time is shown figure 12.8. Intensity of the π-allyl remains unchanged, but the intensity of the π-complexes changes drastically. Based on the infrared results and detailed rate measurements, a mechanism for the isomerization of 1-butene involving *syn* and *anti* π-allyls as intermediates and their inter-conversion has been proposed.

Far from being an exhaustive review on the subject, the above examples taken here gives some idea of how infrared spectroscopy can be used in the study of catalysis.

Figure 12.8: *Intensity of IR bands of different surface species formed by 1-butene on* ZnO.

12.2 RAMAN SPECTROSCOPY

Raman spectroscopy differs from rotational and vibrational spectroscopy (infrared spectroscopy) in that it involves scattering and not absorption of radiation by the sample. Raman spectroscopy can study both rotational and vibrational energy of molecules. The energy of the exciting radiation determines what transition, rotational or vibrational, will occur. Rotational transitions are lower in energy than vibrational transitions. In addition to this, rotational transitions are about three orders of magnitude slower than vibrational transitions. Therefore, collisions with other molecules may occur in the time in which the transition is taking place. A collision is likely to change the rotational state of the molecule, and so the definition of the spectrum obtained will be destroyed. Rotational spectroscopy is therefore carried out in the gas phase at low pressure to ensure that the time between collisions is greater than the time needed for a transition. The basic set-up of a Raman spectrometer is shown in Fig.12.9. The detector is placed perpendicular to the direction of the incident radiation so as to detect only the scattered light. The source should provide intense monochromatic radiation, and so a laser beam is usually used.

The criteria for a molecule to be Raman active are different from

those in other types of spectroscopy. Infrared spectroscopy requires that the molecule has a permanent dipole moment, at least for diatomic molecules. This is not the case for Raman spectroscopy, rather it is the polarizability (α) of the molecule which is important. The oscillating electric field (E) of a photon causes charged particles (electrons and, to a lesser extent, nuclei) in the molecule to oscillate. This leads to an induced electric dipole moment, (μ_{ind}, where $\mu_{\text{ind}} = \alpha E$). This induced dipole moment then emits a photon, leading to either Raman or Raleigh scattering. The energy of this interaction ($-\frac{1}{2}\alpha E^2$) is also dependent on polarizability. By comparison with the equation for the interaction energy for other forms of spectroscopy, it can be seen that the energy of Raman transitions is relatively weak. To counter this, a higher intensity of the exciting radiation is used.

Figure 12.9: *Scheme for Raman Spectroscopy*

For Raman scattering to occur, the polarizability of the molecule must vary with its orientation. One of the strengths of Raman spectroscopy is that this will be true for both heteronuclear and homonuclear diatomic molecules. Homonuclear diatomic molecules do not possess a permanent electric dipole, and so are undetectable by other methods such as infrared.

The polarizabilities of the two orientations of homonuclear diatomic molecule shown above are different. Selection rules arise from quantum mechanics (for details, see standard text books). Here, the quantum

numbers and the allowed transitions involved are only mentioned.

Rotational transitions

In order to find out the allowed rotational transitions, the total angular momentum quantum number for rotational energy states (J), must be considered. Raman spectroscopy involves a 2 photon process, each of which obeys the condition $\Delta J = \pm 1$. Hence, for the overall transition, $\delta J = 0, 2$, where $\Delta J = 0$ corresponds to Raleigh scattering, $\Delta J = +2$ corresponds to a Stokes transition, and $\Delta J = -2$ corresponds to an anti-Stokes transition.

Vibrational transitions

To find the allowed vibrational transitions, the vibrational quantum number υ, must be considered. For the overall transition, $\Delta\upsilon = 1$. Transitions where $\Delta\upsilon = 2$ are also possible, but these are of weaker intensity.

Types of scattering

Consider a light wave as a stream of photons each with energy $h\nu$. Several things may happen when a photon collides with a molecule only two of which are considered.

1. Elastic or Raleigh scattering: This occurs when the photon simply 'bounces' off the molecule without exchanging energy. The vast majority of photons will be scattered in this way.

2. Inelastic or Raman scattering: This occurs when there is an exchange of energy between the photon and the molecule, leading to the emission of another photon with a frequency different from that of the the incident photon. (Probability of this is 1 in 107 photons).

In Raman scattering, the molecule may either gain energy from, or lose energy to, the photon. In the figure next, energy states of the molecule (E_1, E_2, E_3)are shown. Originally, the molecule is in state E_2. The photon interacts with the molecule, exciting it with an energy $h\nu_i$. However, there is no stationary state of the molecule corresponding to this energy, and hence the excitation is to a virtual state that is lower in energy than a real electronic transition with nearly coincident de-excitation and a change in the vibrational energy. The scattering event

occurs in 10^{-14} second or less. The virtual state description of scattering is shown in figure 12.10

The molecule relaxes down to one of the energy levels shown. In doing this, it emits a photon. If the molecule relaxes to energy state E_1, it would lose energy, and so the photon emitted will have energy $h\nu_{r1}$, where $h\nu_{r1} > h\nu_i$. Such transitions are known as anti-Stokes transitions. If the molecule relaxes to energy state E_3, it would gain energy, and so the photon emitted will have energy $h\nu_{r2}$, where $h\nu_{r2} > h\nu_i$. Such transitions are known as Stokes transitions.

For rotational spectroscopy, both Stokes and anti-Stokes transitions are seen. For vibrational spectroscopy, Stokes transitions are far more common, and so anti-Stokes transitions can effectively be ignored.

Figure 12.10: *Energy states responsible for Stokes and anti-Stokes transitions.*

There are various ways Raman spectroscopy can be exploited. Here, only two important modes will be considered. Raman spectroscopy is conventionally carried out with green, red or near infrared lasers. The wavelengths are below the first electronic transitions of most of the molecules. The situation changes if the wavelength of the exciting laser falls within the electronic spectrum of a molecule. In that case the intensity of some Raman active vibrations increases by a factor of $10^2 - 10^4$. This is termed as resonance enhancement or resonance Raman effect (RR) and the intensity enhancement may be quite useful. Resonance enhancement does not begin at a sharply defined wavelength. In fact, enhancement of 5 to 10 times is commonly observed if the exciting laser is even within a few hundred wave numbers below the electronic transition of a mole-

cule. Scattering from a compound (or ion) adsorbed or even within a few Angstroms of a structural metal surface can be $10^3 - 10^6$ times greater than what is observed in solution. This surface enhanced Raman scattering is strongest on silver but is observable on gold, copper and platinum as well.

Surface enhanced Raman scattering (SERS) can arise from at least two mechanisms. The first is an enhanced electromagnetic field produced at the surface of the metal. When the wavelength of the incident light is close to the plasma wavelength of the metal, conduction electrons in the metal surface are excited into an extended surface electronic excited state called a surface plasmon resonance. Molecules adsorbed or in close proximity to the surface experience an exceptionally large electromagnetic field. Vibrational modes normal to the surface are most strongly enhanced. The second mode of enhancement is by the formation of a charge transfer complex between the surface and the molecule on the surface. The electronic transitions of many charge transfer complexes are in the visible region and so resonance enhancement occurs.

One should not, however, conclude that these are the only two mechanisms possible for the SERS. Generally, molecules with lone pair electrons or π clouds show the strongest SERS. The effect was first discovered with pyridine. Other aromatic nitrogen, sulphur or oxygen containing compounds are strongly SERS active. Hence, one has to take these experimental facts also into consideration for the probable mechanism. The RR and SERS spectra of a typical lead(II) complex adsorbed on silver surfaces are shown in figure 12.11. One can easily recognize the intensity increase in the SERS mode since such low concentration as $l5 \times 10^{-7}$ mol dm^{-3} shows similar intensity as that of 103 mol dm^{-3} in the RR spectrum.

12.2.1 Applications of Raman Spectroscopy

Raman spectroscopy is useful for analyzing molecules without a permanent dipole moment which would not show up on an IR spectrum. A useful 'exclusion rule' states that for molecules with an inversion centre, no modes can be both IR and Raman active. It can be used to determine bond lengths in non-polar molecules. It is useful for determining the identity of organic and inorganic species in solution, as the Raman transitions for these species are more characteristic than IR, where the transitions are much more affected by the other species present in the solution.

Like IR spectroscopy, Raman spectroscopy has been used to study

the adsorbents themselves as well as to study the adsorbed states. In the case of adsorbents, studies are mostly on many of the supports like silica, alumina, carbon and also zeolites. In the case of silica, the most extensively studied system is β-quartz for which the complete assignment of the Raman active optical modes has been achieved by Bates and Quist[21] in the case of silica gel. In the case of Vycor glass, well defined bands at 161 (vw),440 (v broad,s) 448 (w,sh) 604 (w),802 (w),930 (sh),980 (vw),1056 (vw),1184 (vw,bd) and 3750 cm^{-1} have been identified and they correlate with those found in nonporous silica and silica-rich glass. In the case of alumina, the report on the base adsorbent is limited though Raman spectroscopy can be utilized to study the s-Cl stretching vibrations of chlorinated alumina (where s represents a surface atom). In the case of zeolites, nine Raman band have been observed between 200 and 1200 cm^{-1} though all the bands did not appear in all samples. The strongest bands were in the 460 to 512 cm^{-1}. Other bands were found at 210 to 263, 268 to 317, 330-395, 403-472, 605-700, 810-990, 1037-1085 and 1100-1160cm^{-1}.

Figure 12.11: *RR and SERS spectra of a typical lead(II) complex adsorbed on silver.*

In spite of these reports, caution has to be exercised as many of these bands could arise from the window material. There is also the possibility of contribution from non-lasing lines.

Raman spectroscopy has been playing a vital role in the characterization of carbon nanotubes. The literature in this area is growing. A typical Raman spectrum of carbon nanotubes is shown in figure 12.12. The important feature in the Raman spectrum of carbon nanotube (CNT) is the radial breathing mode (RBM) which his usually located between 75

[21] J. B. Bates and A. S. Quist, *J.Chem.Phys.*, 56, 1528 (1972).

and 300 cm^{-1}. Frequency of the RBM is directly linked to the reciprocal of the diameter of the nanotube. Another important feature is the D mode (the disorder band located between 1330 to 1360 cm^{-1} is expected in multi-wall carbon nanotues (MWNT). Another characteristic band is the G mode (tangential mode) that corresponds to the stretching mode in the graphite plane. This mode is located around 1580 cm^{-1}. On the whole Raman spectra of carbon tubes are interesting because of resonance phenomena and sensitivity to the tube structure. There is a strong excitation wavelength dependence of the spectra resulting from the electronic band structure. In essence, the features in the Raman spectra are diagnostic of the CNT type.

Figure 12.12: *Typical Raman spectrum carbon nanotubes.*

Raman spectroscopy has played an important role in the characterization of the surface structure of supported molybdenum oxides. These studies have demonstrated the existence of surface compounds which were not detectable by XRD because of their molecular nature or their small particle size and high dispersion. Assignment of the vibrational bands of surface molybdena species has been made on the basis of corresponding solution spectra of a variety of isopolymolybdates and other reference compounds (see table 12.5). In general, the detected surface species are monomeric and polymeric molybdena species anchored to the support surface, two and three dimensional molybdates, crystalline molybdenum-support compounds and crystalline MoO_3. Typical band assignments of such species are given in table 12.6.

12.2.2 Raman Spectra of Adsorbed Molecules

Adsorption of aromatic systems (like benzene, benzaldehyde, benzylamine, benzonitrile, benzoic acid, chlorobenzne, styrene, pyridine (a probe for the determination of acidity of surfaces) has all been studied by Raman spectroscopy. The choice of the molecules is based on the possibility of polarizing the molecules and this is the main reason why most of the SERS studies deal with adsorption of hetero-atom substituted organic molecules adsorbed on Au, Ag, Cu and to some extent on Pt.

Table 12.5: Vibrational bands of some selected molybdenum oxygen compounds.

	Vibrational bands, cm^{-1}				
Compound	Mo=O str.	Mo-O-Mo assym. str.	Mo-O-Mo sym. str.	M=O bending	Mo-O-M deform.
$(NH_4)_2[Mo_8O_{26}]$	963	846	600	468	236
$.4H_2O$, (solid)	947	670	574	365	218
	918		526	338	152
	912				
$H_4[SiMo_{12}O_{40}]$	982	892	680	460	290
(solid)	962	880	680	460	290
	915	805	504	371	210
				340	160
$CoMoO_4$	882	850			
		756			
Na_2MoO_4	892	803		303	
$MoOF_4$	1039	713	666	311	240
solid			506		
$MoOCl_4$	1008	713	666	364	240
			506	354	184
				327	167
					158
MoO_3	996	820	667	469	244
				376	220
				366	199
				335	160
				292	131
				283	114

Among other aliphatic systems, adsorption of ethylene, propylene acrolein, acetone and acetaldehyde have been studied for the same reason. In the case of adsorption of pyridine on most of surfaces, bands are usually observed in the region 990 and 1030 cm^{-1} and these bands have been assigned to physically adsorbed pyridine. This assignment is based

on the position of these bands in liquid and gaseous pyridine and the disappearance of these peaks on evacuation. Similarly, the band close to 1020 cm^{-1} in the spectra of pyridine adsorbed on alumina and other adsorbents have been assigned (by comparison with the spectra of compounds such as pyridine-N-oxide and other coordinated complexes) to adsorbed pyridine coordinated through the nitrogen atom to Lewis site on the surface.

Table 12.6: Band assignment of alumina supported molybdenum catalysts.

Hydrated state		Dehydrated state	
Assignment	Frequency, cm^{-1}	Assignment	Frequency, cm^{-1}
Monomolybdate	900, 300	Monooxo species	1010
Dimolybdate	920–910	Dioxo species	990–970
Polymolybdate	940, 600–500, 200	Polymolybdate	960, 870, 360
MoO_3	995, 820, 665		

Various other types of adsorption of pyridine has been identified, especially the formation of pyridinium ions by interaction with Brönsted acid sites giving rise to bands at 1007 cm^{-1}.

This presentation is restricted only to highlight some typical applications of Raman spectroscopy for the study of adsorbents and also the adsorbed states of some polarizable molecules. The treatment in no way to be considered comprehensive.

12.3 ELECTRON ENERGY LOSS SPECTROSCOPY

Electron energy loss spectroscopy (EELS) is a technique that utilizes the inelastic scattering of low energy electrons in order to measure vibrational spectra of surface species and in a sense, it can be considered as the electron-analogue of Raman spectroscopy. To avoid confusion with other electron energy loss techniques, it is usually referred to as HREELS (high resolution EELS) or VELS (vibrational ELS). During the past few years, EELS has been established as a fairly powerful technique in surface analysis, mainly for the investigation of phonons of adsorbate vibrations but also of electronic transitions. In this chapter, however, discussions will be restricted to the analysis of the structure of adsorbate molecules through the observation of vibrational bands. This analysis, therefore, requires a resolution of a few meV. Unlike IR spectroscopy where resolutions of the order of 0.25 meV is routinely possible, resolution in HREELS is still around 5-7 meV (40-80 cm^{-1}) as seen from the FWHM (full-width at half maximum) of the elastic peak.

Essentially, there are two vibration excitation mechanisms. These are:
(i) Dipole scattering: This is a long range mechanism. The electric field of an incoming electron interacts with the changing electric field by molecular vibration only perpendicular to the surface (surface selection rule). The intensity distribution is sharply peaked in the secular direction.
(ii) Impact scattering: This is a short range mechanism. The incoming electrons impact atoms and molecules at the surface, leading to vibrational excitation. This mechanism excites all vibrations (both parallel and perpendicular to the surface). Since the scattering direction is isotropic, the dipole forbidden mode can be observed in the off-specular direction so as to exclude the intensity by dipole scattering. The selection rules that determine whether a vibrational band may be observed depend upon the nature of the substrate and also the experimental geometry, specifically the angles of the incident and (analyzed) scattered beams with respect to the surface.

Figure 12.13: *Schematic representation of Electron Energy Loss Spectrometer.*

For metallic substrates and a specular geometry, scattering is principally by a long-range dipole mechanism. In this case the loss features are relatively intense, but only those vibrations giving rise to a dipole change normal to the surface can be observed. By contrast, in an off-specular geometry, electrons lose energy to surface species by a short-range impact scattering mechanism. In this case the loss features are relatively weak but all vibrations are allowed and may be observed. Since the technique employs low energy electrons (typically 0.1 -10 eV), it is necessarily restricted for use in high vacuum (HV) and UHV environments. The use of such low energy electrons ensures that it is a surface specific technique and, arguably, it is the vibrational technique of choice for the

study of most adsorbates on single crystal substrates.

However, there are other limitations with respect to the sample. Specimens should be thin (¡50 nm) to avoid plural scattering effects as well as for high spatial resolutions. In addition, the thin films should be beam-insensitive. Thick specimens give rise to plural scattering and thus makes interpretation more difficult.

The basic experimental geometry is fairly simple as illustrated in figure 12.13. It uses an electron monochromator to give a well-defined beam of electrons of fixed incident energy, and then analyzing the scattered electrons using an appropriate electron energy analyzer. Usually for low energy electrons (in the range 1-2 eV), a thermionic source and for still low energies (of the order of 0.5 eV), field emission gun is usually employed.

Electron energy loss spectrum can be used for quantitative elemental analysis, thickness determination, for obtaining band structure of the solid and for the determination of the oxidation states of the elements present. However, the important application of EELS is for the identification of the vibrations of the molecule in the adsorbed state especially for the bond between the adsorbate and adsorbent. This is because in the conventional IR, the intensity of this band is very low. A substantial number of electrons are elastically scattered ($E = E_o$) and this gives rise to a strong elastic peak in the spectrum(see figure 12.13a.). It is seen from the figure 12.13b that additional weak peaks are superimposed on a slightly sloping background on the low kinetic energy side of this main peak ($E < E_o$). These peaks correspond to electrons which have undergone discrete energy losses during the scattering from the surface. For very thin specimens, the most prominent feature is the zero energy loss peaks by purely elastic scattering and this can be taken as the reference for the spectrum. The plasmon peak, due to inelastic scattering by outer shell (valence electrons) in the specimen centered around a plasmon energy E_P generally is in the range 10-30 eV. If there is no additional peaks due to plural scattering, then the intensity of the plasmon peak can be used to determine the thickness of the specimen in terms of the plasmon mean free path using the equation

$$t = \lambda \ln \frac{I_P + I_o}{I_o} \tag{12.2}$$

where λ is the plasmon mean free path, I_o and I_P are the intensities of the zero energy loss peak and plasmon peak respectively.

In figure 12.14, spectrum (a) shows that the predominant peak in the

EELS spectrum is the elastic peak centered around $E = E_o$. Spectrum (b) shows the loss peak at an energy ΔE to the lower energy side of the elastic peak. Elemental quantification can be achieved by integrating the spectral intensity over an energy range and then suitably correcting it for the background. This gives intensity of the core loss (I_c). Then one can make use of the relation $I_c = N(I_o + I_P))\sigma c$ where σ_c is the core loss cross section.

Figure 12.14: *A typical EELS spectrum.*

12.3.1 Application of EELS to the Analysis of Vibrational Excitations

Conventionally, the energy loss peaks in the EELS are associated with vibrational excitations. The magnitude of the energy loss, $E = (E_o - E)$, is equal to the vibrational quantum energy of the vibrational mode of the adsorbate excited in the inelastic scattering process. In practice, the incident energy (E_o) is usually in the range 5-10 eV (although occasionally it may be up to 200 eV) and the data is normally plotted against the energy loss (frequently measured in meV).

There are both advantages and disadvantages in utilizing EELS, as opposed to IR techniques, for the study of surface species. It offers the advantages of: (i) high sensitivity (ii) variable selection rules and (iii) spectral acquisition to below 400 cm^{-1}. The disadvantages are: (i) use of low energy electrons (requiring a high vacuum environment and hence the need for low temperatures to study weakly-bound species), and also

the use of magnetic shielding to reduce the magnetic field in the region of the sample; (ii) requirement of flat, preferably conducting, substrates and (iii) as stated earlier, lower resolution.

In the first section of this chapter we have seen that the adsorbed state of CO on metal surfaces has been widely investigated by infrared technique. Based on the prior knowledge of the coordination complexes, the binding of the CO to the metallic sites is usually inferred from the position of the stretching frequency, ν_{C-O} as shown in the table 12.7.

Table 12.7: Stretching frequency of CO.

	ν_{CO}, cm^{-1}
terminal CO (on top adsorption)	$2100 - 1920$
Bridged CO (between two M sites)	$1920 - 1800$
Multiple bonded CO	< 1800

However, the ν_{M-C} bond is not easily seen in IR while this can be easily observed in EELS around 400 cm^{-1}. This means that EELS enables the direct observation of the adsorption band without resorting to the observation of the changes in the fundamental modes of vibration of the adsorbed molecules.

Oxygen can be adsorbed on silver surfaces both associatively (at low temperature around 100 K) as well as dissociatively at temperatures around 300K. The EELS spectra obtained for these two states of adsorption are shown in figure 12.15.

One can notice that in the case of molecular adsorption of oxygen, the surface to oxygen bond appears at 237 cm^{-1} while dissociatively adsorbed oxygen gives rise to metal oxygen vibration at 324 cm^{-1}. Conventionally, in the IR spectroscopy the changes in the frequency of the stretching vibration of the molecule is usually observed and the changes alone is employed for interpreting the strength of adsorption. This example is chosen to demonstrate how the adsorption bond is directly probed by this technique while in IR, the nature of adsorption bond is only deduced from the variations in the frequency of the fundamental vibrations of the adsorbed molecules. We shall also see how this adsorption directly affects the reactivity of the catalyst surface.

The adsorption and dehydrogenation of cyclohexane have been investigated on the (1x1) and (5x20) surfaces of Pt100. On both surfaces

dehydrogenation of cyclohexane to benzene occurs. The reactivity of the (5x20) surface, however, is three to four orders of magnitude lower than that of both the (1x1) surface and the topographically similar Pt111 surface. The high reactivity of the (1x1) surface is surprising since no softened C-H mode is observed. This shows that the adsorption bond did not cause any major change in the fundamental modes of vibration of the adsorbed molecule though there are differences in the nature of the adsorption bond between cyclohexane and the two surfaces. Probably the metal–C bond is different between the two surfaces and the adsorbed cyclohexane is dehydrogenated more on the (1x1) surface as compared to (5x20) surface.

Figure 12.15: *The EEL spectra for the oxygen adsorption on* Ag (110) *surface.*

The loss features in EELS can be used to study a number of other aspects of the surface like surface contamination, the nature of reduction process (e.g., SiO_2 to Si) and surface plasmon excitations. These aspects are beyond the scope of this presentation. The examples chosen are only representative ones to demonstrate how this technique can compliment infrared and Raman spectroscopy.

SUGGESTED READING

1. C. H. Amberg in *The Solid-Gas Interface*, (Ed. E. A. Flood), Marcell Dekker, New York, 1967.
2. R. B. Anderson (Ed.), *Experimental Methods in Catalytic research*, Academic Press, New York, 1968.
3. J. M. Brown, *Molecular Spectroscopy*, Oxford Chemistry Primer, 1998.
4. J. M. Hollas, *Modern Spectroscopy*, 1996.
5. W. N. Delgass, G. L. Haller, R. Kellerman and J. H. Lunsford, *Spectroscopy in Heterogeneous Catalysis*, Academic Press, (1979).
6. T. A. Egerton and A. H. Hardn, *Catal.Rev.Sci.Eng.*, 11,71(1975).
7. G. Mestl and T. K. K. Srinivasan, *Catal.Rev.Sci Eng.*, 40, 451 (1998).
8. R. F. Egerton, *Electron Energy Loss Spectroscopy* in *The Electron microscope*, Plenum, New York, 1996.
9. H. Ibach and D. L. Mills, *Energy Loss Spectroscopy and Surface Vibrations*, Academic Press, 1982.
10. M. W. Urban, *Vibrational Spectroscopy of Molecules and Macromolecules on Surfaces*, John Wiley and sons Inc, 1993.

Chapter 13

Thermal Methods

13.1 INTRODUCTION

Thermal method here means any study in which the sample is heated in a programmed manner and the consequent effect is monitored. They will be referred as TPX, where TP stands for *temperature programmed* and X stands for the process that is being studied. TPX methods include temperature programmed desorption (TPD), temperature programmed reduction (TPR) and temperature programmed reaction spectroscopy (TPRS). Normally, any kinetic study involves monitoring the concentration of any one or more of the species in the reaction as a function of time and temperature. In the temperature programmed techniques (TPX), time and temperature are related by the expression $T(t) = T_0 + \alpha t$ where T is the temperature at any time t, T_0 is the start temperature and α is the heating rate that is (dT/dt) in the units of K/sec. It therefore provides a means to study two variables of a reaction at the same time, and this method has attracted wide attention.

There is a range of techniques for studying surface reactions based on temperature sweep. Molecular adsorption on surfaces can be studied using temperature programming to discriminate between processes with different activation parameters. Experimentally, this method of analysis is simple requiring a pressure gauge or a chemical analytical tool such as a gas chromatograph or a mass spectrometer. Even pressure measurement as a function of time and temperature may be sufficient in some instances.

The basic experiment is very simple involving the following two steps in the case of desorption.
1. Adsorption of one or more molecular species onto the surface at low temperature (often at 300 K, but sometimes sub-ambient).

2. Heating of the sample in a controlled manner (preferably to give a linear temperature ramp) while monitoring the evolution of the species from the surface back to the gas phase. The data obtained from such an experiment consists of the intensity variation (concentration of the desorbed species) of each recorded mass fragment as a function of time/temperature. In case of a simple reversible adsorption process, it may only be necessary to record one signal that is attributable to the molecular ion of the adsorbate concerned. Typical TPD trace for the desorption of CO adsorbed on Pd(111) at 300 K is shown in figure 13.1.

Figure 13.1: *TPD of carbon monoxide on Pd(111) at 300 K.*

Because mass spectrometric detection is normally used, sensitivity of the technique is good with attainable detection limits below 0.1% of a monolayer of the adsorbate. The following points are worth noting:
1. The area under a peak is proportional to the amount originally adsorbed, i.e. proportional to the surface coverage.
2.Kinetics of desorption (obtained from the peak profile and the coverage dependence of the desorption characteristics) give information on the state of aggregation of the adsorbed species, i.e. it tells us whether adsorption is molecular or it is dissociative adsorption.
3. Position of the peak (peak temperature) is related to the enthalpy of adsorption indicating the binding strength of the adsorbate to the surface. If there is more than one binding site for a molecule on a given surface and if they have significantly different binding enthalpies, it will be possible to distinguish them from the multiple peaks in the TPD spectrum.

13.1.1 Theory of TPX Techniques

In general, rate of desorption of a surface species will be expressed as

$$R_{\text{des}} = \nu N x \exp\left(-E_a^{\text{des}}/RT\right) \tag{13.1}$$

where R_{des} is the desorption rate ($= -dN/dt$), x is the kinetic order of desorption and E_a^{des} is the activation energy of desorption.

In a temperature programmed desorption experiment, temperature and time are related by the expression $T = T_0 + \alpha t$ and $dT = \alpha dt$ where T_0 is the starting temperature. Intensity of the desorption signal $I(T)$ is proportional to the rate at which the surface concentration of adsorbed species is decreasing. This can be expressed as

$$I(T)\alpha\frac{dN}{dT} = (\frac{\nu N^x}{\alpha})\exp -\frac{E_a^{\text{des}}}{RT} \tag{13.2}$$

This problem can also be represented graphically. The equation for signal intensity consists of two terms, one dependent on surface coverage and another exponential term. At low temperature, the exponential term is small and it increases with increase of temperature. The increase is significant when RT approaches the value of E_a^{des}. On the other hand, the coverage dependent term initially remains constant, decreases rapidly as the desorption temperature is approached and becomes zero at some temperature. The graphical representations of the variations in the pre-exponential term and the exponential term are given in figure 13.2. The shaded area can be considered as the desorption trace. The description given here is simplistic, but sufficient to appreciate the shape of the desorption trace.

Let us consider a simple case for understanding the nature of the desorption trace that one will obtain. The case that is considered assumes that (i) the adsorption is of a molecular species and (ii) the order of desorption is unity. The maximum in the desorption trace (the point at which signal $I(T)$ will attain a maximum value) will occur when $\frac{dI}{dT} = 0$, i.e. when

$$(d/dT)[\frac{\nu N^x}{\alpha}\exp\left(-\frac{E_a^{\text{des}}}{RT}\right)] = 0$$

This can be rewritten taking into account that surface coverage N itself is a function of temperature.

$$(\frac{\nu N^x}{\alpha})(\frac{E_a^{\text{des}}}{RT})\exp\left(-\frac{E_a^{\text{des}}}{RT}\right) + \frac{\nu}{\alpha}\exp\left(-\frac{E_a^{\text{des}}}{RT}\right)\frac{dN}{dT} = 0$$

Substituting for dN/dT, one gets

$$(\frac{\nu N}{\alpha})[\frac{E_a^{\rm des}}{RT} - \frac{\nu}{\alpha}\exp(-\frac{E_a^{\rm des}}{RT})]\exp(-\frac{E_a^{\rm des}}{RT}) = 0$$

Putting the expression within the square brackets equal to zero, we get

$$\frac{E_a^{\rm des}}{RT_p^2} = \frac{\nu}{\alpha}\exp(-\frac{E_a^{\rm des}}{RT_p})$$

where T_p represents the peak temperature.

Figure 13.2: *Variation of the pre-exponential and the exponential terms as functions of temperature. The shaded area represents desorption trace.*

It can be seen that
1. Depending on the value of $E_a^{\rm des}$, the peak temperature too varies, being higher for higher values of $E_a^{\rm des}$.
2. Peak maximum temperature is independent of initial coverage.
3. Shape of the trace depends on the rate of the desorption process and it will decrease rapidly after the desorption maximum.

More detailed quantitative information on TPD is beyond the scope of this book and they can be found elsewhere. In general, this technique can provide a variety of information on various aspects of adsorption and catalysis. They are:
1. Mechanistic aspects of reaction under study (the technique in this case is referred as temperature programmed reaction spectroscopy TPRS)

2. Identification of the nature of active sites, binding states of adsorbed species and binding energy of the adsorbed species.
3. The influence of preparation procedures on the catalysts developed.
4. Effects of active phase, chemical composition, promoters dispersion, surface groups.
5. Active phase support interaction, alloy/compound formation

13.2 TEMPERATURE PROGRAMMED DESORPTION

In this section, only very simple cases of desorption spectra are shown as examples for study of surfaces. Details for other specific applications can be found in the literature.

Figure 13.3: *(a) Thermal desorption trace and (b) flash desorption curve for the desorption of CO from tungsten surfaces.*

13.2.1 Binding State of Adsorbed Species

It is often known that the adsorbed molecules can have more than one mode of adsorption. A simple molecule like hydrogen can also be adsorbed in more than one state. These states are often identified from the temperature at which desorption takes place. A simple case is the adsorption of CO on top site, in a two-fold site and multi-fold site depending on coverage and other reaction conditions. The desorption trace of CO from tungsten is shown in figure 13.3 together with the flash desorption curves obtained for the same systems. It can be easily recognized that three adsorbed states of CO are discernable in both the thermal desorption and flash desorption traces indicating that CO is adsorbed on tungsten surfaces in three different forms. It is therefore possible to identify the multiple binding states of the adsorbed species and the binding state that is responsible for a given surface transformation can also be recognized.

Figure 13.4: *Thermal desorption of hydrogen from* W(100) *showing* β_1 *and* β_2 *states.* β_1 *is seen only at higher coverage.*

It can be seen that there are three distinct desorption states shown as α, β_1 and β_2. As stated above even for simple molecules like hydrogen more than one desorption peak can be observed. Even though one may

not be able to visualize more than one adsorption state in some cases, the repulsive interactions among the adsorbed molecules as a function of coverage can result in multiple peaks in traces of desorption profiles. One such example for hydrogen adsorption on tungsten surface is shown in figure 13.4.

TPD is one of the widely used techniques for characterizing the acid sites of most of the catalyst surfaces. Knowledge of the number and strength of the acid sites on surfaces of alumina, silica-alumina and zeolites have been found necessary for understanding surface transformations like cracking of n-hexane, isomerization of xylene,polymerization of propene, methanol to olefins reaction, toluene disproportionation, and cumene cracking that take place on these surfaces. In all these reactions, it is often recognized that the Bronsted acid site density is a crucial factor. Conventionally, there are three types of molecular probes commonly used for characterizing acid sites using TPD. They are:
(i) base molecules like ammonia, pyridine or other amines
(ii) non-reactive vapours, and
(iii) reactive vapours.

Figure 13.5: *Thermal desorption mass spectra of n-butylamine and n-propylamine from* HY *zeolite.*

Even though TPD of ammonia is conventionally employed to monitor the acidity of the solids surfaces, the values obtained are always higher because being a small molecule, ammonia can access almost all the pores of the catalysts while typical reactant molecules may not be able to access all the pores of the catalysts. In addition, ammonia can identify all acid sites including the weak acid sites, although these weak acid sites may not be useful in promoting the reactions mentioned here. These points should be kept in mind while interpreting TPD of ammonia as a measure

of acidity of porous solids as well as in correlating acidity with observed catalytic activity. Larger nonreactive amines such as pyridine and t-butylamine are often preferred alternatives to ammonia because their sizes permit them to access the pores that are required for catalytic cracking and other reactions and also because they identify only the strong and moderate acid sites. Most common application of these pores is the characterization of acid sites by looking at the infrared spectra of adsorbed pyridine.

Ring vibration frequency of pyridine adsorbed on Lewis and Bronsted acid sites are different and their presence can be easily detected from infrared spectra of the adsorbed pyridine. However, determination of extinction coefficients is difficult and IR of pyridine is typically used in a qualitative manner, rather than measuring the acid site densities.

Figure 13.6: *TPR of* $Ni(OH)_2$ *and* NiO.

While using aliphatic amines as probes for monitoring the acid sites and strength of solids, one has to exercise caution. Figure 13.5 shows the TPD traces for the desorption of n-butylamine and n-propylamine from the surface of HY zeolite. Though both amines show distinct desorption patterns, the on-line mass spectral analysis of the desorption products showed the presence of butenes, higher olefins, dienes and aromatics. The observation is significant in view of the fact that uptake and desorption patterns of the alkyl amines are generally used for estimating the acidity

of the catalysts. The observation of such desorption products even from weakly acidic NaY zeolites indicates that caution has to be applied in treating the TPD data of alkylamines for the determination of acidity of solids.

While using reactive probes like alkylamines, it is assumed that the amines are protonated by the Bronsted acid sites to form the alkyl ammonium ions which then decompose giving ammonia and olefins in a well defined temperature range proceeding like a Hoffman elimination reaction. If this were to take place, then acidity of the solids can be monitored using alkyl amines.

13.3 TEMPERATURE PROGRAMMED REDUCTION

TPR has been used to determine the effect of catalyst precursors and also the type of interactions between the active precursor and the support. In figure 13.6, the temperature programmed reduction trace of $Ni(OH)_2$ prepared by urea hydrolysis is shown. It can be seen that the TPR profile shows a pattern with doublet peaks corresponding to the reduction of the rhombohedral and cubic forms of NiO. The controls are also shown in the same figure.

Figure 13.7: *TPR profiles of* Ni/Al_2O_3 *catalyst precursors prepared by different methods (see text).*

Figure 13.7 shows TPR patterns of hydroxides prepared by impreg-

nation of different nickel hydroxides. In all the samples, nickel loading was 30 percent by weight and the support was the same alumina.

In sample A, nickel deposition was carried out from a solution of nickel nitrate by urea hydrolysis. Nickel hexammine complex was used for preparing sample B. Sample C was prepared from nickel nitrate solution by adding ammonia and sample D was prepared from nickel nitrate by equilibrium deposition. Four different stages of NiO reduction characterized by bound states could be identified. They are free NiO in the rhombohedral (a) and cubic (b) forms, NiO getting reduced by an autocatalytic process (c), a bound state of NiO which gets reduced at higher temperature (d) and another state of NiO which is irreducible (see figure 13.7). It is seen that the finer details of the active phase support interactions are manifested in the TPR profiles. The quantitative data generated from these TPR profiles are given in Table 13.1 to substantiate the conclusions made.

Table 13.1: Reduction behaviour of alumina supported nickel precursor.

Sample	Free NiO wt.%	Reduces with difficulty, wt.%	Irreducible bulk spinel, wt.%	Reducibility (total), wt.%
A	7.26	48.74	44.0	56.0
B	7.00	64.0	29.0	71.0
C	8.90	65.10	26.0	65.0
D	18.6	71.54	14.0	86.0

13.4 TP REACTION SPECTROSCOPY

Temperature programmed reaction spectroscopy (TPRS) is another technique that is being employed. In this method, a number of reaction products will normally be detected by employing an analytical tool like a mass spectrometer. We shall illustrate this with a simple example.

Decomposition of formic acid on copper surface has been studied by this method. When formic acid adsorbed on copper surface is heated at a constant rate, the desorption spectrum as shown in figure 13.8 is obtained. The first trace (a) represents the desorption of hydrogen ($m/z = 2$) which shows two peaks, one near room temperature and the other between 400 and 500 K. The second tracing (b) that represents CO_2 ($m/z = 44$) shows only one peak that coincides with the second hydrogen peak. The lower temperature hydrogen peak appears around the temperature at which hydrogen atoms combine and desorb as molecular hydrogen from hydrogen covered Cu(110) surface. The higher

temperature hydrogen peak is observed well above the normal hydrogen desorption temperature. Its appearance must be governed by the kinetics of decomposition of another surface species.The carbon dioxide peak should also be decomposition limited because on clean Cu(110) surface, CO_2 is only weakly physisorbed at very low temperature. Simultaneous desorption of carbon dioxide and hydrogen indicates the surface transformation of adsorbed formic acid.

Detailed mechanistic aspect of surface transformation can also be elucidated from the various species that appear in the temperature programmed reaction traces.

Figure 13.8: *Temperature programmed reaction of formic acid on copper.*

In this brief chapter, only the simpler aspects of the temperature programmed techniques have been discussed. The reader may find more information in the relevant literature.

SUGGESTED READING

1. Cvetanovic, R. J. and Amenomiya, Y. *Catal. Rev.,*, 6, 103 (1972).
2. Kolasinskii, K. W., *Surface Science: Foundation of Catalysis and Naonscience*, John Wiley, 2002.
3. Jones, A. and McNicol, B. D., *Temperature Programmed Reduction for Solid Materials Characterization*, Marcell Dekker, 1986.

Chapter 14

Electron Spectroscopy

Electrons are bound to an atom with different energies. Atoms may be present in free state, in molecules or in a solid. When these atoms are exposed to different stimuli such as a monochromatic photon beam or an electron beam, the bound electrons may be ejected with different kinetic energy. Since an atom has electrons with different binding energies, each of which has some probability of being ejected, a series of electrons having different kinetic energy values will be emitted. In photoelectron spectroscopy, intensity (number of electrons emitted per second) is measured as a function of the kinetic energy of the electrons. This has become possible with the introduction of high resolution β-spectrometer by Siegbahn and co-workers. When a soft X-ray beam is used as the stimulant, it is called *X-ray photoelectron spectroscopy* (XPS). Use of UV radiation can eject only the electrons with low binding energy and this method is known as *Ultraviolet photoelectron spectroscopy* (UPS).

When an atom is subjected to high energy stimulation leading to the ejection of some core electron, the photoionized excited atom may relax by dropping an outer electron to this core level. The difference in energy is then emitted as a X-ray photon. This is *X-ray fluorescence*. On the other hand, if the energy is transferred to an outer electron instead of being emitted as X-ray, that electron may come out with a certain kinetic energy which may be studied by the β-spectrometer. This is an Auger electron. Monitoring the intensity of the Auger electrons is known as *Auger electron spectroscopy* (AES).

As has been said already, electrons scattered from a molecule or a solid may lose energy in many ways. One of these is by exciting the vibrational modes of the molecule. The technique to study the vibrational

energy levels from the electron energy loss is known as *High resolution electron energy loss spectroscopy* (HREELS). The common feature of all these techniques is that all of them use a β-spectrometer. Hence, they all use similar instrumental techniques and can be used in combination. Electrons emitted from atoms in the bulk of a solid material undergo multiple scattering due to collision with other atoms. Only those electrons that are emitted from the atoms at the surface escape without any energy loss due to multiple scattering. Hence, the electron spectroscopic techniques are surface sensitive and are used for studying the surface. This is the reason why electron spectroscopic methods are attractive for studying catalysts. In this chapter, we shall consider the application of XPS and AES for studying solid catalysts.

Figure 14.1: *Two of the several ways of relaxation of a core-ionized atom.*

14.1 X-RAY PHOTOELECTRON SPECTROSCOPY

Kinetic energy E_K of an electron emitted from an atom present in a gaseous molecule is given as

$$E_K = h\nu - E_B \tag{14.1}$$

where $h\nu$ is the photon energy and E_B is the binding energy of the electron. Since the photon energy is fixed, it is possible to plot the spectrum either as a function of E_K or E_B. In the case of gaseous samples, the vacuum level is taken as the zero energy. In the case of a solid sample, where the sample and the spectrometer are in contact, the common Fermi energy is taken as the reference level. That is the reason why the kinetic energy of the same level of an atom in the gaseous state appears lower by about 4 eV as compared to the energy of the same level

when the atom is present in a solid. Here, 4 eV is the work function of the spectrometer which is taken as an instrument constant. Thus, C($1s$) binding energy in a solid sample is 284 eV, whereas the same for gaseous carbon is 288 eV. However, as long as we make all our measurements on solid samples, this difference is of little importance. A typical XPS trace of gold film is shown in figure 14.2.

Figure 14.2: *XPS spectrum of gold film showing binding energy of different electrons*

Chemical shift

It may be noted that E_B is the energy difference between the final state E_f (energy of the core ionized atom present in the solid and the initial state E_i (energy of the initial atom before photoemission). Then

$$E_B = E_f - E_i \tag{14.2}$$

Both E_i and E_f depend on the state of the atom, i.e. on its charge and chemical environment. Hence, any change in binding energy ΔE_B depends on the initial and final state energies. If it is assumed that E_f does not change with the change of state of the atom, ΔE_B is the difference between the initial states of the atom in two different chemical states. ΔE_B is known as the XPS chemical shift. Taking zero oxidation state of an atom as the reference, a positively charged ion will have a positive chemical shift. Higher the positive charge of the ion, more positive will be the chemical shift. Thus the binding energy of the $2p_{1/2}$ level (or any other level) of Ni^{2+} is higher than that in metallic nickel

(positive chemical shift). Similarly, a negatively charged ion will show a negative chemical shift as compared to the neutral atom. This general conclusion is based on the assumption that the final state in the two cases remain unchanged. This is not always true. Thus, it has been found that E_B of a energy level in Pb^{4+} is lower than that for Pb^{2+}.

Surface charging

Due to emission of the photoelectrons, the surface of the sample accumulates positive charge. If the sample is a metal, this charge is quickly neutralized by the flow of electrons from the bulk. If the sample is an insulator, surface charging is appreciable. The emitted electrons will lose some of their kinetic energy to overcome the attraction of the positive surface charge. Hence observed E_B will be higher than its true value and correction for charging is necessary.

There are several ways of making the charging correction. Charging may be avoided by coating the surface of the sample with a thin layer of gold. This method will weaken the intensity of the signal from the sample. Moreover, this may not be always desirable for a catalyst. Alternatively, the surface is flooded with zero energy electrons from an electron gun to neutralize the positive charge. The other approach is to correct the binding energy by referring to a internal standard for which the correct E_B is known. The C1s signal arising from contamination of the surface from pump oil is often used for binding energy correction. For silica or alumina supported catalysts, the known Si2s and Al2s signals are often used as internal standards for binding energy correction.

Line shape and curve resolution

If the XPS peaks are symmetric singlets, obtaining intensity from the peak area is straight-forward. Often, the background is not flat and peaks are asymmetric and overlapping. Curve fitting techniques used in such cases are highly effective in finding the number of lines under a broad band as well as in finding the correct binding energy and intensity.

Peak intensity

The probability N_0 of photoemission is given as

$$N_0 = \sigma n F \tag{14.3}$$

where σ is the photo-ionization cross section of the atomic energy level, n is the concentration of the atom and F is the photon flux. The probability that a photo-electron escapes without loss of kinetic energy due

to multiple collisions is

$$dN = N_0 \exp\left(-\frac{x}{\lambda}\right) dx \tag{14.4}$$

where x is the distance of the atom from the surface. Number of electrons N escaping without loss of kinetic energy

$$N = \int N_0 \exp\left(-\frac{x}{\lambda}\right) dx = \sigma n F \lambda \tag{14.5}$$

where λ is the inelastic mean free path (also known as the escape depth) of the electron.

Experimentally measured peak intensity due to atom A is

$$I_A = \sigma_A n_A F \lambda_A D_A \tag{14.6}$$

where D_A is the fraction of the electrons entering the detector. For two different elements A and B,

$$\frac{I_A}{I_B} = \frac{\sigma_A n_A F \lambda_A D_A}{\sigma_B n_B F \lambda_B D_B} \tag{14.7}$$

Under identical experimental conditions, and approximating $\lambda \propto \sqrt{E_K}$,

$$\frac{I_A}{I_B} = \frac{\sigma_A n_A \sqrt{E_K(A)}}{\sigma_B n_B \sqrt{E_K(B)}} \tag{14.8}$$

Relative concentration of two elements can be expressed as

$$\frac{n_A}{n_B} = \frac{I_A \sigma_B \sqrt{E_K(A)}}{I_B \sigma_A \sqrt{E_K(B)}} \tag{14.9}$$

Photo-ionization cross section σ for a given electronic state depends on the photon energy used. Since most commercial instruments use MgK_α and AlK_α radiations, data on relative cross sections with these X-ray photon energies have been tabulated[1].

It is clear by now that several layers of atoms contribute to the peak intensity in XPS and hence this is not strictly restricted to the top layer of the solid. However, about 95% of the intensity comes from a layer of thickness of 3λ. This means that by properly selecting the binding energy, the effect can be restricted to within $30\mathring{A}$ from the surface. For this reason, it is treated as a technique for surface analysis and XPS is also known as *Electron spectroscopy for chemical analysis* or ESCA.

[1] J. Scofield, *Electron Spectroscopy*, 8, 129, (1976).

14.1.1 Secondary Peaks

Besides the main binding energy peaks, several other peaks are always present in the XPS spectra. In order to interpret the spectra correctly, it is necessary to identify these secondary peaks.

Auger peaks

The origin of the Auger peak has already been explained. The unstable core ionized atom undergoes fast relaxation by emitting X-ray as well as by the emission of Auger electrons. The XPS spectrum always has the additional kinetic energy peaks due to Auger emission. It is easy to identify them since unlike the XPS peaks, the kinetic energy (and hence the binding energy) of the Auger peaks are independent of the photon energy. Position of the Auger peaks remain unchanged by changing the X-ray energy.

Satellite Spectra

Along with the main peaks, additional peaks appear in the lower kinetic energy side. These are the satellite peaks. Some of them are dependent on the pressure in the system. They arise due to the loss of kinetic energy by the electrons due to collision with the gas molecules. These peaks are not observed if the pressure in the spectrometer is maintained at about 10^{-9} torr. The pressure independent satellite peaks are more important of which those arising from multiplet splitting and shake-up are most prominent.

If the atom before photoemission (initial state) has one or more unpaired electrons, the unpaired electron produced during photoemission may have the same spin as the initial unpaired electron, or opposite to it. This gives rise to two different final states leading to two binding energy peaks. This is *multiplet splitting*.

Removal of the core electron by photoemission changes the effective nuclear charge suddenly. As a result, an outer electron may be transferred from its original level to a higher level. Kinetic energy of the emitted photo-electron will be lowered by an amount equal to the energy of this transition. Several such transitions may occur in one photoemission. Photoelectrons will lose kinetic energy equal to these transitions. As a result, a number of low intensity peaks (in addition to the main peak) will appear on the higher binding energy side. These are called the *shake-up* peak. Shake-up lines can sometime provide important clue on the oxidation state of the atom.

14.1.2 The Instrument

The instrument consists of one or more X-ray sources, an electron energy analyzer, the electron detector and a display/recording system. The entire system is backed up by an ultra high vacuum system capable of maintaining a vacuum of 10^{-10} to 10^{-9} torr.

All commercial instruments are provided with MgK_α (1254 eV) and AlK_α (1487 eV) X-ray sources as they have sufficient energy as well as fairly narrow line width. A monochromator can achieve better resolution at the cost of intensity. Two types of kinetic energy analyzers, the cylindrical or the hemi-spherical type, are generally used. The detector is usually a Faraday cup coupled with an electron multiplier tube with a gain 10^6. Multi-detectors are used for the dispersive analyzer. Ultrahigh vacuum is produced using an oil diffusion pump along with a cryogenic pump or a getter. A sample preparation/treatment chamber is connected with the system through a gate valve. This makes it possible to give appropriate pretreatment to the sample. UV and electron sources are also provided as additional attachments.

Figure 14.3: *Schematic diagram of an electron spectrometer*

14.1.3 Application in Catalysis

Application of XPS in the study of catalysts will be illustrated here with a few typical examples. No attempt will be made to make an exhaustive survey of the vast published literature.

Detection of surface phases

Gavalas, Pichitkul and Voecks[2] reported an interesting study. While studying $NiO/\alpha\text{-}Al_2O_3$ catalysts, they could detect the presence of $NiAl_2O_4$ on the surface although this was not found in X-ray diffraction. The sample calcined at 850 and 1050 °C showed XPS spectra similar to that of NiO. After extracting the surface NiO with hydrochloric acid, XPS

[2]G. R. Gavalas, C. Pichitkul and G. E. Voecks, *J. Catal.*, 88, 54, (1984).

showed the presence of $NiAl_2O_4$ that was not detected by X-ray diffraction (figure 14.4).

The extent of reduction of a supported oxide catalyst can be studied by XPS. An example taken here is from the work of Devries, Yao, Baird and Gandhi[3] who had prepared the catalyst by impregnating γ-Al_2O_3 with $(NH_4)_2Mo_2O_7$ and calcining at 400°C. The calcined catalyst showed only Mo3$d_{5/2}$ peak at 238.2 eV due to Mo(VI). As the sample was reduced, molybdenum with lower oxidation states also appeared in the spectrum and the concentration of Mo(IV) increased with increasing reduction temperature (figure 14.5.).

Figure 14.4: NiO/Al_2O_3*: a. calcined at 1050°C and extracted with HCl; b. calcined at 1050°C; c. calcined at 850°C; d.* $NiAl_2O_4$*; e. NiO.*

Supported metal catalysts

Small metal particles on an oxide support constitutes an important class of catalysts. Catalytic activity is often dependent on metal dispersion or metal particle size. The intensity ratio of a peak due to the metal to that of one coming from an atom of the support material after correction for their different emission cross sections (I_m/I_s) gives the true picture for metal dispersion. This is highest when all the metal atoms are atomically dispersed on the top of the support. However, more and more of the metal atoms will be present in the bulk and the emitted electrons from these atoms cannot escape without loss of kinetic energy. This leads to an decrease in I_m/I_s. Although intensity of the XPS peaks depends

[3] J. E. Devries, H. C. Yao, R. J. Baird and H. S. Gandhi, *J. Catal.*, 84, 8, (1983).

on a number of factors, the ratio I_m/I_s can be taken as a qualitative measure of metal dispersion. At very low metal loading, I_m/I_s may be low because the monolayer of the metal is not yet complete and the ratio may initially increase with metal loading. After the completion of the monolayer, further loading would lead to an increase in particle size and I_m/I_s will not increase. The metal signal may be very weak at very low loading if the metal is deposited within the micro-pores of the support. A catalyst with very high metal dispersion may show a decrease in the I_m/I_s ratio when it is subjected to calcination because of the migration of the metal particles on the surface to form bigger metal particles. When used along with additional experiments, I_m/I_s ratio may provide important information about the supported metal catalysts.

Figure 14.5: *XPS of* Mo/Al_2O_3 *reduced at: a.* 300^oC*; b.* 400^oC*; c.* 500^oC*.*

In spite of the stringent conditions maintained in catalyst manufacture, two batches of catalysts prepared in apparently identical conditions do show variation in their catalytic property. In such cases, XPS may be useful in finding out the cause of such a difference.

14.2 AUGER ELECTRON SPECTROSCOPY

Among the various electron spectroscopic techniques, Auger electron spectroscopy occupies a special place in relation to surface analysis. The phenomenon was originally discovered by Pierre Auger in the year 1925. The phenomenon can be described as ionization of an atomic core level by an incident electron beam or X-ray beam, the radiationless transition within the system and the escape of the Auger electron into vacuum

where it is detected with a suitable electron detector. Origin of the Auger electron has been discussed at the introduction where it has been shown that a core-ionized atom may relax by X-ray fluorescence or by emission of Auger electron. If the kinetic energy of the emitted auger electrons is monitored by an electron energy analyzer, the technique is known as Auger electron spectroscopy.

The Auger electrons manifest as small emissions in the total energy distribution function $N(E)$ as a function of E. This small signal can become pronounced by electronic differentiation that removes the large background consisting of backscattered primary electrons and inelastically scattered Auger electrons. The $N(E)$ function also includes a low energy peak corresponding to ejected lattice electrons, a pronounced peak at 1 keV consisting of elastically reflected primary electrons and several small peaks corresponding to characteristic energy losses of reflected primary electrons. However, these events are not relevant in the discussion of the Auger process. A typical $N(E)$ function and the effect of electronic differentiation along with the method of measuring peak to peak height are shown in figure 14.6.

14.2.1 Principles of Auger Process

Let us consider the ionization process from an isolated atom under electron bombardment. The energy levels in an atom can be approximated to the situation shown in figure 14.7. The primary electron beam with sufficient incident energy (E_P) can be expected to ionize a core level with energy E_{K}. The vacancy created in the core level is immediately occupied by transition or relaxation from another level. This is shown in the figure as an electron from the L1 level. The energy released corresponds to $(E_{\mathrm{K}} - E_{\mathrm{L1}})$. This energy released by the relaxation process can be utilized to ionize another electron from the system and in the figure it is shown that an electron from $L2$ level is ionized. This secondary emitted electron is termed as Auger electron. The energy carried by the Auger electron is given by $E_{\mathrm{K}} - E_{L1} - E_{\mathrm{L2}} - \phi_A$ where ϕ_A is the work function of the material with which the analyzer is made of. The Auger transition is termed as KL1L2. Therefore, for an Auger process to take place, a minimum two energy states and three electrons are necessary. It is therefore obvious that hydrogen and helium atoms cannot give rise to any Auger transitions. Li atom which has a single electron in its outermost shell also cannot give rise to Auger transition.

In Auger electron spectroscopy (AES), kinetic energy of the Auger electron arising from WXY transition is measured. This kinetic energy

can be approximated as

$$E_{\mathrm{WXY}} = E_{\mathrm{W}}(Z) - E_{\mathrm{X}}(Z) - E_{\mathrm{Y}}(Z+\Delta) - \phi_A \tag{14.10}$$

where Z is the atomic number of the atom involved.

The term Δ is introduced because the energy of the final doubly ionized state is somewhat different from the sum of the energies for individual ionization of the same levels. There are also other expressions used in the literature to assess the kinetic energy of Auger electrons. Another expression that is commonly employed is

$$E_{\mathrm{WXY}} = E_{\mathrm{W}}(Z) - \frac{1}{2}[E_{\mathrm{X}}(Z) + E_{\mathrm{X}}(Z+1)] - \frac{1}{2}[E_{\mathrm{Y}}(Z) + E_{\mathrm{Y}}(Z+1)] - \phi_A$$

Figure 14.6: *Typical energy distribution of Auger electrons $N(E)$ and dN/dE plot for Auger emission. Usefulness of using differential plot is shown. Peak to peak height is used for qualitative analysis.*

However, only limited calculations have been made to determine the Auger energies from the first principles. Normally, the most prominent Auger peaks result from KLL transitions for elements with $Z = 4 - 14$, LMM transitions for elements with $Z = 14 - 40$, MNN transitions for elements with $Z = 40 - 79$ and NOO transitions for heavier elements.

14.2.2 Auger Electron Escape Depth and Surface Sensitivity

The Auger electron escape depth (which is directly related to the surface sensitivity) is usually determined empirically by depositing atomically

uniform overlayers and then monitoring the Auger peaks from the substrate. The universal escape curve (shown in Fig.14.8) is generated from a variety of experimental data that show that the escape depth is not strongly dependent on the matrix. There are also estimates of the behaviour of the ionization cross section as a function of incident electron beam energy E_P and this appears to reach maximum when $E_P/E_K = 3$. However, it should be remembered that this estimate and other theoretical calculations for estimating the optimum ratio of E_P/E_K have many other complicating factors such as the contribution to the cross section by the backscattered electrons and other instrumental parameters.

Figure 14.7: *Energy scheme showing the Auger process and the three energy levels involved. The core ionization takes place in the K shell. Relaxation into this level occurs from L1 and an electron is ejected from the L2 level.*

Since Auger electron emission in the case of solids involves the valence electrons and also the binding energy of core levels, the line shape as well as the kinetic energy of the Auger electron are strongly influenced by chemical environment. This shift in the kinetic energy of the Auger electrons can be advantageously utilized to derive information on the nature of the species as well as on the nature of bonding involved. However, chemical shifts in Auger electron spectroscopy is not as straight

forward as it is in photoelectron spectroscopy. This is because the energy shifts of Auger peaks involving valence electrons mostly reflect in the redistribution of the density of states in the valence band than in the core level energy shifts. However, the magnitude of the shifts can be considerably different. Depending on the nature of the atom under consideration and its position in the periodic table, one can see some regularities in the chemical shift values with respect to oxidation state of the element. For example, the peak due to LVV transition of SiO_2 appears around 75 eV while that of polycrystalline silicon appears at 91 eV. Similarly, carbon KLL Auger line is monitored for various carbon containing species like CO adsorbed on W(112) surface, W_2C, graphite and diamond. Position of KLL Auger line of carbon for these systems are 274, 272.2, 273.2 and 262.5 eV respectively. From these results, it is clear that although chemical shifts may be observed in the Auger lines, the magnitude and direction of the shifts are not easily predictable.

Shape of the Auger lines is not a direct measure of the density of states, but rather is a reflection of the transition probability density. Therefore, the calculation of the density of states from Auger spectra is a complex problem.

Figure 14.8: *Auger electron escape depth as a function of kinetic energy for various materials.*

Instrumentation for AES essentially consists of a vacuum system, an electron gun, a detector and an electron spectrometer for the energy analysis of the emitted electrons. It is thus no different from that of XPS. Since AES is surface sensitive, a necessary requirement is an ultra high vacuum (UHV) system, which can be routinely evacuated to a

pressure of 10^{-10} torr. At this pressure, it would require about half an hour for the formation of a monolayer of contaminants like oxygen and other residual gases allowing sufficient time for completing the analysis. However, such stringent vacuum requirements may not be necessary for studies with passivated surfaces or for depth profile analysis in which the surface is continuously sputtered by an argon ion beam. The possibility of quantitative analysis is one of the special features of Auger electron spectroscopy (AES).

For carrying out quantitative analysis using AES, one has to relate the Auger current from a specific Auger process from an element to the population density of that element on the surface region. From theoretical point of view, the measured Auger current is proportional to:
(i) the excitation flux density; this parameter can have two components, namely the primary ionization of the core hole and also the excitation flux due to back scattered primary electrons;
(ii) ionization cross section of the core level;
(iii) the atomic density of the element under examination at a defined depth from the surface;
(iv) probability of the Auger electron escape, and
(v) probability factor for the Auger transition.

Table 14.1: Comparison of the analysis of Inconel and 316 Stainless steel alloys for transition metals by atomic absorption spectroscopy and AES.

Alloy	Element	S^a_X	Atomic concentration	
			Atomic absorp.	AES
316 SS	Cr	0.31	0.200	0.18
	Fe	0.21	0.656	0.71
	Ni	0.26	0.127	0.10
	Mo	0.25	0.018	0.01
600T Inconel	Cr	0.31	0.177	0.21
	Fe	0.21	0.084	0.07
	Ni	0.26	0.736	0.71
	Ti	0.44	0.003	0.01

In many cases, however, it is not possible to carry out quantitative analysis from first principles utilizing these five factors. Hence, quantitative analysis is carried out either using external standards or by employing suitable elemental sensitivity factors. In terms of sensitivity factor, the concentration of an element X can be expressed as

$$C_X = \frac{I_X/S_X}{\sum I_\alpha/S_\alpha} \tag{14.11}$$

where S_α is the relative sensitivity of element α. A tabulation of such sensitivity factors is available in standard sources[4]. These factors are based on peak to peak height of the Auger signals and assume the peak shape to be invariant with the matrix.

To demonstrate the utility of the sensitivity factor for quantitative analysis, AES analysis of Inconel alloy is considered. The analyses were carried out for the elements Ti, Fe, Cr and Ni by monitoring the MNN Auger emission. The data given in Table 14.1 demonstrate that the experimental values derived from AES are in good agreement with the values obtained atomic absorption spectroscopy. It should be noted that the spectroscopic analysis is for bulk samples.

The relative elemental sensitivity factor S_X is taken from the hand book of Palmberg et al.

14.2.3 Application of AES for the Study of Catalysts

Most of the applications of AES technique for the study of catalysts is related to finding the surface composition and distribution of species on the surface as a result of catalytic reactions. These studies have established that the surface composition of most of the catalysts can be different from that of the bulk composition. For example, AES analysis of the surface of Ni-Au alloy foil indicated that enrichment of gold on the surface occurs on thermal equilibration at high temperature. This type of surface segregation of one of the metals in the alloys is a common observation. This segregation of one of the constituents to the surface can be due to many factors such as the value of the surface energy of the metals (the one with lower surface free energy will enrich the surface), entropy factors and also preferential segregation due to the preferential interaction with the atmospheric gases.

In the case of Ni-Al alloy catalyst used in methanation of natural gas, AES analysis has shown that the deactivation of the catalyst resulted from coverage of the surface by sulphur. The sulphur accumulation on the surface has been caused by the interaction of sulphur with the segregated Ni on the surface. This could be established by etching the surface which showed that the sulphur concentration was mainly restricted to a few top layers in the spent catalysts.

The sulphur-oxygen reaction on nickel surfaces has also been studied. The reaction steps have been identified as the adsorption of oxygen, the reaction of adsorbed oxygen with adsorbed sulphur followed by the

[4]P. W. Plamberg, G. E. Riach, R. E. Weber and N. C. MacDonald, *Handbook of Auger Electron Spectroscopy*, Physical Electronic Industries, Edina, 1972.

desorption of the sulphur dioxide formed. By monitoring the growth of the oxygen Auger peak and the disappearance of the Auger peak for sulphur at various temperatures and at different partial pressures of oxygen, it has been concluded that the surface reaction between the two adsorbed species is rate controlling.

Auger electron spectroscopy is a powerful surface analytical technique. It can be used to monitor the elemental composition of the surfaces and also for depth profiling by suitable ion bombardment. Several phenomena other than adsorption, surface reactions and surface segregation can be studied employing AES. This includes corrosion, surface oxidation, stress corrosion, adhesion, friction, wear, grain boundary phenomenon, embrittlement in alloys, inter-granular corrosion and stability of grain structures. AES can also be effectively utilized in semiconductor technology to monitor the layer by layer atomic composition and their effect in semiconducting properties. Mechanical properties such as fatigue, wear adhesion resistance to deformation process and surface cracking depend on surface properties and hence these processes can also be studied using AES. Grain boundary chemistry influences mechanical properties such as low and high temperature ductility and fatigue, chemical properties such as inter-granular corrosion and stress corrosion. All these can be effectively studied by AES. However, these applications are beyond the scope of this book.

The main advantages of AES technique can be summarized as:
(i) high spatial resolution;
ii) analysis is relatively rapid;
(iii) surface sensitive analysis can be performed;
(iv) it is sensitive to light elements (except H and He).

AES is expected to find increasing applications in many areas of science and technology requiring detailed information on elemental identification of surface composition, oxidation states and chemical bonding.

SUGGESTED READING

1. Carlson, T. A., *Photoelectron and Auger Spectroscopy*, Plenum Press, 1975.

2. Ghosh, P. K., *A Whiff of Photoelectron Spectroscopy*, IIT Kanpur, 1978.

3. Brundle, C. R. and Baker, A. D., *Electron Spectroscopy: Theory, Techniques and Applications*, Vols. 1-4, Academic Press.

Chapter 15

NMR, EPR and Nuclear Resonance

Three experimental techniques will be considered under the resonance spetroscopic methods. These are nuclear magnetic resonance (NMR), electron paramagnetic resonance (EPR) and Mössbauer spectroscopic method.

15.1 NMR SPECTROSCOPY

Nuclear magnetic resonance spectroscopy is routinely used for molecular structure determination and needs no introduction for the chemist. Any atom with a non-zero nuclear spin can show NMR transitions. Proton and C-13 NMR have become routine tool for the organic chemists. This is because the spin energy of the nucleus is highly sensitive to the chemical environment of the atom giving rise to the so-called chemical shift. In liquid samples, the random tumbling motion of the molecules averages all the anisotropic interactions and it is possible to get sharp spectral lines with line-width less than 1 Hz. In a solid, on the other hand, all the anisotropic interactions are present. The difficulty in getting a good NMR spectrum of a solid sample lies in the enormous line broadening (tens of kHz) mainly due to nuclear dipole-dipole interaction. The mathematical expression for direct dipolar coupling of the nuclei p and q is given as

$$B^{dir}(Hz) = -\frac{h}{4\pi^2}\gamma_p\gamma_q\frac{1}{2}\frac{(3\cos^2\theta_{pq}-1)}{r_{pq}^3} \tag{15.1}$$

where θ_{pq} is the angle that the pq-internuclear axis makes with the direction of the applied magnetic field. The chemical shift B^{dir} is directly

proportional to $(3\cos^2\theta - 1)$. When the sample is in solution, all possible values of θ are possible because the molecules are tumbling and the angle is changing all the time. The moment due to direct dipole-dipole interaction averages to zero. In a polycrystalline solid, all values of θ are possible giving rise to an enormously broad band that is impossible to observe. In a static polycrystalline solid, the magnetic moment vectors are pointing in all directions. When the sample tube is made to spin rapidly at an angle θ with respect to the applied field, every magnetic moment vector gives a resultant that lies along the direction θ. If $\theta = 54^o44'$, the term $(3\cos^2\theta - 1) = 0$ and the dipolar shift disappears. While recording the spectrum, the sample tube is spun at this angle (called the magic angle) at a very high frequency (> 4 kHz) to eliminate dipolar broadening and hence it is called magic angle spinning NMR or simply as MASNMR. This method has made the study of the NMR of solids possible. Here we shall discuss briefly the MASNMR of zeolites and aluminophosphate molecular sieves.

15.1.1 MASNMR of Zeolites

Zeolites have silicon and aluminium (T) atoms surrounded tetrahedrally by oxygen atoms and it has the $T - O - T$ linkages. However, there cannot be any $Al - O - Al$ linkage in a zeolite for structural reasons. Silicon has an isotope ^{29}Si with nuclear spin $\frac{1}{2}$ that has a natural abundance 4.7%. ^{29}Si MASNMR is easily observed at high field with line width of about 20 Hz. The most abundant isotope of aluminium is ^{27}Al that has a nuclear spin $\frac{5}{2}$. In principle, both these nuclei present in a solid can be studied by solid state MASNMR, although the aluminium nuclei that has a nuclear spin I=5/2, show appreciable quadrupole broadening.

Zeolites have different structures and Si/Al ratio in them may vary from 1 to very high values so much so that zeolite structures with only silicon at the T sites could be synthesized. In a zeolite, there can be maximum five different kinds of near-neighbour silicon environment. The Si atom may be linked (via oxygen) to 4 Al and no Si ([Si(0Si)]), 3 Al and 1 Si ([Si(1Si)]), 2 Al and 2 Si ([Si(2Si)]), 1 Al and 3 Si ([Si(3Si)]), and to all four silicon atoms ([Si(4Si)]) (see figure 15.1).

Higher Si/Al ratio increases structural stability and also increases the acid strength of the proton form of the zeolite, although the number of acid sites decreases.

A well resolved MASNMR spectra of a zeolite then can show a maximum of five spectral lines due to the five different tetrahedral silicon in the oxygen environment. These lines generally lie between -80 to about

−120 ppm with reference to tetramethyl silicon (TMS), the negative shift increasing with the number of silicon atoms surrounding a Si.

Figure 15.1: *Five different possible environments of Si in a zeolite.*

^{29}Si MASNMR of an important zeolite called zeolite Y (faujasite) with Si/Al ratio 2.5 is shown in figure 15.2. It can be seen from the figure that the signal due to Si[(4Si)] is absent. This environment is highly unlikely in a Y zeolite where the Si/Al ratio is quite low. This signal would be most prominent in a sample of zeolite ZSM5 that has very high Si/Al ratio. All other types of silicon environment are shown in the MASNMR spectra of zeolite Y.

Because zeolite Y can not be synthesized with high Si/Al ratio, aluminium is partially removed from the synthesized sample in order to increase its structural stability and to increase its acid strength, by a process known as dealumination. However, chemical analysis of such a dealuminated sample may not give the correct Si/Al ratio of the zeolite frame because part of the removed aluminium may stay in the solid mass, or part of silica may also be removed from the structure but may remain in the solid in the form of a silicious mass. These will appear in the results of chemical analysis. Si/Al ratio in such samples may be determined by MASNMR that gives the correct information of the ratio in the zeolite framework.

Si/Al ratio in the framework can be calculated from the spectra[1]

[1] J. Klinowski, *Chem. Rev.*, 91, 1459 (1991)

using the relation:

$$\left(\frac{\mathrm{Si}}{\mathrm{Al}}\right)_{NMR} = \frac{\sum I_4 + I_3 + I_2 + I_1 + I_0}{I_4 + 0.75I_3 + 0.5I_2 + 0.25I_1} \tag{15.2}$$

where I_n is the intensity of the [Si(nSi)] peak.

Figure 15.2: ^{29}Si *MASNMR spectrum of zeolite* Y.

Another high silica crystalline aluminosilicate is zeolite beta. A sample with Si/Al ratio equal to 20 shows only two peaks. The most intense one at -110 ppm is due to [Si(4Si)] and another at -105 ppm due to [Si(3Si)]. ^{27}Al spectrum of the as-synthesized sample show one peak at 52 ppm (with hexahydrated Al^{3+} as the reference) that suggests that all the Al atoms are at tetrahedral sites. After calcination, the ^{27}Al spectrum showed one additional peak that may be assigned to octahedral Al formed due to partial collapse of the structure.

The zeolite ZSM-5 that has very high Si/Al ratio has predominately only [Si(4Si)] environment and shows a single MASNMR peak. Well resolved ^{29}Si MASNMR spectra are shown by high silica zeolites. NMR of the silica-only zeolite with ZSM-5 structure (silicalite-1) on deconvulation shows multiple lines between -110 and -120 ppm. Although all the silicon atoms in silicalite-1 are surrounded by four silicon atoms, they are crystallographically non-equivalent. There are are 24 crystallographically non-equivalent T sites in the ZSM-5 unit cell. Complete deconvulation of the spectrum should give 24 lines, although all of them are not seen.

Study of zeolite crystallization by MASNMR

NMR has been used to study the mechanism of the formation of the zeolite structure from the gel. In order to simplify the writing of the various silicate species, "Q" notations are used. Q stands for a silicon atom tetrahedrally linked to four oxygen. A mononuclear species is represented as Q_0. The notation for a silicon linked to one more silicon (through oxygen) is Q_1 and a that for a silicon linked to two other silicon units is Q_2. According to this notation, a linear binuclear and a linear trinuclear species will be represented as Q_1Q_1 and $Q_1Q_2Q_1$ respectively. A cyclic trimer has the notation $Q_{3/2}$. During crystallization of a zeolite from the silicate solution, various Q species are formed at different stages. Attempts have been made to identify them in solution and in the gel by comparing the chemical shift of the species formed with known chemical shift of crystalline silicate minerals. It has been found that the species and their relative amount depend on the concentration of total silica in solution, amount of alkali, dilution etc. Although extensive studies have been carried out by many workers, interpretation of the results are not unambiguous and this discussion will not be further pursued here.

Figure 15.3: ^{29}Si *MASNMR spectrum of silicalite 1 after deconvulation of the experimental spectrum.*

15.1.2 MASNMR of Aluminophosphate Sieves

MASNMR studies in some substituted aluminophosphate molecular sieves will be considered next. Aluminophosphate (AlPO) molecular sieves have alternating AlO_4 and PO_4 tetrahedra. Aluminium and phosphorus atoms are joined through oxygen atom. They are notable by the

absence of $Al-O-Al$ and $P-O-P$ linkages. They have been synthesized with a variety of crystal structures some of which are analogous to some known zeolites and others are novel. Their framework is flexible and substitution of either phosphorus or aluminium or both by some other atoms is not difficult. In fact, some of the structures are formed only when some silicon atoms are present at the phosphorus sites.

Figure 15.4: *A hypothetical SAPO structure drawn in two dimension showing different possible* Si *environment.*

Silicon substituted (SAPO), metal substituted (MeAPO) and both silicon and metal substituted (MeSAPO) aluminophosphate sieves could be synthesized in large numbers. It has been shown that in SAPO, silicon substitutes only phosphorus atoms and hence $Si-O-Si$ will generally be absent in a SAPO or a MeSAPO, although such a linkage is very much present in zeolites. $Si-O-Si$ linkages can be present in SAPO and MeSAPO if they form silica-only regions within a structure as shown in figure 15.4.

A number of aluminophosphate and related materials have been investigated by MASNMR. Blackwell and Patton investigated AlPO-5, AlPO-11, AlPO-17 and AlPO-31 by ^{27}Al and ^{31}P MASNMR spectroscopy[2]. The ^{31}P MASNMR spectra of all samples showed symmetrical lines in

[2]C. S. Blackwell and R. L. Patton, *J. Phys. Chem.*, 88, 6135, (1984).

the range −19 ppm to −30 ppm (with reference to orthophosphoric acid) consistent with tetrahedral phosphorous in the framework of the material.

^{31}P and ^{27}Al MASNMR of AlPO-14 was reported by Goepper and Guth[3]. Two ^{31}P resonances at −19 ppm and −29 ppm (intensity ratio 1: 2.5) were seen due to tetrahedral phosphorous atoms. The structure AlPO-14 has four crystallographically unique P positions. Three of the Al-O-P angles are similar and the fourth differs appreciably. Hence, two signals may be expected in ^{31}P MASNMR.

Figure 15.5: ^{29}Si *MASNMR spectrum of* SAPO-34.

^{29}Si and ^{31}P MASNMR of SAPO-46 have been studied[4]. The ^{29}Si spectrum consists of two intense peaks at −89 ppm and −92 ppm both of which were assigned to Si(4Al,0Si) environment with Si located at two crystallographically distinct sites. The structure of SAPO-46 is based on doubly capped six-membered rings with a unidimensional 12-ring channel system interconnected through eight-membered rings. The tetrahedral site at the apex of the capped six-ring is in a different environment from those sites located in the six-membered rings. So it is possible to expect two different NMR signals due to silicon atoms located at two distinct sites. The ^{31}P spectrum showed sharp peak at −25 ppm with a shoulder at −31 ppm.

MASNMR of SAPO-34, MgAPO-34, MgSAPO-34 and also of similar

[3]M. Goepper and J. L. Guth *Zeolites*, 11, 477,(1991).

[4]A. M. Prakash, S. Ashtekar and D. K. Chakrabarty,*J. Chem. Soc., Faraday*, 91, 6,(1995).

compounds of the structure -44 have been studied. Structures -34 and -44 are very similar to the natural aluminosilicate zeolite chabazite. The magnesium substituted samples showed distinct multiple ^{31}P spectrum that is very interesting.

Figure 15.5 shows a typical ^{29}Si spectrum of a sample SAPO-34. The spectra could be resolved into five signals, each belonging to a different Si environment [Si(0Si)]. [Si(1Si)], [Si(2Si)], [Si(3Si)] and [Si(4Si)]. If the amount of silicon in the sample is increased, intensity of the peak due to Si(0Si) decreases. Different possible Si environments in a SAPO are shown in figure 15.4. Si can substitute P in isolation or form a five silicon atom cluster with a Si at the centre linked to four other Si atoms. Silicon atoms can also form silicon-only region in the structure. All these can happen without violating the bonding rules.

Table 15.1: Composition of some substituted AlPO samples.

Sample	Mg	Al	P	Si
MgAPO-34/1	0.13	0.39	0.48	0
MgAPO44/1	0.10	0.40	0.50	0
MgAPO-34/2	0.16	0.35	0.49	0
MgAPO-44/2	0.16	0.35	0.49	0
MgSAPO-34/1	0.03	0.47	0.37	0.13
MgSAPO-44/1	0.02	0.47	0.38	0.13
MgSAPO-34/2	0.04	0.45	0.40	0.11
MgSAPO-44/2	0.04	0.45	0.40	0.11
MgSAPO-34/3	0.10	0.38	0.43	0.09
MgSAPO-44/3	0.09	0.40	0.43	0.08

From the relative intensity of the peaks, it is seen that the silicon atoms mostly substitute phosphorus atoms in isolation, but there are also fairly large silicon-only regions present. Similar results were obtained for SAPO-44 as well.

SAPO-34 and SAPO-44 showed a single ^{31}P peak at -27 ppm due to phosphorus tetrahedrally surrounded by oxygen atoms.

MASNMR of MeAPO and MeSAPO

Relative composition of some the samples (taking total number of atoms at the tetrahedral (T) site as unity) are given in Table 15.2. It has been found that Mg^{2+} can be easily substituted in the -34 and -44 frame in fairly large amount.

^{31}P region of the spectra of the MgAPO-34 sample showed multiple peaks[5]. The deconvulated spectrum of MgAPO-34 is shown in figure 15.6. The peaks at -23.9, -16.2 and -8.6 ppm can be assigned to P(3Al,1Mg), P(2Al2Mg) and P(1Al3Mg) respectively. The -23 and -16 ppm peaks sometimes split due to non-equivalent structural sites[6].

Figure 15.6: ^{31}P *MASNMR spectrum of* MgAPO-34/2.

P/Al ratio in the samples has been calculated using equation[7]

$$\frac{\mathrm{P}}{\mathrm{Al}} = \frac{\sum_{\mathrm{n=1}}^{4} \mathrm{I_{P(nAl)}}}{\sum_{\mathrm{n=o}}^{4} 0.25\mathrm{nI_{P(nAl)}}} \tag{15.3}$$

The results obtained from MASNMR are in very good agreement with the results of chemical analysis. Similar results are obtained for MgAPO-44 as well.

Multiple ^{31}P peaks are also seen in the spectra of MgSiAPO-34 and MgSiAPO-44 (figure 15.7). Detailed analysis of these spectra are, however, more complicated. The results clearly indicate that the MASNMR of phosphorus is highly sensitive to the presence metal ions in its immediate neighbourhood.

The ^{31}P spectrum is, however, not sensitive to the presence of Si in the structure. This is because silicon can substitute only phosphorus and not aluminium. This rules out the presence of $\mathrm{P-O-Si}$ linkage and Si

[5]S. Ashtekar, A.M. Prakash, D.K. Chakrabarty and S.V.V. Chilukuri, *J. Chem. Soc., Faraday*, 92, 2481 (1996)

[6]M. Ito, Y. Shimoyama, Y. Saito, Y. Tsurita and M. Otake, *Acta Cryst., Sec. C*, 41, 1968 (1985)

[7]P.J. Barrer and J.K. Klinowski, *J.Phys.Chem*, 93, 103 (1986)

atom in the immediate neighbourhood of P. Si atoms can be present, at best, as the second nearest neighbour to the phosphorus atoms. In this connection, the ^{29}Si MASNMR of MgSAPO-34 samples are revealing.

Figure 15.7: ^{31}P *MASNMR spectra of (a)* MgSAPO-34/1*; (b)* MgSAPO-34/2*; (c)* MgSAPO-34/3*; (d)* MgAPO-34/1*; (e)* MgAPO-34/2.

As the amount of magnesium increases, more silicon goes to form silica-rich regions, although the amount silicon in the sample remained unchanged. This is not difficult to understand if we compare the ionic radii of Mg^{2+} (0.58 Å), Al^{3+} (0.43 Å), P^{5+} (0.25 Å) and Si^{4+} (0.33 Å). As more and more phosphorus goes to replace aluminium, the adjacent sites find it difficult to accommodate the bigger silicon in place of smaller P as that would increase the strain in the structure. The silicon atoms, therefore, form silica-like region within the same structure. This is responsible for the change in the ^{29}Si spectra (see figure 15.8).

^{1}H $-^{29}$ Si CP-MAS NMR

^{29}Si spectra in zeolites can be also observed through cross-polarization. In the zeolites, protons and Si atoms lie close to each other. Magnetiza-

tion can be transferred from ^{1}H to ^{29}Si mediated by ^{1}H $-^{29}$ Si coupling. Protons are much more abundant than ^{29}Si (4.7% abundance) and this will intensify the signal due to the Si atom lying close to a proton. This method not only makes the detection of a signal easier, but also identifies the silicon atoms lying close to protons.

Figure 15.8: ^{29}Si *spectra of (a)*MgSAPO-34/1*;(b)* MgSAPO-34/2*; (c)* MgSAPO-34/3*; (d)* MgSAPO-44/1*; (e)* MgSAPO-44/2*; (f)* MgSAPO-44/3.

The result presented here briefly illustrates how solid state MASNMR spectroscopy can be used in the study of zeolites and aluminophosphate molecular sieves.

15.2 EPR SPECTROSCOPY

15.2.1 Elementary Theory of EPR

We introduce here the most essential of the theory of EPR. The reader should refer to the texts given at the end of this chapter for more detailed discussions.

In electron paramagentic resonance (EPR) also known as electron spin resonance (ESR), the electron spin moment of an unpaired electron ($m_s \pm 1/2$) interacting with the applied magnetic field H gives rise to

two energy states (electronic Zeeman effect). The Hamiltonian of the interaction

$$\hat{H} = g\beta H\hat{S}_z \tag{15.4}$$

where g is the splitting factor that has a value 2.0023 for a free electron, β is the electron Bohr magneton, H is the applied magnetic field and $\hat{S}_z$ is the spin operator. This Hamiltonian operating on the two spin states gives rise to two states. In the presence of a magnetic field H, the energy levels are split as shown in figure 15.9 such that $\Delta E = g\beta H$. If $H = 10,000$ gauss, ΔE has a value that gives $\nu = 28.026$ MHz. EPR experiments are carried out at a fixed ν of 9.5 GHz (X-band) or 35 GHz (Q-band) by varying the magnetic field H.

Figure 15.9: *Splitting of the energy states of an electron spin in a magnetic field.*

What has been discussed so far concerns a free electron. An unpaired electron in a molecule or an ion experiences additional interactions and the complete Hamiltonian for such an unpaired electron is

$$\hat{H} = g\beta H\hat{S} + \sum_{i=1}^{n}(\hat{S}A\hat{I}_i - g_N\beta_n H\hat{I}_i) \tag{15.5}$$

where $\hat{I}_i$ is the nuclear spin operator for the ith nucleus and g_N and β_N are the nuclear g factor and the nuclear magneton respectively. For example, the each of the split electron energy states in the hydrogen atom that has a nuclear spin $1/2$ undergoes further splitting into two states and the EPR spectrum of the hydrogen atom shows two transitions following the selection rule $\Delta m_s \pm 1$. This is known as hyperfine splitting. Both g and the hyperfine coupling constant A are tensors.

The EPR spectrum that is a plot of absorbance of the microwave energy by the sample against the applied magnetic field, is generally presented as the first derivative spectrum from which the value of g and A are obtained. This is illustrated in figure 15.10 with the example of the hydrogen spectrum.

Figure 15.10: *EPR spectrum of hydrogen showing the position from which g and A are calculated.*

When a spectrum is split by n equivalent nuclei each with nuclear spinI_i, the number of spectral lines should be $2nI_i+1$. Thus, the methyl radical that has an electron in the field of three equivalent protons each with $I_i = \frac{1}{2}$ shows a four-line spectrum with intensity ratio $1:3:3:1$. (The relative intensities are given by the coefficients of the binomila expansion). If the odd electron is in the field of n equivalent nuclei with spin I_i and another m equivalent nuclei (different from the first group) of spin I_j, the expected number of spectral lines is $(2nI_i+1)(2mI_j+1)$.

If total electron spin is greater than 1/2, there is interaction between them and the Hamiltonian includes an additional term $\hat{D}$. Because of this, the spin energy states will split even before a magnetic field is applied and this is known as zero-field splitting. Zero field splitting is shown by radicals in triplet states and metal ions with electronic configuration d^2, d^8, d^3, d^7, d^5.

Property of the multi-electron system is summarized in Kramer's rule. The rule states that if the ion has an odd number of electrons, every state should have a two-fold degeneracy (Kramer's doublet) in the absence of a magnetic field. This doublet will split by the application

of a magnetic field. On the other hand, if the ion has an even number of electrons ($m_j = 0, \pm 1, \pm 2... \pm J$), the degeneracy can be removed completely. In such cases, the ground state (a singlet) is separated from the next higher state by a large energy and no transition will be observed in the microwave (EPR) spectrum.

It should be kept in mind that paramagnetism is exhibited whenever the total angular momentum is non-zero ($J \neq 0$). The presence of unpaired electron in an ion is not sufficient to make it paramagentic. For example, the ion Eu^{3+} has six unpaired electron ($4f^6$). Its electronic ground state is $^7F_0$ ($J = 0$) and hence it is diamagnetic.

15.2.2 Powder Samples

Separation of the energy states is dependent on the orientation of the molecule having the unpaired electron with respect to the applied magnetic field. For a polycrystalline solid, the orientations are random and the spectrum is a statistical average. The solution spectrum of a species with $S = 1/2$ and $I = 1/2$ will show a doublet because the molecules are rapidly tumbling. The powder spectrum of such a species will show two g and two A values in trigonal and tetragonal symmetry. At low symmetry, it will show three g and three A parameters. The g values for almost all transition metal ions differ appreciably from the the free electron value g_e. The parameter g is expressed as

$$g = \frac{h\nu}{\beta H} \tag{15.6}$$

Value of A is expressed in gauss or MHz. However, since A has the unit of energy, it is better to express it in energy unit. This is done by multiplying the line separation in gauss by $g\beta$ where β is taken in the unit $\text{cm}^{-1}/\text{gauss}^{-1}$.

15.2.3 Application of EPR in the Study of Solid Catalysts

Heterogeneous catalysis occurs on the surface of the solid catalyst. Hence, the first important step is to distinguish a surface paramagnetic species from the same in the bulk. This is not easy. However, some distingushing features have been identified. If a EPR signal gets affected by adsorption of gases, it may be taken as signal due to a species on the surface. EPR signal of the surface generally broadens on exposure to oxygen. a paramagnetic gas. The same solid with a higher surface area gives a more intense EPR band if the signal is due to a surface paramagnetic species.

Oxygen species

Reactive species like O^-, O_2^- and O_3^- are all paramagnetic. Although the most abundant isotope ^{16}O has zero nuclear spin, ^{17}O has $I = 5/2$.

Figure 15.11: *Expected powder spectra of for $S = 1/2$ and $I = 1/2$.*

The O^- ion has a hole in the $2p$ orbital. The three p orbitals are degenerate in a cubic field that is lifted in tetragonal or orthorhombic symmetry. Because of spin-orbit coupling mixes the orbitals and one expects $g_\perp > g_\parallel$ with $g_\parallel$ close to g_e. EPR spectrum of O^- is shown in figure 15.11. This splits into two sets of six-line patterns in $^{17}O^-$[8]. EPR

[8] J. H. Lunsford, *Catal. Rev.*, 8, 135, (1973).

of $^{16}O^-$ in V_2O_5 shows hyperfine structure because of the V^{5+} showing covalency.

Figure 15.12: *EPR spectrum of* O^-.

In O_2^- species is the most common form formed during surface reactions. The unpaired electron is present in an π^* orbital. Here too the anisotropy in g is due to spin-orbit coupling showing three values (g_{xx}, g_{yy} and g_{zz}) as has been identified on many metal oxide surfaces. The value of g_{zz} has been found to be dependent on the charge of the metal ion stabilizing it. It decreases with increased charge on the metal ion.

Unlike O_2^- that has more than half-filled π^* orbital, in NO^- the π^* orbital is less than half-filled. Adsorbed NO^- has $g_\perp < g_\parallel$. Adsorbed NO^- on MgO surface, for example shows a EPR spectrum with $g_\perp = 1.89$ and $g_\parallel = 1.996$.

EPR has been used to identify the oxidation state and location of transition metal ions in various catalysts. Studies on Cr_2O_3/Al_2O_3 catalysts of ethylene polymerization have shown that Cr^{5+} is the active site [9].

Cu^{2+} exchanged Cu-NaY with small amount of copper showed a spectrum with $g_\perp = 2.05$ and no hyperfine structure for $g_\perp$, and $g_\parallel = 2.38$ with $A_\parallel = 135$ G that may be assigned to $[Cu(H_2O)_6]^{2+}$. When the sample was evacuated at room temperature, a penta-coordinated Cu^{2+} with $g_\parallel = 2.37$ and $g_\perp = 2.06$ is seen. Prolonged evacuation further changed the spectrum to give the EPR of square planar Cu^{2+}. These changes in coordination is due to movement of the copper ion

[9] R. A. Schoonheydt, *J. Phys. Chem.*, 50, 523, (1989).

from the supercage into the sodalite cage[10]. Here, we have selected a few representative examples to demonstrate how EPR spectroscopy has been used to study catalytic surfaces.

15.3 MÖSSBAUER SPECTROSCOPY

The nucleus of an atom may have several energy states and the energy difference between the states are quite high. Suppose the nucleus of an atom are in two states A and B, where A is the excited state and B is the ground state. Then A will emit energy (γ ray) and go to the state B. The state B can absorb the same energy and may rise to the state A. If a nucleus in the state A is used as an emitter and in state B as an absorber, resonance could, in principle, occur. However, unlike in many other cases of resonance fluorescence in the visible, infrared, EPR or NMR regions, the energy emitted during the nuclear transition is very high. This makes the emitting as well as the absorbing nuclei to experience a recoil. As a result, energy of the γ photon (E_γ) is less than the energy difference of the excited and the ground state of the emitter by an amount called the recoil energy (E_R). Since the absorbing nucleus also undergoes recoil, it will need the energy E_R in addition to the energy difference between states A and B to go to the excited state. The recoil energy is related to the photon energy as

$$E_R = \frac{E_\gamma^2}{2Mc^2} \tag{15.7}$$

where M is the nuclear mass and c is the velocity of light. Energy required to excite B to the state A will fall short by $2E_R$ that quite high. This is the reason why gaseous atoms do not show nuclear resonance. If the nuclei are present in a solid matrix, the recoil energy is lost as phonons (lattice vibration) and there is a finite probability that the initial state of some fraction of the nuclei are not changed during emission (or absorption). Such nuclei will have zero loss due to recoil and this fraction is known as *recoil free fraction*. Mössbauer in 1958 for the first time observed recoil free γ-ray emission from ^{191}Ir in a solid and the method of nuclear resonance is now known as Mössbauer transition.

Although nuclear transitions are sharp, there is some broadening because of uncertainty in energy Γ.

$$\Gamma = \frac{0.693h}{2\pi t_{\frac{1}{2}}} \tag{15.8}$$

[10]R. G. Herman and D. R. Flanger, *J. Phys. Chem.*, 82, 720, (1978).

where h is Planck's constant and $t_{\frac{1}{2}}$ is the half-life. For $E_\gamma \approx 10^5$ eV, uncertainty in energy is between $10^{-12} - 10^{-14}$ eV depending on what is $t_{\frac{1}{2}}$. This precise value of energy can give extremely sharp transitions and is the main advantage of this technique. This advantage comes with the disadvantage that not many nuclei fulfill this condition and hence there are not many atoms that can be studied by Mössbauer spectroscopy. Conditions to be satisfied for successful application of this method are:
1. the emitter and the absorber nuclei must be present in a solid,
2. energy of the emitted γ-ray should lie between $10^4 - 10^5$ eV, and
3. half-life should be in the range $10^{-6} - 10^{-11}$ eV, and
4. the γ-emitting nucleus that has the required half-life should have a precursor with a fairly long life.
There are not many nuclei that fulfill all these conditions. Two most exhaustively studied elements are iron and tin using the ^{57}Fe and ^{119}Sn isotopes. The mechanism of their formation and decay is:

$$^{57}_{27}\mathrm{Co} \xrightarrow{270\,\mathrm{days}} {}^{57}_{26}\mathrm{Fe} \xrightarrow{9.77\times10^{-8}\,\mathrm{s}} {}^{67}_{26}\mathrm{Fe}$$

$$^{119}_{50}\mathrm{Sn} \xrightarrow{245\,\mathrm{days}} {}^{119}_{50}\mathrm{Sn} \xrightarrow{1.84\times10^{-8}\,\mathrm{s}} {}^{119}_{50}\mathrm{Sn}$$

In addition to Fe and Sn, some other elements such as Ru, Rh, Ni, Re, Au and Ag too have been studied by Mössbauer method.

Figure 15.13: *Arrangement in a Mössbauer spectrometer.*

In the Mössbauer experiment, one uses the small energy difference in the nucleus of the Mössbauer atom in the source and the sample. Resonance is brought about by supplying a small positive or negative energy to the source by moving it towards the sample or away from it. The essential parts of a Mössbauer spectrometer are (a) a γ-ray source (^{57}Fe,^{119} Sn and some other nuclei.), (b) the sample which is the absorber (containing the stable isotope of the same element, (c) a γ-ray detector and (d) a

drive to impart the Doppler velocity. The experimental arrangement is schematically shown in figure 15.13.

The Mössbauer experiment measures the Doppler velocity needed to cause resonance and the spectrum is a plot of the velocity (mm/s) against the number of counts recorded by the detector. The source generally used for studying the Mösbauer spectra of iron compounds is ^{57}Co in rhodium matrix.

In normal Mössbauer experiments, γ-ray intensity transmitted through a thin sample after absorption is detected. The excited nuclei in the sample may relax in a number of ways. They may relax by emitting electrons from the K shell. These are called *conversion electrons*. For ^{57}Fe, the number of conversion electrons emitted per γ photon is 8.5. Hence, the spectrum recorded by detecting the conversion electrons is more sensitive. Moreover, escape depth of these conversion electrons is only about 100 nm for ^{57}Fe making it more surface sensitive. This makes conversion electron Mössbauer spectroscopy attractive for surface studies.

Figure 15.14: *Mössbauer chemical shift shown schematically: (a) source and absorber have same energy (0 chemical shift); (b) source and absorber are in different states: transition needs Doppler velocity.*

15.3.1 Important Mössbauer Parameters

Nuclear energy levels are perturbed by the electron density near the nucleus. These change in the nuclear energy states are reflected in certain measurable Mössbauer parameters. These are:
1. isomer shift,
2. quadrupole splitting, and
3. magnetic hyperfine interaction or nuclear Zeeman effect.

Isomer shift

Isomer shift or chemical shift (δ) is related to the s electron density in the nucleus in the emitter and the absorber.

$$\delta = \frac{4}{5}\pi Z e^2 R^2 \frac{\Delta R}{R}[|\phi(0)|_a^2 - |\phi(0)|_s^2] \tag{15.9}$$

where Z is the nuclear charge, $\Delta R/R$ is the fractional change in the nuclear radius on excitation and $[|\phi(0)|_a^2 - |\phi(0)|_s^2]$ is the difference in the total s electron density at the nucleus of the absorber and the source. Since s electron density in the nucleus is determined by the chemical state of the atom, this parameter is characteristic of the oxidation state and coordination number of the atom. If the Mössbauer atom in the absorber is in a different chemical environment than in the source, there will be a small energy mismatch for resonance absorption to occur. This extra energy is supplied by the Doppler velocity and the shift is expressed generally as velocity (mm/s).

Figure 15.15: *Spitting of the nuclear energy levels in a non-spherical field and the corresponding quadrupole splitting in* ^{57}*Fe Mössbauer spectrum.*

Quadrupole splitting

A nucleus with spin I has $(2I+1)$ spin states. If the nuclear spin is greater than $\frac{1}{2}$ and the nucleus is in a non-spherical environment, different orientations of the nuclear spin will have different energy of interaction with the applied field. The nuclear energy state will split and the extent of the splitting depends on the nuclear quadrupole moment and the deviation of the electric field from spherical symmetry. For both ^{57}Fe and ^{119}Sn, the nuclear spin $\frac{3}{2}$ and the quadrupole splitting ΔE_q is expressed as

$$\Delta E_q = \frac{1}{2} e^2 q Q \left(1 + \frac{\eta^3}{3}\right)^{1/2} \tag{15.10}$$

where eq is the charge of the metal ion, Q is nuclear quadrupole moment and η is an asymmetry parameter. In the case of ^{57}Fe, the nuclear

quadrupole moment is a positive quantity and the state $m_I = \pm 3/2$ lies higher than $m_I = \pm 1/2$ state. This is reversed in ^{119}Sn for which Q is negative. The major contribution to quadrupole splitting comes from asymmetric charge distribution of the electrons in an atom and the minor contribution is due to other charges in the lattice. Nuclear energy levels in a non-spherical field and the corresponding Mössbauer quadrupole split are shown in figure 15.15.

Low spin Fe^{2+} ($t_{2g}^6 e_g^0$) has a symmetric electron distribution in the t_{2g} level and high spin Fe^{2+} has completely symmetric electron distribution ($t_{2g}^3 e_g^2$). Former is expected to have a small quadrupole splitting. High spin Fe^{3+} should have none. Large quadrupole splitting is expected for low spin Fe^{3+} ($t_{2g}^5 e_g^0$) and high spin Fe^{2+} ($t_{2g}^4 e_g^2$).

Figure 15.16: *Magnetic hyperfine splitting of the ^{57}Fe nucleus.*

Hyperfine splitting

In the presence of a magnetic field (internal or external), each nuclear energy level splits into $(2m_I + 1)$ components. Energy of each level is

$$E_m = -\frac{H_{\text{eff}}\mu}{I} \tag{15.11}$$

where H_{eff} is the magnetic field and μ is the nuclear magnetic dipole moment. Magnetic hyperfine splitting in ^{57}Fe is shown in figure 15.16 and the corresponding spectrum for metallic iron is presented in figure 15.17.

In case of spectra that show hyperfine structure, isomer shift and quadrupole splitting are calculated from the line positions v_n (n is numbered from most negative value to the most positive value of the Doppler velocity) as

$$\delta = \frac{v_1 + v_6 + v_2 + v_5}{4} \tag{15.12}$$

and

$$\Delta E_q = \frac{(v_6 - v_5) - (v_2 - v_1)}{4} \tag{15.13}$$

For a magnetic material, the internal magnetic field can be calculated from the Mössbauer hyperfine splitting. In a polycrystalline magnetic sample, the intensity ratio of the peaks is 3:2:1:1:2:3. Shifts are generally reported after converting them with respect to the shift in an iron foil absorber, although nitroprusside is also used as a reference. For calculating the hyperfine field in a magnetic sample, a iron foil sample ($H_{\text{eff}} = 330$ kOe) is used for calibration.

$$H_{\text{eff}} = \text{total split} \times \text{Y} \tag{15.14}$$

From the known value of $H_{\text{eff}} = 330$ kOe for iron, Y is calculated. This value of Y is used for for calculating hyperfine field in the sample.

Figure 15.17: *Mössbauer spectrum of metallic iron.*

15.3.2 Application to Catalysts

Before going to discuss the application of Mössbauer spectroscopy to catalysts, its limitations should be understtod. There are not many elements that have a Mössbauer active nucleus. We have seen that ^{57}Fe and ^{119}Sn are two good Mössbauer atoms and we shall mostly use iron and tin as examples in our discussion. It should be remembered that only a small fraction of the natural atoms are Mössbauer active. For example, only 2% of natural iron is ^{57}Fe. That many supported catalysts have only a small percent of the active atom complicates the problem further. However, there are some advantages too. Mössbauer transitions

are very sharp and even a small change in the chemical environment of the atom can be detected. Many catalysts consist of nanometer size particles and may escape detection by X-ray diffraction, a limitation that is not present in Mössbauer spectroscopy. However, the sample should be thin in order to get sufficient number of transmission, and at the same time, should have about 10^{18} ^{57}Fe per cm^2 of the sample. The size of the sample can be decreased by using iron enriched with the radioactive isotope.

Experiments are generally carried out by using the sample as the absorber (absorber mode), but experiments can also be done by using the sample as the source. In the last case, it is essential that the sample has sufficient amount of the precursor to the radioactive nuclei undergoing γ-emission. In case of iron, the sample should be prepared by adding ^{57}Co assuming that cobalt and iron will behave in a similar manner in the compound.

Figure 15.18: *Mössbauer spectra of calcined Fe-Mn catalysts supported on silicalite-1 with Fe and Mo mole percent: (a)10:10; (b)10:20.*

Catalyst characterization

The most important application is in catalyst characterization. After preparation, the catalyst needs to be characterized. In the case of iron or tin catalysts, the measured Mössbauer parameters can give information on the oxidation state of the metal, how it is linked to other atoms and can even identify the phases. The various Mössbauer parameters like isomer shift, quadrupole splitting and hyperfine field are useful. Information on these parameters for different iron and tin compounds are already known and are very useful. The application will be demonstrated here with some typical examples.

While preparing iron-manganese catalysts supported on silicalite-1 by impregnation, it was found that the calcined catalyst did not show any X-ray diffraction other than that of the support even at metal loading as high as 20 percent. Mössbauer spectra, on the other hand showed a six-line pattern (δ = 0.44 mm/s; H_{eff} = 503 kOe) characteristic of α-Fe_2O_3 and a central doublet (δ = 0.28 mm/s; ΔE_q = 85 mm/s) due to the presence of superparamagnetic oxide of iron. As the amount of manganese was increased in the catalyst, only the superparamagnetic phase remained (see figure 15.18). This clearly shows that addition of manganese reduces the particle size of the iron oxide[11].

Catalyst preparation

Hobson and Campbell[12] studied the process of reduction of silica supported Fe_2O_3 and found that the amount of Fe^{2+} in the support went on increasing with the temperature of reduction.

Delgass and Boudart[13] studied the effect of dehydration of Fe^{2+}-exchanged Y zeolite by Mössbauer spectroscopy. Intensity of the spectral lines increased with the extent dehydration. Initially, Fe^{2+} was essentially in a dissolved state in the large quantity of water present in the zeolite. The effect of dehydration was to localize the Fe^{2+} ions that lead to the increase in the peak intensity.

Iron catalysts supported on η-Al_2O_3, γ-Al_2O_3 and SiO_2 prepared by impregnation when reduced in hydrogen between 673-973 K showed Fe^{2+} as the most reduced state of iron[14]. Generally, two different ferrous

[11]G. Ravichandran, D. Das and D. K. Chakrabarty, *J. Chem. Soc., Faraday*, 90, 1993, (1994).

[12]M. C. Hobson Jr., and A. D. Campbell, *J. Catal.*, 8, 294, (1967).

[13]W. N. Delgass and M. Boudart, *Catalysis Reviews, Vol.2*, (Ed. H. Heinemann), Marcell Dekker, New York, 1968, p.129.

[14]M. A. Vannice and R. L. Garten, *J. Mol. Catal.*, 1, 201, (1975).

doublets are shown. The doublet that is affected by adsorption of gases such as ammonia is attributed to surface Fe^{2+} and the other to Fe^{2+} present in the bulk.

Another interesting study concerned the $Sn_{1-x}Sb_xO_2$ system obtained by coprecipitation followed by heating[15]. This X-ray amorphous material contained Sn^{4+} and Sb^{5+}. For x¿0.2, phase separation takes place. Mössbauer spectrum shows the presence of Sb^{3+} and Sb^{5+} in approximately octahedral environment. Charge balance is maintained by the formation of Sb^{3+} and not by forming Sn^{2+} is a significant finding.

Adsorption studies

Hobson[16] carried out an interesting study to clearly distinguish surface atoms from bulk atoms. Spectrum of a supported iron oxide catalysts after degassing showed three peaks (figure 15.19). The most intense peak is due to overlap of one band from each of the two quadrupole doublets arising from Fe^{3+} and Fe^{2+}. After ammonia absorption, the peaks due to Fe^{3+} nearly disappear and those of Fe^{2+} become more intense. This is thought to be because of transfer of electron to Fe^{3+}. The doublet due to Fe^{3+} reappears after desorption of ammonia.

Figure 15.19: *Mössbauer spectra of silica supported iron oxide catalysts: A - out-gassed sample; B - after ammonia adsorption; C - after desorption of ammonia.*

Because of the open structure of the zeolites, the exchanged cations inside the pores are accessible to adsorbate molecules. Since the exchanged ions are all on the surface, studying them by Mössbauer spectroscopy will give information on the catalytically active sites. This makes iron exchanged zeolites an ideal candidates for Mössbauer study.

[15]F. J. Berry and P. J. Laundy,J. Chem. Soc., Dalton, 1442, (1098).
[16]M. C. Hobson Jr., *Nature*, 214, 79, (1967)

Goldanskii and co-workers[17] studied the effect of adsorption of methanol and hexane on Fe^{2+} exchanged Y zeolite and mordenite. The sample did not show any Fe^{2+} initially, only Fe^{3+} was shown. After adsorption, Fe^{2+} spectrum appeared. The explanation is that initially only Fe^{3+} ions were bonded and localized and Fe^{2+} were mobile. Adsorption localized the Fe^{2+} giving rise to the spectrum.

Bimetallic catalysts

Bimetallic cluster was observed on supported Fe-M catalysts, when M is ruthenium, rhodium, palladium or platinum[18].

Addition of tin to $Pt/ZnAl_2O_4$ catalyst of butane dehydrogenation is known to have a highly beneficial effect on the life of the catalyst. Gray and Farah[19] studied this catalyst by following the tin Mössbauer spectra during the course of the reaction. They detected the presence of three different tin species such as Sn^{2+}, Sn^{4+} and Pt-Sn alloy. Based on the results, they concluded that PtO_x is active in dehydrogenation of the paraffin and the role of the oxidized form of tin lies in replenishing the oxygen on platinum. The reduced from of tin gets re-oxidized by ZnO.

There are many Mössbauer studies of catalysts. Interpretation of the results are often not straight forward and needs a lot of supplementary information from other studies. Readers may refer to several reviews[20] [21].

SUGGESTED READING

1. Mehring, M., *High Resolution NMR Spectroscopy in Solids*, Springer-Verlag, Berlin, 1983.

2. Engelhardt, G. and Michel, D., *High Resolution Solid-State NMR of Silicates and Zeolites*, John Wlley, New York, 1987.

[17] V. I. Goldanskii, I. P. Suzdalev, A. S. Machindra and Shtyrkov, *Proc. Acad. Sci. USSR*, (English translation), 169, 511, (1966)

[18] A. M. Van der Kraan and J. W. Niemantsverdriet, in *Industrial Applications of Mössbauer Spectroscopy*, (Eds. G. J. Long and J. G. Stevens), Plenum Press, New York, 1986.

[19] P. R. Gray and F. E. Farah, *Mössbauer Method Methodology*, Vol.10, 47, (1976),Ed. L. Mervin, Plenum Press.

[20] J. A. Dumesic and G. B. Raupp, *Adv. Catalysis*, 26, 121, (1977).

[21] S. K. Kulshreshtha, in *Spectroscopic Methods in Heterogeneous Catalysis*, Eds. N. M. Gupta, V. B. Kartha and R. A. Rajadhyaksha, Tata McGraw-Hill, New Delhi, 1991, p.105.

3. Klinowski, J., *Progress in NMR Spectroscopy*, 16, 237, 1984.

4. Wertz, J. and Bolton, J., *Electron Spin Resonance*, McGraw-Hill, New York, 1972.

5. Low, W., *Paramagnetic Resonance in Solids*, Acad. Press, New York and London, 1960.

6. Goldanskii, R. L. and Makarov, E. F., *Chemical Applications of Mössbauer Spectroscopy*, Acad. Press, 1968.

7. Grant, R. W., Mössbauer Effect Methodology, Ed. I. J. Gruvermann, Plenum Press, 1966.

Chapter 16

Preparation of catalysts

Solid catalysts play a key role in chemical industry. Preparation of catalysts plays a dominant role in catalysis research. Preparation of catalysts has always been considered as a skill especially when one is interested in synthesizing such special materials like zeolites and meso-porous substances. The desired properties for a catalyst are (i) high and stable activity; (ii) consistently high selectivity; (iii) controlled surface area and porosity;(iv) good resistance to poisons; (v) good tolerance to high temperatures and temperature fluctuations; (vi) high mechanical strength and (vii) no uncontrollable hazards. After choosing the catalyst system the factors that are to be considered next are : (i) whether the catalyst should be a supported one or not; (ii) what should be the shape of the catalyst (cylinders, rings, spheres, monoliths, coatings); (iii) what should be void fraction; (iv) whether diffusion control is necessary or not and (v) how to achieve the appropriate mechanical strength. There are a variety of preparation methods based on impregnation, precipitation, deposition, calcining, MOCVD, sol-gel techniques, templating and so on.

Catalysts are generally classified in a number of ways. They can be classified on the basis of principal functions or on the basis of the type of reaction they promote. Table 16.1 shows one such way of classification.

A catalyst has several components such as the support, (Al_2O_3, SiO_2, SiO_2-Al_2O_3), the catalytic agent preferably in high dispersion and the promoter that modifies the physical or chemical properties or both, of the catalyst. Figure 16.1 gives a pictorial representation of the various parts of a catalyst.

There are various steps involved in the preparation of a catalyst. One such method involves precipitation of the active component either alone

or on a support.

Figure 16.1: *Pictorial representation of a typical catalyst.*

16.1 PRECIPITATION METHOD

Most catalysts are precipitated from aqueous solutions. Water as a solvent has the following advantages:
1. Water molecules can behave as ligands as well as solvent.
2. It is a Lewis base.
3. It has large dipole moment.
4. Ionic salts easily dissociate completely in it.
5. Ions are solvated in water.
6. Water can react with metal ions (weak Lewis acid) giving species like OH^- or O^{2-} ligand.

Chemical nature of the species in such cases are controlled by variables like pH, temperature, concentration of the salt etc. While using water as a solvent one has to understand the phenomenon of hydrolysis that gives protons and forms metal hydroxyl or oxy species. Coordinated water molecules behave as stronger acid than the solvent molecule themselves because of the electron withdrawal by the metal cations. The hydrolysis reaction can be written as

$$[M(OH_2)_n]^{z+} + nH_2O \rightarrow [M(OH)_h(OH_2)_{n-h}]^{z-h} + +hH_3O^+$$

where h is the hydrolysis ratio, a measure of the number of protons removed from solvation sphere of the metal cation. This hydrolysis ratio depends on the pH of the solution and the oxidation state of the metal cation. However, pH variation can lead to the condensation of the M-OH species. Increase of pH leads to condensation of low valent aquo cations, while decrease of pH condenses high valent oxy-anions.

Large condensed species are obtained at or around *point of zero charge* (PZC) leading to precipitation or gel formation. Below or above the PZC, less condensed solute species (poly anions or poly cations) can be formed. The enthalpy change of the first hydrolysis is positive (often close to the enthalpy of dissociation of water) and hence the tendency

of metal ions to hydrolyze increases with temperature. This is called the hydrothermal concept which is often exploited in the synthesis of molecular sieves and mono dispersed colloids. The condensation of the precursors containing one or more M-OH groups to form polynuclear species takes place through the elimination of water. The water elimination reaction can either be olation or oxolation. In the case of olation reaction, nucleophilic addition of OH^- ion to a hydrated metal cation takes place.

$$M - OH^{\delta-} + M^{\delta+} - OH_2 \rightarrow M - OH - M + H_2O$$

This reaction involves bridging ligand $H_3O_2^-$, with a characteristic distance of about 0.5 nm between the metal atoms.

Table 16.1: Classification of catalysts based on principal functions.

Class	Conductivity type	Functions	Examples
Metals	Conductors	Hydrogenation, hydrogenolysis oxidation	Fe, Ni, Pt Pd, Cu, Ag
Metal oxides and sulphides	Semiconductors, p or n-type	Oxidation, oxidation, cyclization, desulphirisation	NiO, ZnO, CuO WS_2, Cr_2O_3
Metal oxides	Insulators	Dehydration, isomerization	Si_2, MgO, Al_2O_3
Acids		Polymerization, isomerozation, cracking, alkylation	H_3PO_4, H_2SO_4 $AlCl_3$, HF, SiO_2-Al_2O_3

Oxolation is condensation of two OH groups to form one water molecule which is removed by giving an oxo bridge. Dehydration of olate species leads to oxo-species. Olation is generally faster than oxolation.

Normally anions(counter ions) are present in aquesous solutions of metal cations. The counterions can play an important part in hydrothermal chemical transformations. Aquo-cations and anions interact to form a complex. Complexation can be described as the nucleophilic substitution of water molecules by anions in the coordination sphere of the metal cation. However, in the presence of large excess of water molecules in the vicinity of the complex, the reverse can occur. For the stabilization of the complexes the ionic dissociation by solvent molecules or by

hydrolytic dissociation of the M-X bonds have to be avoided. These reactions depend on the extent of charge transfer between the metal and the anion in the MX bond. The complexing ability of an anion will therefore depend on the electronegativity of the complexed precursor and the anion. If the electronegativity of the anion is greater than that of the complexed precursor, then the M-X bond becomes more polar leading to dissociation. In general stable complexation takes place depending on the value for ionic dissociation (χ_{ID}) and hydrolytic dissociation (χ_{HD}). Change in pH, however, can lead to protonation or deportonation and hence the stable complex formation can occur only in a limited pH range. This optimum value of the pH at which complexes can be formed can be shifted towards higher values when the charge on the cation decreases, mean electronegativity of the anion decreases or dentating ability of the ligand increases.

In case of alkoxides where the H in metal hydroxide is replaced by an R group, the chemistry appears to be different. But once the alkoxide is hydrolyzed, the chemical reactions are similar to those taking place in aqueous solutions. Reactivity of metal alkoxides towards hydrolysis and consequent condensation mainly depends on positive charge on the metal centre and ability of the metal atom to expand its coordination number. Hence the stability of metal alkoxide towards hydrolysis decreases with increasing electropositive character of the metal. The stability of metal alkoxide towards hydrolysis increases with increasing chain length or bulkiness of the alkyl group. Notwithstanding this, Si(IV) is four fold coordinated both in the precursor (hydrolyzed or alcoholized) as well as in the oxide form. There is no expansion of coordination number and thereby silicon alkoxides are always monomeric in nature.

Complexation can be used to restrict uncontrolled hydrolysis and condensation. For example, titanium isopropoxide is highly reactive towards hydrolysis. In this case, one can form complexes with alternate ligands like acetyl acetone expanding the coordination number of Ti from four to five thus preventing condensation.

Precipitation is governed by solubility product. The low solubility material in the given reaction medium will be precipitated first. Solubility like any other parameter depends on the temperature and concentration. Co-precipitation is a more complex problem. Precipitation of multiple species with different solubilities under the same temperature and dilution can pose problems. There can also be concentration gradients of the different species and this may also cause additional problems.

Supersaturation may also lead to some problems. In the conventional

precipitation, the process proceeds with the formation of the nuclei and their growth. This kinetics can be of uni-, di- or three-dimensional in nature. Nucleation is dependent on the ratio of prevailing concentration to the concentration under equilibrium conditions. At higher concentration, supersaturation occurs and therefore nucleation can take place. In the case of precipitation, the limiting step will be the diffusion of the species. Precipitation is generally carried out in the formation of an insoluble metal salt. Typically this can be represented as :

Metal(oxalate, nitrate, chloride, sulphate) + NH_3 or Na (urea, hydroxide, and carbonate) + Support = Metal hydroxide or carbonate (on support)

Precipitation conditions (pH, temperature and concentrations) must be carefully controlled for a uniform product. In the case of co-precipitation of double or multiple ions, the relative solubilities of the ions and their solubility products will control the extent of each precipitation.

16.2 IMPREGNATION METHOD

Impregnation from dilute solutions of the precursors of the active component on the support is often resorted to when low loadings of the active component is required. When high loadings are required, then precipitation is preferred. In the impregnation method, a metal ion is contacted with an oxide with high surface area with the idea to create small metal particles with large exposed surface area. When choosing an oxide support to contact with a metal it must have a large surface area and should be compatible with the corresponding metal that is loaded on the support oxide. In this case the first step would be to determine the point of zero charge (PZC) of the oxide. The PZC is the pH where the net surface charge of the oxide is zero. In solution when the pH is greater than the PZC, the surface of the oxide is negatively charged and deprotonated. When the pH is less than PZC, the surface of the oxide is positively charged and protonated. So oxides placed in solutions with a pH greater than its PZC adsorbs cations, and oxides contacted with a solution with pH less that of its PZC will adsorb anions. Metal uptake depends on the pH of the solution and the oxide used.

Impregnation can be achieved by filling the pores of a preformed support with a solution of the metal salt. This procedure is often called wet impregnation or incipient wetness impregnation. In the wet impregnation method, the volume of the solution is substantially larger than

the pore volume of the support while in the incipient wetness method the amount of the solution added is equal to or slightly less than the pore volume of support. The quantitative aspect of impregnation can be realized by the following equation

$$g = a + V_P.C$$

where g is the amount of the precursor in catalyst (mol), a is the amount of the precursor adsorbed on the support (mol), C is the equilibrium concentration of the precursor in the solution (mol/cm^3) and V_P is the pore volume in cm^3. If $a \ll V_P.C$, impregnation takes place and if $a \gg V_P.C$ sorption and ion exchange may be predominant.

Figure 16.2: *Schematic representation of sol-gel process and polymer modified sol-gel process.*

Another method of loading active component on a support is the ion exchange method. This method therefore requires some functionalization of the support and exchanging the functional species with the species to be loaded. This method is often referred by various terms like anchoring, grafting and also ion exchange.

16.3 ROLE OF SUPPORT

One of the essential components of an active catalyst is the support (see Fig.16.1). The support serves the purpose of effective dispersion of the

active component. It is therefore necessary to understand the properties of a support. If necessary, the support can be chosen so that it possesses reactivity towards the reaction mixture. In this case, the support should be capable of interacting with the active component. These interactions have been termed as *weak metal support interaction* (WMSI) or *strong metal support interaction* (SMSI). These interactions have been associated with either charge transfer or decoration of the reduced support on the active component. The support active component interaction could result in the formation of inactive catalyst phase like the formation of spinel $CuAl_2O_4$ in CuO/Al_2O_3 catalyst system. SMSI state has been associated with noble metals supported on reducible supports like TiO_2.

The support imparts mechanical strength to the catalyst to withstand severe experimental conditions like in fluidization. The support should be thermally stable and should also act as a heat sink for the dissipation of the heat of the reaction. The support should possess appropriate porous texture for effective dispersion of the active component but also provide porous architecture which will promote the reaction in an uninhibited fashion.

Normally supports are prepared by any one of the following methods.
1. Solid state reaction (precipitation, drying, coagulation).
2. Reduction, carbonization and leaching (supports like WC, MoC, CoN, are prepared by the use of appropriate precursors which are subjected to temperature controlled reaction). Alloy leaching method is employed for the preparation of catalysts like Raney Nickel.
3. Sol-gel method that has been employed in a variety of ways. A pictorial representation of this process is shown in figure 16.2
4. Flame hydrolysis of chlorides has been employed for the preparation of supports like TiO_2, SnO_2, Al_2O_3 and Fe_2O_3 from $TiCl_4$, $SnCl_4$, $AlCl_3$ and $Fe(CO)_5$.

16.3.1 Loading of the Support

Loading of the active component on the support can also be carried out in a variety of ways. These can be classified as :
1. Traditional chemical methods such as grafting, precipitation and impregnation that have been discussed earlier.
2. Modern methods (based on the methods employed in electronics industry) like physical and chemical vapour deposition and atomic layer deposition.

Anchoring and grafting are the methods based on stable covalent bond formation between homogeneous transition metal complex cata-

lysts and inorganic support. A typical example is shown next:

In case of supported systems, the various stages of formation and growth of particles can occur from monomer dispersion. This is shown pictorially in figure 16.3.

Figure 16.3: *Various stages of formation and growth of particles that take place from the formation of monolayer dispersion.*

3.Micro emulsion method.
Water, oil and amphiphile, (surfactant) constitute a micro-emulsion system. Such systems are optically isotropic and thermodynamically stable. At macroscopic level, micro-emulsion looks like a homogeneous solution, but at molecular state, it is heterogeneous. The internal structure of the micro-emulsion at any temperature is dependent on the ratio of the constituents. The structure can be either nano-spherical nano-sized droplets or a bi-continuous phase. At high concentration of water, the internal structure of micro-emulsion consists of small oil droplets in a continuous water phase. At increased oil concentration a bi-continuous phase without any clear defined shape is formed. At high oil concentration, the system transforms to small water droplets in a continuous oil phase (reverse micelles). The size of the droplets varies from 10 to 100 nm depending on the type of surfactant employed. In the hydrophilic interior of these droplets a certain amount of water soluble material like transition metal salts is dissolved. Two preparation methods possible. These are:

1. Mixing two micro-emulsions, one containing the precursor and the other containing the precipitating agent (this is shown in figure 16.4).

Figure 16.4: *Typical mechanism where a reverse micro emulsion can be used for the preparation of solid catalysts.*

2. Adding the precipitating agent directly to the micro-emulsion containing the metal precursor.

The size of the metallic particle depends on the size of the water droplets in the micro-emulsion. This will depend on the water to surfactant ratio. In the droplet only the nucleation takes place and the size of the particles is controlled by the surrounding surfactant molecules.

Generally a fast nucleation process will result in the production of small particles. The nature of the precipitating agent as well as the concentration of the reducing agent (like hydrazine instead of hydrogen) employed can also control the particle size.

Since the micro-emulsions are stable suspensions, it is a challenge to separate the particles form the constituents of the micro-emulsion, especially when the surfactant molecules are strongly adsorbed on the particles. A homogenous distribution of the particles on the support is required for the preparation of supported catalyst and these distributed particles should not undergo sintering at high temperatures. This has been achieved by adding solvents like tetrahydrofuran (THF) which can compete with surfactant molecules which will destabilize the solution and bring about the sedimentation of the particles. Simultaneous addition of the support and the solvent can bring about uniform distribution of the particles on the support.

There has been some developments in the micro-emulsion mediated synthesis of catalysts. One of the methods employs supercritical carbon dioxide. In one method the rapid expansion of a supercritical micro-emulsion is carried out into a liquid containing the reducing agent for the production of metal particles. In this case silver nitrate was incorporated in reversed micelles formed by perflouoropolyether ammonium carboxylate molecules in supercritical carbon dioxide. The formation of silver particles takes place when the micellar solution is expanded in a room temperature solution of sodium borohydride.

Another method involves the spraying the micro-emulsion solution into an air/acetylene flame. This method allows the deposition of large amounts of particles. Yet another method, involves cross flow ultra filtration to recover metal particles prepared by micro-emulsion. The method allows the possibility of recycling components of the micro-emulsion. There are some advantages and disadvantages of the micro emulsion technique. They are :

1. The metal particles are reduced directly in the micro-emulsion and can be used as a catalyst in suspension without further thermal treatment.
2. A narrow particle size distribution can be obtained.
3. The particle size can be controlled to a great extent Bimetallic particles can be obtained at room temperature.
4. No effect of the support is found on the formation of the particles.

Limitations of this method are :
1. The amount of the catalyst prepared from a single micro-emulsion may be limited.
2. Recovery and recycling of the liquid phase may be difficult.

16.4 MICROPOROUS SOLIDS

The essential steps involved in the synthesis of zeolites and molecular sieve type of materials are :
1. These syntheses are carried out normally under hydrothermal conditions and hence involves a series of complex physico-chemical processes.
2. The reaction starts with the hydrolysis of silicon, aluminium or metal source to form a gel or a solution.
3. In the next step, the dissolution or mineralization of the gel takes place.
4. Nucleation of the zeolite architecture takes place from the gel or the solution as the case may be.
5. This is followed by continuation of the crystallization and crystal growth in various dimensions.
6. This can also be attended with the dissolution of any of the metastable phases that would have formed initially.
7. Finally, the crystallization and crystal growth occurs in the condensed phase to give the final solid product.

Table 16.2: Factors that affect the synthesis of micro porous solids.

Chemical factors	Physical factors
pH of the medium	temperature
Dilution(water/S ratio)	time
Presence of atoms like Fe, Ti etc.	Stirring
Nature of template	Aging

Factors that affect or influence the synthesis of micro- and mesoporous solids are listed in Table 16.2.

The gel composition is an important parameter in the synthesis of micro porous solids especially zeolites. This must take into account all the possible chemical reactions and the ratios of the constituents have to be computed carefully taking into account all possible species. Essentially in the synthesis of zeolites, the OH^-/SiO_2 is an important parameter and the OH^- concentration is computed taking into account the concentration of the alkali cations and the sulphate anions that will be generated in the chemical reactions involved in the synthesis. The al-

kalinity (OH^-/Si) controls the solubility of the silicate species which is required for nucleation and growth. The alkali metal ions exhibit significant influence in stabilizing the desired product. Charge balancing role is attributed to the M^{3+} ions in silicate. The templates (normally N-containing organic bases) fulfill the following functions :

1. Structure and architecture directing.
2. Void space filling.
3. Charge balancing.

The factors that influence the incorporation of hetero-metallic atoms in the zeolite framework are :
1. The ionic size should be comparable to that of Si^{4+}. Too small or too big ions are not compatible.
2. Solubility in reaction medium - insoluble or sparingly soluble metal oxides or hydroxides are difficult to incorporate.
3. Chemical nature towards hydrolysis - hydrolysis of metal salts or complexes of metal like Ti, Zr should be controlled to avoid the formation of metal hydroxide or oxides.
4. The rate of hydrolysis of silicon alkoxide is slow compared to that of titanium alkoxide or zirconium alkoxides. Iron forms insoluble oxides in basic pH range.

16.4.1 Mesoporous Solids

Pore size limitations in zeolites have led to the search of mesoporous solids. A variety of mesorporous solids have been synthesized and used as catalysts in recent times. These materials ushered in a new synthetic approach where instead of a single molecule as templating agent as in the case of zeolites, self assembled molecular aggregates or supramolecular assemblies are employed as templating agents. There have been a number of models proposed to explain the formation of mesoporous materials. Normally surfactants contain hydrophilic head groups and hydrophobic tail within the same molecule and will self organize so as to minimize the contact with incompatible ends. Among the various synthetic routes, the main difference is the way in which the surfactants interact with the inorganic species. In earlier stages, it was thought that the formation of these materials is a result of electrostatic complementarity between charged surfactant and inorganic species. But later on, the meso structured materials have been prepared by exploring possible interactions other than electrostatic path ways. The formation of these materials can be viewed alternatively as the interface chemistry between

the surfactant and inorganic species. The meso porous materials can be prepared by exploiting ionic and hydrogen bonding as well as covalent bonding interactions. Based on possible interactions various synthetic routes have been evolved and they are given in Table 16.3

Figure 16.5: *A typical representation of liquid crystal templating mechanism (single molecule templating is shown at the top).*

The formation of meso porous materials is considered through the liquid crystal templating mechanism. Two mechanistic pathways are postulated to understand the formation of meso porous materials.
(i) The aluminosilicate precursor species occupied the space between a pre-existing hexagonal lyotropic liquid crystalline (LC) phase initiated by the LC phase,
(ii) The inorganic species mediated in some manner, the ordering of the surfactants into the hexagonal arrangement (cooperative templating mechanism). In both cases the inorganic components which are negatively charged under high pH conditions interact strongly with cationic surfactants. Condensation followed by polymerization of silica leads to the meso structure. A pictorial representation of this mechanism is given in figure 16.5 together with single molecule mechanism employed for the synthesis of zeolites.

A three step mechanism for the formation of the surfactant silicate complex has also been proposed. In the first step the oligomeric silicate poly anions act as multidentate ligands for the cationic surfactant head groups leading to a strongly interacted surfactant silica interface with the lamellar phase. In the second step preferential polymerization of silicate

occurs at the interface. Charge density matching takes place between the surfactant and inorganic species that leads to the phase transition from lamellar to hexagonal phase. Another puckering layer model where the silicate species in aqueous solution form a layered structure and further ordering leads to puckering which results in hexagonal structure has been proposed.

Table 16.3: Possible synthetic routes for mesoporous materials.

Pathway	Surfactant	Inorganic precursors	Type	Examples
Direct (ionic interactions)	Cationic Anionic	Anionic Cationic	S^+I^- S^-I^+	MCM type materials
Mediated (ionic interactions)	Cationic Anionic	Cationic Anionic	$S^+X^-I^+$ $S^-M^+I^-$	Acid prepared materials
Neutral pathways	Neutral Neutral	Neutral Neutral	S^0I^0 N^0I^0	Hexagonal mesoporous Mesoporous units
Ligand assisted pathway	Neutral	Neutral	S-I	Technical molecular sieves

16.4.2 Other Unit Operations

The prepared catalysts are subjected to a variety of subsequent unit operations like drying, calcining and shaping. These unit operations and the conditions employed like the temperature of calcinations, atmosphere in which drying and calcination are carried out, the shape of the catalysts like pellets, rings, extrudates depend on the conditions employed in catalytic reactions.

SUGGESTED READING

1. Okamoto, Y. *et al. Appl.Catal., A. General*, 170, 315-379 (1998).
2. Jacobs, P. A., and Poncelet, G., *Preparation of Catalysts, (Ed.B.Delmon)*, 1-VII, Elsevier, 1975, 1978,1982,1988,1998.
3. Indovina, V., *Catalysis Today*, 41, 129 (1998).
4. Pinna, F., *Catalysis Today*, 41, 129 (1988).
5. Schawarz, J. A. et al., *Chem.*, 95, 477 (1995).

Chapter 17

Role of Diffusion

Most of the solids used as catalysts have porous texture. Depending on the pore size distribution of the catalytic solid, some of the molecules may not have access to the total available surface area contained within the pores. The size and geometry of the molecules may also impose restrictions on the accessibility of the molecules to the total surface area available in small pores. A variety of methods is available to determine the pore size distribution in a solid of which adsorption of inert gases like nitrogen at its boiling point is most widely used employing a procedure developed by Barret Joyner and Halenda (BJH) and the details of this procedure can be seen in the original literature. Other physical methods like the pressure porosity meter and density measurement are also used to obtain the total pore volume in a given solid. The pores can adopt a variety of geometries though it is usually visualized as if the pores are cylindrical in shape, an assumption that may not be quite true.

17.1 TYPES OF MASS TRANSPORT

Under the conditions in which a catalytic reaction takes place, it is possible that the rate of transport of the gaseous molecules through the porous structure is comparable with the rate of the chemical reaction and hence can influence the observed kinetics. It is therefore necessary to consider the various modes of transport of the gaseous molecules through porous media. Normally the rate at which molecules diffuse through the porous media is less than the translational velocity of the molecules. This is due to the collisions with the pore walls and with other molecules during their motion through the catalyst texture resulting in a completely random motion. Essentially, there can be three different types of mass transport in porous solids. These are:

17.1.1 Knudsen Flow

When the mean free path of molecules is considerably greater than the pore diameter, Knudsen follow is the predominant mode of molecular transport. This will be the situation when the catalytic reactions are carried out at moderate pressure on solids with small pores. For example, the mean free path of a molecule with a diameter of 2 Å is of the order of 10^{-5} cm and many catalysts have pore diameters in the range 100 Å and hence Knudsen flow will predominate for these molecules at and around atmospheric pressure. Under the Knudsen flow conditions the collision of the molecules with the pore walls is predominant and the reflections from the walls obey the cosine law. The number of molecules crossing unit area in unit time is given by

$$\frac{Ncu}{4} = \frac{p}{\sqrt{(2\pi MRT)}} \tag{17.1}$$

where N is the Avogadro's number, c is the concentration, u is the mean Maxwellian velocity, M is the molecular mass and p the pressure at the plane under consideration. So the rate of flow along the length of the capillary will be proportional to the pressure gradient between two places at a distance, and hence to the concentration gradient. Therefore Knudsen diffusion coefficient D_K can be defined as

$$D_K = (2/3)r\sqrt{(8RT/pM)} = (2/3)ru \tag{17.2}$$

17.1.2 Bulk Flow of Gases

If the pore diameters are of the order of 10^{-4} cm and at atmospheric pressure the mean free path is about 10^{-5} cm, then collision between the molecules is predominant and hence rate of diffusion will be independent of the pore radius (r). The net flow of one set of molecules in one direction will be given by

$$\frac{\partial n_A}{\partial t} = \frac{nA}{3}\lambda\frac{\partial c_A}{\partial x} \tag{17.3}$$

where λ is the distance traveled between two points (the mean free path). Since there will be equal number of molecule of another kind passing through the same area in the opposite direction, the diffusion coefficient for bulk flow can be defined as

$$D_B = \frac{1}{3}\lambda u \tag{17.4}$$

17.1.3 Forced flow

The two diffusive processes that have been considered, namely Knudsen and bulk flow processes, are independent of the total pressure differences across the pore. If a pressure difference is maintained, forced flow occurs and when the mean free path of the molecule is large compared to the pore diameter, then forced flow is indistinguishable from Knudsen flow and is not affected by pressure differentials. But if the mean free path is small compared to the pore diameter and a pressure difference is maintained, there will be a flow due to the pressure difference in addition to the bulk flow. The relationship for the forced flow resulting from such a pressure difference has been deduced by Hagen and Poiseuille. The diffusion coefficient for forced flow has been written as

$$D_P = \frac{r^2 c_T RT}{8\eta} \tag{17.5}$$

where r is the cylindrical pore radius, η is the viscosity and C_T is the concentration. However, unless the reaction is carried out at high pressures, and the pressure drop necessary to maintain flow through the packed reactor is sufficient to cause forced flow through the capillaries of the catalyst pellet, the gas flow will be diverted through the exterior of the pellet. Under these conditions, the reactants reach the interior surface of the catalyst either by Knudsen flow or by bulk flow.

17.2 IMPORTANCE OF DIFFUSION

It is clear that when diffusion into the catalyst particle is fast compared to the chemical reaction, the entire internal surface of the catalyst will be available for the reaction. If on the contrary an active catalyst was used, the reaction will be fast and the reactants will be converted into products before they had time to diffuse into the pores and the most of the reaction will occur in the pore mouth or in the periphery of the catalyst pellet. The interior pore structure is not utilized. Thiele developed the differential equations, solutions of which give the variation of concentration along the length of the pores of different pellet shapes. Wheeler extended Thiele's treatment in such a way that the equations would be adaptable to a practical catalyst pellet. Only a few important cases will be considered where conclusions can be drawn on reaction rates in commercial catalysts.

17.2.1 A Single Cylindrical Pore

Consider a single cylindrical pore of radius r and length 2L. The concentration of the reactant at the pore mouth ($L = 0$) is c_0. Now consider

any volume element dx in the cylindrical pellet. Under steady state, the change in mass flow rate of the reactant in and out of this section must be equal to the rate of the reaction. If the reaction is assumed to be first order, the change in mass flow rate as a result of diffusion alone the pore length will be

$$\pi r^2 D(\frac{\partial c}{\partial x})_x - \pi r^2 D(\frac{\partial c}{\partial x})_{x+dx} = -\pi r^2 D\frac{\partial^2 c}{\partial x^2}dx \tag{17.6}$$

where c is the concentration at a point x along the pore and D is the diffusion coefficient the form of which depends on the experimental conditions (Knudsen, bulk or forced flow).

Figure 17.1: *Fraction of the surface available for reaction as a function of the Thiele Modulus: A. for first order reaction; B. for second order reaction; C. For Zero order reaction. D. For first order on spherical pellets.*

Equating this with the reaction rate in a surface area of $2\pi r dx$,

$$\pi r^2 D\frac{\partial^2 c}{\partial x^2}dx = 2\pi r dx k_1 c \tag{17.7}$$

where k_1 is the first order rate constant per unit area of the solid. The boundary conditions applicable are $c = c_0$ at $L = 0$ and $dc/dx = 0$ at $x = L$. The second condition implies that at the centre of the pore there is no net flow of the reactant. The solution of this equation is

$$c = c_0\frac{\cosh[L\sqrt{\frac{2k_1}{rD}} - x\sqrt{\frac{2k_1}{rD}}]}{\cosh[L\sqrt{\frac{2k_1}{rD}}]} \tag{17.8}$$

One can now obtain the fraction of the pore area available for the reaction by dividing the rate of the reaction by the rate of the reaction when there is no concentration gradient $R_0 = 2\pi r L k_1 c_0$.

Fraction of the surface available for the reaction is given by $f = \frac{1}{h_1} \tanh h_1$ where h_1(dimensuionless) $= L\sqrt{\frac{2k_1}{rD}}$. (This is called Thiele modulus).

When $h_1 > 2$ (the reaction is fast, small pores) $f = 1/h_1$ and the fraction of surface available is inversely proportional to the pore length, which to a first approximation, is proportional to the pellet size. The fraction f is plotted as a function of h in figure 17.1. Similar treatment will hold good for other reaction orders. The fraction of the available surface as a function of h is also shown in figure 17.1.

17.2.2 Influence of Diffusion on Adsorption and Desorption in Pores

In this case, it is reasonable to assume that the first order rate constant will decrease linearly with the fraction of the surface remaining uncovered by reactants or products. In this case the dimensionless group h_o can be defined as

$$h_0 = L\sqrt{\frac{2k_1(1-\theta)}{rD}} = h_0^0\sqrt{(1-\theta)} \tag{17.9}$$

where h_0^0 is the value of h_0 when the pore is free of adsorbed molecules and θ is the coverage. The ratio of the activity of the pore containing adsorbate to that of the uncovered pore will be the fraction of the surface available for reaction and is therefore

$$f = \frac{h_0^0\sqrt{(1-\theta)}\tanh[h_0^0\sqrt{(1-\theta)}]}{h_0^0 \tanh h_0^0} \tag{17.10}$$

When h_0^0 is small, the fraction of the surface is available for the reaction is simply $\sqrt{(1-\theta)}$. This will be the case for slow reactions in large pores.

If on the other hand the catalyst is very active, the pore mouth will be covered by the adsorbate and the reactant molecules will have to travel inside the pores to reach the uncovered surface. If the transport of the reactant molecules through the pore which are covered with adsorbate is by diffusion, one can then calculate the ratio of the rate of the reaction on the uncovered part of the pore to that on the covered part of the pore which is given as

$$f = \frac{1}{1+h_0^0\theta}.\frac{\tanh[h_0^0\sqrt{(1-\theta)}]}{\tanh h_0^0} \tag{17.11}$$

This is a measure of the extent to which the reaction rate is retarded by strong adsorption in small pores. If the rate is high and the pores are very small, the reaction is retarded by a factor $1/(1 + h_0^0\theta)$. In these cases the temperature coefficient of the reaction will be simply the effect of temperature on diffusion since the reactant molecules have to diffuse into the pore to reach the uncovered surface. Hence under these conditions the reaction rate will be proportional to $\sqrt{T}$. In this case, the value of the apparent activation deduced from normal treatment of data will be small since the line will be almost parallel to the abscissa. However, at a sufficiently low temperature the true value of the activation energy can be obtained from these plots. This is because at such low temperatures the rate constant will be small and the fraction of the surface available will be near unity and hence one can obtain the true value of the activation energy. This implies that as the temperature is increased the rate changes from the true chemical rate to the diffusion controlled rate. In the case of desorption, the diameter of the pores decide the magnitude of h_0 and in small pores (when h_0 is large) rate becomes proportional to $\sqrt{k_0}$. The apparent activation energy is only one half of its true value and desorption is accelerated.

17.2.3 Reaction Rate in Spherical Particles

The assumptions are:
1. The reaction is considered to be first order,
2. The radius of the spherical pellet is assumed to be R. In this case, since the reaction inside the pellet must balance the rate of diffusion into the particle, one writes the balanced equation as

$$4\pi R^2 D_e \left(\frac{\partial c}{\partial x}\right)_{a=R} = 4\pi R^2 D_e c_0 \sqrt{\frac{k_v}{D_e}} \left[\frac{1}{\tanh(R\frac{\sqrt{k_v}}{D_e})} - \frac{1}{(R\frac{\sqrt{k_v}}{D_e})}\right] \quad (17.12)$$

The dimensionless quantity is now

$$\phi_s = R\sqrt{\frac{k_v}{D_e}} \quad (17.13)$$

Wheeler, however, defined this as $3h_1 = \phi_s$. (ϕ_s is another dimensionless quantity like Thiele modulus).

If there is no resistance to diffusion, the reaction rate is $k_v c_0$ per unit internal area. Since the internal pore volume of the pellet is $\frac{4}{3}\pi R^3$, the uninhibited rate of the reaction is $\frac{4}{3}\pi R^3 k_v c_0$. The ratio of the rate in the

pellet to the uninhibited rate in the absence of diffusion is a measure of the fraction f of the surface available for the reaction.

$$f = \frac{4\pi R D_e c_0 \phi_s}{(k_v c_0 4\pi R^3)/3}\left[\frac{1}{\tanh\phi_s} - \frac{1}{\phi_s}\right] = \frac{3}{4}\left[\frac{1}{\tanh\phi_s} - \frac{1}{\phi_s}\right] \tag{17.14}$$

This fraction is plotted as curve D in figure 17.1.

When the reactants and/or products retard the reaction, the fraction of the surface available for reaction may be different from that calculated based on some assumptions like the order of the reaction. This is termed as *effectiveness factor*.

17.3 REACTION IN PORES OF ARBITRARY SHAPE

In most of the cases one cannot ascertain the porous texture in a well defined manner. Hence, analytical solutions may not be always possible. Wheeler has considered this case wherein he assumed that the experimental surface area and pore volume conform to the geometric surface area and pore volume of the model catalyst. If a pellet is a composite of N pores of length L, the rate of the reaction per catalyst pellet is an N times the rate per pore. Since the number of pores is $n_p S_x$ where n_p is the number of pores per unit external surface area S_x, then the rate R_p per pellet is given by

$$R_p = S_x n_p R_{1/2} = \left(\frac{S_x \psi}{\pi r^2 \sqrt{2}}\right)\frac{\pi r^2 D}{L} c_0 h_p \tanh h_p \tag{17.15}$$

where $R_{1/2}$ is the rate per pore and ψ is porosity. h_p is defined as

$$h_p = L\sqrt{\frac{k_1 c_1 (1-\psi)\tau}{rD}} = \frac{2v_p}{S_x}\sqrt{\frac{k_1'}{rD}} \tag{17.16}$$

where $k_1(1-\psi)\tau = k_1'$ is the modified value of k_1 due to pore intersections and tortuosity. The fraction of the surface available for reaction is then given by $(1/h_p)\tanh h_p$. The quantity measured experimentally is usually the activity per unit bulk volume of the reactor. This may be obtained by multiplying the rate per pellet by the number of pellets per unit volume. The rate per unit bulk volume is given by

$$R_b = \frac{\rho_b}{\rho_b V_p}\left(\frac{S_x \psi D}{\sqrt{2}L}\right)^2 c_0 h_p \tanh h_p = \frac{1}{2}\left(\frac{S_x}{V_p}\right)^2 \rho_p V_g D c_0 h_p \tanh h_p \tag{17.17}$$

Substituting appropriate quantities for porosity in terms of pellet density and specific volume V_g per gram and also substituting $L = \sqrt{2V_p/S_x}$, one gets the expression for the rate for practical pellets as

$$R_b = \frac{6}{a_p}\rho_b V_g c_0 \sqrt{\frac{k_1 D}{r}} \tanh\left(\frac{a_p}{3}\sqrt{\frac{k_1}{rD}}\right) \tag{17.18}$$

where a_p is the pellet size.

17.3.1 Pressure and Temperature Gradients in Porous Pellets

Depending on the stoichiometry of the reaction considered and the nature of diffusion prevalent, there may be sharp partial pressure gradients in the pores of the pellet. The stoichiometry coefficient ν decides the concentration inside the pellet as compared to the exterior and if $\nu > 1$ and Knudsen diffusion is prevalent, the pressure is greater at the centre than at the exterior surface. In some cracking reactions ν can be higher than 4 and the pressure at the centre of the pellet may be twice as that found in the bulk gas stream. It is also possible that high temperature gradients may be present inside the pores of the pellet depending on the nature of the reaction (i.e., whether it is exothermic or endothermic) and the thermal conductivity of the catalyst. Under steady state conditions the heat flux within the pore must be balanced by the that produced by the chemical reaction and the rate of the chemical reaction must equal the rate of diffusion of reactant into the pore. The temperature profile inside the pore can be written by a heat balance equation of the type

$$\frac{\partial^2 T}{\partial a^2} + \frac{2}{a}\frac{\partial T}{\partial a} = \frac{\Delta H k_v c}{K} \tag{17.19}$$

The temperature profile within the pellet can be obtained by solving equation (17.19) with the equation

$$\frac{\partial^2 C}{\partial a^2} + \frac{2\partial c}{a\partial a} = \frac{S_v k_1 c}{D_e} = \frac{k_v c}{D_e} \tag{17.20}$$

where $k_v = S_v.k_1$, the rate constant per unit volume and D_e is the effective diffusivity. These two equations are solved only numerically by an iterative procedure. These two equations contain two independent variables (termed α and β) namely the exponent of the Arrhenius equation and the heat generation function ($-\frac{\Delta H D c_0}{k T_0}$). The solutions obtained are

given in the form of plots of the ratio of inhibited and uninhibited reaction rates (or the fraction of the surface available for reaction) and for non-isothermal cases, it is referred to as effectiveness factor as a function of the Thiele modulus for spherical pellets, $\phi_s = R\sqrt{(k_v/D_e)}$ with the independent variables (α and β) being constants. Such a plot is shown in figure 17.2.

Figure 17.2: *The effectiveness factor η as a function of ϕ_s.* $\Gamma = E/RT$; $\beta = (-\Delta H D c_0)/(kT - 0)$.

β represents the maximum temperature difference that could exist in the particle relative to the temperature at the particle periphery and this can be written as $(T - T_0)_{max}/T_0$. For exothermic reaction beta is positive and the effectiveness factor can exceed unity. This is due to the increase in rate due to increase in temperature (because of the reaction) may and may more than compensate the decrease in rate caused by the negative concentration gradient effecting a decrease in concentration towards the centre of the particle. The plot for $\beta = 0$ corresponds to the isothermal case.

It is necessary to consider the possibility of diffusion in pores in designing reactors and also catalyst sizes. It may be advantageous assessing the suitable pellet size for commercial reactors. The choice of appropriate size of the catalyst pellets will give rise to fuel economy for heating

purposes and also in the reactor design.

The observed orders of the reaction will also be different from the true orders of the reaction if diffusion were to play a major role in catalytic reaction. This will be true if the molecular weight of the reactants were different since the diffusion of the heavier reactant will be slower than that of the lighter substrates. This will give rise preferential concentration gradient and hence there will be additional pressure dependence of reaction rate on the pressure of heavier substrate due to slower diffusion of this reactant.

Diffusion in the pores of the catalyst can also manifest in the Arrhenius plot. The dimensionless quantity h contains the rate constant and more so on $\sqrt{k}$. Hence the variation of this dimensionless parameter with reciprocal of temperature will show a gradual change of slope indicating that true activation energy is observed only at comparatively low temperatures where h is small and so the factor $\tanh h$ becomes equal to h. The rate now depends on h^2 (hence proportional to k) and not its square root. This transition from apparent kinetics to true kinetics is there fore can be expected (a) with increasing pore size at a fixed temperature and (b) for pores of a given size if the temperature is decreased. Similarly there can be a variety of parameters like surface area, pore volume on which the reaction rate may depend. In two typical extreme cases of slow reactions in large pores and fast reactions in small pores, the observable parameters differ. This information is given in Table 17.1.

Table 17.1: Observable parameters for two extreme cases of pore diffusion.

	Slow reactions (large pores)	Fast reactions (small pores)
Reaction order	n	$\frac{(n+1)}{2}$
Activation energy	E	$E/2$
Bulk diffusion		
Pore radius	r	$r^{3/2}$
Surface area	S_g	$\sqrt{S_g}$
Pore volume	independent	$\sqrt{V_g}$
Knudsen diffusion		
Pore radius	-	r
Surface area	-	independent
Pore volume	-	V_g

Poisoning of the catalysts is a general phenomenon. If the poisoning were to take place homogeneously, the intrinsic activity of the pore walls will decrease as $k(1-\theta)$ where θ is the total fraction of the surface covered with poison. The ratio of the activity of the poisoned pore to that of the unpoisoned pore is given by

$$f = \frac{h_0^0\sqrt{(1-\theta)}\tanh[h_0^0\sqrt{(1-\theta)}]}{h_0^0\tanh h_0^0} \tag{17.21}$$

where h_0^0 is the value of the Thiele modulus for the unpoisoned pore. This equation is analogous to the equation of the effect of diffusion on adsorption.

Figure 17.3: *Poisoning of the catalyst pores: (a) effect of homogeneous distribution of poison on a slow reaction; (b) effect of homogeneous reaction on a fast reaction; (c) selective poisoning of active catalysts; (d) selective poisoning in small pores.*

Selective poisoning occurs with very active catalysts. In this case pore mouths adsorb poison and then more poison was to add an increasing fraction of the pore length becomes covered and become inaccessible to reactant molecules. In this case the ratio of the activity in the poisoned length to the unpoisoned length has to be obtained by considering the diffusion of the reactant through the length L to the rate of the reaction in the length $(1-\theta)L$. Various types of poisoning and its effect on the ratio of the rates of poisoned to unpoisoned pore are shown in figure 17.3.

For more detailed discussion on the role of diffusion in pores the books in suggested reading may be consulted.

SUGGESTED READING

1. Satterfield, C. N. and Sherwood, T. K., *The Role of Diffusion in Catalysis*, Addition-Wesley Publ. Co., Reading, 1963.

2. Thomas, J. M. and Thomas, W. S., *Introduction to the principles of Heterogeneous Catalysis*, Academic Press, London, 1967.